Recovery and Sequestration of CO₂ from Stationary Combustion Systems by Photosynthesis of Microalgae

Final Report

Reporting Period Start Date: October 1, 2000
Reporting Period End Date: March 31, 2005

Dr. T. Nakamura and Dr. C.L. Senior
Physical Sciences Inc.
20 New England Business Center
Andover, MA 01810-1077

Miguel Olaizola, Terry Bridges, Sonolynne Flores, and Laurence Sombardier
Aquasearch Inc./Mera Pharmaceutical Inc.
73-4460 Queen Kaahumanu Highway
Suite 110, Kailua-Kona, HI 96740

S.M. Masutani
University of Hawaii
Hawaii Natural Energy Institute
1680 East-West Rd. POST 109
Honolulu, HI 96822

April 2005

DISCLAIMER

This report was prepared as an account of work sponsored by an agency of the United States Government. Neither the United States Government nor any agency thereof, nor any of their employees, makes any warranty, express or implied, or assumes any legal liability or responsibility for the accuracy, completeness, or usefulness of any information, apparatus, product, or process disclosed, or represents that its use would not infringe privately owned rights. Reference herein to any specific commercial product, process, or service by trade name, trademark, manufacturer, or otherwise does not necessarily constitute or imply its endorsement, recommendation, or favoring by the Untied States Government or any agency thereof. The views and opinions of authors expressed herein do not necessarily state or reflect those of the United States Government or any agency thereof.

ABSTRACT

Most of the anthropogenic emissions of carbon dioxide result from the combustion of fossil fuels for energy production. Photosynthesis has long been recognized as a means, at least in theory, to sequester anthropogenic carbon dioxide. Aquatic microalgae have been identified as fast growing species whose carbon fixing rates are higher than those of land-based plants by one order of magnitude. Physical Sciences Inc. (PSI), Aquasearch, and the Hawaii Natural Energy Institute at the University of Hawaii are jointly developing technologies for recovery and sequestration of CO_2 from stationary combustion systems by photosynthesis of microalgae. The research is aimed primarily at demonstrating the ability of selected species of microalgae to effectively fix carbon from typical power plant exhaust gases.

This report covers the reporting period 1 October 2000 to 31 March 2005 in which PSI, Aquasearch and University of Hawaii conducted their tasks. This report discusses results of the work pertaining to five tasks: Task 1 - Supply of CO_2 from Power Plant Flue Gas to Photobioreactor; Task 2 - Selection of Microalgae; Task 3 - Optimization and Demonstration of Industrial Scale Photobioreactor; Task 4 - Carbon Sequestration System Design; and Task 5 - Economic Analysis. Based on the work conducted in each task summary conclusion is presented.

TABLE OF CONTENTS

TABLE OF CONTENTS (Continued)

LIST OF FIGURES

LIST OF TABLES

1. INTRODUCTION

Emissions of carbon dioxide are predicted to increase in the next century (U.S. DoE, Energy Information Agency, 1997) leading to increased concentrations of carbon dioxide in the atmosphere. While there is still much debate on the effects of increased CO_2 levels on global climate, many scientists agree that the projected increases could have a profound effect on the environment. Most of the anthropogenic emissions of carbon dioxide result from the combustion of fossil fuels for energy production. It is the increased demand for energy, particularly in the developing world, which underlies the projected increase in CO_2 emissions. Meeting this demand without huge increases in CO_2 emissions requires more than merely increasing the efficiency of energy production. Carbon sequestration, capturing and storing carbon emitted from the global energy system, could be a major tool for reducing atmospheric CO_2 emissions from fossil fuel usage.

The costs of removing CO_2 from a conventional coal-fired power plant with flue gas desulfurization were estimated to be in the range of $35 to $264 per ton of CO_2 (IEA, 1998). The cost of power was projected to increase by anywhere from 25 to 130 mills/kWh. DOE's goal is to reduce the cost of carbon sequestration to below $10 /ton of avoided net cost.

Photosynthesis has long been recognized as a means, at least in theory, to sequester anthropogenic carbon dioxide. There has been relatively little research aimed at developing the technology to produce a gaseous combustion effluent that can be used for photosynthetic carbon sequestration. However, the photosynthetic reaction process by plants is too slow to significantly offset the point source emissions of CO_2 within a localized area. Aquatic microalgae have been identified as fast growing species whose carbon fixing rates are higher than those of land-based plants by one order of magnitude.

The Department of Energy has been sponsoring development of large scale photovoltaic power systems for electricity generation. By this analogy, a large scale microalgae plantation may be viewed as one form of renewable energy utilization. While the PV array converts solar energy to electricity, the microalgae plant converts CO_2 from fossil combustion systems to stable carbon compounds for sequestration <u>and</u> high commercial value products to offset the carbon seques-tration cost. The solar utilization efficiency of some microalgae is ~ 5%, as compared to ~ 0.2% for typical land based plants. Furthermore, a dedicated photobioreactor for growth of microalgae may be optimized for high efficiency utilization of solar energy, comparable to those of some photovoltaic cells. It is logical, therefore, that photosynthetic reaction of microalgae be considered as a mean for recovery and sequestration of CO_2 emitted from fossil fuel combustion systems.

Stationary combustion sources, particularly electric utility plants, represent 35% of the carbon dioxide emissions from end-use of energy in the United States (U.S. DoE, Energy Information Agency, 1997). The proposed process addresses this goal through the production of high value products from carbon dioxide emissions. Microalgae can produce high-value pharmaceuticals, fine chemicals, and commodities. In these markets, microalgal carbon can produce revenues of order $100,000 per kg C. These markets are currently estimated at >$5 billion per year, and projected to grow to >$50 billion per year within the next 10-15 years. Revenues can offset carbon sequestration costs.

An ideal methodology for photosynthetic sequestration of anthropogenic carbon dioxide has the following attributes:

1. Highest possible rates of CO_2 uptake
2. Mineralization of CO_2, resulting in permanently sequestered carbon
3. Revenues from substances of high economic value
4. Use of concentrated, anthropogenic CO_2 before it is allowed to enter the atmosphere.

In this research program, Physical Sciences Inc. (PSI), Aquasearch, and the Hawaii Natural Energy Institute at the University of Hawaii have jointly developed technologies for recovery and sequestration of CO_2 from stationary combustion systems by photosynthesis of microalgae. The research we proposed aimed primarily at quantifying the efficacy of microalgae-based carbon sequestration at industrial scale. Our principal research activities were focused on demonstrating the ability of selected species of microalgae to effectively fix carbon from typical power plant exhaust gases. Our final results will be used as the basis to evaluate the technical efficacy and associated economic performance of large-scale carbon sequestration facilities.

Our vision of a viable strategy for carbon sequestration based on photosynthetic micro-algae is shown conceptually in Figure 1. In this figure, CO_2 from the fossil fuel combustion system and nutrients are added to a photobioreactor where microalgae photosynthetically convert the CO_2 into compounds for high commercial values or mineralized carbon for sequestration. The advantages of the proposed process include the following.

1. High purity CO_2 gas is not required for algae culture. It is possible that flue gas containing 2~5% CO_2 can be fed directly to the photobioreactor. This will simplify CO_2 separation from flue gas significantly.
2. Some combustion products such as NO_x or SO_x can be effectively used as nutrients for microalgae. This could simplify flue gas scrubbing for the combustion system.
3. Microalgae culturing yields high value commercial products that could offset the capital and the operation costs of the process. Products of the proposed process are:
   (a) mineralized carbon for stable sequestration; and (b) compounds of high commercial value. By selecting algae species, either one or combination or two can be produced.
4. The proposed process is a renewable cycle with minimal negative impacts on environment.

The research and experimentation we propose will examine and quantify the critical underlying processes. To our knowledge, the research we conducted represents a radical departure from the large body of science and engineering in the area of gas separation. We believe the proposed research has significant potential to create scientific and engineering breakthroughs in controlled, high-throughput, photosynthetic carbon sequestration systems.

The research program calls for development of key technologies pertaining to: (1) treatment of effluent gases from the fossil fuel combustion systems; (2) transferring the recovered CO_2 into aquatic media; and (3) converting CO_2 efficiently by photosynthetic reactions to materials to be re-used or sequestered.
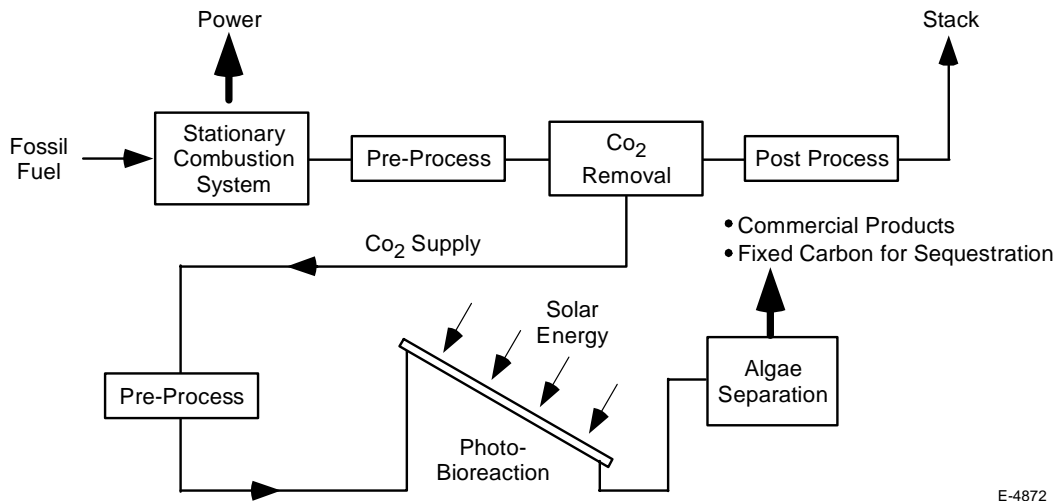
Figure 1.   Recovery and sequestration of CO_2 from stationary combustion systems by photosynthesis of microalgae.

The challenging nature of our program required a qualified an multidisciplinary team. Aquasearch Inc., a U.S. company, has developed full-scale, operating photobioreactor technology with its own investment of more than $13 million. Aquasearch photobioreactor technology now produces commercial quantities of high-value microalgae products. The University of Hawaii provides unique expertise in the understanding and analysis of carbon sequestration processes. PSI has extensive government program management experience and unique technical expertise in the areas of pollution control from stationary power systems and solar engineering.

The 3-year program consisted of the following tasks; (1) recovery of CO_2 from power plant flue gas to photobioreactor; (2) selection of microalgae best suited for the proposed process; (3) optimization and demonstration of industrial scale photobioreactor; (4) carbon sequestration system design; and (5) economic analysis. Figure 2 shows the organization of the program with five main tasks. The tasks (as expressed in our Phase II proposal) are explained in more detail below.

In Task 1, we will survey and characterize flue gas from different fossil combustion systems and identify suitable carbon separation methods for the proposed system. There are several technologies currently available to separate and capture CO_2 from fossil-fueled power plants including absorption from gas streams by contact with amine-based solvents, cold methanol or sorbents and passing the gas stream through special membranes. Merely bringing a gaseous CO_2 stream to the photobioreactor is not sufficient to ensure high utilization of CO_2; effective dissolution of CO_2 into the aqueous phase is needed. In Task 1, we will optimize the gas-liquid mass transfer into the photobioreactor.

DOE Program Manager

Program Management and Reporting
Task 6
PSI

Carbon Dioxide Supply to Bioreactor Task 1 PSI	Selection of Microalgae Task 2 Aquasearch	Demonstration of Industrial Scale Photobioreactor Task 3 Aquasearch	Carbon Sequestration System Design Task 4 Univ. Hawaii	Economic Analysis Task 5 Aquasearch
Power Plant Exhaust Task 1.1 PSI	Microalgae Requirements Task 2.1 Aquasearch	Pilot Scale Evaluation Task 3.1 Aquasearch	Component Development and Design Task 4.1 PSI	Gas Separation Task 5.1 PSI
CO_2 Separation Process Selection Task 1.2 PSI	Photosynthetic Fixation Rates Task 2.2 Aquasearch	Full Scale Evaluation Task 3.2 Aquasearch	System Integration Task 4.2 Univ. Hawaii	Photobioreactor Carbon Fixation Task 5.2 Aquasearch
CO_2 Dissolution Task 1.3 PSI		Product Processing Task 3.3 Aquasearch		

E-4877

Figure 2. Program organization.

In Task 2 selection of microalgae best suited for the proposed carbon recovery and sequestration system will be made. We will quantify the performance of 15 to 20 microalgae species at a small laboratory scale according to the following criteria.

- Ability to withstand the most untreated forms of industrial exhaust gases;
- High rate of photosynthetic carbon fixation; and
- Ability to produce high-value products; _or_
- Ability to produce carbonate minerals

These experiments will involve the use of exhaust gases that are manipulated to represent exhaust streams from a variety of typical power plants. We will then determine, based on the preceding experiments, the degree to which separation or purification of the gas exhaust is necessary, and which species of microalgae are best suited to a scaled up demonstration.

In Task 3, we will demonstrate the carbon sequestration process at large scale. This approach will employ two to three species from each category (high-value _or_ carbon-mineralizing), cultivated with industrial-scale photobioreactors and using selected power plant exhaust gases as the primary carbon source. The nature of the exhaust gases may be modified by separation, purification or other alterations in physical characteristics as dictated by preceding experiments.

4

Task 4 will involve component development and study of subsystem integration of a large-scale carbon sequestration facility. Optimization of each component and of the integrated system will be made. The purpose of this study is to provide the design parameters for such a facility in sufficient detail to enable a detailed economic analysis of capital and operating cost requirements, expected return on capital, and a variety of related performance characteristics, both technical and economic nature.

Based on the results of Tasks 1 through 4, we will conduct a detailed economic study in Task 5 to assess viability of the proposed system for recovery and sequestration of CO_2 from stationary combustion systems.

2. EXECUTIVE SUMMARY

This program calls for development of key technologies pertaining to: (1) treatment of effluent gases from the fossil fuel combustion systems; (2) transferring the recovered CO_2 into aquatic media; and (3) converting CO_2 efficiently by photosynthetic reactions to materials to be re-used or sequestered. The work we have conducted may be summarized as follows.

Task 1 - Supply of CO_2 from Power Plant Flue Gas to Photobioreactor

- Completed characterization of power plant exhaust gas;
- Identified a number of CO_2 separation processes;

Task 2 - Selection of Microalgae

- Analyzed 34 different strains for high value pigments;
- Determined the productivity parameters for 25 different algae grown at three different pH;
- Determined the productivity parameters for 21 different algae with 5 different simulated flue gases;
- Tested three different strains for carbon sequestration potential into carbonates for long-term storage of carbon;

Task 3 - Optimization and Demonstration of Industrial Scale Photobioreactor

- Successfully carried out scale up of eight microalgal strains in pilot scale photobioreactors (0.18 m diameter, up to 2,000 liter capacity);
- Conducted CO_2 mineralization study for *Haematococcus* in laboratory and in open-pond experiment;
- Installed the diagnostic instrumentation for characterization of coal combustion gas at Aquasearch Inc.;
- Delivered to Aquasearch the PSI coal reactor to be used with the Aquasearch 2000 liter outdoor photobioreactor for direct feeding of coal combustion gas to microalgae;
- Tested the coal reactor and conducted the first pilot scale production run with coal combustion gases and modified the coal combustor to allow for longer-term burns;
- Ran microalgal carbon sequestration experiments with actual coal combustion gases with six different stains of microalgae;
- Successfully carried out scale up of six microalgal strains in full commercial scale photobioreactors (0.41 m diameter, up to 25,000 liter capacity);
- Ran microalgal carbon sequestration experiments with actual propane combustion gases with six different stains of microalgae;
- Carried out bench-top scale centrifugation experiments on twenty two microalgal strains;
- Carried out experimental work on biomass separation for five microalgal strains grown in pilot and full scale outdoor photobioreactors;
- Modeled the costs associated with biomass harvested from different microalgal strains;

Task 4 - Carbon Sequestration System Design

- Conducted work on designing key components including: CO_2 removal process; CO_2 injection device; photobioreactor; product algae separation process; and process control devices;
- Developed a photobioreactor design concept for biofixation of CO_2 and photovoltaic power generation.
- Shared the ASPEN model with UH, PSI and Aquasearch for review and discussion;
- UH research staff visited Aquasearch and worked on-site for 1 week to gather information on the performance of the photobioreactor;
- Photobioreactor data from Aquasearch were analyzed and simple linear relationships for biomass productivity as a function of solar irradiance and CO_2 were developed using multiple regression;
- A review of the technical literature on tubular photobioreactors progressed;
- A literature study progressed to develop the CO_2 flue gas separation subsystem model for both Aspen Plus and Excel models;

Task 5 - Economic Analysis

- Conducted economic analysis for photobioreactor carbon fixation process; and
- Developed an economic model to be used in predictions of carbon sequestration cost for a number of scenarios.

3. EXPERIMENTAL

3.1   Task 1 - Supply of CO$_2$ from Power Plant Flue Gas to Photobioreactor

There was no experimental work conducted under Task 1. Results and discussion of Task 1 is given in Section 4.1.

3.2   Task 2 - Selection of Microalgae

The objective of 2 is to select microalgae best suited for the proposed carbon recovery and sequestration system. We have quantified the performance of over 20 microalgae species at a small laboratory scale according to the following criteria.

- Ability to grow at high temperatures;
- Ability to withstand the most untreated forms of industrial exhaust gases;
- High rate of photosynthetic carbon fixation; and
- Ability to produce high-value products; *or*
- Ability to produce carbonate minerals.

3.2.1   Subtask 2.1 - Characterization of Physiology, Metabolism and Requirements of Microalgae

3.2.1.1 Mera's Culture Collection

The microalgal strains used in this work were selected from our microalgal culture collection. The Mera Culture Collection consists at the present time of 78 different strains of microalgae representing an estimated 68 species (Figure 3). Sixty strains have been isolated locally (i.e., in Hawaii) from 71 water samples collected from aquaculture ponds, water treatment plants, birdbaths, puddles, and the seashore) by the staff at Mera. Selected colonies of microalgae were plated repeatedly resulting in unialgal cultures.

H-1682

Figure 3. The Aquasearch Culture Collection.

For this work, a total of 41 locally isolated strains and 13 strains imported from other collections were used. The local strains (Hawaii) were expected to have relatively high temperature tolerances. The imported strains were selected based on their ability to accumulate high value metabolites or to mineralize CO_2 into carbonates. Table 1 lists all the strains that were used in this research project.

Table 1. List of Microalgal Strains Used in this Work

Strain ID	Class	Source
AQ0008	Chlorophyta	**Haematococcus pluvialis**
AQ0011	Chlorophyta	Local isolate, unidentified
AQ0012	Cyanophyta	Local isolate, unidentified
AQ0013	Chlorophyta	Local isolate, unidentified
AQ0015	Cyanophyta	Local isolate, unidentified
AQ0017	Bacillariophyta	Local isolate, unidentified
AQ0018	Cyanophyta	Local isolate, unidentified
AQ0019	Chlorophyta	Local isolate, unidentified
AQ0022	Chlorophyta	Local isolate, *Scenedesmus* sp.
AQ0024	Chlorophyta	Local isolate, *Scenedesmus* sp.
AQ0025	Chlorophyta	Local isolate, *Schroederia* sp.
AQ0028	Chlorophyta	Local isolate, unidentified
AQ0029	Chlorophyta	Local isolate, unidentified
AQ0031	Cyanophyta	Local isolate, unidentified
AQ0033	Rhodophyta	UTEX 637, *Porphyridium* sp.
AQ0034	Rhodophyta	UTEX 161, *Porphyridium cruentum*
AQ0035	Rhodophyta	UTEX LB2618, *Porphyridium aerugineum*
AQ0036	Rhodophyta	UTEX 755, *Porphyridium aerugineum*
AQ0037	Cyanophyta	Local isolate, unidentified
AQ0038	Cyanophyta	Local isolate, *Merismopedia* sp.
AQ0040	Chlorophyta	Local isolate, unidentified
AQ0041	Chlorophyta	Local isolate, unidentified
AQ0042	Chlorophyta	Local isolate, unidentified
AQ0044	Chlorophyta	Local isolate, unidentified
AQ0046	Chlorophyta	Local isolate, unidentified
AQ0052	Chlorophyta	HCC P2, *Dunaliella* sp.
AQ0053	Chlorophyta	HCC P7, *Dunaliella* sp.
AQ0054	Bacillariophyta	Local isolate, unidentified
AQ0058	Eustigmatophyta	HCC NANNP01, *Nannochloropsis sp.*
AQ0059	Chlorophyta	*Chlorella sp.*
AQ0062	Chlorophyta	*Tetraselmis suecica*
AQ0067	Chlorophyta	Local isolate, unidentified
AQ0073	Chlorophyta	UTEX LB572 *Botryococcus braunii*
AQ0074	Chlorophyta	UTEX LB142 *Phacotus lenticularis*

The strains are maintained on an agar-based nutrient medium. When needed for an experiment, cells from the agar cultures are transferred to test tubes containing liquid growth medium. After a few days of growth (may vary depending on the strain) the cultures are transferred to larger containers such as 250 ml Erlenmeyer flasks. Further scale up is performed according to the type of experiment planned. All cultures were grown using a proprietary medium formulation based on Bold's Basal medium (Bischoff and Bold, 1963). For marine isolates, the same nutrient enrichments were used but added to deep ocean seawater obtained from the Natural Energy Laboratory of Hawaii Authority (NELHA, http://www.nelha.org/). Here we identify the strains by our collection ID number (e.g., Table 1) unless genus identification is available. Identification is tentative for the locally isolated strains.

3.2.1.2 Culture Systems

Batch Cultures

Batch cultures are defined as those cultures where a container with a fixed volume of nutrient medium is inoculated with microalgal cells. The cells grow until a nutrient becomes limiting (or light, as in our case). While the cells are not limited, the growth rate is high. As the cells encounter limiting conditions, the growth rate slows down and finally growth ceases. Batch cultures were used in the temperature tolerance experiments, below.

Chemostat Cultures

Chemostat cultures, as opposed to batch cultures (above), receive a continuous supply of nutrient medium. Our cultures are grown under light limitation. As the cells are diluted by the continuous medium addition more light/cell is available, permitting cell growth. Thus, the growth rate is dependent on the rate of medium addition. At steady state (no change in cell concentration in the chemostat culture) the growth rate is equivalent to the dilution rate. Also, at steady state, the growth conditions stay constant, allowing for better characterization of the physiological state of the cells. pH is automatically maintained (using pure CO_2 injections or simulated flue gases) by a computerized data acquisition and control system developed in house. Chemostat cultures were used in the pH and flue gas tolerance experiments, below.

While at steady state the dilution rate (or rate of nutrient addition to the culture) determines the growth rate, during the initial ramp up phase the chemostat culture is managed as a batch culture. A 3.3 liter chemostat vessel (Figure 4) is inoculated with a starter culture and allowed to grow. Once the culture reaches a sufficiently high biomass (the culture starts to reach light limitation), nutrients are continuously added using a pump. Over the first few days, then, we can estimate a maximal growth rate can be estimated from changes in daily biomass estimated from fluorescence measurements (below). This estimated growth rate is considered 'maximal' under since during that period in the cultures life light is not yet limiting (i.e., the culture is sufficiently dilute still).
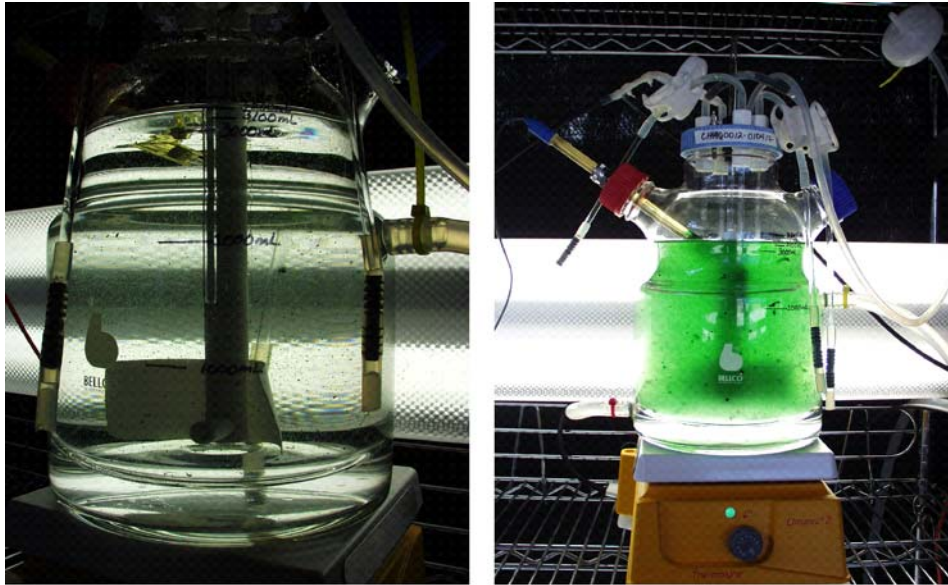
Figure 4. Photographs of the same chemostat culture (AQ0012) seven days apart showing the large capacity for carbon sequestration of microalgal cultures. The panel on the left shows little biomass, mostly concentrated in 3-4 mm clumps. The panel on the right is the same culture after seven days of photosynthetic growth.

To carry out these experiments while controlling the pH of the cultures, we have constructed a unique, computer controlled, pH control and gas distribution system. The apparatus uses a data acquisition and control system to control, monitor and acquire data through a multichannel Ethernet, I/O modules, sensors and electrodes. The system provides intelligent signal conditioning, analog I/O, digital I/O, RS-232 and RS-485 communication. The systems communicate with their controlling host computer over a multi-drop RS-485 network. The data is analyzed and converted to usable information through applications software. This software must be written to query the I/O modules for the raw data and send control commands to the proper channels. The I/O modules must be configured for output and input of the proper data formats.

In the application of pH monitoring and control, a pH electrode is immersed into a live algal culture (Figure 4). The pH electrode sends an electronic message through a signal amplifier to the respective I/O control point (
Figure 5). The host computer queries the I/O module; when the pH signal passes above the alarm setting, a command is sent to a separate relay module control point, which opens a solenoid valve allowing CO_2 gas to flow though a rotameter into the chemostat, thereby controlling the pH in the growth module. This process is repeated in reverse when the pH in the growth module reaches the low threshold and the solenoid is switched to the off position. By adding an RTD or thermocouple and the proper I/O module, this system also supports the monitoring and control of temperature in the growth module. A system of three solenoid valves, controlled by simple on/off switches, is used to distribute up to three different gases to each growth module (
Figure 5). When the channel is switched on, the gas passes through a rotameter for flow control and flow rate measurement before entering into the growing chemostat.

H-1684

Figure 5. Rear and side view of the pH control and gas distribution system showing the I/O modules as well as tubes and solenoids that distribute and feed the gas mixtures to the chemostat cultures and two ports (right panel, top) to accept gas mixtures for distribution to 12 different channels and 6 ports to accept input from 6 different pH probes. Six more probe ports are found on the opposite side (out of view).

In order to facilitate the accurate measurement of carbon uptake in the algae during the process of photosynthesis, a time base and flow measuring system has been added to this control system. This consists of two pulse generators combined with the appropriate frequency counting I/O modules. The first pulse generator generates a frequency, which is used to increase the accuracy of the rotameters. A pulsing current is sent to the solenoid valves, reducing the mass flow rate as the gas passes through the valves and respective rotameters. The naturally low flow rate of the different gases into the growth module necessitates this increase in accuracy of flow measurement. The frequency generated by the second generator creates a time base, which is used to measure the time the solenoid valves are open. The pulse generators give the system the capability to accurately measure the amount of gas (and carbon) entering the individual growth modules and a historic record of the data.

3.2.1.3 Temperature Tolerance Experiments

To determine the growth rates of microalgae at different temperatures, cultures were batch grown in 250 ml Erlenmeyer flasks. The flasks and medium were sterilized by autoclaving. Once inoculated, the flasks were immersed in temperature controlled water baths and were illuminated from below (fluorescent bulbs, 60 μE m^{-2} s^{-1}, 14:10 light:dark). The flasks were manually agitated three times daily. A total of 41 locally isolated strains and 13 strains imported from other collections were used. The local strains (Hawaii) were expected to have relatively high temperature tolerances.

Algal growth was estimated from daily changes in biomass concentration estimated from *in vivo* fluorescence. A Pulse Amplitude Modulated fluorometer (MINI PAM, Walz, Germany) was used to measure culture *in vivo* fluorescence of the cultures at the end of the dark period (Schreiber et al, 1986). The cultures were manually shaken and the end of the MINI PAM fiber optic guide was placed directly against the bottom of the each flask in a darkened room.

Following the *in vivo* fluorescence determination, the culture was shaken again and the procedure repeated for a total of three determinations of the maximum fluorescence yield (F_m). The three values for F_m thus obtained were averaged and assumed proportional to the biomass concentration in the flask.

The growth rate (d^{-1}) was calculated as:

$$\mu = Ln\left(\frac{F_2/F_1}{\Delta T}\right) \tag{1}$$

where μ is the growth rate (d^{-1}), F_2 is the fluorescence at time 2, F_1 is the fluorescence at time 1 and ΔT is the difference between time 2 and time 1 in days. For each strain two separate experiments were conducted. On the one hand, flasks at 25, 30 and 35ºC were grown. A second run was conducted at 25, 20, and 15ºC.

3.2.1.4 pH Tolerance Experiments

Microalgal cells were grown in 3.3 liter chemostats. Temperature was maintained at 25°C (±1°C) by recirculating water baths. Light was provided by fluorescent bulbs (120 uE m^{-2} s^{-1}, 14:10 light:dark).

Changes in biomass concentration in the chemostats were estimated from *in vivo* fluorescence measurements taken at the end of the dark period (see above). The end of the MINI PAM fiber optic guide was brought in contact with the outside of the chemostat vessel wall and three measurements of the dark adapted maximum and minimum fluorescence yields (F_m and F_o) were taken and averaged. The physiological state of the cells was also determined daily using fluorescence techniques based on the techniques developed by Schreiber et al. (1986). The maximum quantum yield of photosystem II (F_v/F_m) provides an estimate of the fraction of open reaction centers in photosystem II of photosynthetic organisms. The fraction of open reaction centers is directly proportional to the probability that the energy of an absorbed photon will participate in photosynthesis. Thus, it is a measure of the photosynthetic efficiency of the cells and of their physiological state.

To test the pH tolerance of the different microalgal strains (20 strains tested), the cultures were exposed to different pH conditions. Initially, the cultures were grown in chemostats at a nominal pH of 7.5. The pH of the cultures was automatically controlled by pure CO_2 injections into the growth medium in response to raises in pH. The system was programmed with set points at 7.4 and 7.6 pH. Thus, when the pH of the culture reached 7.6 in response to photosynthetic carbon uptake, a solenoid valve opened allowing the introduction of gaseous CO_2 into the culture. As the pH dropped and reached 7.4 in response to the injection of CO_2, the valve closed.

Once the flow of nutrient medium into the chemostats was started and steady state was reached (no change in fluorescence-based biomass estimates from day to day) the chemostats were allowed to grow using pH set points at 7.4 and 7.6 for a week. Next, the pH set points were changed to either 6.4-6.5 or 8.4-8.6 for another week. Data obtained during the period under each set of conditions (fluorescence-based biomass and F_v/F_m) were averaged for the period. Negative

changes in those values in response to exposure to different pH conditions were used to indicate whether the cells were negatively affected by those conditions.

3.2.1.5 <u>Flue Gas Tolerance Experiments</u>

To test the flue gas tolerance of the different microalgal strains, the cultures were grown in chemostats ($22 \pm 2°C$) and exposed to different gas mixtures (BOC Gases, Lebanon, New Jersey, USA) selected to mimic the flue gas from power plants utilizing different fuels (Table 2). Initially, the cultures were grown at a pH range of 7.4-7.6. The pH of the cultures was automatically controlled by pure CO_2 injections into the growth medium in response to raises in pH (see above). Once the cultures reached steady state, the stream of pure CO2 for pH control was substituted with commercial mixtures of gases specific to mimic different flue gas compositions (Table 2, 100% CO_2 and five different gas mixtures). Each culture was exposed to each gas mixture for 1 week of continuous culture. Addition of gas mixtures was controlled by the culture pH. As the cells photosynthesized and the pH of the culture rose to 7.6, solenoid valves automatically injected the gas mixture into the chemostat. The valve closed when the pH of the culture dropped to 7.4 following the gas mixture injection.

Table 2. Composition of Simulated Flue Gases Used in the Flue Gas Tolerance Experiments According to the Combusted Material

Fuel type	A. Bituminous coal	B. Sub-bituminous coal	C. Natural gas	D. Natural gas	E. Fuel oil
Gas (ppm)	Utility boilers			Gas Turb Comb	Diesel
CO_2	181000	240000	131000	57000	62000
O_2	66000	70000	76000	159000	170000
N_2	719000	681000	793000	784000	767000
SO_2	3504.0	929.7	0.0	0.0	113.1
NO	328.5	174.3	95.1	22.1	169.7
NO_2	125.9	66.8	36.5	8.5	65.0

As in the pH tolerance experiments (above), changes in the fluorescence-based estimates of biomass and F_v/F_m in response to exposure to different gas mixtures were used to indicate whether the cells were negatively affected by the flue gases.

3.2.2   <u>Subtask 2.2 - Achievable Photosynthetic Rates, High Value Product Potential and Carbon Sequestration into Carbonates</u>

3.2.2.1 <u>CO_2 Utilization Efficiency</u>

Task 1 deals with the supply of CO_2 to the microalgal cultures. Here, we have investigated the capacity of the microalgal cultures to take up the delivered CO_2. Furthermore, we report on experiments conducted to estimate the efficiency with which the algae assimilate CO_2 from the growth medium under different conditions of pH and flue gas composition. Specifically, we estimated the fraction of the CO_2 dissolved in the growth medium taken up by

the microalgal cells versus the fraction that was lost to the atmosphere through passive degassing from the medium. In these experiments, we did not attempt to measure the efficiency of gas dissolution into the growth medium as that is addressed in Task 1.

CO_2 Utilization Capacity and Efficiency of a Commercial Microalgal Facility

The amount of carbon that can be captured by a microalgal facility can be estimated from the amount of microalgal biomass (as carbon) that the facility produces versus the amount of carbon (as CO_2) that is used in growing the microalgal biomass. Production of biomass is scaled to the surface area (m^{-2}) of the cultivation systems. Here, we have used historical estimates of biomass production at Mera's commercial facility (Olaizola, 2000). We have estimated the CO_2 utilization efficiency of Mera's commercial facility, which produces a high value pigment (astaxanthin) from the microalga *Haematococcus pluvialis*. Using historical data, the efficiency was calculated as the ratio of the amount of carbon contained in the biomass of *H. pluvialis* produced by Mera to the amount of CO_2 that Mera purchases for biomass production.

CO_2 Utilization Capacity of Experimental Chemostat Cultures

We made measurements of CO_2 utilization capacity by 25 strains of microalgae grown at three different pH (6.5, 7.5 and 8.5 pH ($\pm$ 0.1)) and by 21 strains of microalgae grown exposed to 5 different experimental gas mixtures plus CO_2 at pH 7.5 (see sections 3.2.1.4 and 3.2.1.5).

The automated pH monitoring and control system allows us to closely follow changes in pH in all the chemostat cultures. As an example, Figure 6 shows the changes in pH over the life history of a chemostat culture of strain AQ0022.
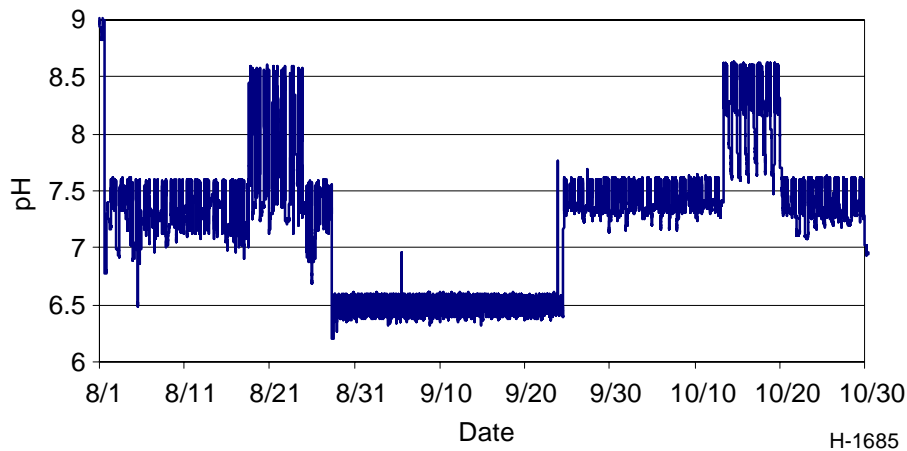
Figure 6. Computer generated trace of culture pH in a chemostat culture (strain AQ0022) showing the periods of time during which the culture's pH was maintained at 6.5, 7.5, and 8.5.

15

We used the logged changes in pH plus alkalinity estimates to calculate the changes in concentration of dissolved inorganic carbon (DIC = dissolved $CO_2 + HCO_3^- + CO_3^=$) in the medium. We estimate the amount of dissolved carbon species in the medium using a standard titration method (Clesceri et al., 1998). Following an injection of CO_2 into the medium (see above, Figure 6), the pH of the medium decreases, reflecting an increase in the concentration of CO_2. After the injection period, the pH increases as a result of photosynthetic uptake of CO_2 by the algae plus physical processes such as degassing of CO_2. The slope of this increase results from the rate of CO_2 loss from the culture system.

We have assumed that changes in DIC in the medium caused by CO_2 injections, degassing or photosynthesis and respiration by the cells have no or negligible effect on the alkalinity of the chemostat at steady state. Thus, decreases in medium DIC reflect either photosynthetic uptake of CO_2 by the microalgae or degassing of CO_2 from the medium. Then, increases in medium DIC are produced either by respiration by the microalgae or by injections of CO_2.

Figure 7 shows an example of such changes. The figure shows two traces. The first trace is the pH of the culture medium over 36 hours a microalgal culture grown at a nominal pH of 7.5. Decreases in pH correspond to increases in DIC produced by CO_2 injections and algal respiration. Increases in pH correspond to decreases in DIC caused by photosynthetic uptake of CO_2 by the algae or degassing of CO_2 from the medium.

H-1686
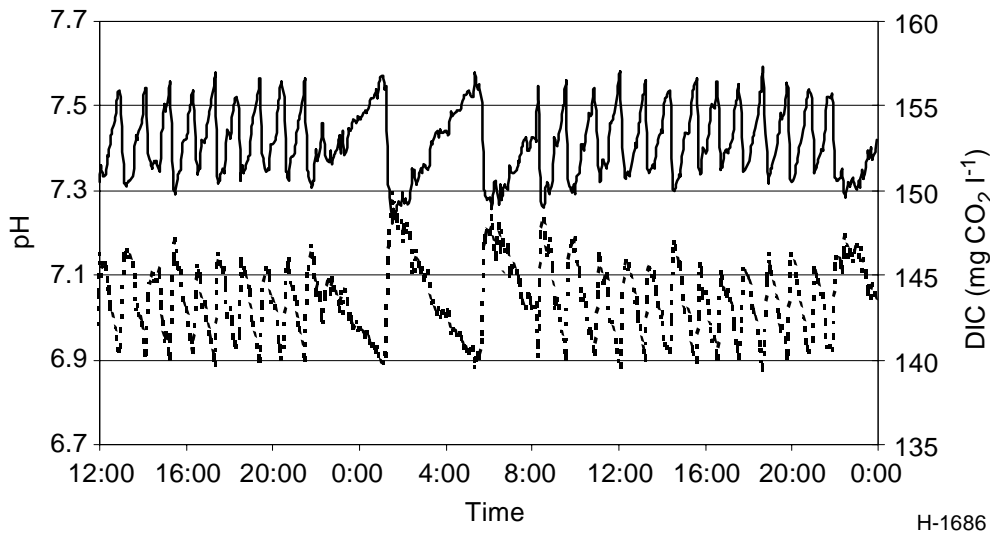
Figure 7. Sample pH trace (solid line) and DIC (broken line) for a microalgal culture grown at 7.5 pH. Note the difference in the slope of the DIC trace over time between the light periods and the dark period (22:00-08:00).

Using the changing concentrations of DIC over time we can calculate the net rate of DIC concentration change (mg CO_2 l^{-1} min^{-1}), essentially the slope of the decreases in DIC shown in Figure 7. By subtracting the values obtained during the dark period (i.e., night periods) from the values obtained during daylight hours we obtain estimates of net photosynthetic carbon uptake by the microalgal cells in culture.

CO$_2$ Utilization Efficiency of Experimental Chemostat Cultures

We made measurements of CO$_2$ capture efficiency by 25 strains of microalgae grown on 100% CO$_2$ at three different pH (6.5, 7.5 and 8.5 pH ($\pm$ 0.1)) and we also made measurements of CO$_2$ capture efficiency by 21 strains of microalgae grown exposed to 5 different experimental gas mixtures plus CO$_2$ at pH 7.5 (see sections 3.2.1.4 and 3.2.1.5).

The CO$_2$ utilization efficiency of the experimental chemostat cultures was calculated as the ratio of the amount of carbon photosynthetically taken up by the experimental culture per unit time to the total amount of CO$_2$ that was lost from the culture medium per unit time (see section 3.2.2.1.2, above) during daylight hours. The total loss of CO$_2$ from the medium is the sum of the CO$_2$ taken up by the algae and the CO$_2$ lost via physical processes (e.g., degassing).

3.2.2.2 Production of High Value Products to Offset Cost of Carbon Sequestration

Microalgae are a diverse group of over 30,000 species of microscopic plants that have a wide range of physiological and biochemical characteristics. Microalgae produce many different substances and bioactive compounds that have existing and potential applications in a variety of commercial areas, including human nutrition, pharmaceuticals, and high value commodities. Algal pigments (carotenoids and phycobiliproteins) are one such group of molecules. Examples of natural algal pigments that already been commercialized include B-carotene (food additive grade worth about $1,400 per kg, market size estimated >$500 million per year), astaxanthin (feed additive grade worth about $2,500 per kg-market size about $200 million- but up to >$100,000 per kg for nutraceutical grade-market size not know at this point).

High Value Pigment Analysis

Phycobiliprotein Pigments

Presence/absence of phycobiliproteins is determined by visual inspection of microalgal biomass after extraction of chlorophylls and carotenoids using an organic solvent (100% acetone). Samples for analysis were obtained form our cultures systems. The microalgal biomass was concentrated by centrifugation and the overlying medium decanted. The remaining pellet was mixed with an appropriate amount of solvent (acetone) and centrifuged a second time. The supernatant was decanted removing the chlorophyll and carotenoids. The resulting pellet was then visually inspected for color. A blue colored pellet is indicative of phycocyanin while a pink colored pellet is indicative of phycoerythrin.

Carotenoid Pigments

Carotenoids were analyzed via High Performance Liquid Chromatography (HPLC) using the method described by Zapata et al. 2000. The carotenoid pigments were extracted from the algal biomass with dimethyl sulfoxide (DMSO). The extract was then injected into the HPLC system. The HPLC system consisted of a Beckman System Gold with a model 126 programmable solvent module, a model 168 diode-array detector, and a model 508 injector with a 100 uL loop. The column used was a Supelco Discovery C8 column 150x4.6 mm, 5 um particle size. The solvent system consisted of

17

A   MeOH: Acetonitrile: Acetone at 20:60:80
B   MeOH: Ammonium Acetate 0.25M: Acetonitrile at 50:25:25 using the following
        time program:
%B   100--> 60 over 22 minutes
%B   60--> 5 over 6 minutes
%B   5 for 10 minutes
%B   5--> 100 over 2 minutes.

The total run time is 40 minutes at a flow rate of 1.5 ml/min.

The HPLC chromatograms were analyzed by identifying the peaks of zeaxanthin, lutein, β-carotene, and chlorophyll according to published spectral data (Jeffrey et al, 1997). The concentration of the biomass was determined by centrifuging a known volume of culture and transferring the pellet to a preweighed 15 ml tube, which was placed in a 65°C drying oven for 24 hours. After drying, the tube was re-weighed and the concentration of biomass per ml of culture was calculated. Pigments were quantified based on the areas of the peaks, which were multiplied by previously determined response factors of standard pigment samples. The amount of pigment (ng) injected was divided by the volume injected into the HPLC to determine the concentration of the extract (ng/ml), and then multiplied by the volume of DMSO used for the extraction. This determined the total amount of pigment in the extract, which was divided by the original volume of culture used for extraction. Averages were taken of duplicate samples. Percent lutein, zeaxanthin, and β-carotene were determined by dividing the concentration of the pigment by the concentration of biomass in the sample.

<u>Pigment Concentrations of Microalgae Grown under Standard Conditions</u>

Cultures were grown under our standard conditions (temperature: 25°C; irradiance: 60 uE m^{-2} s^{-1}; light/dark: 14 hr/10 hr). The first group of strains that we tested for high value pigment content was made up of 11 cyanobacterial strains grown in batch cultures. This group was tested first since the Cyanobacteria are good potential candidates as sources of high value pigments. Two different cultures were analyzed from each strain; a relatively young culture and a relatively older culture. A second group of pigment analysis was carried out on strains grown at the flask scale (150 ml cultures) also grown under standard conditions. These strains represent the microalgal Classes Chlorophyceae, Bacillariophyceae, Eustigmatophyceae and Prymnesiophyceae. A third group of pigment analysis was carried out on strains grown at the chemostat scale (3.3 liters) under standard conditions. In this group, we have representatives of the Chlorophyceae, Bacillariophyceae and Cyanophyceae.

<u>Pigment Concentrations of Microalgae Grown under Non-Standard Conditions</u>

It is well known that microalgal pigment content may vary depending on the growth conditions (e.g.: light, nutrients). Here, we report results of analysis carried out on cultures grown continuously in chemostat and then transferred to stress conditions believed to be conducive to carotenogenesis (described below).

Six strains of microalgae were selected for the pigmentation experiments. The chlorophyte strain AQ0011 and cyanobacterium strain AQ0012 were isolated locally in Kona, Hawaii. The Porphyridium strains AQ0033 and AQ0036 represent Rhodophyta, obtained from the University of Texas at Austin, while AQ0052 and AQ0053 are *Dunaliella* species of the division Chlorophyta, obtained from the Hawaii Culture Collection.

The cultures were grown in 3.3 L chemostats, using a 10:14 light:dark cycle, with temperature (25ºC)and pH control (7.4-7.6). The chemostats provided the culture material for the experimental treatments. Daily fluorescence readings with a Pulse Amplitude Modulator Fluorometer (PAM) monitored the biomass indirectly. PAM measures minimal (F_o) and maximal fluorescence (F_m) of the culture in a dark adapted state. The difference between F_o and F_m was F_v. The ratio F_v/F_m was used to estimate the photosynthetic efficiency of the cells. Initially, the chemostats were grown in batch mode. When a certain cell density was reached, the cultures were switched to continuous mode, which allowed the cells to attain a well-defined physiological state (Nyholm and Peterson, 1997).

PAM data measured in darkness was utilized to determine the percent functional reaction centers in the photosystem of the algal cells. The dark PAM reading of each hour was divided by the initial PAM reading to determine this value for the light intensity experiments. For the nitrate deprivation and salt/sodium acetate experiments (below), daily PAM readings helped to monitor the health of the cells. A decline in these F_v/F_m values indicated that the cells were experiencing stress. The F_v/F_m value from each flask was plotted each day and a linear regression analysis was performed to measure the trends.

Light Intensity Experiments

Each species of microalgae was first tested under intense light conditions (sunlight). Preliminary PAM readings and pH measurements were taken before exposure to light. Flasks with 200 ml of culture were placed in an outdoor water bath at 25°C in full sunlight for a period up to 5 or 8 hours. Light intensity was monitored by roof top solar panels. Each hour, PAM readings were first taken in ambient sunlight and again in darkness. Flasks were swirled, and the pH was monitored hourly. In addition, 45-50 ml samples were collected for pigment extraction from each sample and 175 ml of culture was used for dried biomass analysis of the initial and final flasks. Samples were collected in duplicate. Pigments were extracted using 5 ml of dimethyl sulfoxide (DMSO), and re-extracted with 2 ml DMSO until the extract color was very pale. Irradiance readings from roof top solar panels recorded the sunlight intensity on the dates when the light intensity experiments were conducted.

Nitrate Deprivation Experiments

Nitrate deprivation experiments were conducted with AQ0033, AQ0036, AQ0011, and AQ0012. Two hundred ml of each culture was collected from the chemostat and inoculated in 800 ml of 413 media without nitrate. Freshwater media was prepared for AQ0011 and AQ0012, while AQ0033 and AQ0036 were grown in 9 ppt salt media. The cultures were grown in 2800 ml Fernbach flasks in a 25°C water bath on a 14:10 light:dark cycle, with lights measuring an intensity of 60 $\mu E\ m^{-2}\ s^{-1}$. The flasks were mixed by air agitation, and it is probable that ambient

CO_2 contributed slightly as a source of carbon. PAM readings were taken daily and pH was monitored. Two additional light banks were added on day 6 of the experiment to increase photosynthesis and expedite the nutrient deprivation effects. The average light intensity was measured to be 175 $\mu E\ m^{-2}\ s^{-1}$. After 10 days, pigments were extracted from 50 ml of each culture and dried biomass analysis was conducted using 350 ml of culture.

Salt/Sodium Acetate Experiments

The third experiment exposed *Dunaliella* species AQ0053 to high sodium chloride and sodium acetate concentrations. Triplicate samples of 200 ml of culture were collected from the chemostat and grown in batch mode in 250 ml Erlenmeyer flasks. Initial samples were collected from the chemostat for dried biomass (170 ml) and pigment analysis (50 ml). Initial PAM readings were taken of each flask. Sodium chloride was then added to three flasks, creating a 10% salt solution. Sodium acetate was also added to three flasks bringing the concentration of sodium acetate to 1g/l. This additive serves as a source of organic carbon readily taken up by the cells and has been used to increase carotenoid yields. Both sodium chloride and sodium acetate were added to three additional flasks in the previously determined amounts. Flasks were grown in batch mode in a 25°C water bath on a 14:10 light:dark cycle for 3 days. Pigments were extracted from 50 ml of culture, and 150 ml samples were used for dried biomass analysis.

3.2.2.3 Carbon Sequestration into Carbonate Minerals Utilizing Microalgae

One of the goals of this project is to identify under what conditions microalgal cultures can be induced to precipitate $CaCO_3$. This would represent a stable, long term, sink of atmospheric CO_2, a goal of the US Department of Energy. Initially, we proposed to carry out this research by growing microalgal species known to produce cellular structures out of $CaCO_3$. We have decided to take the concept a step further. We have endeavored to describe culture conditions that will induce the precipitation of carbon into $CaCO_3$ via photosynthetically mediated changes in medium pH. As cells photosynthetise and take up CO_2 from the culture medium, the pH of the medium raises. This change in pH produces an increase in the concentration of CO_3^{2-} ions in the medium. In the presence of sufficient amounts of Ca^{2+}, $CaCO_3$ is expected to precipitate out of solution. Because the photosynthetically mediated change in pH is not specific to species that produce cellular carbonate structures, in principle, any species of microalgae could be used for this process.

These experiments were conducted using the following strains of microalgae: AQ0008 (*Haematococcus pluvialis*), AQ0053 (*Duneliella sp*. obtained from the Hawaii Culture Collection), AQ0011 (an unidentified locally isolated Chlorophyte), and AQ0012 (an unidentified species of filamentous cyanobacteria also isolated locally). All experiments were conducted using a 14:10 light:dark cycle with a light intensity of 60 $\mu E\ m^{-2}\ s^{-1}$. The source of the culture material for these experiments was our chemostat system.

Our standard growth medium was enriched in Ca^{2+} by the addition of $CaSO_4*2H_2O$ (gypsum) for these experiments. Changes in the concentration of dissolved inorganic carbon species (CO_2, HCO_3^-, CO_3^{2-}) were determined using a standard titration method (Clesceri et al., 1998). Production of $CaCO_3$ was determined by observing the formation of a white precipitate.

The precipitate was collected by filtration or centrifugation and dried (70°C overnight). A few drops of hydrochloric acid were mixed with the powder thus obtained. A positive reaction (bubbling caused by CO_2 effervescence) was interpreted to indicate the presence of $CaCO_3$.

The first experiment was conducted with species AQ0011. Two types of media were prepared for the experiment. Standard growth medium was prepared for flasks 1 and 3, and medium without bicarbonate was prepared for flasks 2 and 4. Each 250 ml flask was filled with 200 ml of its respective media. Flasks 3 and 4 were enriched with 6.16×10^{-4} moles of Ca^{2+}. Four 50 ml samples of AQ0011 were centrifuged and the pellets were used to inoculate each flask. Initial pH and alkalinity was measured and recorded. All flasks were placed in a 25°C water bath under the above mentioned growth conditions. The pH of each flask was monitored periodically. Fluorescence measurements were also measured throughout the five day experiment using a Pulse Amplitude Modulated Flourometer (PAM). After the cultures had grown for five days, final pH and alkalinity measurements were taken from each flask. The contents of each flask were gravity filtered using Whatman 15.0 cm filter paper. The filtrate was then tested for the presence of $CaCO_3$ by adding concentrated HCl and observing whether or not a reaction occurred. Bubbling of the filtrate would indicate that $CaCO_3$ was present.

A second experiment was performed with strain AQ0011, this time on a larger scale. A volume of 2500 ml of culture and media were removed from our chemostat system. The sample was divided into two 1600 ml volumes, one of which was enriched with 2.09×10^{-2} moles Ca^{2+} and stirred until dissolved. Alkalinity and pH measurements were taken from 40 ml of both the Ca^{2+} and non-Ca^{2+} enriched mediums. Four 1 L flasks were used and 780 ml of non-calcium culture was added to both flasks 1 and 2. A volume of 780 ml of Ca^{2+}-enriched culture was added to both flasks 3 and 4. All flasks were grown as previously described. After the pH in each flask reached 9.0 or higher, the contents of each was centrifuged and the pellet dried. The concentrated HCl bubble test was used on the dried pellets to determine if $CaCO_3$ precipitation had occurred.

Another experiment examined strain AQ0012. Approximately 800 ml of culture in medium was removed from the chemostat system. This volume was divided in half, and 5.60×10^{-3} moles Ca^{2+} was dissolved into one half. It was necessary to add an additional 20 ml of deionized water while stirring the sample in order to dissolve all of the Ca^{2+}. Two flasks were filled with 200 ml of culture each, and two were filled with culture enriched with calcium. Alkalinity and pH measurements were taken initially from each flask. All flasks were then placed in a 25°C water bath and grown as mentioned. Alkalinity and pH measurements were taken periodically. After the flasks had reached a pH of 9.0 or higher, the contents of each were examined under a microscope for $CaCO_3$ precipitates. Also, the contents of each flask was filtered and tested for $CaCO_3$ precipitation using the HCl bubble test.

A second experiment was conducted with AQ0012 on a larger scale using greater volumes and biomass. Approximately 2 L of culture was removed from the chemostat system. Initial pH and alkalinity measurements were taken from 50 ml of this sample. Flasks 1 and 2 were filled with 975 ml each of the culture. Again, approximately 2 L of culture was removed from the receiver and was enriched with 2.80×10^{-2} moles of Ca^{2+}. Initial pH and alkalinity measurements were taken from 50 ml of this sample. Flasks 3 and 4 were filled with 975 ml of the sample. All flasks were grown under the same conditions as the previous experiments and pH

and alkalinity measurements were taken periodically. After the pH of each flask reached 9.0 or higher, the contents of each flask was centrifuged, filtered, and dried overnight. The HCl bubble test was conducted on the dried samples to determine whether $CaCO_3$ was present.

A similar experiment was done with strain AQ0052. One liter of culture was removed from the chemostat system. Initial pH and alkalinity measurements were taken and 200 ml were added to flasks 1 and 2. A volume of 500 ml of the culture was enriched with 6.39×10^{-3} moles of Ca^{2+} and stirred until dissolved. Flasks 3 and 4 were filled with 200 ml of this solution and the remaining culture was used for initial pH and alkalinity measurements. Flasks were grown under the same conditions and pH and alkalinity measurements were taken periodically.

Another series of experiments were conducted in which microalgal growth was allowed to increase the pH of the medium. Two flasks were filled with 2 L of either AQ0008 or AQ0012 culture. The AQ0008 culture was obtained from an outdoor commercial photobioreactor (Olaizola, 2000), where the AQ0012 culture was again obtained from the chemostat system. The growth medium was enriched by adding 0.58×10^{-2} moles of Ca^{2+} to each flask. Alkalinity and pH measurements were taken of each culture before and after the addition of the Ca^{2+} solution. The flasks were then exposed to light for 14 hours in order for photosynthesis to increase the pH. Samples were taken after the pH of each flask reached 9.0 or higher. CO_2 was then bubbled into the culture while stirring and two 170 ml samples were taken at a pH of 9.0, 8.5, 7.5, and 6.5. The samples were centrifuged and the pellets were dried on pre-weighed aluminum weigh boats. The supernatant of each centrifuged sample was used for pH and alkalinity measurements.

Finally, two more cultures (strain AQ0008) were grown to test the changes in medium chemistry when the microalgae were allowed, through photosynthesis, to raise the pH well above 9. We used 20 liter cultures grown in carboys. The first culture was allowed to grow without CO_2 supplementation and exposed to natural light conditions (sun light) for four days. The culture was mixed by continuously bubbling air through the culture. Discrete samples were taken from the culture for pH determination and biomass concentration. On the fourth day, samples were also taken for alkalinity determination (described above) to calculate the concentrations of dissolved inorganic carbon in the culture. Alkalinity was measured in the culture sample before and after centrifugation. By centrifuging the sample we are able to eliminate all particulates, including cells and any possible carbon that may have precipitated as carbonates. The difference in the values thus obtained are presumed to represent the amount of carbon that would have precipitated.

The second culture was grown without CO_2 supplementation for three days as above. In this experiment, however, alkalinity and inorganic carbon species were measured several times each day.

3.3   Task 3 - Optimization and Demonstration of Industrial Scale Photobioreactor

The goal of Task 3 of this research program is to optimize carbon sequestration, high value component production and CO_2 carbonation utilizing microalgal cultures at a commercially significant scale. This was done in three phases. First, we conducted a pilot evaluation using 2,000 liter enclosed photobioreactors (pilot scale MGM, Subtask 3.1) and, second, we conducted full scale production runs using 24,000 liter enclosed photobioreactors

(full scale MGM, Subtask 3.2). Finally, we conducted experiments to determine the costs associated with harvesting the produced biomass to use in our economic model (Subtask 3.3).

3.3.1   Subtask 3.1 - Pilot Evaluation

The pilot evaluation consisted in growing selected strains of microalgae in scale-up Mera Growth Modules (MGM). The MGM is an enclosed outdoor recirculating photobioreactor of the serpentine type (Olaizola, 2000). The MGMs consist of an end assembly made up of PVC pipe parts where temperature and pH probes are inserted into the culture medium as well as ports for CO_2 and air to aid in gas exchange. The part of the MGM exposed to sunlight is made up of a series of parallel polyethylene tubes that are transparent to sunlight (Figure 8). The flow rate of the medium inside the MGM provides turbulence to the culture. Scale-up MGMs used here have capacities of up 2,000 liters of culture growth medium.

H-1687
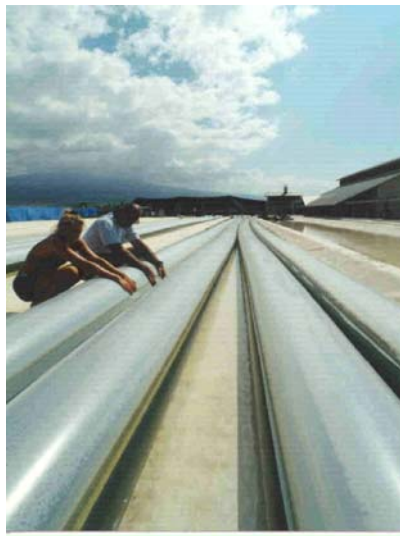
Figure 8. Part of an MGM exposed to sunlight.

Cultures to be used in the MGM units are first scaled up in the laboratory using flasks, chemostats and carboys. Once inoculated, the MGM cultures temperature was automatically controlled by our computerized monitoring and control system. pH is also automatically controlled by either injections of CO_2, or by injections of flue gas from the coal combustor in the case experimental cultures.

The MGM cultures were managed as per Mera's standard operating procedures. The cultures are allowed to grow in batch fashion until a predetermined biomass level (determined empirically) is reached. At that point, a fraction of the culture volume is disposed of and fresh medium added to the fraction of the culture remaining inside the MGM to allow for more growth.

Every morning at sunrise, the cultures were sampled for biomass concentration (fluorescence, see below). On some experimental cultures, samples were also taken at this time for biomass concentration estimates based on dry weights. For dry weight determinations, up to

4 liters of culture were centrifuged and the pellet dried for 24-48 hrs. Changes in biomass were used to estimate daily growth rates.

On some experimental cultures, morning samples were also collected for pH and alkalinity determinations as described earlier. We used this information plus the monitored pH values to estimate the rates of carbon disappearance from the culture medium, as we did for the chemostat cultures (above).

Estimates of dissolved inorganic carbon (DIC) concentration in the medium were calculated from the pH logged every 5 minutes, as described in previous sections, and estimates of alkalinity based on the morning alkalinity measurements. It was assumed that the alkalinity does not change during the night hours since there is no photosynthetic energy available for nitrate assimilation. Then, we estimated changes in alkalinity during the light hours by assuming a linear increase from the alkalinity value measured in the morning on any one day to the value measured the next morning. An example of the results of the DIC calculation is shown in Figure 9. From the DIC values we, then, calculated the rate of change in DIC with units of mg CO_2 l^{-1} min^{-1} for 5 minute intervals. A decrease in medium DIC is assumed to represent disappearance of DIC from the medium to photosynthesis and/or degassing of CO_2. An increase in medium DIC represents cell respiration and/or an injection of CO_2 into the system (Figure 10). In our calculation, positive values in the rate of DIC change indicate net uptake of CO_2 by the cells and degassing form the medium while negative values indicate injection of CO_2 into the medium and cellular respiration. If we consider only the positive values and compare those obtained during daylight hours from those obtained during the night, the difference is the photosynthetic carbon uptake rate.
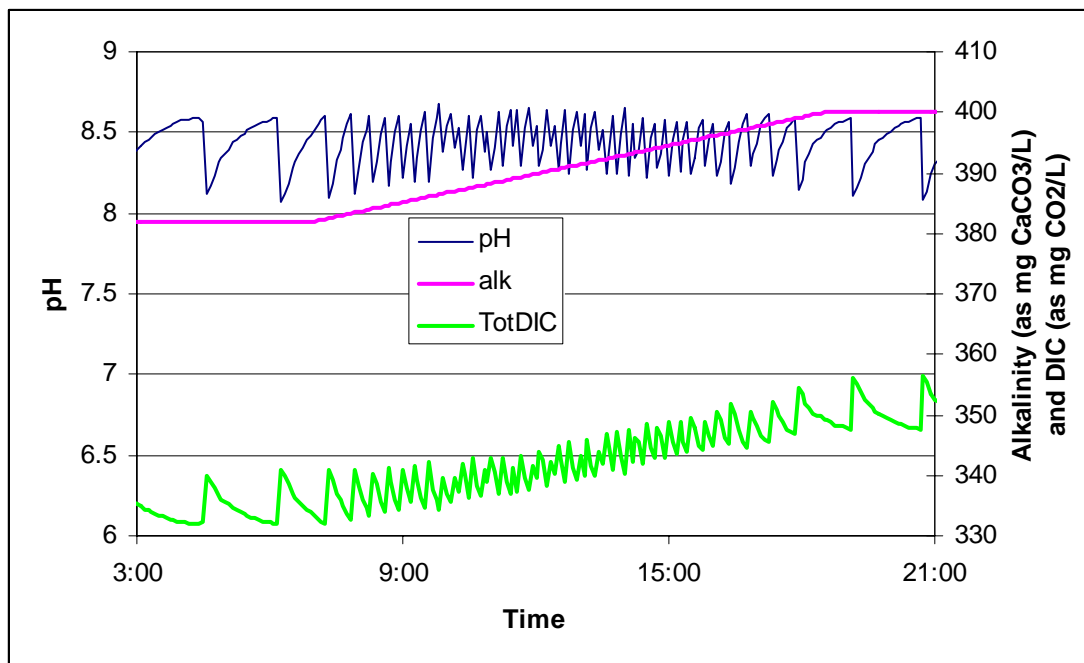
Figure 9. Logged pH values, estimated alkalinity and calculated dissolved inorganic carbon (DIC) in an algal culture over an 18 hour period.
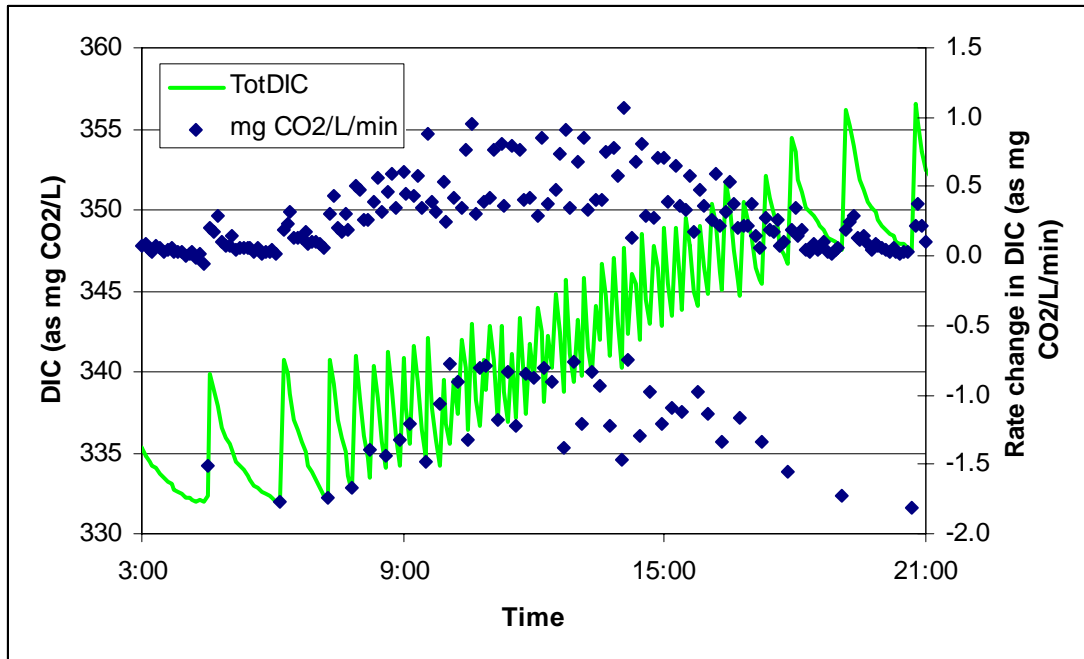
Figure 10. Changes in dissolved inorganic carbon (DIC) in the culture medium and the corresponding rates of disappearance in DIC concentration. Positive rates of DIC disappearance represent degassing and/or photosynthesis. Negative rates represent injection of CO_2 into the medium in response to increases in medium pH.

3.3.1.1 Coal Reactor

The work we conducted in this subtask accomplished reflects the directives we received from the DOE technical contract representative (COTR) as a result of our first annual progress review meeting in February 2002. The DOE directives included the following elements:

- Test the most promising algal species with simulated flue gas in bioreactors while varying the appropriate parameters such as pH, temperature, etc.;
- Testing actual flue gas from coal-fired power plants on the most promising algal species should follow this effort, as synthetic flue gas tends not to reflect all of the conditions encountered in actual flue gas from power plants fired with various types of fuels;
- Because of NETL's interest in biofixing/sequestering CO_2 from coal-fired electrical power generating plants, it is imperative that this project demonstrate the effectiveness of various microalgae for removing CO_2 from flue gas from coal-fired power plants and not from oil or natural gas fired power plants; and
- Flue gas from coal-fired power plants should be used on the most promising microalgae in a type of photobioreactor that would allow testing realistically the maximum amount of algal biomass for CO_2 removal.

The main goal of this task is to demonstrate the feasibility and to quantify the performance of microalgae for biofixation/sequestration of CO_2 from coal-fired electrical power generating plants. We recognized that it is imperative that this project demonstrate the effectiveness of

various microalgae for removing CO_2 from the flue gas from coal-fired electrical power generating power plants. To fully implement this objective, it was necessary to conduct a series of tests using actual coal combustion gas. Synthetic flue gas tends not to reflect all of the conditions encountered in actual flue gas from power plants fired with various types of fuels.

To comply with DOE directives we chose the following scheme:

1. Employ a coal combustor which can operate with different types of pulverized coal.
2. Use diagnostic instruments to monitor and quantify chemical constituents (CO_2, NO_x, SO_x) of the combustion gas.
3. Feed the coal combustion gas directly to the Aquasearch photobioreactor.

Figure 11 shows the scheme of the project.
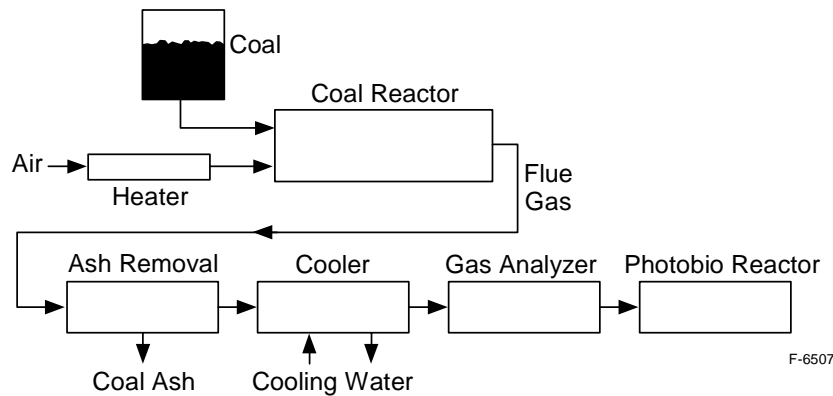
Figure 11. Coal combustion gas for photobioreactor.

In this reporting period we have started preparations for the pilot scale experiment to assess feasibility of using coal flue gas as a feeder for microalgae. For this experiment it is highly desirable to simulate the use of real coal combustion flue gas. The facility for pilot scale evaluation is the Aquasearch 2000 liter photobioreactor. Approximate characteristics of the reactor are given in Table 3.

We need to supply coal combustion gas compatible with the specifications required by the photobioreactor discussed in Table 3.

Table 3. Aquasearch 2000 liter Photobioreactor - Standard Configuration

Photobioreactor area:	30 m^2
Carbon fixation capacity:	225 gram/day
Necessary carbon supply:	1.875 kg/day*
Carbon feed:	1.3 gram/min**

  * Based on the empirical overall carbon utilization of 12%
  ** Based on continuous 24 hour carbon feed

About 10 years ago PSI developed a coal combustion test facility to study coal ash characteristics. The facility consists of an auger type pulverized coal feeder, an entrained flow reactor, a six-way cross, and an ash collection system. This facility, as shown schematically in Figure 12, was developed to study coal ash by in-situ X-ray Ash Fine Structure (XAFS) method. It is designed to be separable in two pieces so that each can be wheeled into the experimental hatch. The furnace top section is composed of the furnace, pre-heater, feeder, diffuser, six-way cross, and detector mount. The furnace base section is composed of the ash collection chamber, filter, heat exchanger, and furnace alignment system. For our purpose, the "exhaust gas" which is pumped out of the furnace system is the important product. The six-way cross is not necessary. Table 4 summarizes the air flow rate, preheat temperature and the coal feed rate.
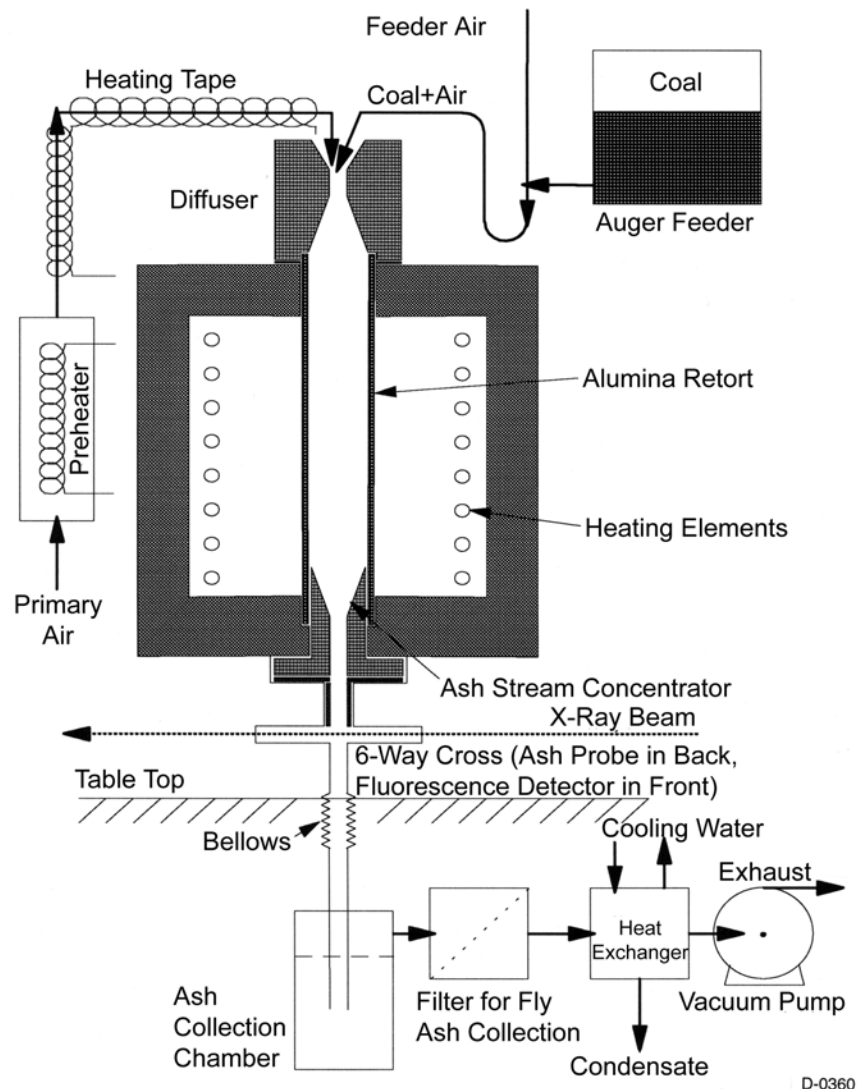
Figure 12. Schematic of the PSI coal reactor system.

Table 4. Specifications of the PSI Coal Reactor System

Total gas flow rate:	~ 1 scfm
Primary air:	~ 0.8 scfm
Feeder air:	~ 0.2 scfm
Preheat temperature:	up to 550°C
Coal feed:	1 ~ 10 gram/min; 4 gram/min recommended

Combustion of the reactants mixed in the diffuser takes place in the vertically-oriented, electrically-heated furnace placed underneath the diffuser. The furnace is composed of a vertically-oriented 30-in. long, 3-in. ID alumina retort surrounded by 18 silicon carbide heating elements placed inside a brick chamber and has a constant temperature zone of 20 in. A gas temperature profile along the axis of the retort at furnace wall temperature of 1300°C and total gas flow rate of 1 scfm is shown in Figure 13. The residence time of the coal particles is 2.5 seconds. About 90% of coal ash is captured by the ash collection chamber and the rest is captured by a filter placed downstream of the furnace. The heat exchanger is used to condense the moisture in the exhaust stream and cool the exhaust to room temperature.
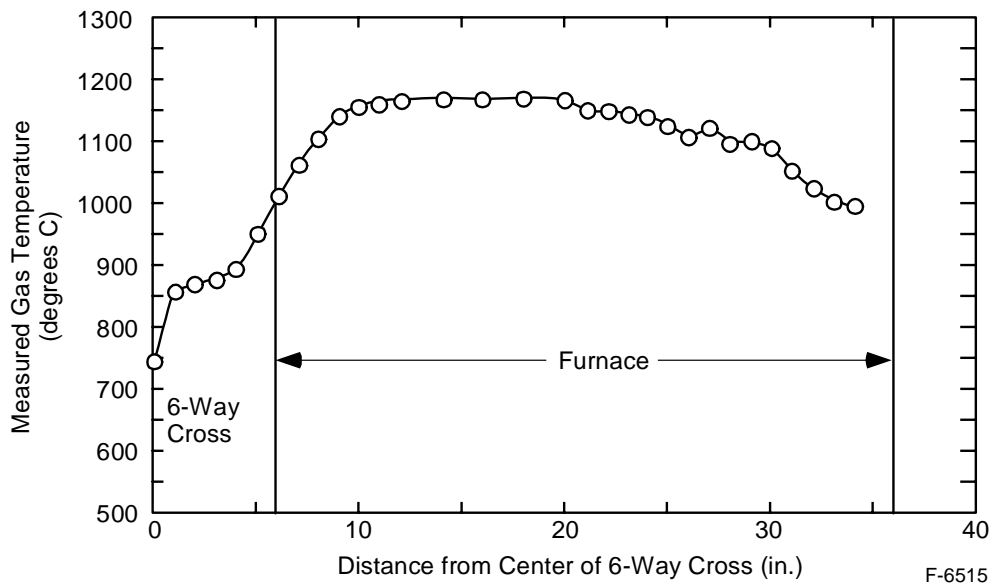
Figure 13. Axial gas temperature profile along the center of the alumina retort.

The recommended feed rate of the pulverized coal (4 gram/min) shown in Table 4 translates to approximately 2.8 gram/min of carbon (assuming 70% of coal is carbon). This indicates that the PSI coal reactor is capable of supplying adequate carbon to the Aquasearch Photobioreactor as shown in Table 3.

3.3.1.2 Coal Combustion Gas Diagnostics

PSI has also been preparing the instruments to measure the combustion gas composition: CO_2, NO_x; and SO_x. The expected composition of the coal combustion gas is given in Table 5 below.

Table 5. Typical Flue Gas Compositions for Coal Combustion Systems

	Bituminous Coal	**Sub-Bituminous Coal**	**Combustion Gas Diagnostics Measurement Range**
CO_2	12.7%	15.1%	$0 \sim 100\%$
H_2O	5.0%	12.2%	
O_2	6.0%	6.0%	
N_2	76.9%	71.0%	
SO_2 [ppm]	50-500	300-500	$0 \sim 4000$
NO_x [ppm]	50-500	50-500	$0 \sim 500$

We measure the composition of the coal combustion gas at the inlet and the vent of the photobioreactor. The locations of the gas composition measureant are shown in Figure 14. The current concept is to inject the coal combustion gas through the port which was used for injection of pure CO_2. As the volume of the coal combustion gas is expected to be about five times larger than the pure CO_2, it is possible that the coal combustion gas cannot be injected through the port for the counter flow dissolution section. If this is the case, the coal combustion gas may have to be injected at the air lift port.
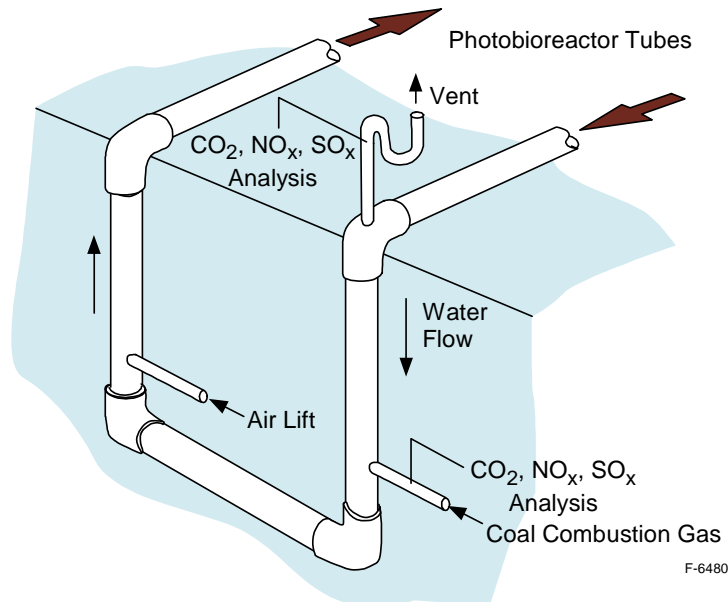
Figure 14. Coal combustion gas diagnostics.

The diagnostic instruments consists of the gas dryer main box, IMR 400 Gas Dryer Main Box shown in Figure 15. There are two sets of heated hose which takes gas sample from the inlet and the outlet of the photobioreactor (Figure 16). The sample gas is dried in the dryer box and is sent to IMR5000 Gas Analyzer Main Box shown in Figure 17. Concentration of CO_2, NO_x and SO_2 will be determined.

The analyzer was programmed to alternate between analyzing gases from the combustor smoke stack for a period of 20 minutes, switch to a purge period for five minutes, switch to the photobioreactor exhaust for 30 minutes and again to a five minute purge period. Then, the cycle repeated itself.

Initially, MGM cultures were grown using 100% CO_2 to control the pH in the culture medium. In some cases, after initial grow out, the pure CO_2 stream was substituted with combustion gases from a coal burning reactor (Figure 18, left panel). The custom-built coal combustor is utilized to burn bituminous coal from the Upper Freeport Mine. A vacuum pump is used to transfer the gases from the combustor to the MGM. Gas concentrations (of CO_2, NO_X and SO_X) in the flue gases were measured using a gas analyzer consisting of an IMR400 gas dryer and an IMR5000 analyzer (Figure 18, right panel).

Figure 15. IMR 400 gas dryer main box.

Figure 16. Gas sample hoses, probes and flanges.

Figure 17. IMR5000 gas analyzer main box.

H-1688

Figure 18. Photographs showing the coal combustor installed at Mera's facility (left panel) and the IMR gas analyzer used to measure the concentration of CO_2, NO_X and SO_X in the flue gases.

3.3.1.3 Fluorescence-based Biomass and Growth Estimates in Photobioreactors

Estimates of culture growth are calculated from changes in culture biomass estimated once daily. Culture biomass was estimated from *in vivo* fluorescence. Samples collected at dawn were placed in an opaque Nalgene bottle (250 ml). A Pulse Amplitude Modulated (MINI PAM, Walz, Germany) fluorometer was used to measure culture *in vivo* fluorescence (F_m) by placing the tip of the fiber optic guide just below the level of culture in the sample container in the dark. Three measurements of each sample were averaged. The fluorescence measured is proportional to the amount of chlorophyll, and thus biomass, of the culture. The following formula is then used to estimate growth rates:

$$\mu = Ln\left(\frac{F_2/F_1}{\Delta T}\right) \tag{2}$$

where μ is the growth rate (d^{-1}), F_2 is the fluorescence at time 2, F_1 is the fluorescence at time 1 and ΔT is the difference between time 2 and time 1 in days.

The amount of carbon that can be captured by a microalgal culture is dependent on the biomass concentration and the growth rate. We have used the growth rates estimated during the initial phase of growth in outdoor photobioreactor cultures to estimate the carbon capture capacity of these cultures. These measured growth rates are believed to be maximal since, during this phase of growth, the microalgae are not experiencing any limitations.

3.3.1.4 <u>Dissolved Inorganic Carbon Analysis and CO_2 Utilization Capacity and Efficiency</u>

A standard titration method was used to estimate alkalinity throughout all experiments (Clesceri et al., 1998). In short, acid (HCl) is added to a sample of known volume with a pH probe submerged until an endpoint of pH 4.3 was reached. Normality of the acid, volume of acid used, volume of the sample, and initial pH of the sample were noted an used in a series of equations (Clesceri et al., 1998) in order to determine total alkalinity, CO_3^{-2} ion, HCO_3^- ion, free CO_2, and total dissolved inorganic carbon concentrations (DIC). Samples that were analyzed before and after centrifugation to eliminate particulates produced the same results indicating the absence of any precipitated carbon. CO_2 utilization capacity and efficiency were estimated as described above for the chemostat cultures.

3.3.1.5 <u>Carbon Sequestration into Inorganic Carbonate Species Utilizing Microalgae</u>

<u>Model Showing the Dependence of Alkalinity on Microalgal Growth</u>

The data obtained on changes in dissolved inorganic carbon species (Section 3.3.1.4) was also used to obtain estimates of carbon capture and sequestration into inorganic carbon species, an integral part of our objectives. Carbon sequestered into relatively stable compounds such as carbonates would generate a long-lived and easy-to-store form of sequestered carbon. As will be seen in the Results obtained from the small scale experiments, we demonstrated that microalgal cultures can modify the chemistry of the culture medium sufficiently to induce the precipitation of carbonates.

In our previous work, at bench-top scale, we made the argument that as the pH of a culture increases caused by photosynthetic CO_2 uptake, the proportion of $CO_3^=$ in the medium increases. The increased availability of $CO_3^=$ in the medium increases the probability that it would react with Ca^{2+} ions to form $CaCO_3$, which represents a stable for of carbon useful for long-term sequestration of CO_2. Furthermore, the concentration of $CO_3^=$ can also be increased without a change in pH if the total alkalinity of the medium increases. Here, we report our first attempts to model the changes in alkalinity in the medium that results from the cells photosynthetic and growth activities.

Photosynthetic uptake of CO_2 produces changes in the pH of the medium but does not change the alkalinity *per se*. However, other growth processes, such as the uptake of NO_3^- and $H_2PO_4^-$ do (Eq. (3) below). The stoichiometry of photosynthesis-based cellular growth indicates that for every 106 moles of CO_2 taken up 16 moles of NO_3^- and 1 mole $H_2PO_4^-$ are taken up. At the same time, 17 moles of H^+ are taken up from the medium which results in an equivalent increase in alkalinity.

$$106CO_2 + 16NO_3^- + H_2PO_4^- + 122H_2O + 17H^+ \xrightarrow{\quad photosynthesis \quad} \{C_{106}H_{263}O_{110}N_{16}P_1\} + 138O_2 \quad (3)$$
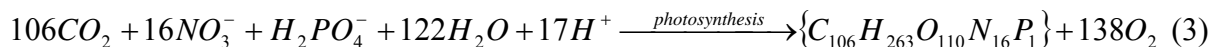
Based on the equation we have modeled the expected change in alkalinity caused by photosynthetic growth equivalent to 1 mM of carbon and estimated the resulting changes in nutrient concentrations (N, P) as well as in inorganic carbon species. We have then extended that analysis to estimate the changes expected in a long-term microalgal culture assuming reasonable

growth rates as obtained from our experimental cultures. Finally, we have compared the modeled results with those obtained from an actual culture of *Haematococcus pluvialis* at commercial scale (25,000 liters). The culture was grown as per our standard operating procedures. The culture's pH was controlled (7.4-7.6) by direct injections of CO_2 into the medium. Every morning, pH and alkalinity determinations were conducted on samples from the MGM as described previously. Biomass estimates were carried out on the same samples by cells counts using a hematocytometer under the microscope. The amount of CO_2 taken up photosynthetically by the cells was estimated from changes in daily cell concentration and assuming a mean cell mass of 8.39 x 10^{-10} grams and a mean carbon content in the cellular biomass of 45%. These values were derived for our cultures by Mr. Shu Ki Tsang, a student in Dr. Masutani's laboratory and our partner in this project. The calculated carbon taken up by the cells was used to estimate the amount of N and P taken up by the cells assuming the stoichiometry implied in the equation above (106C:16N:1P). Finally, from the estimated consumption of N and P we estimated the expected change in alkalinity after each day of growth. This value was then compared with the actual alkalinity measured in the morning. For morning values following days in which the culture was diluted with fresh medium, the estimated alkalinity value was assumed to be equal to the actual alkalinity measured.

Carbon Sequestration into Dissolved Inorganic Carbon Species

The fact that the alkalinity of the culture medium increases fueled by microalgal uptake of nutrients such as NO_3^- and $H_2PO_4^-$ (see Section 3.3.1.5), provides a means to capture and sequester carbon in an inorganic chemical form besides the algal biomass produced thus enhancing the total capacity for carbon sequestration of microalgal cultures. In this section we will present the results of measurements carried out on experimental cultures to determine the concentration of DIC in the culture medium.

3.3.2   Subtask 3.2 - Full Scale Production Runs

For Task 3.2, we scaled microalgal cultures to full scale MGMs (up to 25,000 liters). Culture performance was examined in cultures feed 100% CO_2 versus in cultures fed flue gases from a commercial propane-fed water heater (Figure 19). Culture sampling and sample analysis was conducted as described for the scale-up reactors (above, Section 3.3.1).

Initially, full scale MGM cultures were grown using 100% CO_2 to control the pH in the culture medium. In some cases, after initial grow out, the pure CO_2 stream was substituted with combustion gases from a propane burning reactor.

We have developed a propane combustion system (see Figure 19 for a schematic diagram) that consists of a Bosch Aquastar 125HX water heater producing 125,000 BTUs. The gases from the propane combustion are transported to the photobioreactor via a 4" vent pipe using a 5 horsepower regenerative blower. The gas is then cooled by submerging a carrier pipe into a cold water bath. Finally, the combustion gases are introduced into the photobioreactor at the bottom of the airlift.
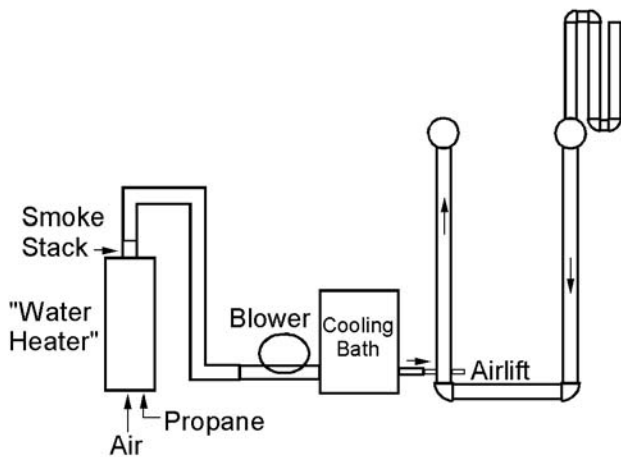
Figure 19. Schematic diagram showing the components of the system used to deliver propane combustion gases to the photobioreactor's airlift (left panel) and photograph of the water heater installed (right panel).

As was the case for pilot scale cultures, initially, all full scale MGM cultures were grown using 100% CO_2 to control the pH in the culture medium. In some cases, after initial grow out, the pure CO_2 stream was substituted with combustion gases from the propane burner. On many cultures, samples were also collected for pH and alkalinity determinations (see above). We used this information plus the monitored pH values to estimate the rates of carbon disappearance from the culture medium, as we did for the chemostat cultures (above).

3.3.3 Subtask 3.3 - Algae Separation and Final Product

The objective of this subtask was to investigate the processes and model the costs associated with separating the algal biomass from the growth medium. Harvesting entails concentrating the biomass produced from a concentration of <1 g l^{-1} in the MGM to as much as 250 g l^{-1}. The harvesting technique to be used is dependent on characteristics of the microalgae, such as size and density. Reviews of the different techniques available (including flocculation, filtration, centrifugation and air flotation) have concluded that centrifugation is possibly the most reliable technique and only slightly more expensive than other techniques (Molina-Grima et al 2003). First, we did a number of pilot centrifugation measurements in flask grown cultures using a benchtop centrifuge. Second, we tested an alternative technique for harvesting the microalgal biomass consisting of a simple lamellar settler. Finally, full centrifugation runs using an industrial centrifugation separator.

3.3.3.1 Pilot Studies

Bench-top Centrifugation Experiments

We carried out a set of bench scale centrifugation tests to determine the settling characteristics of different species of microalgae. These tests are designed to make relative estimates of centrifugation capacity needed for different species of microalgae. It is expected that different species of microalgae will be more or less difficult to separate from the growth medium by centrifugation because of different physical characteristics such a density and particle size. This information will then be used in our economic model to support our cost estimates of algal biomass harvesting and separation form the growth medium.

Essentially, the tests consist in centrifuging samples of different microalgal cultures in 15 ml tubes for specific amounts of time, noting the volume of pellet formed at those times and estimating the amount of biomass (using fluorescence) left in the supernatant. A digital photograph of the tubes following centrifugation was also be used to record the results.

Microalgal cultures were grown in 250 ml Erlenmeyer flasks under standard conditions (irradiance: ~60 uE m^{-2} s^{-1}, 14:10 L:D, temperature: 22 ±3 °C). The flasks were manually shaken three times daily. Culture biomass was estimated from *in vivo* fluorescence. A Pulse Amplitude Modulated (MINI PAM, Walz, Germany) fluorometer was used to measure culture *in vivo* fluorescence. The fluorescence measured is proportional to the amount of chlorophyll, and thus biomass, of the culture. Once grown, the cultures were used in our centrifugation experiments as follows. A 2-5 ml sample (approximate) of culture was placed into a glass t-tube and its fluorescence measured. The measurement was repeated twice. The sample was then returned to the Erlenmeyer flask and the flask was thoroughly mixed. Next, six 15 ml samples of the culture were then placed in 15 ml centrifuge tubes. The samples were centrifuged in a Eppendorf 5810R centrifuge programmed for 0, 30", 60", 120", 300" and 600" at 400 rpm. The 0" centrifugation sample was spun up to 400 rpm and immediately stopped. We calculated that the centrifugation force experienced by the samples during speed-up and slow-down was equivalent to 6.5" at 400 rpm so this time was added to all our samples. After each tube was centrifuged, the tubes were photographed and the pellet volume noted. Finally, a 2-3 ml of supernatant was taken from each tube and its fluorescence determined using the MINIPAM fluorometer. The change in fluorescence between pre- and post-centrifugation was used as an estimate of centrifugation efficiency. The values thus calculated were fit to a hyperbolic tangent model to estimate a centrifugation efficiency factor that will later be used in estimating centrifugation needs for a commercial sized facility producing the specific strains.

Lamellar Settlers

Algae separation from the growth medium represents a significant fraction of the costs associated with microalgal biomass processing. So far, we have considered the use of centrifuges because of its high efficiency. However, centrifugation is relatively costly, in capital costs (centrifuges at several hundred thousand dollars each would be necessary for even a small operation) and running costs (high electricity usage and associated CO_2 production). In this quarter, we have investigated the use of passive lamellar settlers as an alternative. Lamellar

settlers are an existing technology used in the separation of solids from, e.g., waste waters. Their use in microalgal biotechnology is nearly non-existing because the specific density of most microalgae is too close to that of the medium in which they grow. However, we feel that this technology can be successfully applied to specific microalgal products. Specifically, cells of *Haematococcus pluvialis* cells become significantly heavier following physiological stress. Thus, we have tested whether lamellar settling can be useful in harvesting *H. pluvialis* cells.

A lamellar settler (L/S) consists of a container with vertical walls. Inside the container, a series of sheets (the lamellae-plural- or lamella-singular) are stacked up at some angle off the horizontal (about 10°-40°). The operating principle of a L/S is that it accelerates gravity settling by shortening the distance over which the particles need to travel before hitting a surface. An example is shown in Figure 20.
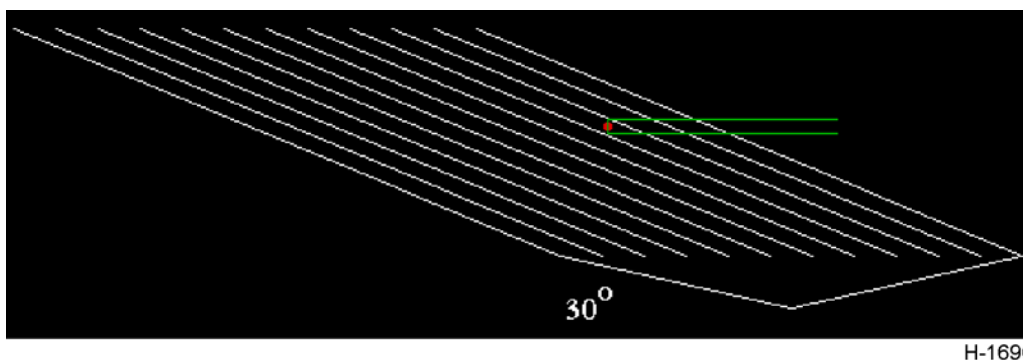
Figure 20. Diagram of a lamellar settler with lamellae at 30° (from http://www.rpi.edu/dept/chem-eng/Biotech-Environ/SEDIMENT/lamel.html).

To test this concept we have built a simple unit consisting of a clear PVC box (0.10 x 0.08 x 103 cm; WxHxL). Essentially, this is a one-lamella lamellar settler (Figure 21). Calculations based on the design constrains and the settling velocity of *H. pluvialis*, we estimated that this unit should be able to harvest 100% of the cells at a through put of 0.5 liter/minute.

To measure the harvest efficiency of the model lamellar settler, we estimated the biomass concentration of the culture fed into the unit by measuring its fluorescence and comparing it with the fluorescence of the culture at the outflow of the unit.
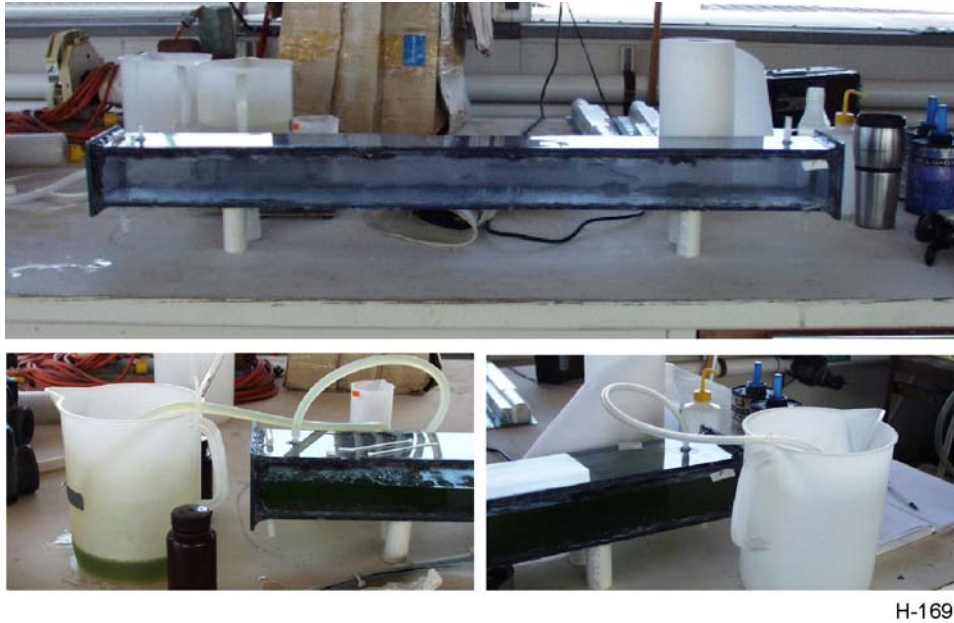
Figure 21. Model lamellar settler (one-lamella, top) and inlet and outlet details (bottom left and right.

3.3.3.2 Full Scale Centrifugation Experiments

We have carried several separation of algal biomass produced in MGMs. We have harvested up to 2000 L volumes utilizing pilot scale industrial centrifuges (Clinton Separators, Model # 9021). The centrifugation of the algal biomass is carried out by placing the volume of culture in a feed tank about two feet above the centrifuge. The material is fed by gravity and the amount of feed (liters per minute) adjusted via the feed tank's drain valve.

The optimum rate of flow into the centrifuge is arrived to empirically. It is expected that cells of different physical characteristics (density, size, shape) will present different settling rates and, thus, will affect the capacity of the centrifuge. We adjust the flow into the centrifuge to the point where less than 10% (estimated optically) of the feed biomass appears in the outflow (i.e., >90% capture of biomass).

3.4   Task 4 - Carbon Sequestration System Design

3.4.1   Task 4.1 - Component Design and Development

There was no experimental work conducted under Task 4.1. Results and discussion of Task 4.1 is given in Section 4.4.

3.4.2   Subtask 4.2 - System Integration

The original objective of this Subtask was to develop a model of the commercial *Haematococcus pluvialis* cultivation process that could be applied to optimize system performance with respect to CO_2 sequestration and the generation of an income stream to offset

capital and recurring costs. During the first year of the UH subcontract, model development was pursued using the ASPEN Plus software package. This strategy, however, evolved as the project progressed and the goals of the Subtask were refined based on information that emerged from the technical effort of the team.

After careful review, it was decided to focus on optimizing harvesting strategies as a means to improve carbon capture and revenues. Harvesting strategies are commonly used in managing aquaculture operations to identify practices that maximize profit (Leung et al., 1989). In the production of *Haematococcus pluvialis,* a small portion of culture in the photobioreactor is collected periodically and stressed in ponds to produce astaxanthin. The harvesting strategy in this application is based on meeting two criteria: (1) a specific number of cells needed to inoculate the open ponds and (2) a minimum cell concentration in the photobioreactor that must be achieved before harvesting.

The approach taken to investigate the effects of modifying the harvesting strategy on CO_2 utilization and cell production comprised the following activities:

- Develop and verify a model that accurately depicts the *Haematococcus pluvialis* production process in the photobioreactors.
- Apply the model to simulate and quantitatively evaluate different harvesting strategy scenarios.
- Identify the harvesting strategy that will provide the maximum carbon capture by *Haematococcus pluvialis*.

Functional relationships for the dependence of the *Haematococcus pluvialis* population on operating parameters were determined. These relationships were employed to synthesize a process model based on the STELLA biological systems simulation software which was verified by comparison with operational data. Parametric studies were then performed using the model to identify the target cell concentration and the harvesting cell quantity that provides maximum carbon capture by *Haematococcus pluvialis*.

3.4.2.1 <u>Operational Data</u>

Model relationships were derived by analysis of data provided by Mera Pharmaceuticals, Inc. on the operation of two photobioreactors identified as M13A-030423 and M10A-040810. Some supplementary experiments were also conducted. M10A-040810 was a standard size photobioreactor with a volume of 25,000 L; M13A-030423 was a smaller unit with a volume of 16,500 L. The data included records of pH and temperature of the media, CO_2 injection, and information about the sampling and harvesting of *Haematococcus pluvialis*. The data from M13A-030423 included values of media alkalinity measured each morning and alkalinity during the nights for the first few days of operation of the MGM. The pH data set comprised measurements of media taken every minute for M13A-030423 and every five minutes for M10A-040810. The temperature data set included measurements of media taken every five minutes for M10A-040810 and every fifteen minutes for M13A-030423. The CO_2 data set consisted of injection times and volumetric flow rate of the CO_2 injection stream. The cell sampling data set comprised sampling times and cell concentrations (typically three replications

of each sample) and the harvesting data included the volumes of harvested microalgae and media and the corresponding dates and times.

3.4.2.2 Carbon Mass Balance

CO$_2$ was the primary carbon source for cell biomass production. CO$_2$ injected into the photobioreactor was partitioned between the biomass, media, and the gas headspace. The carbon balance relationship for the photobioreactor is:

$$C_{in} - C_{out} = V_l M_C \left(\frac{d[C_{biomass}]}{dt} + \frac{d[DIC]}{dt} \right) + V_g M_C \left(\frac{d[C_{headspace}]}{dt} \right) \quad (4)$$

where C$_{in}$ is the daily mass flow rate of carbon from both CO$_2$ and air (airlift) injections into the photobioreactor (g/day), C$_{out}$ is the daily mass flow rate of carbon out of the photobioreactor via venting (g/day), V$_l$ is the volume of the media (L), M$_C$ is the atomic weight of carbon (g/mol), $\frac{d[C_{biomass}]}{dt}$ is the daily rate of change in concentration of carbon bound in the biomass in the media (mol/L/day), $\frac{d[DIC]}{dt}$ is the daily rate of change in dissolved inorganic carbon concentration (mol/L/day), V$_g$ is the volume of the headspace (L), and $\frac{d[C_{headspace}]}{dt}$ is the daily rate of change in carbon concentration in the headspace (mol/L/day).

3.4.2.3 Evaluation of Terms of the Carbon Mass Balance

Several of the terms in the carbon mass balance Eq. (4) could be determined from operational data provided by Mera Pharmaceuticals, Inc. The first term on the left hand side of Eq. (4), C$_{in}$, the daily mass flow rate of carbon from both CO$_2$ and air injections into the photobioreactor, was estimated from data on CO$_2$ and air injections. CO$_2$ injection data included the frequency, duration, and volumetric flow rate of the injections of pure CO$_2$. The mass of carbon injected as CO$_2$ per day could be calculated from this information. Air containing about 0.038% CO$_2$ by volume was injected every minute, and the volumetric flow rate of the air was recorded. These data were used to calculate the mass flow rate of carbon transported into the photobioreactor with the air.

Another term that could be estimated from operational data on alkalinity, pH, and media temperature was the daily rate of change in dissolved inorganic carbon concentration, $\frac{d[DIC]}{dt}$. Dissolved inorganic carbon (DIC) is the sum of carbonic acid, bicarbonate, and carbonate in the aqueous solution. DIC, along with total alkalinity and temperature, describe the CO$_2$ chemical system in freshwater media. The relationship for dissolved inorganic carbon is:

$$[DIC] = \left(\frac{TA + [H^+] - \dfrac{K_w}{[H^+]}}{\dfrac{[H^+]}{K_2} + 2} \right) \left(1 + \frac{[H^+]}{K_2} + \frac{[H^+]^2}{K_1 K_2} \right) \tag{5}$$

where [DIC] is the inorganic carbon concentration in meq/L, TA is the total alkalinity in meq/L, $[H^+]$ is the hydrogen ion activity (i.e., 10^{-pH}), K_w is the acid dissociation constant of water, K_1 is the first apparent dissociation constant for carbonic acid in water, and K_2 is the second apparent dissociation constant for carbonic acid in water.

Values of the dissociation constant of water and first and second dissociation constants can be determined from the following equations (Millero, 1979; UNESCO 1987) if the temperature of the media, T (K), is known:

$$K_w = e^{\left(148.9802 - \frac{13847.29}{T} - 23.6521 \ln T \right)} \tag{6}$$

$$K_1 = 10^{-\left(\frac{6320.81}{T} - 126.3405 + 19.568 \ln T \right)} \tag{7}$$

and

$$K_2 = 10^{-\left(\frac{5143.69}{T} - 90.1833 + 14.613 \ln T \right)} \tag{8}$$

Operational data provided by Mera Pharmaceuticals, Inc. were not sufficient to evaluate the terms C_{out}, $\dfrac{d[C_{biomass}]}{dt}$, and $\dfrac{d[C_{headspace}]}{dt}$ in the carbon mass balance. This required additional experiments.

3.4.2.4 Carbon Venting from the Photobioreactor

Neither the gas venting rate nor the composition of the gas discharged from the photobioreactor are monitored. Experiments were conducted to obtain this information and to estimate the value of C_{out}. These experiments consisted of measuring the volume of gas exiting the photobioreactor during typical operation, collecting samples of the gas, and analyzing these samples for CO_2 (carbon) content with a gas chromatograph.

An orifice flow meter was employed to measure the gas venting rate from the photobioreactor. Gas is regularly discharged from the photobioreactor through a nominal 3 inch diameter PVC pipe connected to the headspace to prevent over-pressurization due to the injections of air (for the airlift system) and CO_2. The orifice flow meter was attached to the end of the 3 inch vent tube. The orifice flow meter consisted of a nominal 3 inch diameter PVC pipe and fittings upstream and downstream of the orifice plate. The ASME sharp edge orifice was machined from a Plexiglas plate and was sandwiched between the PVC pipe flanges. Several orifices were fabricated with different diameters to accommodate a range of possible flow rates.

The orifice that was used in the tests had an internal diameter of 1.2 inches (3.0 cm). Pressure drop across the *vena contracta* taps was monitored with a Magnehelic differential pressure gauge. ASME relationships for sharp edge orifice response were then used to determine the flow rate from the measured pressure drop.

Samples of the vented gas were collected and brought to UH for GC analysis of carbon content. Tygon tubing was inserted into the vent downstream of the orifice and gas was extracted with a vacuum pump and stored in 1 liter teflon sampling bags. An inline filter removed water vapor from the vented gas.

During the gas venting experiments, the automated CO_2 injection system that supplies the photobioreactor was turned off so that the start time and duration of the CO_2 injections could be manually adjusted. Tests were performed where CO_2 was injected continuously for 21 minute periods. The amount of pure CO_2 injected was monitored and recorded. Vent gas samples and differential pressure readings (i.e., vent gas flow rates) were taken before, during, and after the injections.

The gas samples were subsequently analyzed at UH using a Shimadzu Model 14A gas chromatograph. 0.2 mL of gas extracted from the teflon sampling bags was manually injected into the GC using a gastight syringe. The injected sample was carried through the column by an inert carrier gas consisting of 8% hydrogen and 92% helium by volume. The sample was partitioned between the carrier gas and a stationary phase supported on an inert size-graded solid (solid support) in a packed column. A Carbonex 1000 packed column was used for this analysis.

Measurements were performed with a thermal conductivity detector (TCD) in which a tungsten filament is heated by a constant 100 mA electrical current. In these measurements, both the temperatures of the injection port and the detector were set at 140°C. The column temperature was programmed to start at 45°C, maintain that temperature for 1 minute, increase 20°C for each of the next seven minutes, maintain 185°C for 1 minute, and finally cool down for 11 minutes before the next run.

The GC was calibrated using three gas standards: pure N_2; 0.038% CO_2 in atmospheric air; and a mixture of 2.1% CO_2 in 97.9 % N_2. The same protocol was used during the calibration and the sample analysis with the exception that the gas standards were injected automatically into the GC.

The mass flow rate of carbon vented out of the photobioreactor was calculated from the measured gas venting rate and the concentration of carbon in the gas samples. The total mass of carbon vented over the duration of the experiment was determined by integration of the experimental values of the mass flow rate of carbon. This value is divided by the total mass of carbon injected into the photobioreactor during the duration of the experiment to estimate the percentage of injected carbon vented from the system. This percentage was used in the carbon mass balance and the process model.

Carbon Bound in Biomass

The daily rate of change in the concentration of carbon bound in the *Haematococcus pluvialis* biomass, $\frac{d[C_{biomass}]}{dt}$ could not be determined directly from operational data provided by Mera Pharmaceuticals, Inc. but was estimated by analysis of cell samples collected on a daily basis. $\frac{d[C_{biomass}]}{dt}$ was estimated by comparing the mass of carbon bound in the cells on consecutive days. The mass of carbon in the cell biomass pool is the product of the total cell count (or concentration) in the photobioreactor, the average dry cell mass, and the average % total organic carbon (%TOC) of a cell on a dry mass basis. Mera Pharmaceuticals regularly monitors the quantity of cells in the photobioreactor and this information was included in the operational data set. Occasionally, Mera Pharmaceuticals collects cell samples to determine the dry cell mass, but does not monitor the %TOC in a cell.

Dried samples of *Haematococcus pluvialis* were analyzed for %TOC. These samples were collected from M13A-030423 over a period of 6 days at different times during both the day and night cycles. Table 6 summarizes the information for this set of samples, including sampling dates and times, ages relative to the time of initial inoculation of the photobioreactor, average cell count, liters of culture and media sampled, and dry masses. Using this information, the daily average dry cell mass and the average dry cell mass over the 6 days that samples were collected were calculated. The Agricultural Diagnostic Service Center of UH analyzed the *Haematococcus pluvialis* samples for %TOC on a dry mass basis. The product of the %TOC results, the data on cell counts (concentrations), and average dry cell mass was the daily mass of carbon bound in the biomass. The change in mass of carbon bound in the biomass between consecutive days could then be used to estimate $\frac{d[C_{biomass}]}{dt}$.

Table 6. *Haematococcus pluvialis* Samples

Date	Time	Age (days)	Average Cell Count (cells/mL)	Liters used	Dry Mass (g)
4/26/03	5:40	3	156,513	3	0.3498
4/26/03	18:45	3	237,617	3	0.6309
4/27/03	5:40	4	211,803	3	0.4901
4/27/03	18:30	4	298,501	3	0.6839
4/28/03	6:05	5	304,173	3	0.6213
4/28/03	18:50	5	336,370	1.95	0.6501
4/29/03	5:30	6	410,071	3	0.9152
4/29/03	18:45	6	441,130	2	0.7105
4/30/03	6:00	7	431,003	2	0.7581
4/30/03	19:00	7	538,085	2	1.0871
5/1/03	5:25	8	520,702	2	0.9908

Change in Carbon Concentration in the Headspace

Determination of the final unknown term in the mass balance equation, $\dfrac{d[C_{headspace}]}{dt}$, the daily rate of change in carbon concentration in the headspace posed a problem, since this requires a detailed time history of the headspace gas concentration, which is not monitored by Mera Pharmaceuticals. Resources were not available to conduct long term extractive sampling of the vent gas and subsequent GC sample analysis. Given that the efficiency of carbon capture by the biomass (which is essentially the ratio of $V_l M_c \dfrac{d[C_{biomass}]}{dt}$ and C_{in}) was the primary interest of this study and that the carbon mass balance served as a check to verify the values of $\dfrac{d[C_{biomass}]}{dt}$ and C_{in}, it was decided to forego experiments needed to determine $\dfrac{d[C_{headspace}]}{dt}$. $\dfrac{d[C_{headspace}]}{dt}$ was instead inferred from the carbon mass balance equation (since it is the only unknown) and its values were assessed on the assumption that CO_2 equilibrium existed between the liquid media and gas headspace.

Relationships Between Variables in the Carbon Mass Balance Equation

After all terms in the carbon mass balance equation were calculated, relationships between different variables in this equation were developed and used in the process model. One relationship of interest was the variation in mass flow rate of carbon injected into photobioreactor over time. The mass flow rate of carbon is controlled automatically in response to changes in media pH. Specifically, we were interested in whether carbon injections were random, constant, increasing, or decreasing. Relationships also were derived to determine if the quantity of carbon dissolved in the media or the quantity of carbon degassed out of the media is affected by a change in the quantity of carbon injected into the MGM; and if either the change in mass of carbon bound in the biomass or the change in dissolved inorganic carbon concentration is affected by a change in the total carbon in the media.

Haematococcus pluvialis Population Dynamics

Haematococcus pluvialis utilizes carbon from the CO_2 and air injections for cell production (division). The relationship between the cell division rate and the average rate of carbon uptake per cell was of interest in this study.

The specific growth rate (i.e., the population-averaged rate of cell divisions per cell) is given by:

$$\mu = \frac{\ln\left[\dfrac{B_0 + Y}{B_0}\right]}{\delta t} \tag{9}$$

where B_0 is the initial number of cells in the culture and Y is the number of cells created over the time interval δt (Geider and Osborne, 1992). The average rate of carbon uptake per cell could be estimated by dividing the change in the total mass of carbon bound in the biomass between two consecutive days by the *Haematococcus pluvialis* population on the first day of the two consecutive days. These data were analyzed and a relationship between carbon uptake and specific growth rate was developed.

Harvesting Strategy

The criteria for the harvesting strategy applied in the process model simulations were determined by reviewing Mera Pharmaceuticals' operating records. The records indicate that the current Mera Pharmaceuticals harvesting criteria are based on two parameters: (1) a specific number of cells needed to inoculate the open ponds and (2) a minimum cell concentration in the photobioreactor that must be achieved before harvesting. Values of these two parameters were identified by examination of the operational data.

STELLA Model

The process model was developed using the STELLA software. STELLA is a computer software program with an interface for building dynamic models that realistically simulate biological systems (Rice et al., 2002). The procedure used in STELLA modeling involves: (1) constructing a relational model of the system using icons that represent state and rate variables and arrows and flows that represent interrelated components; (2) quantifying the relationships among elements in the model; and (3) running the model to observe the system dynamics (American Society for Horticultural Science, 2004; Rice et al., 2002).

The process model integrates the partitioning of the carbon, *Haematococcus pluvialis* population dynamics, and the harvesting strategy. The carbon component of the model incorporated different variables of the carbon mass balance, Eq. (4), such as the mass flow rates of carbon injected into and vented out of the photobioreactor, and changes in mass of dissolved inorganic carbon, carbon bound in the biomass, and carbon in the headspace. The relationships between variables in the carbon mass balance equation described above were included in the model. The *Haematococcus pluvialis* population dynamics component of the model describes the growth rate of the cells and their ability to capture and assimilate CO_2 as a function of operating conditions.

Model Verification

The process model was verified by comparison of its results with operational data from a different photobioreactor than the one used to develop the functional relationships between variables used by the model. Data from photobioreactor identified as M10A-040810 were employed. Model inputs from the operational records of this unit included the carbon injection mass flow rates, the initial cell population, media volume, target concentration (for harvesting), and the harvesting cell quantity. The simulated output was the cell population size. Statistical techniques were used to compare the simulated outputs and the data to determine whether the model provides an accurate representation of the photobioreactor (Law and McComas, 2001).

<u>Sensitivity Analysis</u>

After the model was verified, analyses were conducted to determine the sensitivity of the predicted amount of carbon captured to varying the target cell concentration and the harvesting cell quantity. One of these two inputs was varied at a time, while other model parameters were held constant, to see the resulting impact on the model output.

<u>Model Simulations</u>

Different operating scenarios were simulated with the process model to identify the combination of the target cell concentration and the harvesting cell quantity that would yield maximum carbon capture. Maximizing carbon capture is the same as maximizing cumulative cell yield since the model assumes a constant %TOC per cell.

3.5   <u>Task 5 - Economic Analysis</u>

There are two subtasks under Task 5 to deal separately with the economic analysis of the gas separation process and the photobioreactor carbon fixation process.

3.5.1   <u>Subtask 5.1 - Gas Separation Process</u>

No experimental work was performed under this subtask.

3.5.2   <u>Subtask 5.2 - Photobioreactor Carbon Fixation Process</u>

To carry out the economic analysis of the photobioreactor carbon fixation process we have put together an economic model that results in predicted costs for a microalgal-based carbon sequestration plant. The economic models are driven by scientific/technical variables (e.g., microalgal growth rate) and can be applied to a variety of product scenarios. At present, the models are designed for facility sizes of 5 to 50 ha, but may be changed for application to larger facilities. The model includes over 500 variables that go into calculating monthly cost of goods, capital equipment requirements, land requirements and cash flow and balance sheets for 15 years of operation.

The model produces a detailed breakdown of operating expenses, capital costs, and human resources, each of which is analyzed with regard to functional subsystems (e.g., water pretreatment, media formulation, photobioreactor operation, product processing, quality control). Finally, the model also includes detailed analysis of area requirements, utility usage, and product flows within the production system.

Costs in the Mera economic models are currently based on historical data for actual costs incurred. One of our key activities in this project has been to research the costs of equipment and supplies at significantly larger scales. All model assumptions are stated in detail and, where applicable, all model results will comply with international GAAP (Generally Accepted Accounting Principles) standards.

3.5.2.1 Microalgal Plant Design

Our first activity under this subtask includes the design of a microalgal facility of commercially significant scale that would produce a high value product, such as astaxanthin. The design parameters are based on Mera's experience in commercial production and historical data. Thus, this first design effort assumes no optimization concerning efficiency of CO_2 utilization, including gas dissolution into the growth medium or losses due to degassing from the medium.

The design parameters for this plant are

Total plant surface area: 12 ha
Culture surface area: 7 ha
Support systems: 5 ha

where the support systems' area includes areas needed for laboratories, nutrient storage, biomass harvesting and processing, utilities, maintenance, CO_2 storage, drive access, pump stations, pipe runs, and office space.

Assuming no optimization, as stated above, we can also assume the following parameters (based on historical production data collected at Mera's microalgal facility in Kona, Hawaii):

Productivity: 8 g C m^{-2} d^{-1}
Efficiency of CO_2 utilization: 12%
Percent of culture area under cultivation: 81.6%

which are the parameters used as the starting point for our microalgal facility design

We can estimate that this plant would capture up to about 1.6 tons of CO_2 per day. Again, assuming no optimization in CO_2 utilization efficiency (12% based on the results of Section 4.2.2.1), the plant would need to be fed by a combustion source generating about 13 tons CO_2 d^{-1}. This is approximately the amount of CO_2 generated when producing 1.7 MW of thermal power by burning bituminous coal. The same plant can be expected to produce about 8 kg of nutraceutical grade astaxanthin d^{-1}, which at a wholesale price of US $10,000 would generate about US$2.5 million month^{-1}.

As a first step in the design process, we have specified the mass flows of the different materials necessary to run Mera's actual plant in Kona, Hawaii. The plant under consideration will be, however, significantly larger (about 30x more capacity). It should be noted that this plant's characteristics are specific to the production of a high value product, astaxanthin, from *Haematococcus*. Thus, the plant utilizes both enclosed photobioreactors (MGM), depicted green in the figure, and open pond systems, depicted red in the figure. As we continue work on this design, alternate designs can be generated for similar sized plants to produce other types of materials which might utilize only open pond reactors (e.g., *Spirulina* for biomass) or only enclosed photobioreactors (e.g., *Nanochloropsis* for lutein production).

3.5.2.2 Capital and Recurring Costs of Microalgal Plant

The model has been designed to be flexible and accept parameters for significantly larger microalgal plants that would produce a number of different microalgal products (e.g., astaxanthin from *Haematococcus*, biomass from *Spirulina*, and B-carotene and lutein from *Dunaliella* and *Nannochloropsis* respectively) utilizing open and closed photobioreactors while capturing carbon from smoke stack gases. We have determined the capital and recurring costs of the microalgal plant based on our own experiences at the Mera Production plant.

3.5.2.3 Calculation of "Economies of Scale" Factors in Microalgal Plant Engineering

We expect that as the size (scale) of the microalgal facility increases, the costs per unit biomass produced/costs per unit CO_2 sequestered will decrease. We have modeled this ESF (Economy of Scale Factor) as follows. First, we determine the costs associated with what we consider, based on our experience and economic models at Mera's microalgal plant, to be the smallest size microalgal plant that is economically viable (Smallest Economical Unit or SEU). Based on the capacity of the different units of material handling equipment used in these processes we will determine at what scale (e.g., 2x, 5x, 20x, 200x capacity of the smallest size plant) the change in ESF becomes 0 (zero). We will then determine the costs for two or more microalgal plants of intermediate size. Using our calculated cost results we will formulate an equation that will relate microalgal plant scale to ESF.

4. RESULTS AND DISCUSSION

4.1   Task 1 - Supply of CO_2 from Power Plant Flue Gas to Photobioreactor

The issue of supplying CO_2 from power plant flue gas to the photobioreactor system entails that the team reproduce representative types of industrial flue gas and test their ability to support microalgal carbon fixation. In this Subtask, we will first undertake to reproduce a variety of flue gas types at a scale sufficient only for laboratory experiments with microalgae. For the laboratory scale experiments in microalgae growth and carbon fixed to be carried out in Task 2, small amounts of simulated flue gas are needed and can be mixed using bottled gases. The results of the laboratory experiments (Task 2) will guide the selection of appropriate flue gas generation for large-scale demonstration (Task 3). At the larger scale (2,000 and 25,000 liter bioreactors), the flue gas will be generated using exhaust from the existing propane-fired boiler at the Aquasearch facility.

4.1.1   Subtask 1.1 - Power Plant Exhaust Characterization

In the United States about two-thirds of the capacity in the utility power generation sector is based on fossil fuel combustion (Table 7). Coal and natural gas are the primary fuels for power generation; fuel oil is important in specific regions. All fossil fuels amount to 71% of the electricity generating capacity. Fossil fuels represent an even larger segment of the non-utility power generation market (approximately 90%, if the use of biomass is included).

Table 7. Electricity Production (Nameplate capacity) for 1999, by Sector and Energy Source

Sector/Fuel	Megawatts	
Utility		
Coal-Fired	296,883	
Petroleum-Fired	54,444	
Gas-Fired	129,510	
Nuclear-Powered	102,291	
Hydroelectric	89,800	
Other	4,883	
Total Utility		677,811
Non-Utility		
Coal-Fired	48,501	
Petroleum-Fired	40,508	
Gas-Fired	49,353	
Nuclear-Powered	1,542	
Hydroelectric	5,662	
Other	21,791	
Total Non-Utility		167,357
Total		**845,168**

Source: Energy Information Agency

To be effective, sequestration of CO_2 using the photobioreactor needs to be located in an area with higher solar flux and warmer temperatures. If we consider only the sunnier and more southern regions of the US, as shown in Table 8, the capacity represents about half of the total US capacity. Generalizations have been made about climate in this exercise, which is intended to show only that a significant amount of fossil fuel combustion sources exist in places with climates most conducive to the photobioreactor.

Table 8. Electricity Production for 1999, by Sector and Region

Region	Utility		Non-Utility	
	Number of Units	Nameplate Capacity (MW)	Number of Units	Nameplate Capacity (MW)
*Other**	*4,372*	*235,165*	*2,974*	*88,908*
South Atlantic	1,345	152,463	726	14,416
East South Central	490	66,150	185	6,009
West South Central	795	109,473	576	17,929
Mountain	783	52,265	376	6,842
Pacific	1,708	62,296	1,167	33,254
Total	**9,493**	**677,812**	**6,004**	**167,358**

*Northeast, Middle Atlantic, and North Central Regions
Source: Energy Information Administration

Based on the information in Table 7, non-utility electricity generators using fossil fuels may be attractive for application of a photobioreactor because the average size of such plants is smaller than that of utility plants (28 MW versus 71 MW). Implementation of the concept may be easier on a smaller scale, particularly initially.

As shown in Table 9, the CO_2 content of flue gas from boilers (as opposed to gas turbine combustors) has low amounts of excess oxygen (typically 6 vol%) and CO_2 concentrations on the order of 12-15 vol%. Gas turbine combustors have much lower CO_2 and higher excess oxygen.

Table 9. Typical Flue Gas Compositions for Different Fuels and Combustion Systems

Volume %	Utility Boilers					GTCC Natural Gas	Diesel Fuel Oil
	Bituminous Coal	Sub-bituminous Coal	Fuel Oil	Biomass	Natural Gas		
CO_2	12.7%	15.1%	12.1%	19.0%	7.4%	3.4%	3.8%
H_2O	5.0%	12.2%	7.5%	13.0%	14.8%	6.9%	3.4%
O_2	6.0%	6.0%	6.0%	6.0%	6.0%	13.8%	15.0%
N_2	76.9%	71.0%	76.0%	62.0%	71.8%	75.0%	77.7%
SO_2 [ppm]	50-500	300-500	300-1300	100-200	0	0	10-100
NO_x [ppm]	50-500	50-500	300-500	200-400	100-300	25	150

Concentrations of trace acid gas species such as NO_x and SO_2 depend on the composition of the fuel and on the air pollution control system employed. Natural gas-fired combustors have virtually no SO_2 in the flue gas, while coal-fired systems have hundred of parts per millions. The range of NO_x emissions given in Table 3 reflects the use of low NO_x burners and/or post-combustion NO_x control to remove some of the NO_x from the flue gas.

Future efforts to aid CO_2 capture from combustion sources may include modifications to the combustion system that result in much higher concentrations of CO_2 in the exhaust. Oxygen-enriched combustion and recycle of flue gas back into the boiler are currently being investigated at the laboratory- and pilot-scale in the US and in other countries. Since the photobioreactors currently use a pure CO_2 stream, using a very CO_2-rich flue gas stream would require less modifications to existing commercial practice for growth of microalgae.

4.1.2 Subtask 1.2 - Selection of CO_2 Separation and Clean-Up Technologies

There are several technologies currently available to separate and capture CO_2 from fossil-fueled power plants including absorption from gas streams by contact with amine-based solvents, cold methanol or sorbents and passing the gas stream through special membranes. The optimum process for capturing CO_2 is largely influenced by the concentration or partial pressure of CO_2 in the flue gas; this depends, in turn, on the characteristics of the fuel and combustion system. The results of the laboratory screening experiments with microalgae will dictate the type and degree to which separation and clean up technologies may be necessary. Ideally, the no such procedures would be necessary. However, this will be dependent on the tolerance of the microalgae to certain components of the gas mixtures. Such tolerance will likely depend not only on the nature of the constituent compounds, but also on their concentration. Therefore, in this Subtask, we will characterize the effluents and processing conditions of processes applicable to separation of CO_2 from flue gas.

According to recent reports (Perry and Chilton, 1973) the most likely options currently available for CO_2 separation from combustion flue gas include: gas adsorption (both physical and chemical), cryogenic separation, and membrane separation. Some of the major commercial applications of these processes are given in Table 10.

In gas adsorption systems, CO_2 reacts with a liquid solvent in which it is soluble. Both physical and chemical solvents have been used. Physical solvents take up CO_2, but do not react with it, whereas chemical solvents cause the formation of an intermediate compound with CO_2.

Physical adsorption processes are more suitable for mixed gas streams that are under high pressure because the solubility of CO_2 increases with increasing gas pressure. Physical adsorption can be carried out in a solvent according to Henry's law; regeneration is accomplished using heat or pressure reduction. Solvents used for physical adsorption include dimethylether of polyethylene glycol (Selecol process) or cold methanol (Rectisol process). Physical adsorption processes are more economical if the CO_2 partial pressure is above 200 psia. At low CO_2 partial pressure, chemical adsorption processes are favored.

Table 10. Examples of Commercial Applications of CO_2 Removal by Gas Adsorption

Process	Owner	Uses	Comments
Sulfinol	Shell Oil Company	Natural gas, refinery gas, and synthesis gas	180 commercial units in operation or under construction in 1996
Selexol	UOP	Natural gas, refinery gas, and synthesis gas	53 commercial units installed by 1992
Rectisol	Lurgi GmbH and Linde AG	Heavy oil partial oxidation process of Shell and Texaco, also Lurgi gasification	More than 100 commercial units in operation or under construction in 1996
Purisol	Lurgi GmbH	Natural gas, hydrogen, and synthesis gas	Seven commercial units in operation or under construction in 1996
Catacarb	Eickmeyer & Associates	Any gaseous stream	
Benfield	UOP	Synthesis gas, hydrogen, natural gas, town gas	600 commercial plants had been installed by 1992
Alkanolamines	No specific owner	Any gaseous stream	Chemicals produced and supplied by Dow, DuPont, Union Carbide; they do not supply process equipment

Chemical solvents (for example, monoethanolamine (MEA), dimethanolamine (DEA), ammonia, or hot potassium carbonate) form an intermediate compound that can be broken down by heating to give the original solvent and CO_2. These processes can be used at low partial pressure of CO_2, but the flue gas must be free of SO_2, hydrocarbons, and particulate matter. In particular, SO_2 must be reduced to below 5 to 10 ppmv for MEA adsorption.

Pressure-swing adsorption (PSA) or temperature-swing adsorption (TSA) are used in chemical process streams and have also been proposed for removal of CO_2 from flue gas. A combination of chemical and physical adsorption is used with beds of solid sorbents, for example, of alumina, zeolite, or activated carbon.

Gas adsorption or gas separation membranes have the potential to remove CO_2 from flue gas. Gas separation membranes employ a membrane that is selective for transport of CO_2 and high pressure on the flue gas side to concentrate CO_2 on the low pressure side of the membrane. Gas adsorption membranes employ a liquid on the other side of the membrane instead of a gas stream.

Application of these carbon dioxide separation processes to flue gas depends on the concentration of CO_2 in the stream, on the presence of impurities in the gas, and on the pressure of the flue gas stream. Chemical adsorption may be preferred for cases in which the concentration of CO_2 is low and the pressure is near atmospheric. Physical adsorption is favored for higher total pressure and concentration of CO_2.

52

Chemical adsorption using MEA is the most mature technology and looks to be the most economically viable in the near future. An example of an MEA system applied to flue gas is given here, taken from a DOE report (United Technologies Research Center, 1999). Figure 22 shows a process flow diagram for an MEA absorption process as applied to flue gas from a coal-fired power plant. In this implementation, gas leaves the flue gas desulfurization (FGD) unit at 56°C and is drawn into a fan and the pressure is boosted to 19.7 psia. The gas stream is cooled slightly and then enters the absorber where it contacts the lean MEA stream flowing countercurrently. The lean MEA stream contains 30 wt% MEA and absorbs more than 90% of the CO_2 in the flue gas (which can now be discharged to the atmosphere). The rich MEA solution is pumped from the bottom of the absorber to a stripper in which water vapor (produced in the reboiler) is used to strip CO_2 from the solution. The CO_2 and water vapor go to a condenser and gas/liquid separator. The condensed water is recovered and the CO_2 can be further processed downstream.
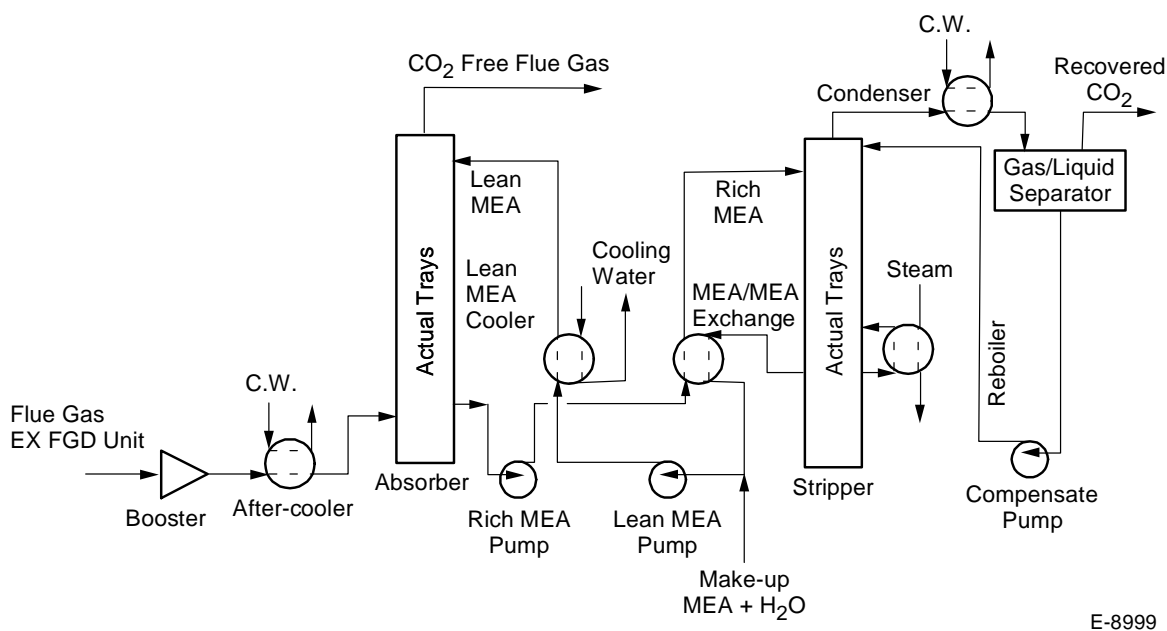
Figure 22. Process flow diagram for MEA absorber unit for removal of CO_2 from coal-fired flue gas (United Technologies Research Center, 1999).

A unit sized for a 25 MWe plant burning a bituminous coal would process 235,000 lb/hr of flue gas and produce 42,000 lb/hr of CO_2. Table 11 lists the major equipment and costs. The total major equipment cost is approximately $5M (1999 dollars). The total capital cost is on the order of $11M.

The processes discussed above are currently demonstrated on a commercial scale, but for the production of CO_2 (from chemical plants or natural gas processing plants, for example). The cost of these technologies is too high for the reduction of greenhouse gases. Research into less expensive processes that are aimed at carbon emissions reductions is still in the early stages. The hope is that in the near future, less costly options will be available for fossil fuel-fired combustion sources. Some of the technologies now being developed include membranes, novel gas-liquid contactors, solid sorbents, and the formation of CO_2/water hydrates.

Table 11. Cost for Major Equipment in MEA Absorber
(United Technologies Research Center, 1999)

Equipment		Cost, in 1999 Dollars
Absorber	1	210,000
Stripper	1	17,000
MEA Make Up Tank	1	29,000
After Cooler	1	127,000
MEA Cooler	1	344,000
MEA/MEA Exchanger	1	481,000
Condenser	1	1,921,000
Reboiler	1	1,324,000
Booster	1	601,000
Rich-MEA Pump	2	34,000
Lean-MEA Pump	2	31,000
Condensate Pump	2	6,000
Total		5,125,00

4.1.3 Subtask 1.3 - Carbon Dioxide Dissolution Method

In the small, laboratory scale reactors used in Task 2, any introduced gases are effectively mixed instantaneously throughout the culture medium. This is not so in larger scale reactors (particularly the 25,000 L AGM), due to the physical configuration of the photobioreactor. In this task, we will undertake theoretical and experimental investigations of the optimum method for dissolving CO_2 from the flue gas mixtures into the aqueous environment of the bioreactors. The results of this investigation will be implemented in Task 3 in the 25,000-L AGM.

In this task, we undertook theoretical and experimental investigations of the optimum method for dissolving carbon dioxide from the flue gas mixtures into the aqueous environment of the bioreactors. In the current Aquasearch commercial reactor, there are two gas streams added to the photobioreactor. A large stream of transport air is added using multiple injectors arranged radially near the walls of the photobioreactor. Large (~1.25 cm (~ ½ in.)) diameter nozzles are used. This air is used to add momentum to the liquid and promote liquid circulation in the long tube that comprises the photobioreactor. In the current design, a high-volume, low-pressure flow of filtered ambient atmosphere is introduced in a 2-m vertical airlift section of the reactor in which fluid rises, creating the head pressure necessary for recirculation.

Slightly upstream of the air injection location, pure CO_2 is added through a small pipe with a sparger on the end to produce small bubbles. The CO_2 is introduced in a 2-m "down-flowing" section, where it rises against the fluid flow. This procedure dramatically improves the dissolution of CO_2. CO_2 is not added continuously, but rather is added when the pH of the liquid rises to a certain level. CO_2 is used both to provide carbon for growth of microalgae and to keep the pH in an optimum regime for growth.

54

In the commercial-scale photobioreactors, air is needed for circulating the liquid. In the smaller chemostats that are used to grow microalgae in the laboratory, CO_2 is sometimes used by itself, without adding any air to promote mixing. This can result in much higher carbon conversion (or efficiency of CO_2 utilization) than in the larger scale system. As far as the growth rate of microalgae is concerned, air has both advantages and disadvantages.

The chief advantage of the transport air is that it removes some of the dissolved oxygen in the water. Photosynthesis results in the production of O_2 by the microalgae. Under some conditions, the water can be supersaturated with oxygen. When this occurs, the rate of photosynthesis (and growth) falls rapidly. The relatively large flow of air through the photobioreactors strips out some of the dissolved oxygen and prevents high levels of supersaturation.

The chief disadvantage of the transport air addition is that is strips CO_2 as well as O_2 from the water. The removal of CO_2 lowers the efficiency of carbon utilization by 50% to 80%. Thus, in the commercial photobioreactors, the efficiency of CO_2 utilization (based on carbon production and CO_2 usage) is only 12.5%.

What determines the efficiency of CO_2 utilization by the microalgae: the rate of incorporation of CO_2 into the liquid or the rate of uptake of CO_2 by the microalgae? In the former situation, the microalgal growth is limited by the rate that CO_2 is dissolved into the liquid. In the latter, there is adequate CO_2 in the water and the rate is limited by the available sunlight. We would like to find a balance in which as much of the CO_2 added as possible is incorporated into biomass.

If we introduce a flue gas containing 5 to 10% CO_2 in the downflowing section where pure CO_2 is currently introduced, the 10 to 20-fold increase in flow rate could create a substantial back-pressure on the airlift-driven circulation. We may be able to solve this problem by simply increasing the flow rate of the airlift supply to overcome the flow rate of the flue gas. However, the solution may not be so simple. The flue gas supply will be pulsed (because it is used to regulate pH), whereas the airlift is continuous. Thus, we might create a strongly modulated fluid flow rate that is not favorable to the microalgae cultures. Other solutions could involve (a) decreasing bubble size of the flue gas to provide for higher dissolution rates, or (b) automatic modulation of the airlift flow rate to offset the counter-flow of flue gas.

We have conducted a theoretical investigation to explore the limits of the mass transfer and the dependence of mass transfer on operating parameters, in preparation for a more detailed experimental and theoretical investigation. The mass transfer rate to bubbles is controlled by:

- The concentration driving force between the interface and the bulk liquid;
- The interfacial area for mass transport, a;
- The mass transfer coefficient in the liquid, k_x.

The resistance on the gas-side in the bubble is usually negligible unless the gas in question is very soluble in the liquid; therefore, mass transfer in the gas will be neglected. The overall mass transfer rate, in moles per sec per volume of liquid is (McCabe and Smith, 1976):

$$N_A/V = k_x a(x_i - x) \tag{10}$$

where x and x_i are the mole fractions of component A in the liquid at the bulk and interface, respectively. Once again, a is the interfacial area per unit volume and k_x is the mass transfer coefficient in the liquid.

For small bubbles (diameters less than 0.5 mm), the liquid mass transfer coefficient is calculated from the following relationship (McCabe and Smith, 1976):

$$\frac{k_x D_P M_\ell}{\rho \mathscr{D}v} \tag{11}$$

where:

D_p is the bubble diameter
M_l is the mean molecular weight of the liquid
D is the liquid density
$\mathscr{D}_v$ is the diffusivity of the dissolved gas in the liquid
: is the liquid viscosity
) D is the difference between the liquid and gas density (~D)
g is the gravitational acceleration

For large bubbles (diameters greater than 2.5 mm), the following should be used (McCabe and Smith, 1976):

$$\frac{k_x D_P M_\ell}{\rho\,\mathscr{D}v} = 2.0 + 0.31\left(\frac{\mu}{\rho\,\mathscr{D}v}\right)^{1/3}\left(\frac{D_p^3\,\rho\Delta\rho g}{\mu^2}\right)^{1/3} \tag{12}$$

In order to use Eq. (1), we need to have the mean diameter of the bubbles and the interfacial area. The interfacial area can be calculated from (McCabe and Smith, 1976):

$$a = \frac{6\varepsilon}{D_p} \tag{13}$$

where , is the gas hold-up (the relative volume of the dispersed phase, i.e., the gas). Equation 4 was used to calculate the interfacial area using values for , taken from Figure 18-129 in Perry and Chilton, 1973.

Using Eq. (10), the maximum rate of mass transfer can be estimated by setting the bulk concentration of the gas species A to zero and by using the saturated value for the interfacial concentration. Thus

$$N_A/V \approx k_x a x_i \tag{14}$$

There will be two regimes: the small bubble regime is probably more typical of the CO_2 injection sparger, which is designed to produce fine bubbles; the large bubble regime is more like the air injectors which are one-half inch pipes. For formation of single bubbles from a submerged orifice of diameter D_o, the bubble diameter is given by McCabe and Smith, 1976.

$$D_p = \left[\frac{6D_o\sigma}{g\Delta\rho} \right]^{1/3} \quad (15)$$

where F is the interfacial tension. Using this equation, the diameter of the bubbles from the air nozzles in the Aquasearch photobioreactors is estimated to be 8 mm.

In Figure 23, this maximum mass transfer rate is plotted as a function of diameter using the "small" bubble relationship (Eq. (11)), which applies to the conditions under which the CO_2-containing gas is added, and the "large" bubble relationship (Eq. (12)), which applies to the conditions under which the transport air is added. The calculations were carried out for pure water at 20°C. One set of curves applies to O_2 and the other, to CO_2. The differences in solubilities between the two molecules account for the differences in maximum amount of mass transfer.
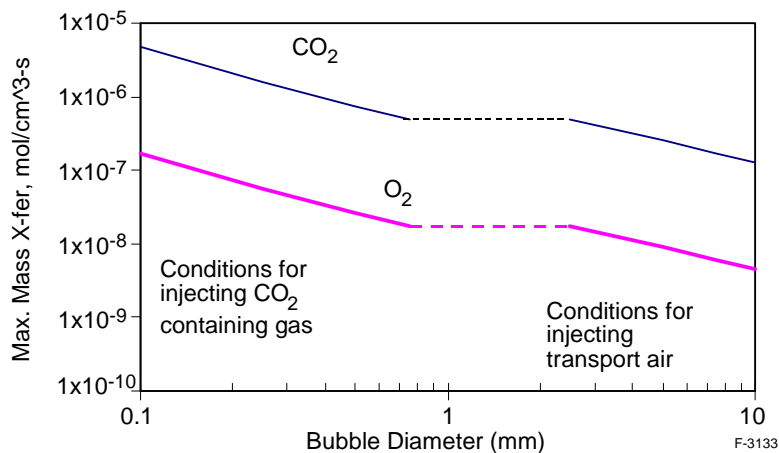
Figure 23. Maximum mass transfer rate from bubbles in water at 20°C as a function of bubble diameter.

In the photobioreactor, we would like to maximize the transfer of CO_2 to the water, while minimizing the amount of CO_2-stripping by the air that is being injected. At the level of this analysis, it is obvious that if the CO_2 is to be injected separately from the air, then the size of the bubbles from the air injectors should be large to produce the largest possible bubbles. This will reduce CO_2-stripping. At the same time, the bubble size for the CO_2 inlet stream should be as small as possible. This is what one would expect, of course, but Figure 23 shows how strong the dependence is on diameter.

57

If we introduce a flue gas containing 5 to 10% CO_2 in the down-flowing section where pure CO_2 is currently introduced, the 10 to 20-fold increase in flow rate could create a substantial back-pressure on the airlift-driven circulation. We may be able to solve this problem by simply increasing the flow rate of the airlift supply to overcome the flow rate of the flue gas. However, the solution may not be so simple. The flue gas supply will be pulsed (because it is used to regulate pH), whereas the airlift is continuous. Thus, we might create a strongly modulated fluid flow rate that is not favorable to the microalgae cultures. Other solutions could involve (a) decreasing bubble size of the flue gas to provide for higher dissolution rates, or (b) automatic modulation of the airlift flow rate to offset the counter-flow of flue gas.

4.2   Task 2 – Selection of Microalgae

4.2.1   Subtask 2.1 - Characterization of Physiology, Metabolism and Requirements of Microalgae

4.2.1.1 Temperature Tolerance Experiments

These experiments were designed to quickly test the tolerance of the different microalgal strains to different temperatures. As such, the cultures were grown in batch mode. The data indicated that there is a large degree of uncertainty about the mean growth (not shown). This is the case for two reasons. First, these experiments were designed to quickly provide information on temperature tolerances for the different strains. Cultures in batch mode show different growth rates at different stages of the cultures' growth curve. Second, a number of these cultures are of a filamentous and clumping nature (see, for example Figure 24). Thus, the cells are not uniformly distributed throughout the growth medium. This translates into inherently noisy data.

Figure 24. An example of cultures of strain AQ0064 (a locally isolated, fresh water, diatom) grown at three different temperatures.

However, the results from the experiment allow us to determine the temperature tolerances of the different microalgal strains. Figure 25 summarizes the results of culture growth for 54 strains at up to five different temperatures. The results show that for the tested strains five did not grow at 15ºC, one did not grow at 20ºC, one did not grow at 30°C and eleven did not grow at 35ºC. In general, local isolates were able to better tolerate the higher temperatures than the imported strains (Figure 26).
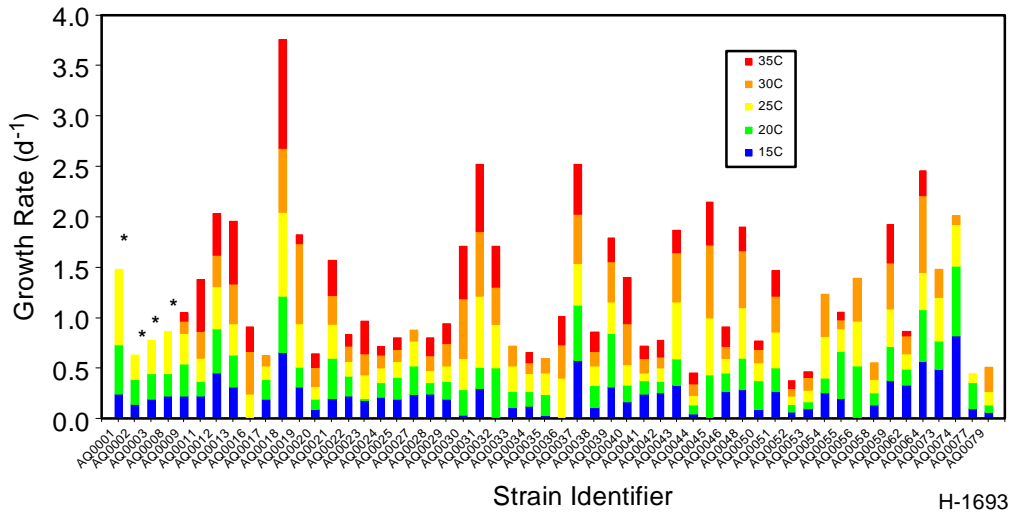
Figure 25. Growth rate estimates for 54 strains of microalgae at five different temperatures. * Incubations for these strains were not carried out at 30 and 35 °C.
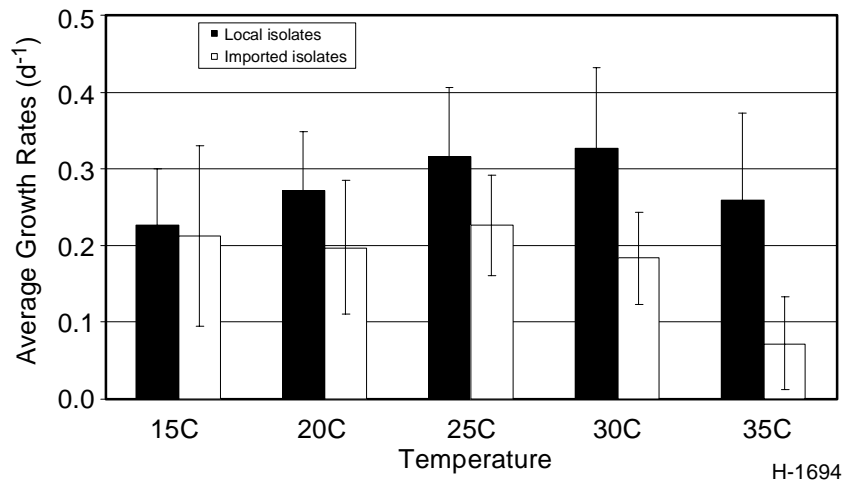
Figure 26. Average growth rates under 5 different temperatures for locally isolated vs. imported strains.

4.2.1.2 pH Tolerance Experiments

Biomass Under Different pH Conditions

Fluorescence-based biomass estimates in chemostat cultures are used to determine whether the experimental culture conditions result in a negative impact on the culture growth rate. In Figure 27 we summarize the biomass maintained by 20 different strains grown at 6.5, 7.5 and 8.5 pH. Lower biomass levels at high pH (8.5) could be interpreted as CO_2 limitation of the cultures. Lower biomass levels at low pH (6.5) could be interpreted as a detrimental effect on the cells due to the acidity of the medium. The biomass estimates, however, must be interpreted with caution. Several strains produced clumps of cells and some strains fouled the inside of the chemostat vessels. Thus, the biomass estimates obtained may not have always reflected the biomass concentration of equivalent homogeneous cultures.
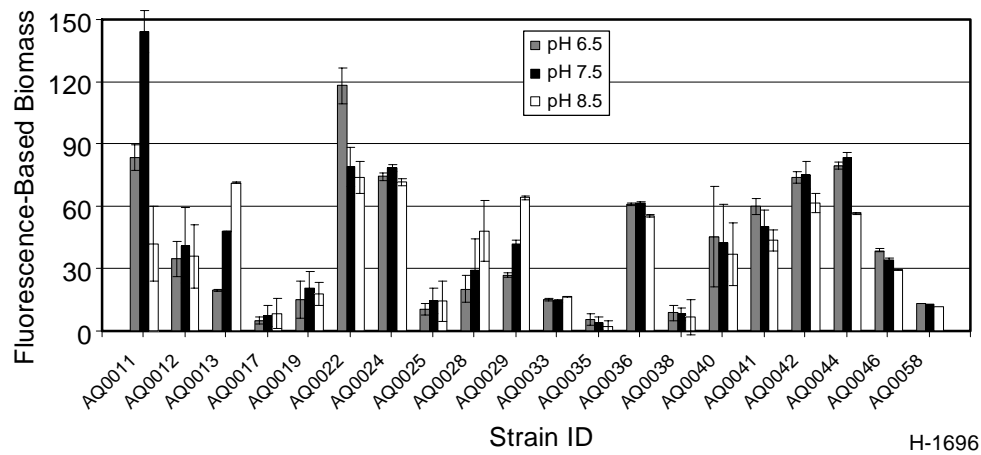
Figure 27   Fluorescence-based estimates of biomass in chemostat cultures grown at three different pH. Error bars are one standard deviation wide.

Photochemical Efficiency Under Different pH Conditions

Figure 28 shows the results of the F_v/F_m measurements, averaged over several days, for the chemostat cultures grown at three different pH levels. The values are normalized to the maximum F_v/F_m value obtained for each specific strain and, thus, reflect relative changes in the maximum quantum yield of photosystem II in response to the changes in pH for each strain.

Maximum absolute F_v/F_m values ranged between 0.37 and 0.39 for Cyanobacterial strains (AQ0012, a locally isolated filamentous strain, and AQ0038, tentatively identified as *Merismopedia* sp.), between 0.58 and 0.65 for Rhodophytes (three *Porphyridium* strains: AQ0033, AQ0035, and AQ0036) and between 0.65 and 0.78 for all other strains (mostly Chlorophytes and including one diatom).

Interestingly, different pH growth conditions resulted in (for most cases) negligible changes in F_v/F_m. Only in Strain AQ0013 did we measure a significant reduction in F_v/F_m in

60

response to 6.5 pH. Strains AQ0012 and AQ0038 are representatives of the Cyanophyceae, or blue-green algae. In this case there appears to be a reduction in photochemical efficiency at the higher pH values (equivalent to lower levels of dissolved CO_2 in the culture medium).

Previous reports have indicated that addition of high concentration CO_2 gas to microalgal cultures may reduce their productivity (Hanagata et al 1993, Sung et al, 1999). In our system, pure CO_2 gas is used as the carbon source in microalgal cultures without any negative effects. However, pure CO_2 is added to the culture on demand, that is, when photosynthetic carbon uptake results in an increase in pH, which triggers the addition of the gas. The three pH conditions that we used in our experiments (6.5, 7.5 and 8.5 pH) correspond to dissolve CO_2 concentrations ranging over 2 orders of magnitude (from 0.7 to over 70 mg/L). However, in most cases, the photochemical efficiency was found near the maximum (Figure 28). We conclude that as long as the pH of the system is controlled and CO_2 is fed on demand (such as with automatic pH control), no deleterious effects on photochemical efficiency will be found from using gases of different CO_2 content.
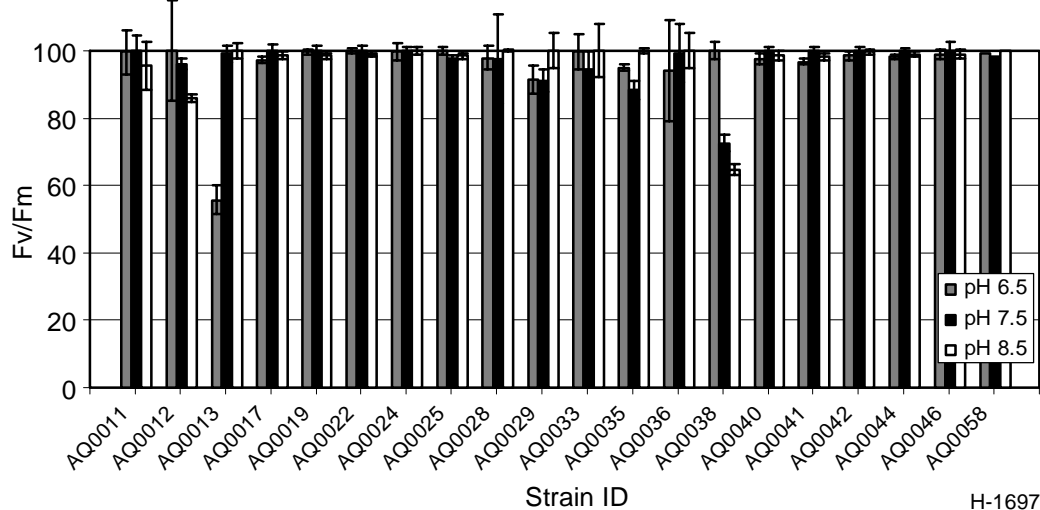
Figure 28. Fluorescence-based estimates of photochemical efficiency normalized to the maximum measured. Error bars are one standard deviation wide.

4.2.1.3 Flue Gas Tolerance Experiments

Biomass Under Different Gas Conditions

Twenty four microalgal strains were grown in chemostat cultures while exposed to pure CO_2 and five different gas mixtures representing five different flue gas sources (Table 12). The gases were injected into the chemostat cultures in response to increases in pH. The range of gas concentrations that the cells were exposed to were 5.7-100% CO_2, 0-3504 ppm SO_2, 0-328 ppm NO, and 0-126 ppm NO_2.

Table 12 summarizes the fluorescence-based biomass levels maintained by the different strains under the six different growth conditions. Our fluorescence-based biomass estimates are, however, to be taken with caution. As was the case in the chemostat pH experiments, clumping of cells and fouling on the inside of the chemostats mean that the biomass estimates obtained may not have always reflected the biomass concentration of equivalent homogeneous cultures. In the case of the flue gas experiments, this is more so since the experiments were of longer duration than that of the pH experiments.

Table 12. Summary of Results from the Flue-Gas Experiments: Fluorescence Based
Biomass Estimates of the Cultures Under Pure CO_2 and
Five Different Flue Gas Mixtures.
For an explanation of the gas mixtures see Table 2.

Strain	CO_2	MIX A	MIX B	MIX C	MIX D	MIX E
AQ0008	14	32	30	38	41	32
AQ0011	33	27	29	32	36	29
AQ0012	15	22	23	15	19	21
AQ0013	21	43	21	23	27	33
AQ0017	3	33	29	8	16	28
AQ0022	35	33	39	40	35	32
AQ0024	28	24	27	28	24	21
AQ0025	31	41	40	44	39	40
AQ0028	25	67	88	25	29	49
AQ0033	3	3	4	3	3	3
AQ0034	2	4	2	2	3	4
AQ0035	7	11	10	9	9	11
AQ0036	13	18	18	17	19	22
AQ0037	11	41	16	20	26	34
AQ0038	12	14	12	13	11	13
AQ0040	17	22	27	24	16	10
AQ0041	31	41	42	25	26	31
AQ0042	28	21	29	26	25	23
AQ0044	22	17	19	25	21	18
AQ0046	37	37	39	37	37	41
AQ0052	N/D	22	28	26	31	25
AQ0053	N/D	31	39	38	33	23
AQ0054	3	2	3	3	2	2
AQ0067	26	33	31	37	40	35

Photochemical Efficiency Under Different Gas Conditions

Table 13 summarizes the measured F_v/F_m values averaged for 7 consecutive days, at each gas condition. As opposed to the biomass estimates, it is expected that changes in detected biomass concentration (e.g., caused by fouling or clumping, above) does not affect the measured F_v/F_m. Our data indicate that changes in flue gas composition did not induce reductions in the measured F_v/F_m. Thus, the photochemical efficiency of the cells was not negatively affected by

Table 13. Summary of Results from the Flue Gas Experiments: F_v/F_m of the Cells under Pure CO_2 and Five Different Flue Gas Mixtures.
For an explanation of the gas mixtures see Table 2.

Strain	CO₂	MIX A	MIX B	MIX C	MIX D	MIX E
AQ0008	0.72	0.73	0.73	0.72	0.72	0.73
AQ0011	0.73	0.72	0.74	0.73	0.74	0.74
AQ0012	0.41	0.38	0.42	0.36	0.38	0.35
AQ0013	0.77	0.78	0.77	0.78	0.78	0.79
AQ0017	0.76	0.71	0.66	0.73	0.71	0.70
AQ0022	0.76	0.76	0.77	0.77	0.76	0.77
AQ0024	0.73	0.72	0.72	0.73	0.72	0.73
AQ0025	0.72	0.72	0.73	0.71	0.72	0.74
AQ0028	0.79	0.79	0.79	0.80	0.79	0.79
AQ0033	0.63	0.54	0.59	0.63	0.61	0.64
AQ0034	0.57	0.56	0.56	0.53	0.54	0.63
AQ0035	0.55	0.55	0.52	0.58	0.58	0.52
AQ0036	0.61	0.60	0.61	0.60	0.59	0.58
AQ0037	0.50	0.51	0.53	0.54	0.51	0.51
AQ0038	0.31	0.49	0.52	0.32	0.31	0.32
AQ0040	0.73	0.72	0.74	0.73	0.73	0.68
AQ0041	0.69	0.69	0.69	0.71	0.70	0.69
AQ0042	0.74	0.75	0.75	0.75	0.75	0.74
AQ0044	0.73	0.73	0.73	0.74	0.72	0.74
AQ0046	0.73	0.74	0.74	0.73	0.73	0.74
AQ0052	N/D	0.67	0.68	0.67	0.69	0.69
AQ0053	N/D	0.69	0.69	0.70	0.70	0.67
AQ0054	0.70	0.64	0.68	0.63	0.71	0.69
AQ0067	0.71	0.72	0.72	0.71	0.71	0.71

that toxicity (Lee et al., 2000). Furthermore, it has been suggested that NO_x species present in the flue gas can be used as a nitrogen source by the algae (Brown, 1996). NO could oxidize in the medium before being assimilated by the cells (Nagase et al., 1997) or could diffuse directly into the cells where it might be oxidized before being used in the cell's metabolism (Nagase et al., 2001). Our results support the conclusion that SO_x and NO_x components in flue gas do not represent any negative impacts in microalgal photochemical efficiency, as long as the pH of the medium is under control. This can easily be done by buffering the culture medium (e.g., with bicarbonate) and controlling the addition of flue gas to the culture on an on-demand basis as in our system.

4.2.2 Subtask 2.2 - Achievable Photosynthetic Rates, High Value Product Potential and Carbon Sequestration into Carbonates

4.2.2.1 CO_2 Utilization Efficiency

CO_2 Utilization Capacity and Efficiency of a Commercial Microalgal Facility

An analysis of biomass production by the enclosed photobioreactor system at the Mera facility over a 9 month period resulted in production rate of 13 g m^{-2} d^{-1} (Olaizola, 2000) when growing *Haematococcus pluvialis* for the production of astaxanthin. This is equivalent to a photosynthetic CO_2 capture rate of 24 g m^{-2} d^{-1}.

The calculated CO_2 utilization efficiency for Mera's commercial facility for the production of astaxanthin from *H. pluvialis* is about 12.5%. This means that 12.5% of the CO_2 purchased by Mera to control the pH of, and provide carbon nutrition to, its cultures is captured in the biomass harvested. The rest of the carbon is presumably lost to the atmosphere (degassing) and, to some degree, captured as dissolved inorganic carbon forms (HCO_3^- and $CO_3^=$) dissolved in the growth medium (see Section 4.3).

CO_2 Utilization Capacity of Experimental Chemostat Cultures under Different pH and Gas Conditions

Maximum Growth Rates

During the initial batch grow out period of the chemostat cultures, maximum growth rates are observed as the cells' growth is not yet limiting. We pooled the growth data from all the cultures used in the pH and gas tolerance experiments during this initial phase of culture growth. For the 27 strains grown, the calculated maximum growth rates ranged between 0.17 and 0.81 d^{-1} (Figure 29). We consider these rates only to be indicative of potential growth and, thus carbon capture potential into microalgal biomass. It must be kept in mind that in outdoor industrial applications of microalgal photosynthesis growth is always limited, usually by solar flux.
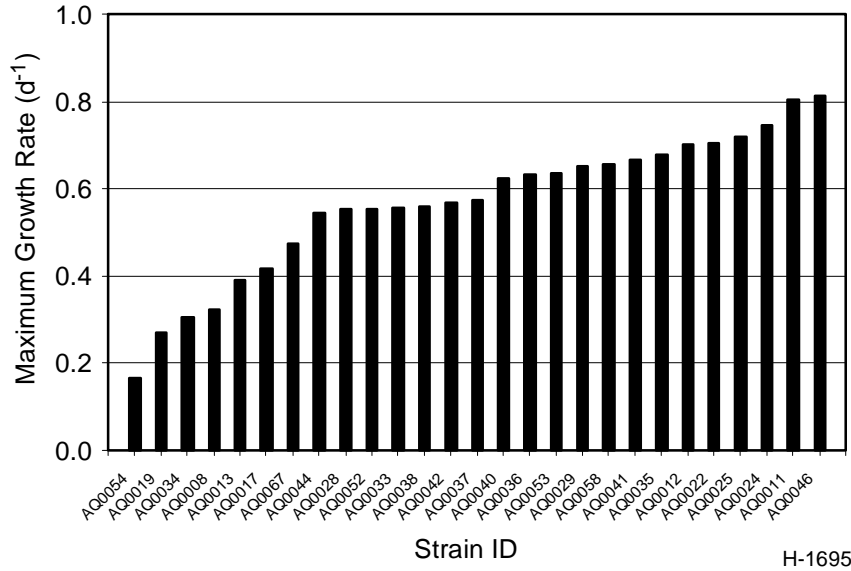
Figure 29. Maximum growth rates obtained during the log phase of growth in chemostat cultures
for 27 microalgal strains.

CO$_2$ Capture Rates by Chemostat Cultures Under Different pH Conditions

Changes in DIC in the cultures were used to estimate the relative importance of pathways that affect the concentration of DIC in the culture medium under different pH conditions. First, we consider the rate of DIC loss from the medium measured during the dark periods (no light available for photosynthesis), for all strains, at three different pH levels. This "dark" rate represents net loses of DIC from the medium (degassing – respiration). The individual dark rate values measured for each strain ranged from less than 0.01 to 0.03, 0.02 to 0.08, and 0.20 to 0.49 at pH 8.5, 7.5 and 6.5 respectively. Thus, at lower culture pH, the DIC loss rates (degassing - respiration) are, on average, much larger than at higher medium pH (Figure 30). Changes in DIC in the cultures were used to estimate the relative importance of pathways that affect the concentration of DIC in the culture medium under different pH conditions. First, we consider the rate of DIC loss from the medium measured during the dark periods (no light available for photosynthesis), for all strains, at three different pH levels. This "dark" rate represents net loses of DIC from the medium (degassing – respiration). The individual dark rate values measured for each strain ranged from less than 0.01 to 0.03, 0.02 to 0.08, and 0.20 to 0.49 at pH 8.5, 7.5 and 6.5 respectively. Thus, at lower culture pH, the DIC loss rates (degassing - respiration) are, on average, much larger than at higher medium pH (Figure 30).

The rates of DIC loss during the light periods represent the net loss of DIC from the medium (degassing + photosynthesis – respiration). We assume that, barring large changes in respiration between dark and light periods, the difference between the "light" and "dark" rates correspond to net photosynthesis. The highest net photosynthetic rate was 0.13 mg CO$_2$ l^{-1} min^{-1} (Figure 31).
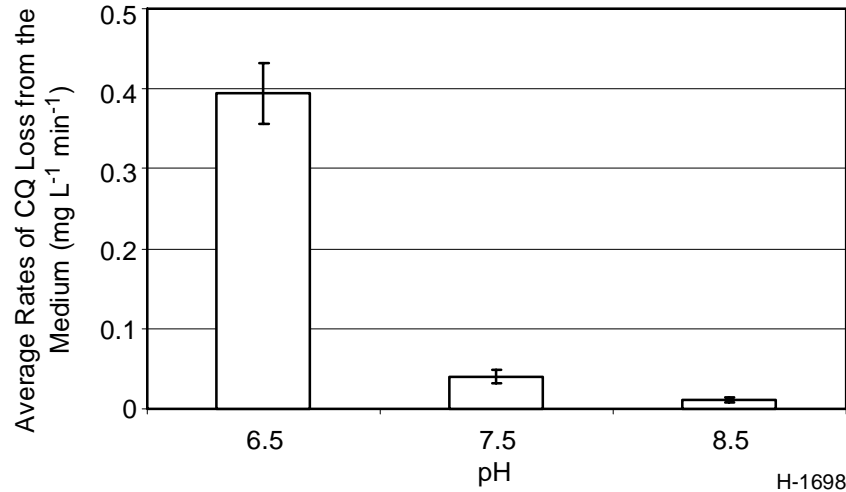
Figure 30. Average rates of CO_2 loss from the growth medium during darkness at three different pH. Error bars are one standard deviation wide.
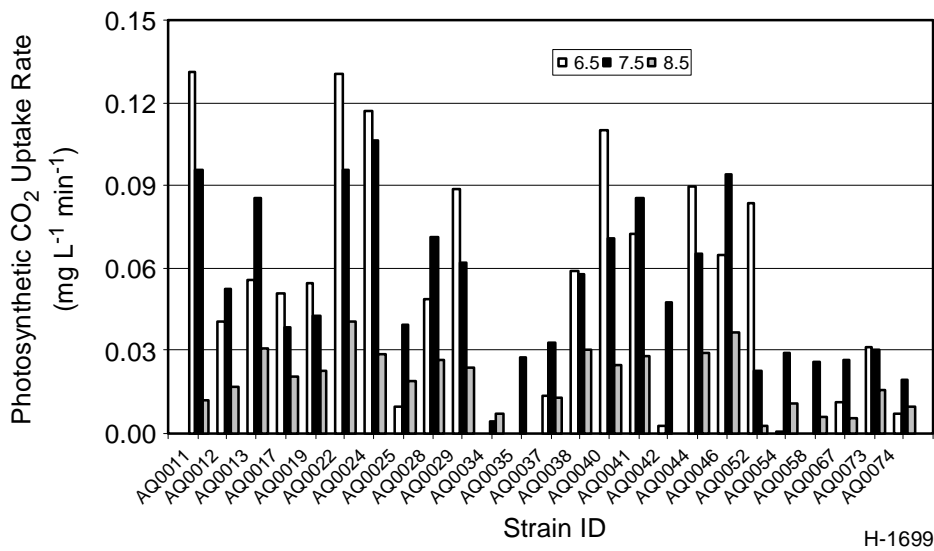
Figure 31. Net photosynthetic rates measured for 25 strains at three pH conditions.

CO_2 Capture Rates by Chemostat Cultures Under Different Gas Conditions

The rate of DIC loss from the medium measured during the dark periods for all strains grown with 100% CO_2 and the five experimental gas mixtures was essentially the same (Figure 32). However, we did find differences between the results obtained here and the results obtained in the pH experiment chemostats at 7.5 pH (Figure 32). The 'dark' rate of DIC loss from the medium was higher in the flue gas experiments. We ascribe this difference to the fact that the gas phase in flue gas chemostats was constantly flushed with atmospheric air (nearly no CO_2) to allow for the removal of excess culture volume.
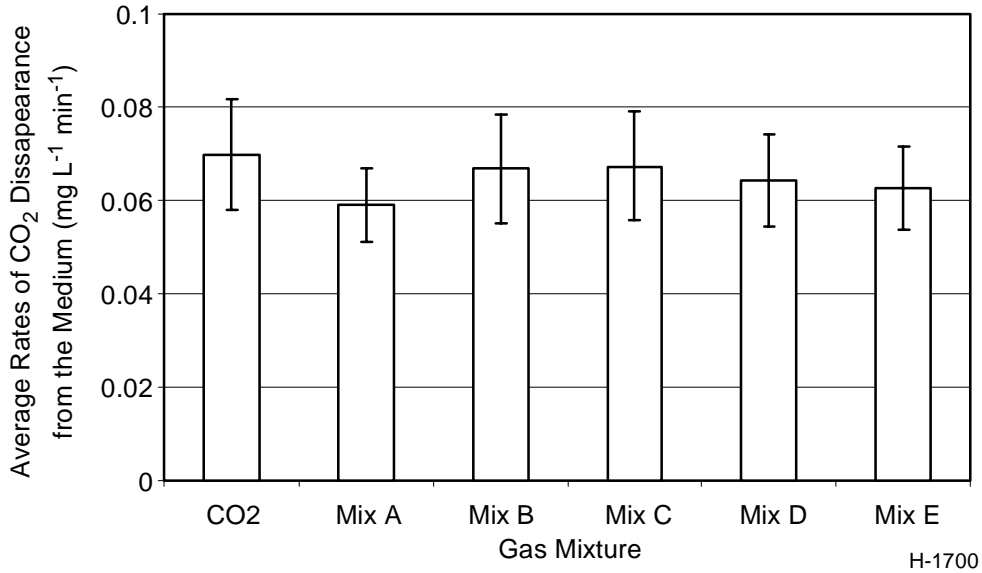
Figure 32. Average rates of CO_2 loss from the growth medium during darkness at 7.5 pH in cultures exposed to 100% CO_2 or one of the five gas mixtures (see Table 2) for an explanation of the gas mixtures). Error bars are one standard deviation wide.

The rates of DIC loss during the light periods represent the net loss of DIC from the medium (degassing + photosynthesis – respiration). As in the pH experiments, we assume that the differences between the "light" and "dark" rates correspond to net photosynthesis. The photosynthetic values thus obtained are summarized in Figure 33 and they indicate large differences among strains.
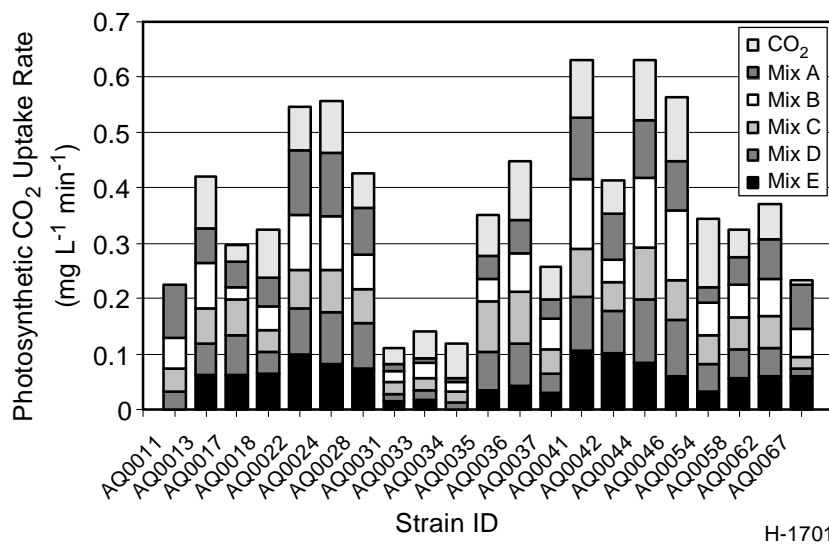
Figure 33. Net photosynthetic rates for 21 microalgal strains exposed to 100% CO_2 or one of the five gas mixtures.

<u>CO$_2$ Utilization Efficiency of Experimental Chemostat Cultures</u>

<u>Effects of pH</u>

We have calculated the efficiency with which microalgae captured CO$_2$ from the medium by normalizing the calculated net photosynthetic rates to the rate of DIC disappearance from the medium during the light periods for each strain. When the efficiency values are plotted against the net photosynthetic rates (above) three different relationships result (Figure 34). It is clear that the efficiency of photosynthetic CO$_2$ capture is, first, dependent on the actual photosynthetic rate accomplished by the cultures (the actual data points on the three different lines in the figure) but, second, also dependent on the pH of the culture (i.e., the difference between the three lines). The results indicate that, on average, the efficiency of photosynthetic CO$_2$ capture is higher at higher medium pH values, i.e., the probability for CO$_2$ to be lost from the medium back to the gas phase is less at high pH.
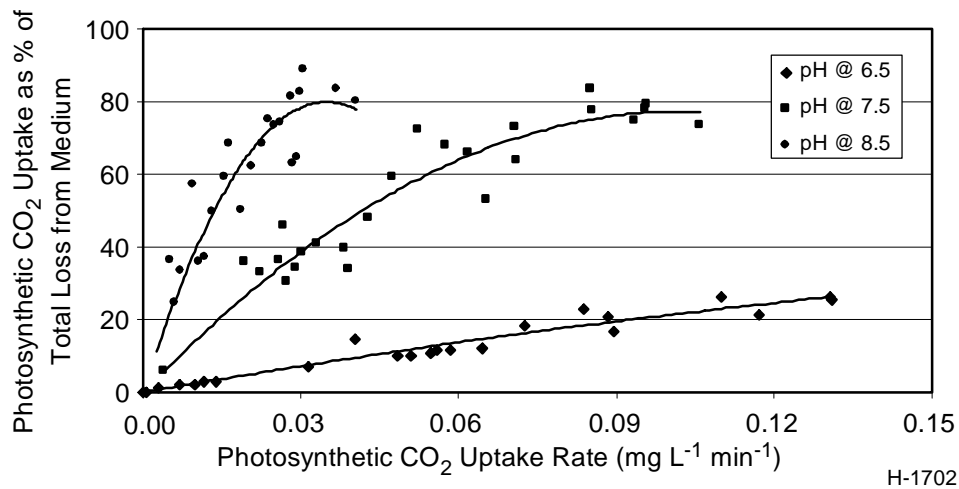
Figure 34. Relationship between photosynthesis and the percent efficiency of photosynthetic CO$_2$ capture from the medium at three different pH.

<u>Effects of Gas Composition</u>

For this set of experiments, the relationships between photosynthetic rate and CO$_2$ capture efficiency are indistinguishable for the 5 gas mixtures and the 100% CO$_2$ treatment (Figure 35). However, the slope of those relationships is less for these cultures than for the cultures kept at 7.5 pH during the pH experiments (Figure 36). This means that renovation of the headspace in the gas chemostats with atmospheric air resulted in lowered CO$_2$ capture efficiencies for those cultures.

68
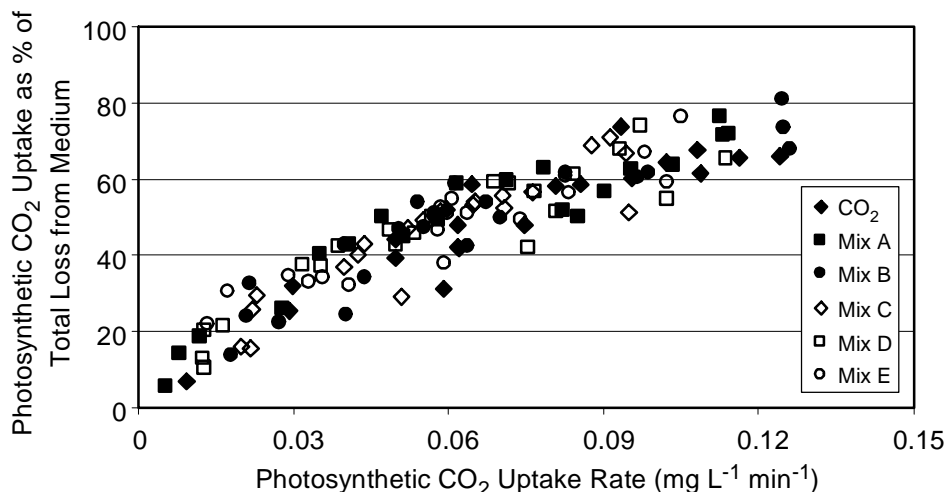
Figure 35. Relationship between photosynthesis and the percent efficiency of photosynthetic CO_2 capture from the medium for cultures exposed to 100% CO_2 or one of the five gas mixtures.
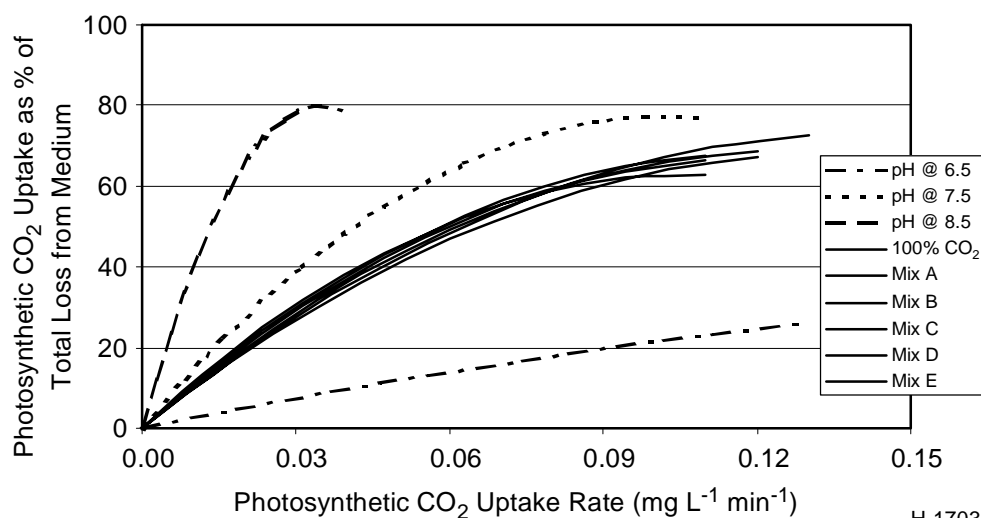
H-1703

Figure 36. Comparison of the relationship between photosynthesis and the percent efficiency of photosynthetic CO_2 capture from the medium for cultures exposed to three different pH plus the cultures exposed to 100% CO_2 or one of the five gas mixtures.

Here, we have investigated the effects of culture medium pH and flue gas composition on the efficiency of CO_2 capture by over 20 microalgal strains at the laboratory bench scale. Our results indicate that the pH of the culture medium is a critical determinant of the efficiency of CO_2 capture from the medium by microalgae. First, we found that the rate of CO_2 degassing from the culture medium (i.e., lost from the system and unavailable for photosynthesis) is much higher at 6.5 than at 7.5 and 8.5 pH (Figure 34). However, on average, photosynthetic rates for most of the strains used was higher at pH 6.5 and 7.5. This means that to maximize absolute CO_2 capture one would want to control the culture medium's pH at 6.5. However, such a system

69

would be relatively inefficient: According to the relationships described in Figure 34, in a culture with a photosynthetic rate of 0.03 mg CO_2 l^{-1} min^{-1}, about 93% of the available DIC in the medium would be lost to the atmosphere. On the other hand, in a culture with the same photosynthetic rate but maintained at 7.5 and 8.5 pH the losses would amount to 61% and 22% respectively.

Using simulated flue gases and pure CO_2, we subjected our cultures to 5.7-100% CO_2, 0-3504 ppm SO_2, 0-328 ppm NO, and 0-126 ppm NO_2. Individual strains showed changes in photosynthetic rate when exposed to the different gas mixtures (Figure 33) but found that flue gas composition had no effect on the relationship between photosynthetic rate and the CO_2 capture efficiency (Figure 35). We had also suspected that use of combustion gases containing NO_X and SO_X (see Table 2) might lower the CO_2 capture efficiency by acidifying the medium (e.g., [12, 13]) but this was not the case. However, the CO_2 capturing efficiencies measured in the flue gas experiments (run at 7.5 pH) was lower than those measured during the pH experiments at 7.5 pH (Figure 36). We ascribe this difference to the fact that the gas phase in the former was flushed with air to allow for the removal of excess culture volume. Flushing with air would have lowered the concentration of CO_2 in the gas phase above the culture medium which, in turn, would have increased the rate of CO_2 degassing from the medium, as our results show. This implies that photobioreactor design parameters will also have a bearing on the CO_2 capture efficiency of the microalgal cultures (e.g., airlift driven versus pump driven photobioreactors).

If we consider the individual values for each culture, we find that there is large variability in photosynthetic rates under different culture conditions among the strains (Figure 31 and Figure 33). Previously we showed that changes in pH and flue gas composition did not negatively affect the, dark adapted, maximum photochemical yield of microalgal cultures (Figure 28, Table 13). A discussion on the reasons why different strains respond differently pH conditions is beyond the scope of this manuscript (e.g., presence or absence of a carbon concentrating mechanism, ability to take up bicarbonate from the medium, differences in respiration rates or pH- and gas-related toxicities). However, it is noteworthy that the relationships between culture pH and the efficiency of CO_2 uptake from the medium are consistent over a large range of photosynthetic rates (e.g., Figure 36).

From an industrial point of view, we can envision how culture strategies may be optimized for a particular application. First, changes in culture pH are expected to cause differences in CO_2 capture efficiency independently of the culture's photosynthetic rate (Figure 34). Second, our results show that differences in reactor design will similarly cause differences in capture efficiency (Figure 36). While these results apply specifically to the vessels used here it is expected that changes in reactor design and culture management at larger scales will also result in differences in the efficiency of CO_2 capture from the medium (e.g., Mazzuca-Sabczuk et al., 2000).

In real world applications of CO_2 capture by microalgae, two scenarios are envisioned, taking into account that outdoor microalgal cultivation productivity maximizes at about 110 g CO_2 captured m^{-2} d^{-1} (see above). First, we consider a power plant that is not limited by the availability of surrounding land area for microalgal cultivation. By this definition, this power plant should be able to capture all the CO_2 that it produces during the generation of electricity.

To capture all the CO_2 produced this power plant would be expected to strive to be as efficient as possible either by selecting for microalgae that perform satisfactorily at a relatively high pH and utilizing efficient reactor designs (Tredici, 2003) or by recycling the gases after passage through the culture. Second, we consider a power plant limited by the amount of land surface available for microalgal cultivation. Let us assume that only 20% of the CO_2 generated can be captured, i.e., 80% of the CO_2 emissions will be lost to the atmosphere. Here, the CO_2 capture efficiency of the culture is not important but the productivity per m^2 is. Thus, the strategy in this scenario would be to select for the most productive algae and reactor design (on a m^{-2} basis), even at low capture efficiencies such as at low pH. Indeed, a number of efforts have been carried out to select for microalgal species amenable to this application (Chang et al., 2003; Maeda et al., 1995; Murakami and Ikenouchi, 1997; Sung et al., 1999).

4.2.2.2 <u>Production of High Value Products to Offset Cost of Carbon Sequestration</u>

Microalgae are a diverse group of over 30,000 species of microscopic plants that have a wide range of physiological and biochemical characteristics. Microalgae produce many different substances and bioactive compounds (Borowitzka, 1995) that have existing and potential applications in a variety of commercial areas, including human nutrition, pharmaceuticals, and high value commodities. Algal pigments (carotenoids and phycobiliproteins) are one such group of molecules. Examples of natural algal pigments that already been commercialized include B-carotene (food additive grade worth about $1,400 per kg, market size estimated >$500 million per year), astaxanthin (feed additive grade worth about $2,500 per kg-market size about $200 million - but up to >$100,000 per kg for nutraceutical grade-market size not know at this point).

<u>Pigment Concentrations of Microalgae Grown under Standard Conditions</u>

We have analyzed the pigment content of 34 different microalgal strains. First we will report on results of pigment analysis carried out on microalgal cultures grown under standard conditions (temperature: 25°C; irradiance: 60 uE m^{-2} s^{-1}; light/dark: 14 hr/10 hr).

The first group of strains for which we report pigment content was made up of 11 cyanobacterial strains grown in batch cultures. This group was tested first since the Cyanobacteria are good potential candidates as sources of high value pigments. Two different cultures were analyzed from each strain; a relatively young culture and a relatively older culture (Figure 37). The most abundant carotenoids present in these strains are zeaxanthin and B-carotene and are reported as the mass ratios to chlorophyll-a, an indicator of algal biomass. B-carotene is used widely as a food coloring in margarine, butter, drinks, cakes and candies. It is also sold as a nutritional supplement or nutraceutical. Zeaxanthin is a carotenoid believed to be important in human nutrition and, specially, eye health. Of the 11 strains tested, AQ0012 showed potential as a source of zeaxanthin. Five other strains may be considered potential sources of B-carotene, also a high value pigment. All strains had phycobiliproteins as part of their pigment complement (characteristic of the Cyanobacteria). Of those, seven strains contained phycocyanin and four contained phycoerythrin. The phycobiliproteins are also high value molecules used to produce fluorescent probes useful in diagnostic biochemistry.

A second group of pigment analysis was carried out on strains grown at the flask scale (150 ml cultures) also grown under standard conditions. These strains represent the microalgal Classes Chlorophyceae, Bacillariophyceae, Eustigmatophyceae and Prymnesiophyceae. The results of that analysis are summarized in Figure 38. Based on the results obtained we consider strain AQ0056 (a diatom, Bacillariophyceae) a possible good source of fucoxanthin. Recent reports in the literature indicate that fucoxanthin may have anticancer activities (Kim et al., 1998). Our results also indicate that strain AQ0059 can be considered a good source of lutein. Lutein, as zeaxanthin, has been identified as a carotenoid with application in human eye health.

A third group of pigment analysis was carried out on strains grown at the chemostat scale (3.3 liters) under standard conditions. In this group we have representatives of the Chlorophyceae, Bacillariophyceae and Cyanophyceae. The results of that analysis are summarized in Figure 39. Based on those results we can consider strain AQ0038 a very good source of lutein (even better than strain AQ0059, Figure 38). Strain AQ0042 can also be considered a good source of the high value carotenoids lutein and B-carotene. Finally, strain AQ0044 can be considered a good source of carotenoid complex or mixture since it contains high levels of B-carotene, lutein and violaxanthin. Although violaxanthin has not yet been identified as a high value carotenoid it can be considered a precursor of zeaxanthin (via the xanthophyll cycle, Yamamoto and Kamite, 1972).
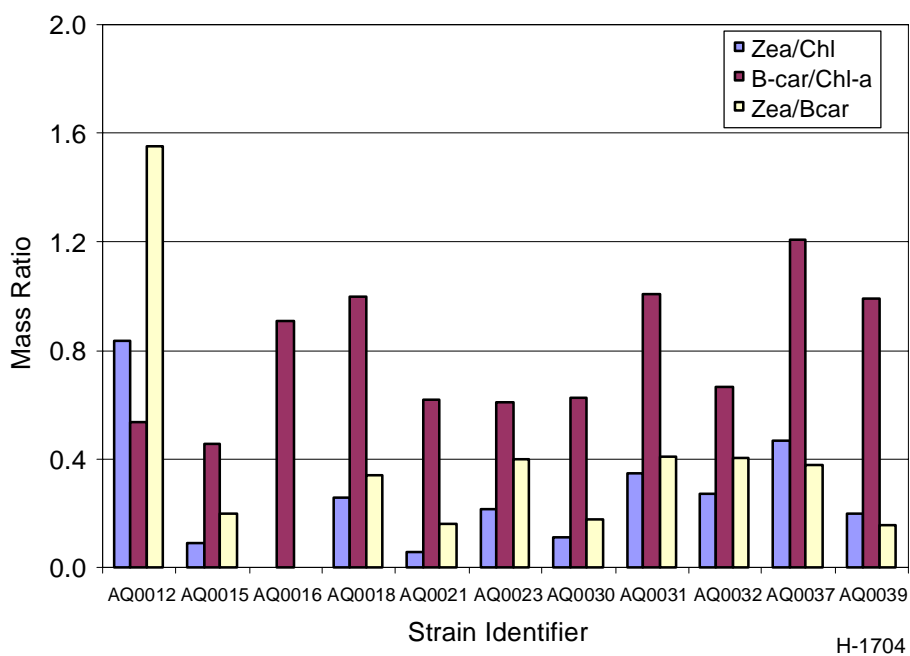
Figure 37. Summary of carotenoid pigment analysis of 11 strains of Cyanobacteria. Zea/Chl: mass ratio of zeaxanthin to chlorophyll-a, B-car/Chl: mass ratio of B-carotene to chlorophyll-a, Zea/Bcar: mass ratio of zeaxanthin to B-carotene. The values reported are the average of measured concentrations in two different cultures of each strain.
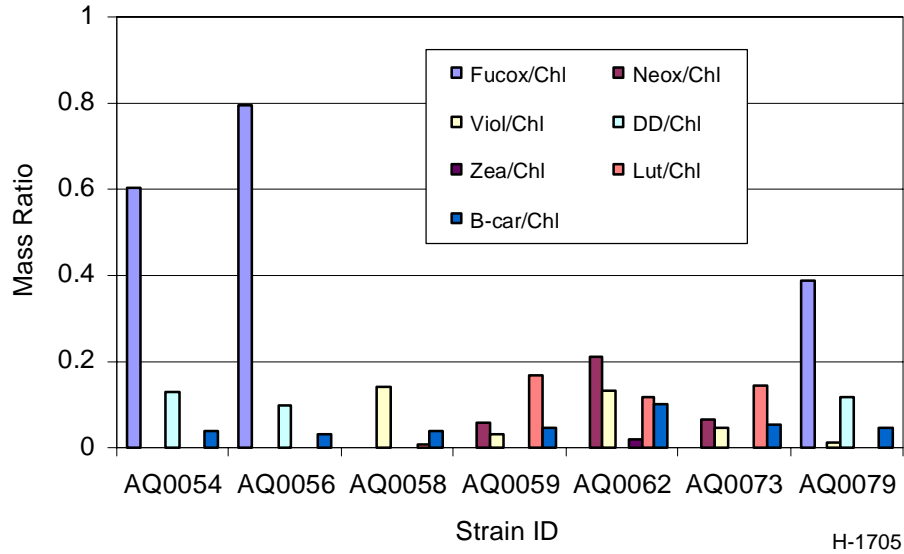
Figure 38. Summary of carotenoid pigment analysis of 6 microalgal strains grown at flask scale (150 ml). Fucox: fucoxanthin; Neox: neoxanthin; Viol: violaxanthin; DD: diadinoxanthin; Lut: lutein; Zea: zeaxanthin; B-car: B-carotene; Chl: chlorophyll-a.
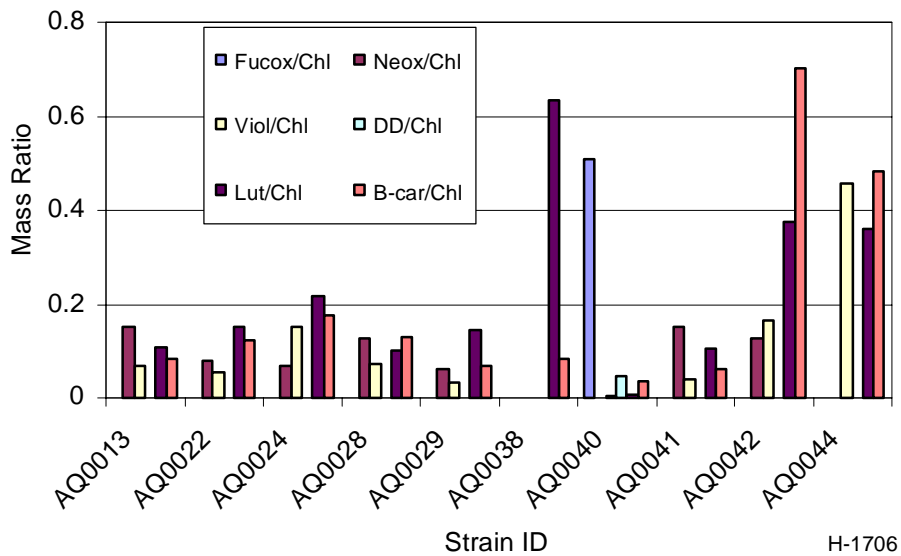
Figure 39. Summary of carotenoid pigment analysis of 10 microalgal strains grown at chemostat scale (3.3 l). Fucox: fucoxanthin; Neox: neoxanthin; Viol: violaxanthin; DD: diadinoxanthin; Lut: lutein; B-car: B-carotene; Chl: chlorophyll-a.

Pigment Concentrations of Microalgae Grown under Non-Standard Conditions

Light Intensity Experiments

Irradiance readings from roof top solar panels recorded the sunlight intensity on the dates when the light intensity experiments were conducted (Figure 40). Decreases in intensity represent clouds. PAM data showed that after one hour in the sun, 30% of the reaction centers were functional and remained functional throughout the 5 hour period (Figure 41).
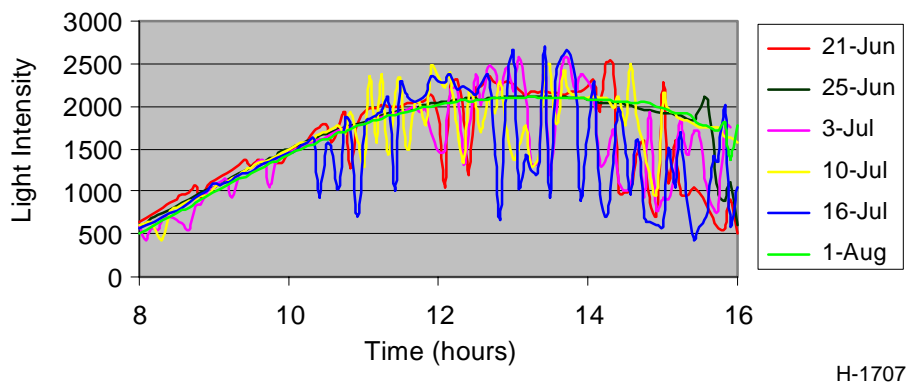
Figure 40. Light intensity ($\mu E\ m^{-2}\ s^{-1}$) measured outdoors on days when light experiments were carried out with strains AQ0011 (6/21, 7/11), AQ0012 (6/25, 7/11), AQ0052 (7/3, 7/11), AQ0053 (8/1), AQ0033 and AQ0036 (7/16).
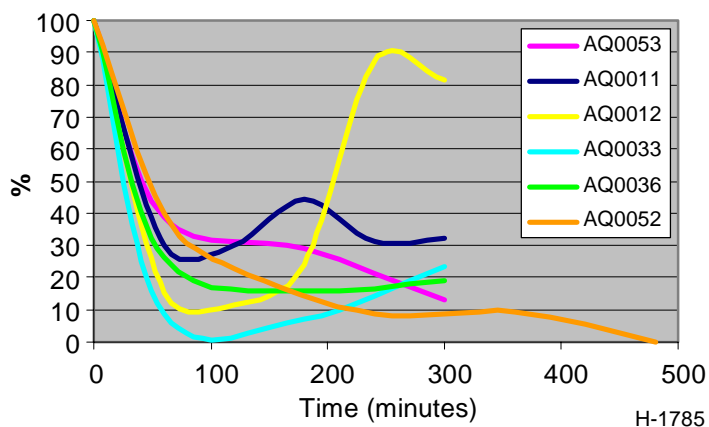
Figure 41. Percent functional reaction centers for each species from initial sample to final calculated with PAM Fv/Fm reading.

The unidentified chlorophyte AQ0011 did not increase in biomass during the 5 hour period. HPLC confirmed the presence of large amounts of lutein present throughout the experiment, as percent lutein per dried biomass increased from 0.25% (initial) to 0.28% (5 hour). Initially, no zeaxanthin was detected by HPLC, but after five hours, the percent zeaxanthin per ml dried biomass had increased to 0.12%. Lutein and Zeaxanthin increased per volume as well

74

(Figure 42). In addition, a small amount of β-β carotene was present in varying levels throughout the experiment. Examples of HPLC chromatograms are shown in Figure 43.
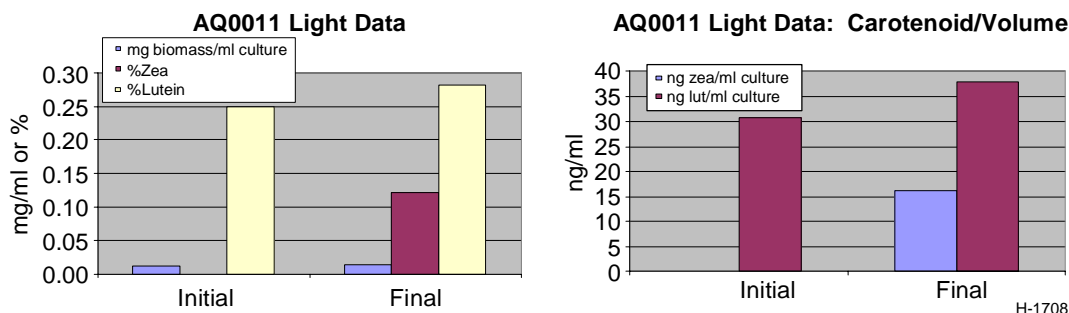
Figure 42. Biomass and % carotenoids from initial (0 hr) to final (5 hr) after intense light exposure (left panel) and carotenoid amount per culture volume initially and after 5 hr of intense sunlight (right panel).
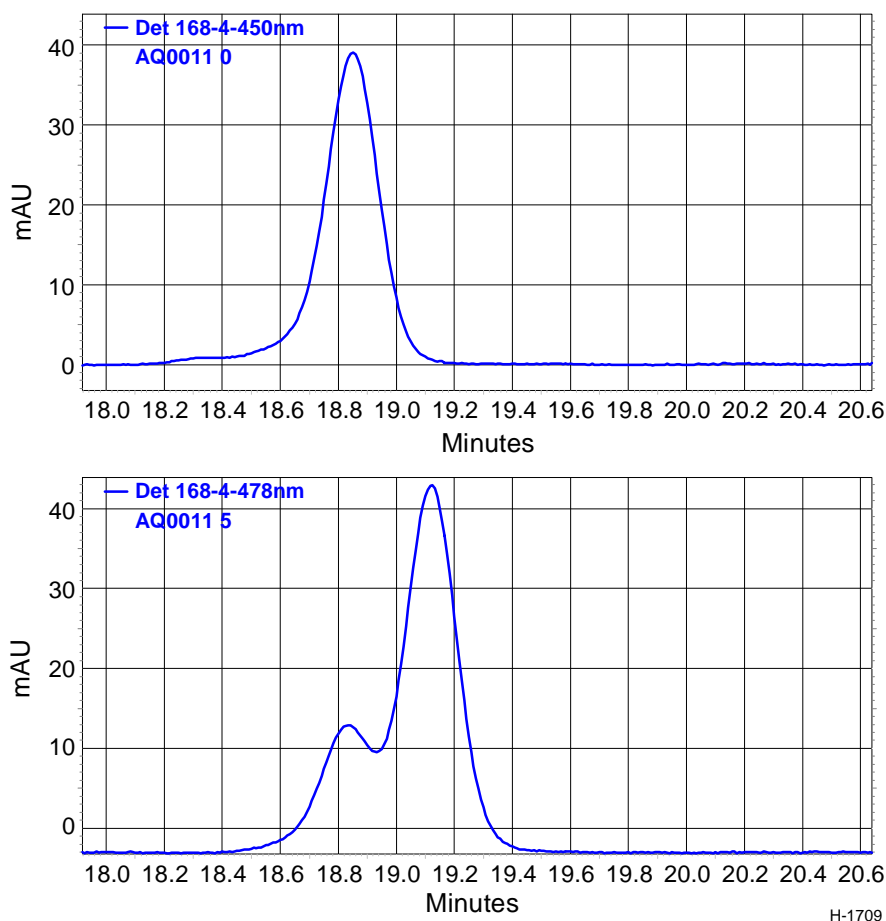
Figure 43. AQ0011 HPLC chromatogram showing the lutein peak at 0 hr: no zeaxanthin present (top panel). AQ0011 HPLC chromatogram of the 5 hr sample. Zeaxanthin peak present at base of the lutein peak (bottom panel).

The biomass of AQ0012, an unidentified strain of cyanobacteria, increased through time. After one hour of light exposure, the biomass in the flask was floating at the top of the liquid in a tight clump. It is likely that this is morphological defense mechanism of the microalgae to increase shading of the cells. Data collected with the Pulse Amplitude Modulator (PAM) in the light show that after two hours of intense light exposure, only one-tenth of the initial reaction centers are functioning (Figure 44). HPLC analysis revealed the initial percent of zeaxanthin per dried biomass to be 0.15% and final percentage was 0.14%. The amount of zeaxanthin per volume increases proportionately with the increasing biomass (Figure 44). It was also noted that AQ0012 produced β-β carotene, but the amount was small and did not change significantly with time.
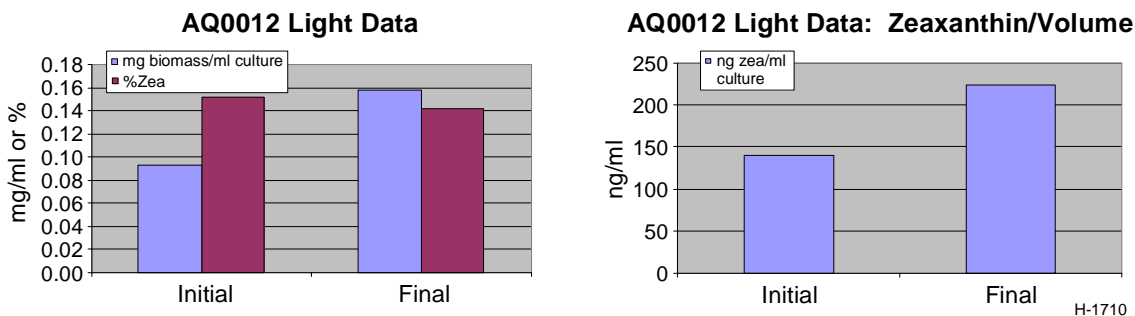
Figure 44. Biomass and % zeaxanthin from initial (0 hr) to final sample (5 hr) (left panel and zeaxanthin measured per culture volume from initial (0 hr) to final (5 hr) (right panel).

Dunaliella strain AQ0052 was exposed to intense sunlight for a period of 8 hours to determine if extended light exposure would induce additional zeaxanthin production. After two hours of sunlight, 22% of reaction centers were operating, and this percentage continued to decrease until no reaction centers were functional at 8 hours (Figure 45). The biomass increased slightly, and the zeaxanthin increased from 0% to 0.05% per dried biomass. AQ0052 also contained lutein, which decreased during the light exposure from 0.2% to 0.11% per ml dried biomass. Chlorophyll a decreased dramatically throughout the experiment, and was not detectable in the 8 hour sample by HPLC.
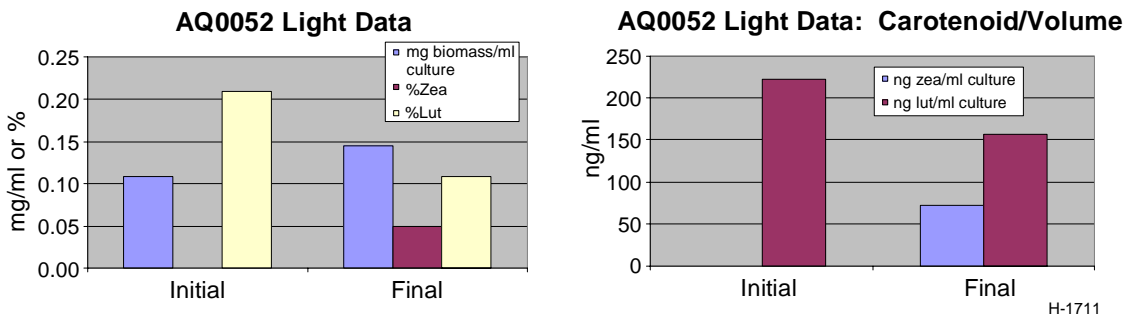
Figure 45. Biomass and % carotenoids from initial sample (0 hr) to final sample (8 hr) (left panel) and carotenoid per volume of culture from initial (0 hr) to final sample (8 hr of intense sunlight) (right panel).

76

Dunaliella strain AQ0053 was exposed to intense light conditions for 5 hours and PAM data showed that after 5 hours of intense light exposure, 12% of reaction centers were functioning (Figure 46). The biomass began to settle to the bottom center of the 1000 mL flask during the experiment, and some small clumps of cells were visible at the end of the time period. Biomass increased from initial to final sample. HPLC data showed that the % lutein increased from 0.31% to 0.35% per dried biomass. Lutein also increased on a volumetric basis.
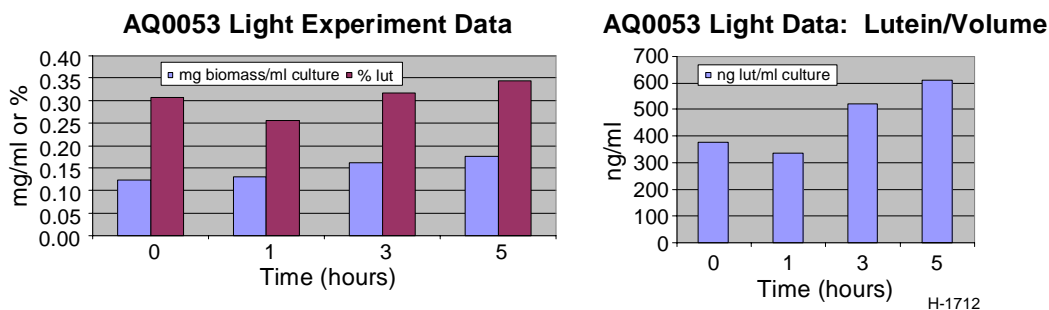
Figure 46. Biomass and % lutein after 0, 1, 3, and 5 hours of intense light (left panel) and lutein per culture volume (right panel).

Strain AQ0033 (*Porphyridium*) was exposed to intense light conditions for 5 hours, and the biomass decreased slightly. Similar to AQ0012, the biomass clustered together in the flask, but formed a loose mass rather than a tight clump. PAM data showed that only 7% of reaction centers were functional after 3 hours of sunlight (Figure 41). HPLC data confirmed that the 0 hour sample contained 0.2% zeaxanthin per dried biomass, a value higher than any percent zeaxanthin obtained. However, after intense light exposure, this amount decreased to 0.1%.

The biomass of *Porphyridium* strain AQ0036 significantly increased during the 5 hour experiment. PAM data showed that after one hour of light exposure, 25% of the reaction centers that harvest light for photosynthesis were operating (Figure 47). This number remained fairly constant throughout the experiment. The amount of zeaxanthin per dried biomass also decreased from 0.13% to 0.05% (Figure 47).
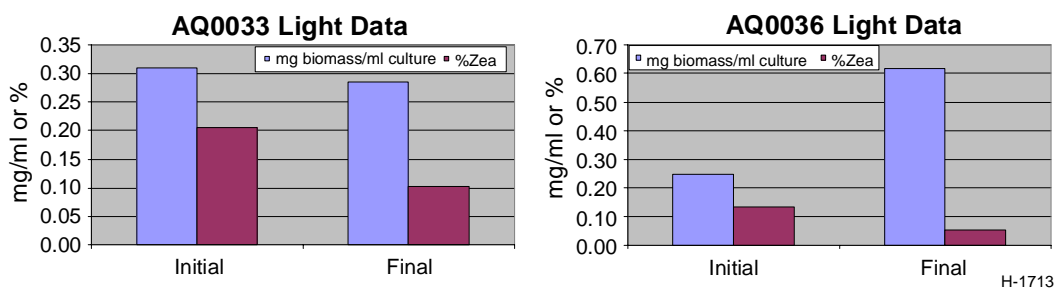
Figure 47. Biomass and zeaxanthin from initial (0 hr) to final sample (5 hr) for strains AQ0033 (left panel) and AQ0036 (right panel).

Zeaxanthin decreased on a per volume basis as well for AQ0033 (Figure 48) and stayed constant for AQ0036. The reasons for the measured decrease are unknown and are still under investigation. It is possible that because *Porphyridium* was originally a soil algae (Lee, 1989), these strains do not have the ability to efficiently adapt under intense light.

AQ0033 and AQ0036 Light Data
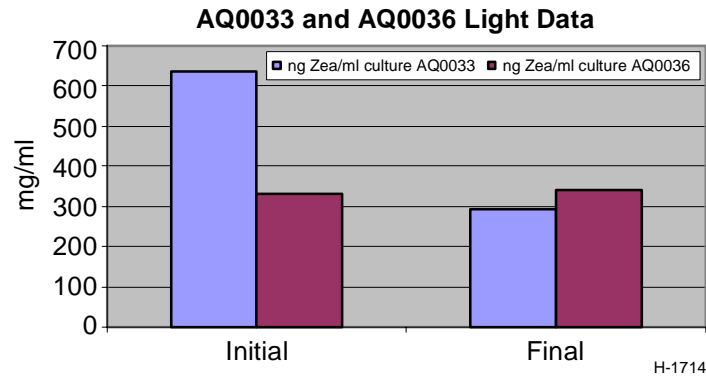
Figure 48. Zeaxanthin per culture volume from initial (0 hr) to final sample (5 hr) for strains AQ0033 and AQ0036.

Nitrate Deprivation Experiments

Daily PAM readings showed that the Fv/Fm values varied greatly for each strain tested. In Figure 49, the slope of the line for AQ0033 was –0.0218, representing the rate of decrease in F_v/F_m. A flask of AQ0033 was broken on day 9 of the experiment, but data until this point was included in the analysis. For AQ0036, the linear regression line was nearly flat, with a slope of -0.0039. The slope for AQ0011 also decreased, but at a rate of –0.0167. In addition, the line for AQ0012 had a negative value of -0.0019, which represents that the cells were experiencing only slight stress after ten days of nitrate deprivation.
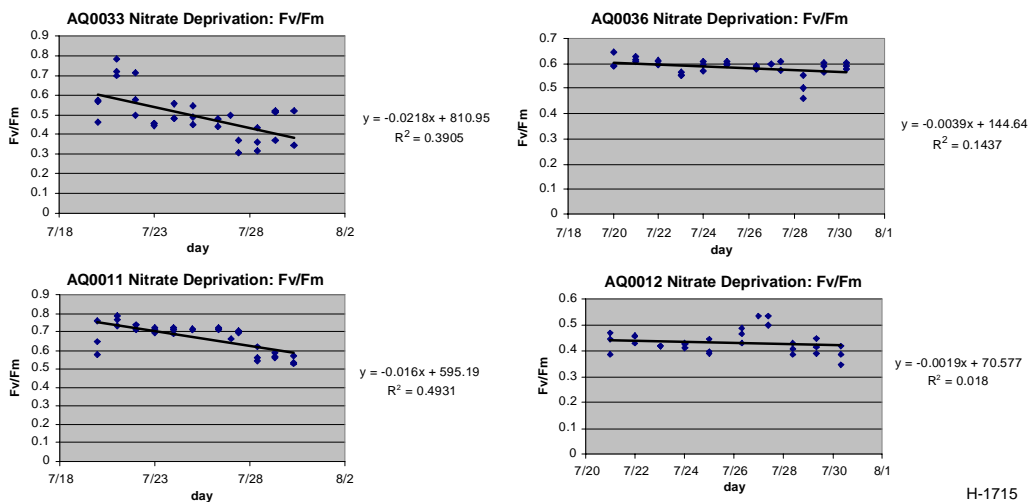
Figure 49. F_v/F_m readings from PAM data over 10 day nitrate deprivation experiment with linear regression analysis for strains AQ0033, AQ0036, AQ0011 and AQ0012.

78
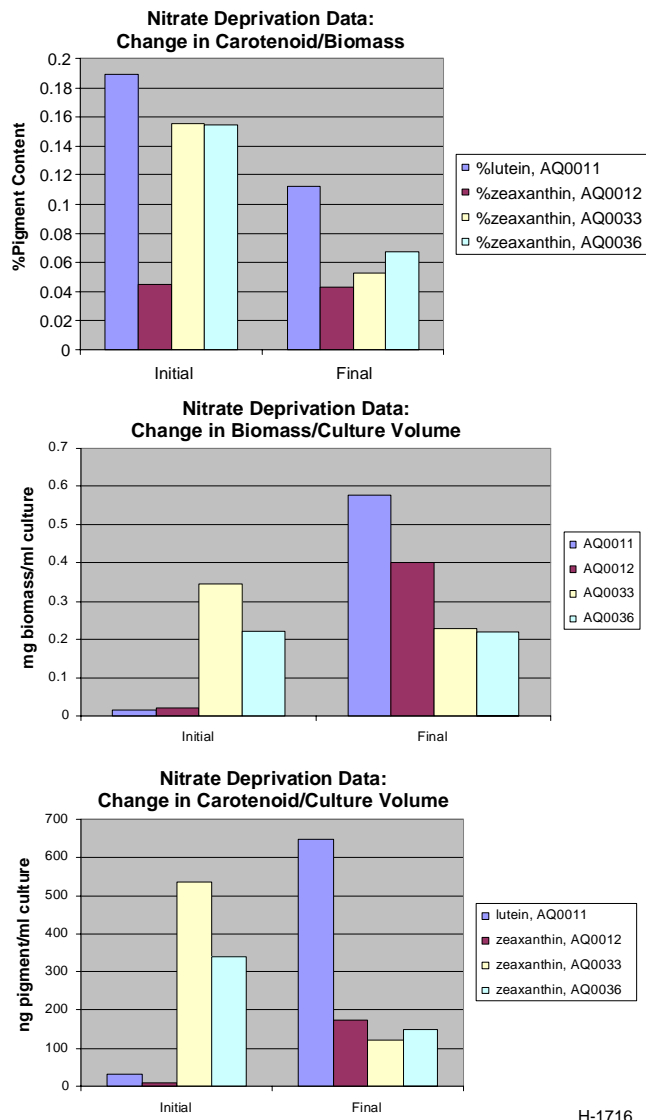
Figure 50. Carotenoid percentages per biomass, biomass per culture volume and carotenoid per culture volume over 10 day nitrate deprivation experiments.

Salt/Sodium Acetate Experiments

PAM data showed that the F_v/F_m values of AQ0053 were the same for the initial samples before additions of salt and/or sodium acetate were made compared to the F_v/F_m values immediately after the additions. However, the F_v/F_m value decreased from 0.7 on day one to 0.2-0.3 on day 2. The dramatic decrease was unexpected, and it is possible that the media was contaminated or that the concentrations were higher than calculated.

The biomass per culture volume increased for all flasks slightly during the 3 day experiment, with the greatest increase seen in the flasks with NaCl and NaAc in combination. AQ0053 produced lutein initially at 0.34% per dried biomass, a level higher than any carotenoid for all strains. The % lut decreased for all flasks from initial to final sample, with the lowest value for the NaCl/NaAc flasks at 0.09% (Figure 51). The amount of lutein decreased for all samples volumetrically as well.
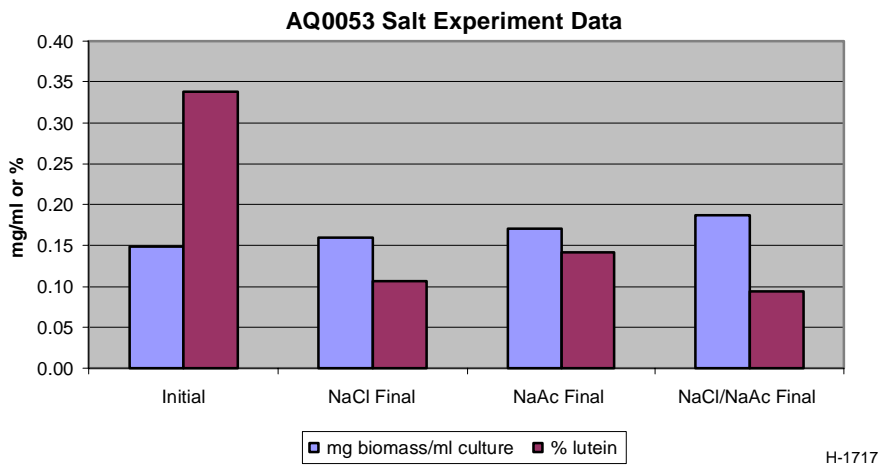
Figure 51. Biomass and % lutein for initial sample (0 day) and samples with additives after 3 days.

Potential for Commercial Production

One goal of these experiments was to determine which strains would be worthwhile to grow at a commercial level to offset the cost associated with microalgal mediated carbon sequestration. The pigment composition of each strain was analyzed before and after exposure to environmental stress to evaluate how the stress affected pigment production. This research was conducted at Aquasearch Inc., where the 25,000 L enclosed outdoor photobioreactors, known as the Aquasearch Growth Modules (AGMs), are producing *Haematococcus pluvialis* at a rate of 9 to 13 g m^{-2} d^{-1} (Olaizola, 2000). Similar growth rates or higher could be expected by growing the tested strains in the AGMs. For AQ0033, AQ0036, AQ0012, and AQ0052 the highest % zea was found in the initial sample before treatment with environmental stress (Table 14). Thus, the most pigment per dried biomass was produced when the cultures were grown in nutrient rich media at low light intensities. On the other hand, AQ0011 and AQ0053 produced the greatest amount of pigments after 5 hours of intense light exposure. AQ0052 produced the most lutein without treatment, but produced a small amount of zeaxanthin after 8 hours of intense sunlight. The ability of AQ0011 to produce both lutein and zeaxanthin makes it a highly attractive strain to grow in the AGM. AQ0053 could be expected to produce 0.04487 g m^{-2} d^{-1} lutein after 5 hours of intense light exposure, which is the highest value found of any carotenoid of any strain in this study. The values in Table 14 most likely represent the minimal amounts of carotenoids that can be obtained from these strains, as yields will increase with optimization of mass cultures.

Table 14. Highest percent carotenoids per dried biomass obtained in experiments
and predicted pigment production rates at a production rate of
13 g dry biomass m^{-2} d^{-1}, a typical rate of Aquasearch growth modules

Strain	Treatment Which Gave Highest % Pigment	Pigment	% Pigment	Production @ Growth Rate of 13 g m^{-2} d^{-1}
AQ0011	5 hours sunlight	Lutein	0.28	0.037 g m^{-2} d^{-1}
AQ0011	5 hours sunlight	Zeaxanthin	0.12	0.016 g m^{-2} d^{-1}
AQ0012	No treatment	Zeaxanthin	0.15	0.020 g m^{-2} d^{-1}
AQ0033	No treatment	Zeaxanthin	0.21	0.027 g m^{-2} d^{-1}
AQ0036	No treatment	Zeaxanthin	0.13	0.017 g m^{-2} d^{-1}
AQ0052	No treatment	Lutein	0.21	0.027 g m^{-2} d^{-1}
AQ0052	8 hours sunlight	Zeaxanthin	0.05	0.006 g m^{-2} d^{-1}
AQ0053	5 hours sunlight	Lutein	0.35	0.049 g m^{-2} d^{-1}

4.2.2.3 <u>Carbon Sequestration into Carbonate Minerals Utilizing Microalgae</u>

One of the goals of this project is to identify under what conditions microalgal cultures can be induced to precipitate $CaCO_3$. This would represent a stable, long term, sink of atmospheric CO_2, a goal of the US Department of Energy. Initially, we proposed to carry out this research by growing microalgal species known to produce cellular structures out of $CaCO_3$. We have decided to take the concept a step further. We have endeavored to describe culture conditions that will induce the precipitation of carbon into $CaCO_3$ via photosynthetically mediated changes in medium pH. As cells photosynthesize and take up CO_2 from the culture medium, the pH of the medium raises. This change in pH produces an increase in the concentration of CO_3^{2-} ions in the medium. In the presence of sufficient amounts of Ca^{2+} $CaCO_3$ is expected to precipitate out of solution. Because the photosynthetically mediated change in pH is not specific to species that produce cellular carbonate structures, in principle, any species of microalgae could be used for this process.

Initial experimentation with species AQ0011 gave no visual indication that $CaCO_3$ precipitation via algal mediation could occur under the conditions tested with these species. Flasks lacking bicarbonate did not increase in biomass and did not produce data indicative of $CaCO_3$ formation. This was possibly due to the intolerance of algae to the low pH of the growth medium caused by lack of HCO_3^-. After examining the ion concentrations of the media enriched with bicarbonate, it was apparent that a portion of carbon was missing from the calcium-enriched medium (Figure 52). A greater decrease in total inorganic carbon concentration, along with a decreased amount of dissolved carbonate ions in the calcium-enriched flask with bicarbonate indicates the possible formation of $CaCO_3$ (Figure 48). However, this was not visually confirmed through identification of $CaCO_3$ particles or through a reaction of the filtrate with concentrated HCl.
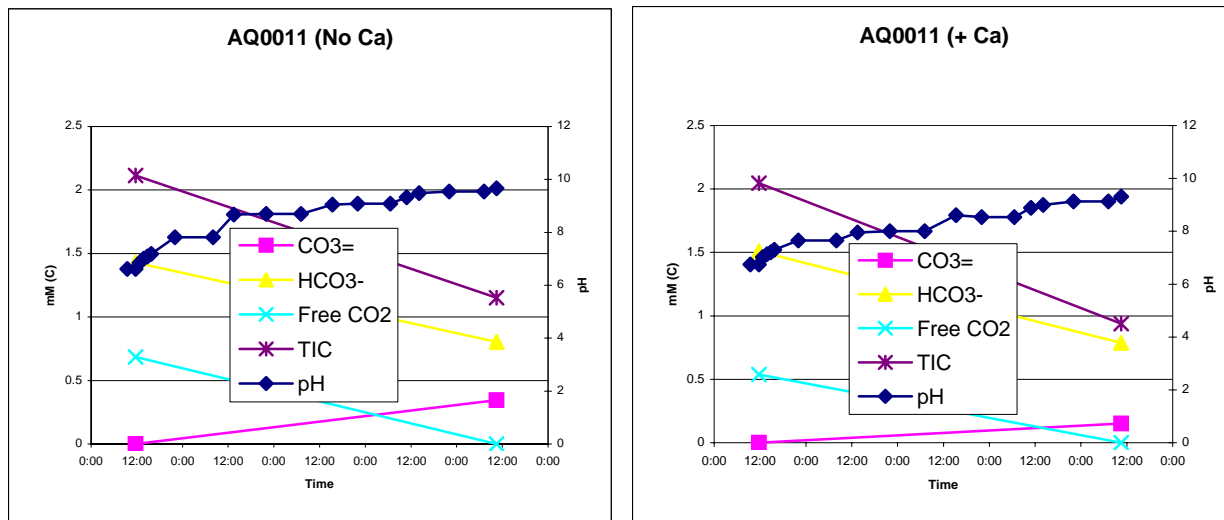
Figure 52. pH and dissolved inorganic carbon species concentrations in AQ0011 without Ca (left panel and with Ca (right panel)

A second experiment with AQ0011 demonstrated similar ion concentrations, although the second experiment displays a clearer depiction of differences in ion concentrations in control and experimental flasks (Figure 53). The solid was identified as $CaCO_3$ due to the identification of a reaction occurring after the addition of concentrated HCl. Results from the second experiment with AQ0011 were more conclusive because of the method of testing for $CaCO_3$ precipitate. In the initial experiment, the contents of each flask were filtered and exposed to HCl while still damp. Centrifuging and drying of the pellets from each flask better prepared the samples for the "bubble test" with concentrated HCl. In both experiments, it can be recognized that as the pH of the medium increases, the carbon species shift towards CO_3^{-2}. In flasks with Ca, the CO_3^{-2} concentrations are significantly lower than those not enriched with calcium, indicating the binding of CO_3^{-2} ions with the Ca^{2+} ions in solution and ultimately the formation and precipitation of $CaCO_3$. The precipitate was not visually apparent due to the biomass of algae in the flasks and the small particle size of the $CaCO_3$ crystals. This dust-like form of $CaCO_3$ is similar to that identified as the source of Bahamas whiting incidents where biologically induced precipitates cloud surface waters (Robbins and Yates 2001).

Experimentation with Cyanobacteria species AQ0012 also yielded promising results. The initial experiment resulted in white particles observed in suspension among the biomass. Dissolved carbon concentrations were found to decrease throughout the experiment in the experimental flasks containing calcium (Figure 54). In addition, the total dissolved inorganic carbon at the end of the experiment was lower in the experimental flasks. This indicates that carbon has been successfully removed from the system, once again suggesting the formation of solid $CaCO_3$. Data from the first experiment using species AQ0012 indicated a difference in initial bicarbonate ion concentration of the medium.
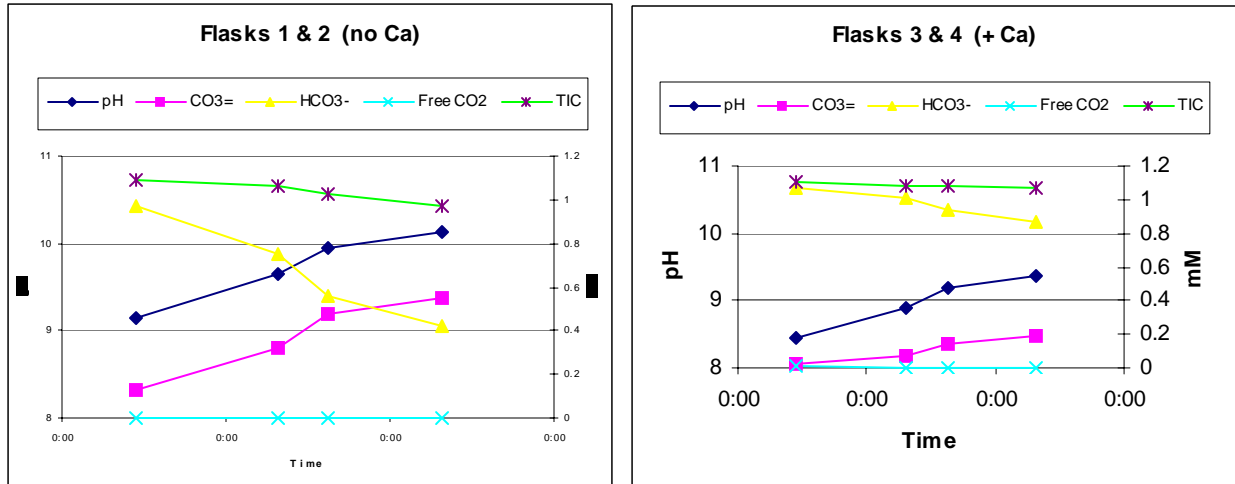
Figure 53. pH and dissolved inorganic carbon species concentrations in AQ0011 exp. 2 without and with Ca (average of 2 flasks).
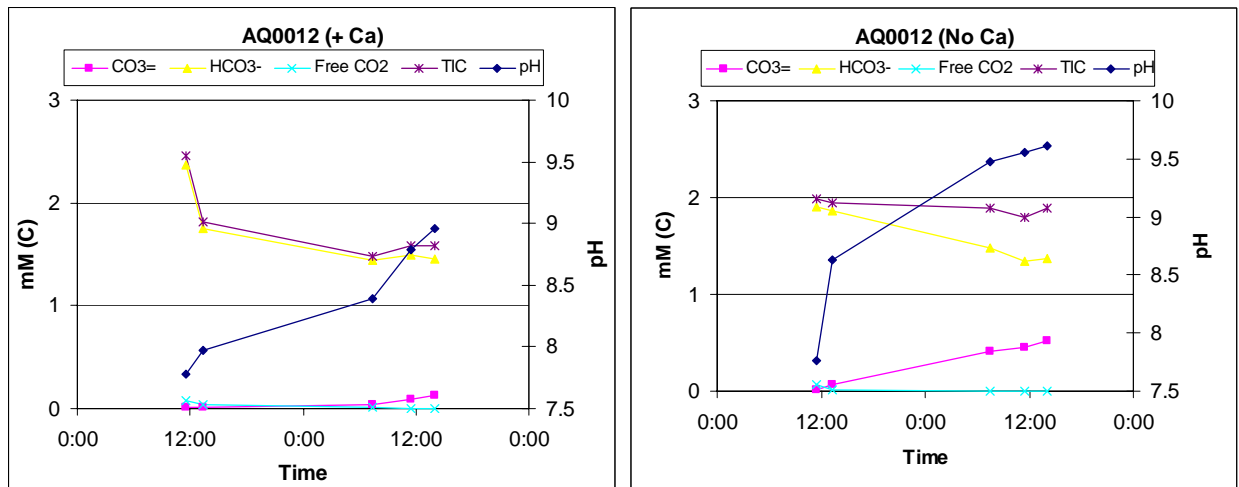
Figure 54. pH and dissolved inorganic carbon species concentrations in AQ0012 without and with Ca (average of 2 flasks).

The experiment was therefore repeated to ensure equal initial ion concentrations. A greater biomass was used to ensure a more rapid increase in pH in order to quickly induce the precipitation of $CaCO_3$. Ion concentrations from the second AQ0012 experiment demonstrate decreased total inorganic carbon, HCO_3^-, and CO_3^{-2} concentrations at the end of the experiment compared to the control flasks (Figure 55). The white amorphous particles found within the culture of both experiments were determined to be calcium carbonate after being tested for a reaction with concentrated HCl. It is not known why larger particulate $CaCO_3$ was formed in experiments using Cyanobacteria. Prior examination of calcification in cyanobacteria by Merz-Preiss (2000) shows that under certain conditions, filaments of the organism can become encrusted with $CaCO_3$. However, upon examination of the culture, particulate $CaCO_3$ was not encrusted on the cells of the organism (Figure 56), however were abundant in close proximity with clumps of the algal filaments.
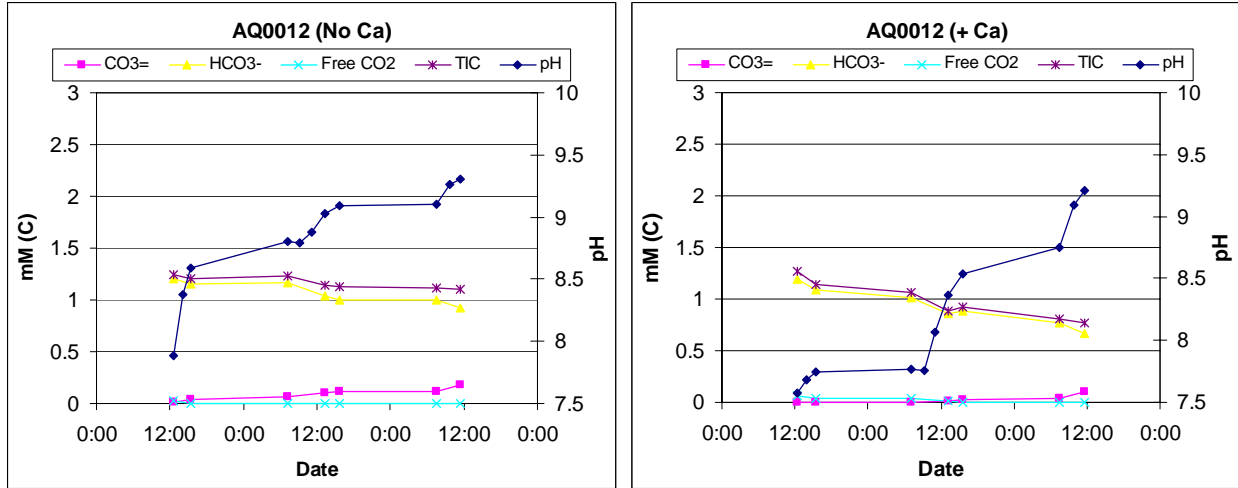
Figure 55. pH and dissolved inorganic carbon species concentrations in AQ0012 2nd exp. without and with Ca (average of 2 flasks).
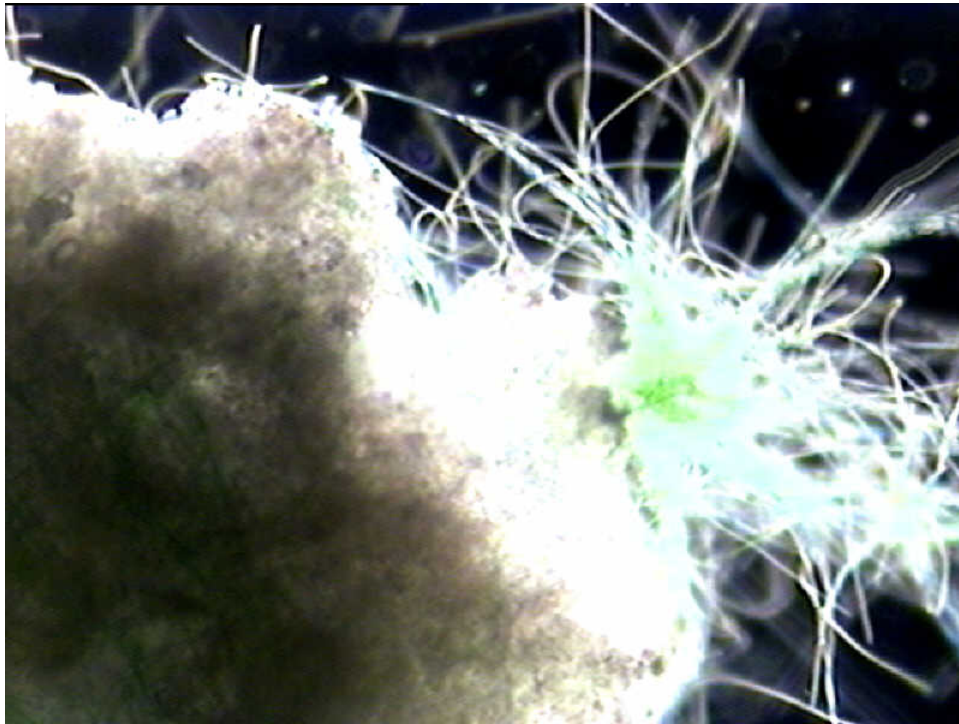
Figure 56. Photomicrograph of a clump of AQ0012 culture. The green filaments are the alga itself. The large white mass is precipitated $CaCO_3$. Although the $CaCO_3$ mass is closely associated with the algal filaments it doesn't seem to crust the filaments.

Microalgal strain AQ0052 did not increase significantly in biomass from the beginning to the end of experiment. The culture did not photosynthesize enough to raise the pH of the medium to a level where $CaCO_3$ could possibly precipitate. Also, the ion concentrations did not differ between experimental and control flasks (Figure 57) indicating that carbon had not been removed from the system. It has not been determined why AQ0052 did not increase in biomass, but a low initial biomass may have been the cause for the lack of rapid growth.
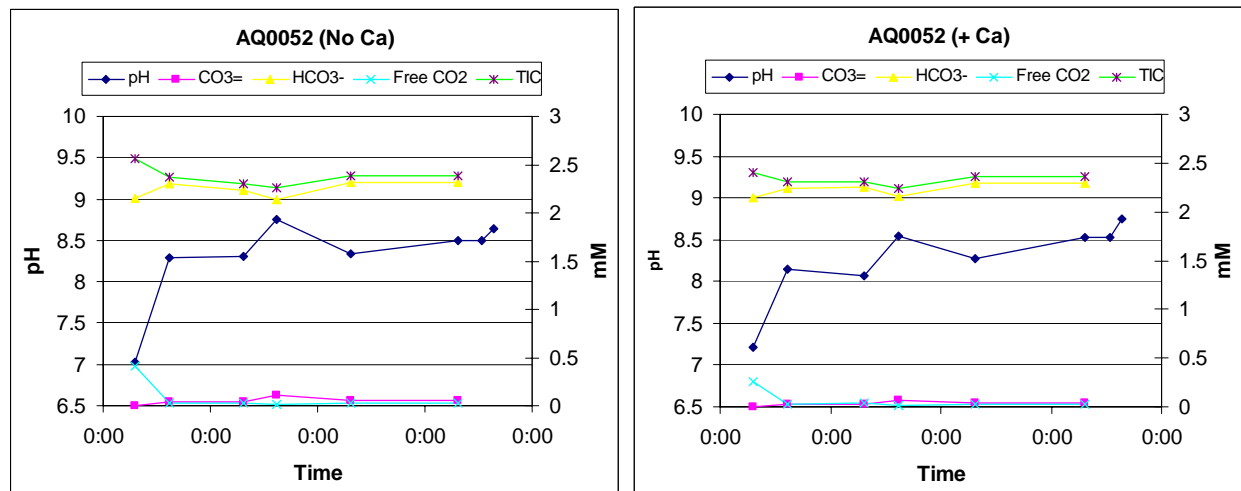
Figure 57. pH and dissolved inorganic carbon species concentrations in AQ0052 without and with Ca (average of 2 flasks).

The experiments conducted using both AQ0012 and AQ0008 to increase the pH of the medium yielded similar trends. The initial ion and total inorganic carbon concentrations of the AQ0008 culture were greater than those found in the AQ0012 culture media. Regardless of the initial difference, however, both cultures displayed a decrease in HCO_3^- and an increase in CO_3^{-2} concentrations as the pH of the media was biologically increased (Figure 58). Likewise, both culture mediums were replenished with HCO_3^- ions after the addition of CO_2 to each flask. According to Libes (1992) HCO_3^- ions are still dominant when compared to CO_3^{-2} at a pH of approximately 9.0. It is not until an approximate pH of 10.0 is reached when the majority of HCO_3^- ions have been converted to CO_3^{-2}.

The two carboy scale experiments conducted showed that microalgal cultures can quickly increase the culture pH when exposed to natural sunlight in the absence of CO_2 supplementation. In the first case (Figure 59), the pH of the culture rose rapidly within the first few hours (between 10:30 and 15:00 on the first day of culture) from 7.2 to 10.5, assumedly caused by photosynthetic CO_2 uptake. Overnight, the pH decreased to 8.4 due to respiration and possibly to the small amount of CO_2 present in atmospheric air used for mixing in the carboy. The second day, the pH of the culture rose to 10.5 by 12:30. On the third and four days, the pH rose only to 10.1 and 9.8 respectively. The smaller increases in pH can be attributed to loss of culture vitality probably caused by carbon limitation.
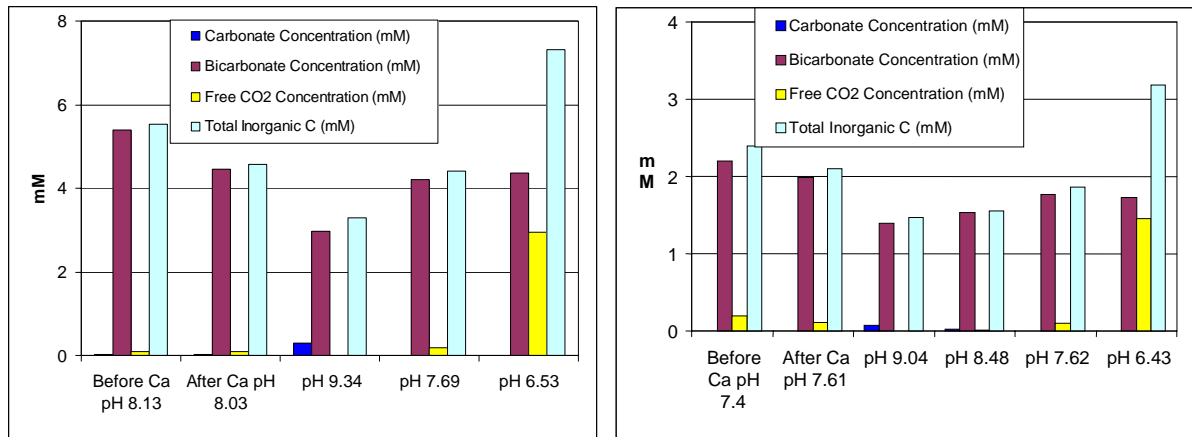
Figure 58. pH and dissolved inorganic carbon species with AQ0008 culture + Ca^{2+} (left panel) and with AQ0012 culture + Ca^{2+} (right panel).
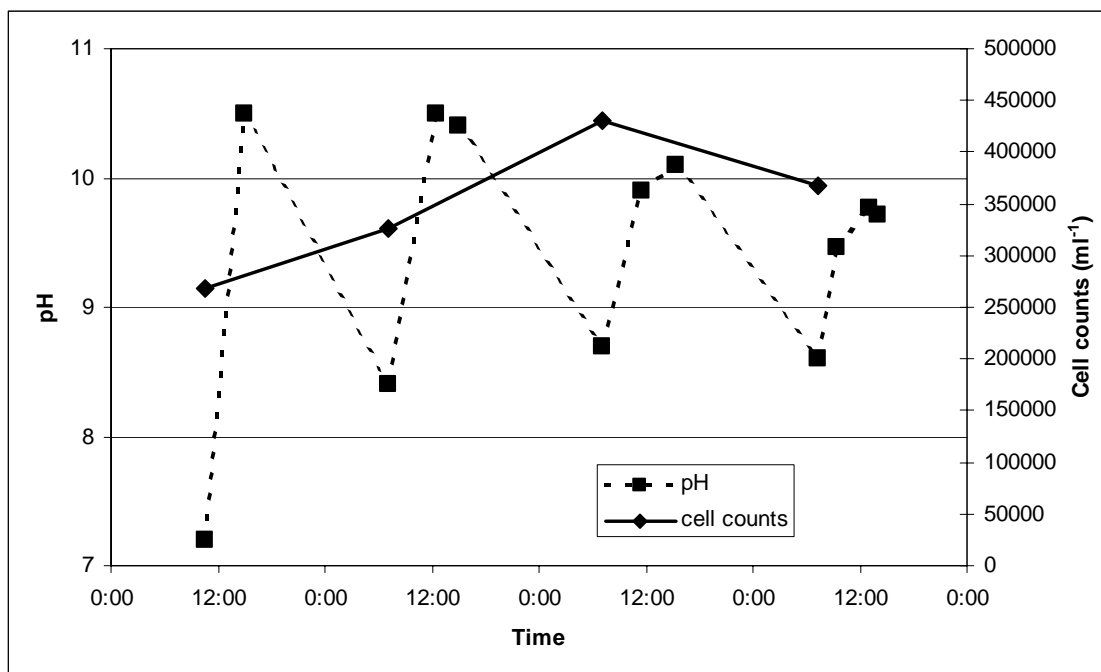
Figure 59. Changes in pH in a 20 liter carboy *Haematococcus* culture showing rapid rise in pH during daylight hours during four consecutive days.

On the last day of the experiment, measurements of alkalinity were conducted before and after centrifugation of the sample. By centrifuging the culture we are able to eliminate all particulates, including cells and any possible carbon that may have precipitated as carbonates. Thus, the values measured before centrifugation provide us with total inorganic carbon content in the culture, the values measured after centrifugation provide us with inorganic carbon content in the dissolved fraction, and the difference between the two is assumed to represent the amount of inorganic carbon in the particulate fraction. The results are presented in Figure 60 and show that a significant fraction of the carbon had apparently precipitated (i.e., present in the particulate fraction).
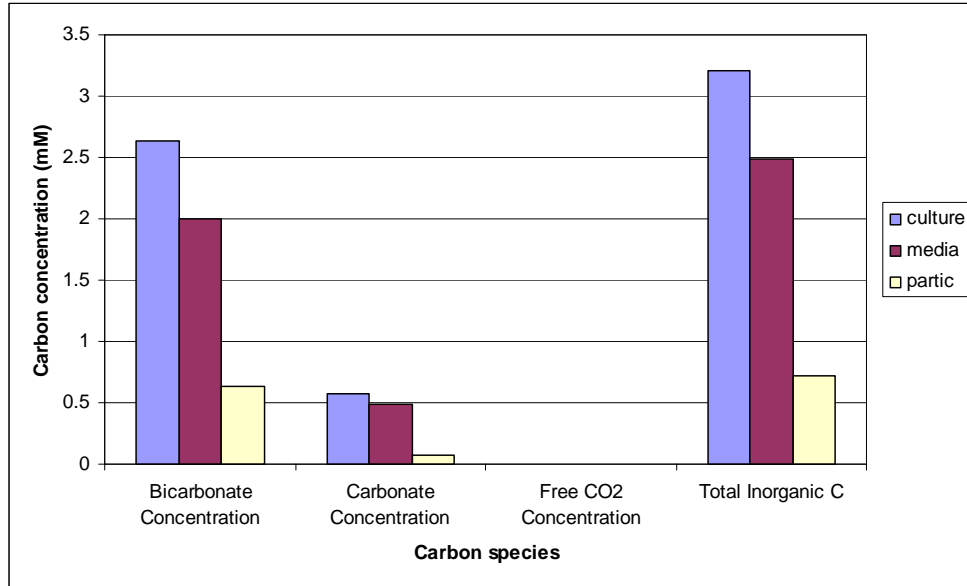
Figure 60. Concentration of the different forms of inorganic carbon in the culture, medium, and particulates (= culture-medium). Note that at the high pH reached (> 9.5) there is virtually no free CO_2.

The pH in the second 20 liter culture also rose caused by photosynthetic CO_2 uptake by the microalgal cells (Figure 61) as was the case in the previous experiment.
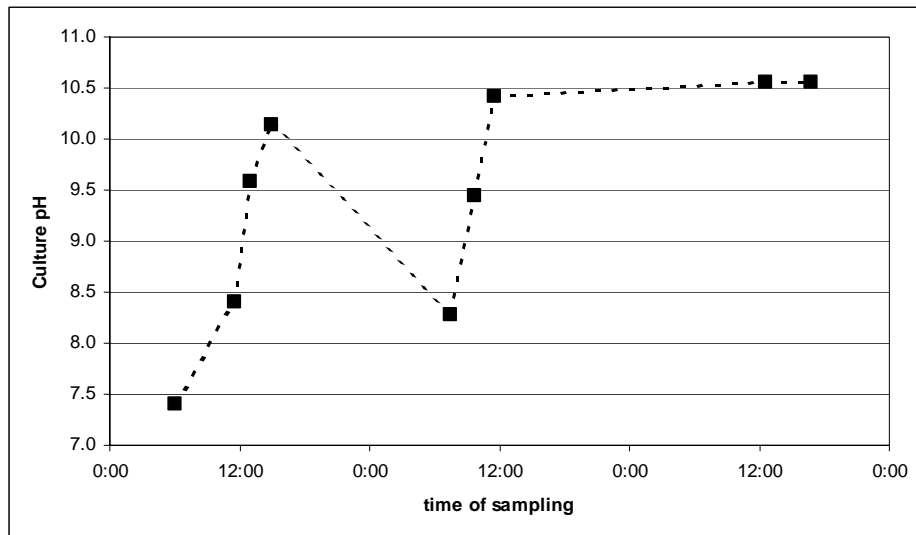
Figure 61. Changes in pH in a 20 liter carboy *Haematococcus* culture showing rapid rise in pH during daylight hours during three consecutive days.
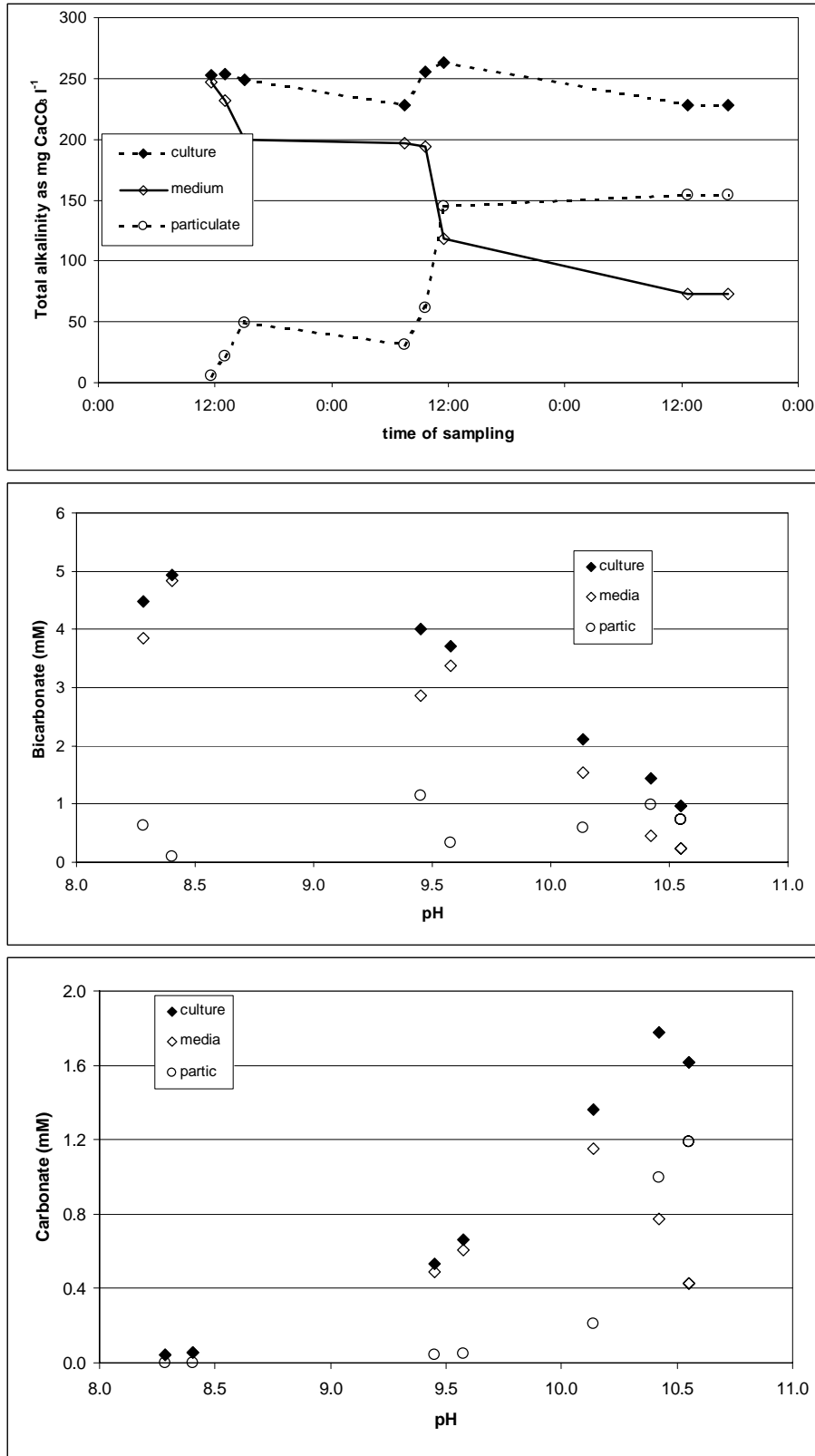
Figure 62. Changes in total alkalinity (top panel), bicarbonate ion (middle panel) and carbonate ion (bottom panel) over three days of growth for a culture of *Haematococcus* not supplemented with CO_2.

The measurements of alkalinity of the culture indicated that as the pH of the culture rose the total alkalinity (TAlk) changed little for the culture but the value of TAlk in the dissolved fraction decreased while the value in the particulate fraction increased (Figure 62, top panel). Similarly, analysis of the inorganic carbon species indicates that as the pH of the culture rose, a larger fraction of the inorganic carbon was in the form of carbonate (at the expense of bicarbonate) and a larger fraction of carbonate was present in the particulate fraction (Figure 62 middle and bottom panels).

Significance of the Results

From an industrial perspective, this process has the possibility of decreasing carbon emissions that lead to global warming. However, this process must be cost effective in order to promote the energy production industry to utilize its potential. In the past few decades, microalgae have been grown for the production of valuable byproducts of certain physiological characteristics. Some carotenoid pigments produced by algae have been identified as valuable antioxidants and present many health benefits (see section on high value products). Some are presently utilized in the nutraceutical industry. This byproduct of microalgal growth will help to offset the cost of implementing the algal mediated sequestration of carbon. As the sequestration method requires a calcium supply, a relatively inexpensive source is $CaSO_4*2H_2O$, or gypsum. Deposits of this mineral are abundant throughout the world and it is readily available for use in agriculture as well as other venues. The preceding experiments were all conducted using gypsum as the calcium source, and this mineral has proven successful in its ability to supply calcium to an algal medium. The use of this mineral does have limited potential, however, due to its relatively low solubility. $CaSO_4*2H_2O$ is less soluble than other species of Ca, and therefore limits the number of moles of Ca available for binding with free CO_3^{-2} ions in the experiments. Another Ca source could be used to provide more Ca^{2+} ions to a medium, however some more reactive and soluble species require energy to produce. This in essence defeats the purpose when viewed on a global perspective because CO_2 is released during energy production. Another species of Ca, more soluble than $CaSO_4*2H_2O$ that requires no energy to produce would be a better alternative, however more research must be done to determine the most suitable Ca species.

In conclusion, microalgal photosynthesis can be used to induce the precipitation of $CaCO_3$ from a Ca-enriched medium. This process can be used to reduce the amounts of CO_2 degassed from industrial fossil fuel combustion, reducing the large amounts of anthropogenic CO_2 contributed to the global carbon cycle each year. More information is necessary to successfully establish an industrial scale carbon sequestration system, but the research presented demonstrates the feasibility of this method. In conjunction with high value product generation, this process can prove to be affordable to industry and environmentally beneficial.

4.2.3   Selection of Microalgal Strains for Scale Up Experiments

We chose eight microalgal strains for the scale-up experiments reported in Task 3: AQ0008, AQ0011, AQ0012, AQ0015, AQ0024, AQ0033, AQ0059, and AQ0073. The strains were chosen based on their growth characteristics under the culture conditions tested here (temperature, pH, flue gas composition), on their ability to accumulate high value compounds,

on their perceived ease of harvest, and on either perceived or existing markets already available for those products. The strains chosen represent a large variety of cell morphologies (from small coccoid cells of 3-4 μm diameter to filaments several mm long) and phylogenetic groups (Chlorophytes, Cyanobacteria, Rhodophytes).

4.3   Task 3 – Optimization and Demonstration of Industrial Scale Photobioreactor

The objective of Task 3 is to demonstrate algal-mediated carbon sequestration at a commercially significant scale. This includes delivery of CO_2 to the microalgal cultures, capture of carbon into organic (biomass) and inorganic (carbonates) forms of carbon and processing of the resulting biomass. First, Subtask 3.1, we will present results of experiments designed to demonstrate carbon capture and sequestration at pilot scale in outdoor photobioreactors (up to 2,000 liter capacity) fed either pure CO_2 or combustion gases from an actual coal burning reactor. Next, Subtask 3.2, we will report on experiments conducted at a commercially significant scale in outdoor photobioreactors (up to 25,000 liter capacity) fed either pure CO_2 or combustion gases from an actual propane burning reactor. Finally, Subtask 3.3, we report on experiments carried out to determine costs associated with harvesting of the produced biomass for processing.

4.3.1   Subtask 3.1 – Pilot Evaluation

4.3.1.1 Initial Growth Rates and Productivity

During the initial batch grow out period of photobioreactor cultures, maximum growth rates are observed as the cells' growth is not yet limiting. We pooled the growth data grown in pilot scale photobioreactors (up to 2,000 liters) during this initial phase of culture growth.

A total of 30 cultures were grown in pilot scale MGMs representing 8 different strains of microalgae. The growth rates of the cultures were calculated from the daily changes in fluorescence-based biomass estimates (Figure 63).

For the 8 strains grown in pilot scale MGMs, the maximum daily growth rates ranged between 0.17 and 1.22 d^{-1} while average growth rates for each culture ranged between 0.04 and 0.55 d^{-1} (Figure 64).
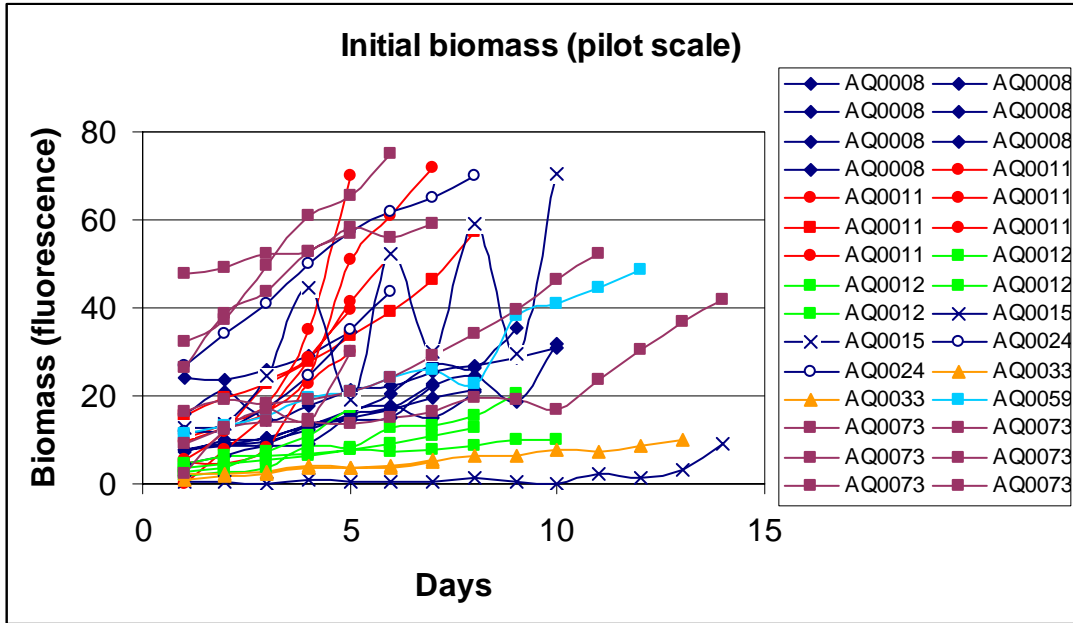
Figure 63. Daily fluorescence-based biomass estimates.
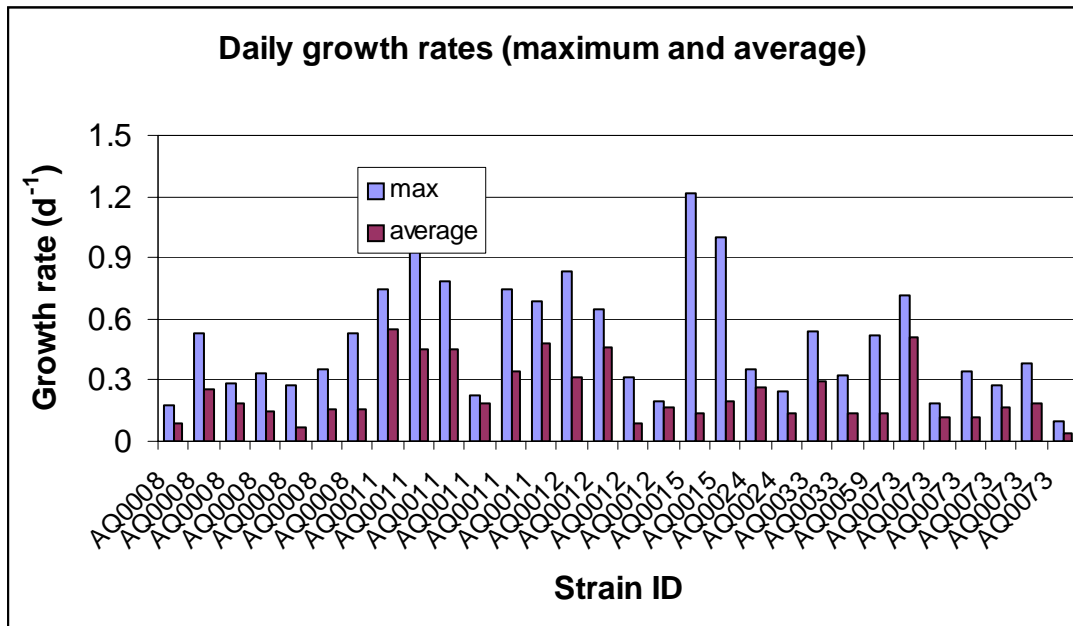
Figure 64. Growth rates measured in 30 individual pilot scale cultures.

If we average the obtained growth rates for all cultures representing any one strain we find the following:

Strain AQ0008	0.15 d^{-1}
Strain AQ0011	0.41 d^{-1}
Strain AQ0012	0.26 d^{-1}
Strain AQ0015	0.16 d^{-1}
Strain AQ0024	0.20 d^{-1}
Strain AQ0033	0.21 d^{-1}
Strain AQ0059	0.13 d^{-1}
Strain AQ0073	0.19 d^{-1}

We consider these rates only to be indicative of potential growth and, thus carbon capture potential into microalgal biomass. It must be kept in mind that in outdoor industrial applications of microalgal photosynthesis growth is always limited, usually by solar flux.

Next we consider the biomass productivities obtained during the same culture start up period. We established fluorescence vs. biomass relationships for the strains, above (except for AQ0015; difficulty sampling the large clumps formed by this strain precluded us from obtaining accurate estimates of biomass). Figure 65 shows the biomass (dry weight) estimates for the same cultures.

From these values we calculated the actual biomass production rates for this period (Figure 66). Cultures of strains AQ0011 and AQ0012 were the most productive cultures.
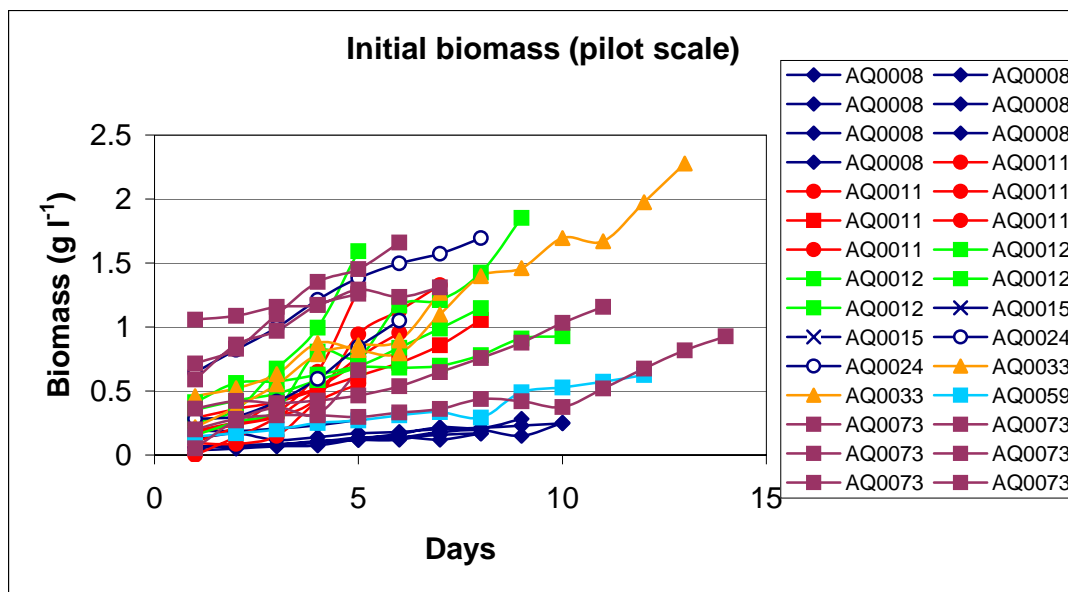
Figure 65. Biomass estimates (g l^{-1}) during the initial ramp up phase.
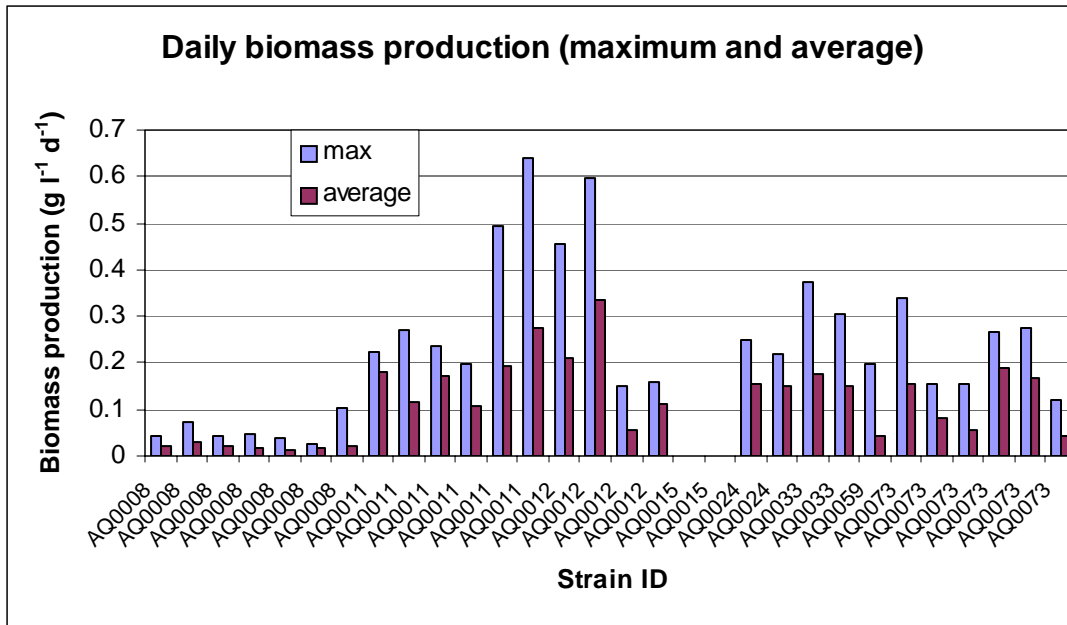
Figure 66. Daily biomass productivities during the ramp up phase.

4.3.1.2 Photosynthetic Carbon Uptake

Effects of culture pH at pilot scale (2,000 liter photobioreactors)

One of the main conclusions that we reached in Task 2 is that culture pH has a profound effect on the carbon capture efficiency of microalgal cultures. Our first experiment in scale up photobioreactors was used to test whether the same effect could be measured at this larger scale.

Two 2000 liter photobioreactors growing *Haematococcus pluvialis* (AQ0008) were prepared for testing the effects of culture pH. The objective of the test was to estimate changes in the CO_2 capture efficiency at two different pH levels, 7.5 and 8.5. Our previous tests at the chemostat scale (Task 2) indicated that the efficiency of CO_2 capture by microalgal cultures is higher at higher pH levels.

Photobioreactors AQ0008-M09 and AQ0008-M10 were inoculated from the same mother culture and at the same time. The pH set points for M10 were programmed at 7.4 and 7.6 while the set points for M09 were programmed at 8.4 and 8.6 starting one day after inoculation. After 8 days of growth, the pH set points were reversed.

Figure 67 shows the pH recorded, at a frequency of every 5 minutes, for the two modules. Both cultures were started at a nominal pH of 7.5, i.e., the controlling set points were 7.4 and 7.6. On the second day, M09 pH was changed to 8.5, the set points were 8.4 and 8.6. The pH of the cultures was reversed after 8 days of growth.
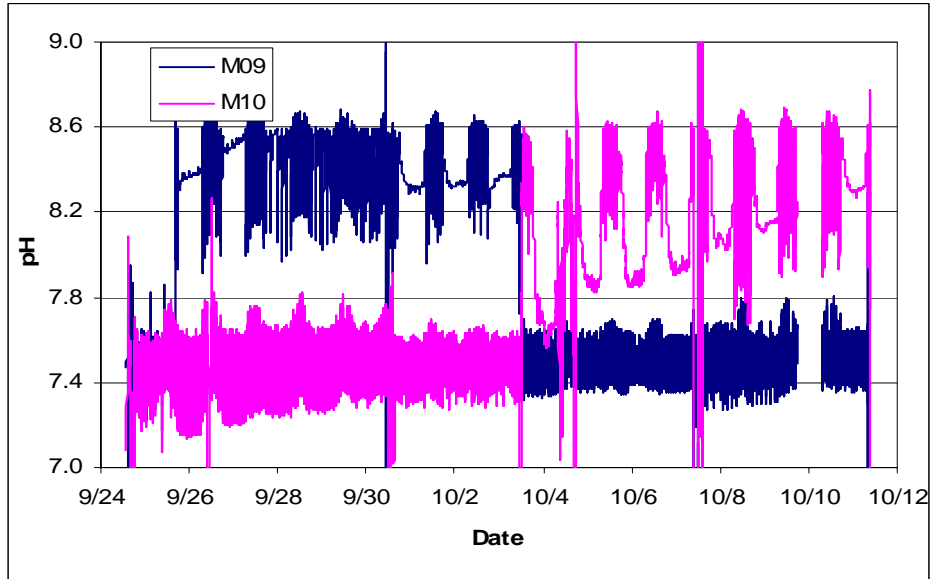
Figure 67. pH traces obtained from photobioreactors M09 and M10.

Figure 68 shows the alkalinity measured in both photobioreactors during the experiment. Alkalinity increased over time due to nitrate uptake by the microalgal cells, indicating growth. Large decreases in alkalinity occurred when the culture was diluted with freshly made nutrient medium.
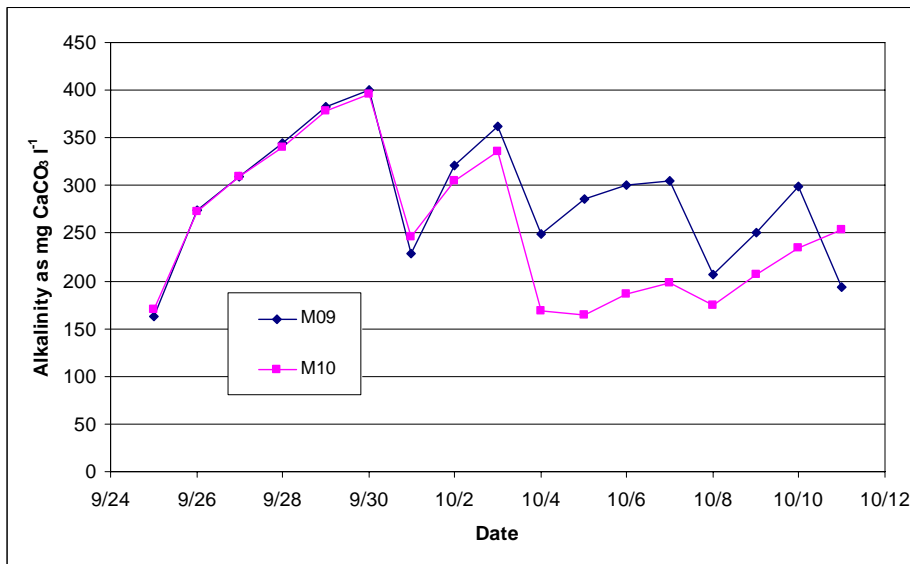
Figure 68. Alkalinity values measured in photobioreactors M09 and M10.

Figure 69 shows the fluorescence-based biomass estimates obtained once daily and Figure 70 shows the growth rates accomplished by the cultures during the experimental period, based on cell counts.
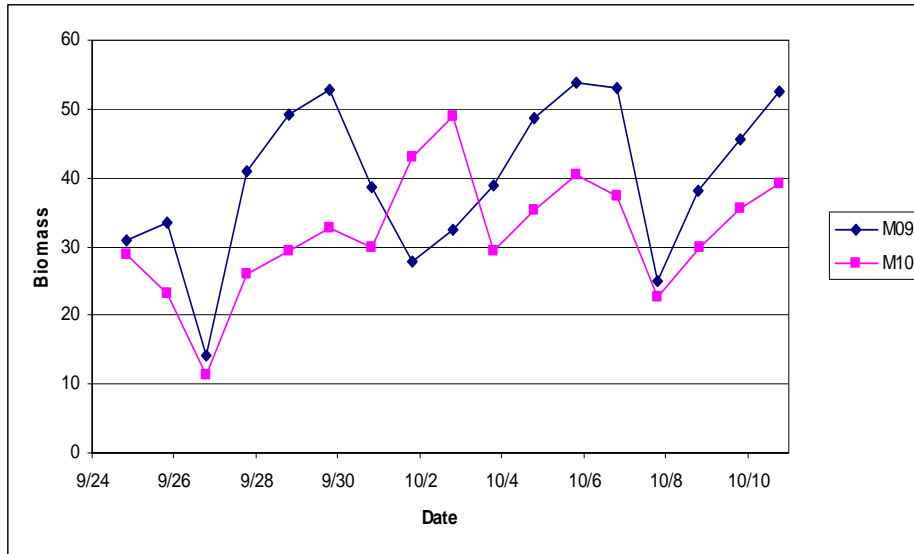
Figure 69. Fluorescence-based estimates of daily biomass.
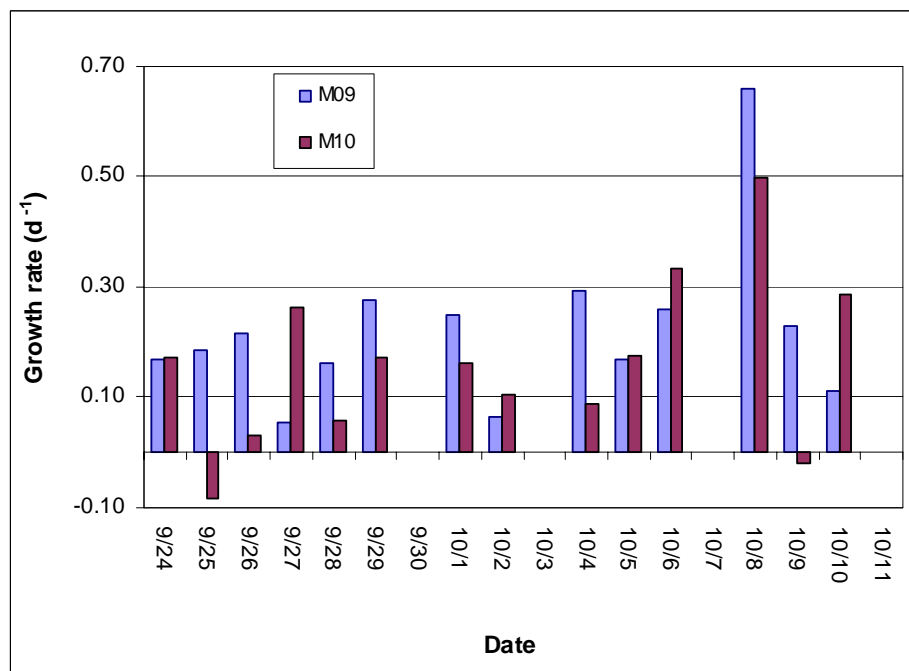
Figure 70. Growth rates for M09 and M10 based on cell counts. Data missing is from days when culture dilutions took place.

The calculated rates of CO_2 disappearance from the medium are shown in Figure 71. It is clearly seen that the rates are larger when the culture pH is maintained near 7.5 than when maintained near 8.5 in both photobioreactors. These results reflected those obtained in our chemostat scale experiments reported on earlier.
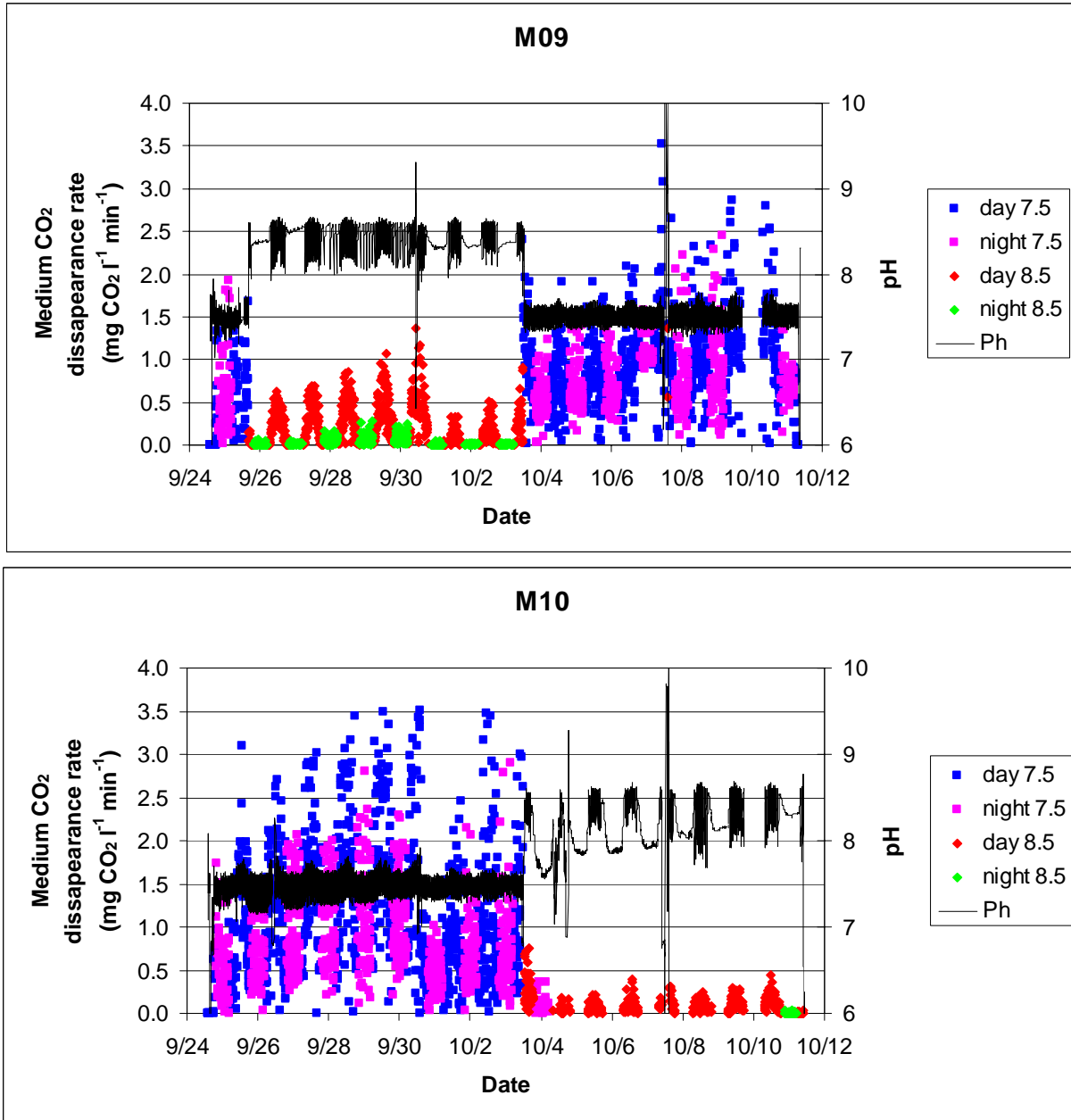
Figure 71. Rates of dissolved inorganic carbon (DIC) disappearance from the medium (photosynthesis and/or degassing) for M09 and M10. The different symbols indicate the different conditions under which these data were obtained (night vs. day, pH 7.5 vs. pH 8.5).

We have then averaged the CO_2 disappearance rate over each day and night period, eliminating those days during which culture dilutions took place from the calculations (since the alkalinity of the medium was significantly changed). We have further averaged the day and night values for each pH condition for each photobioreactor. Our results indicate that the night-time rate of CO_2 disappearance from the medium averaged 0.76 (M09 at 7.5 pH), 0.03 (M09 at 8.5 pH), 0.82 (M10 at 7.5 pH), and 0.01 (M10 at 8.5 pH) mg CO_2 l^{-1} min^{-1} (Table 15). If we calculate the average concentration of CO_2 in the medium for each individual night period at the appropriate pH levels (7.5 or 8.5) we find a linear relationship between the concentration of CO_2 in the medium and the rate of degassing (Figure 72). According to this relationship, significant amounts of dissolved CO_2 are lost from the medium at CO_2 concentrations as small as 1 mg CO_2 l^{-1} and above.

Finally, we consider the difference between the rates of CO_2 disappearance from the medium obtained during the day and night periods. Assuming similar degassing and respiration rates, the difference between night and day can be ascribed to photosynthesis. We have averaged the calculated photosynthetic rates and present those results in Table 15 which show faster photosynthetic rates were obtained at pH 7.5 than at pH 8.5 in M10 but not in M09.

Table 15. Average Rates of DIC Disappearance from the Medium (mg CO_2 l^{-1} min^{-1}) for M09 and M10 at Either 7.5 or 8.5 pH and Either During the Day or Night Periods. The difference is assumed to be the photosynthetic rate.

PH	7.5			8.5		
Period	Day	Night	Difference	Day	Night	Difference
M09	0.93	0.76	0.17	0.21	0.03	0.18
M10	1.24	0.82	0.42	0.09	0.01	0.08
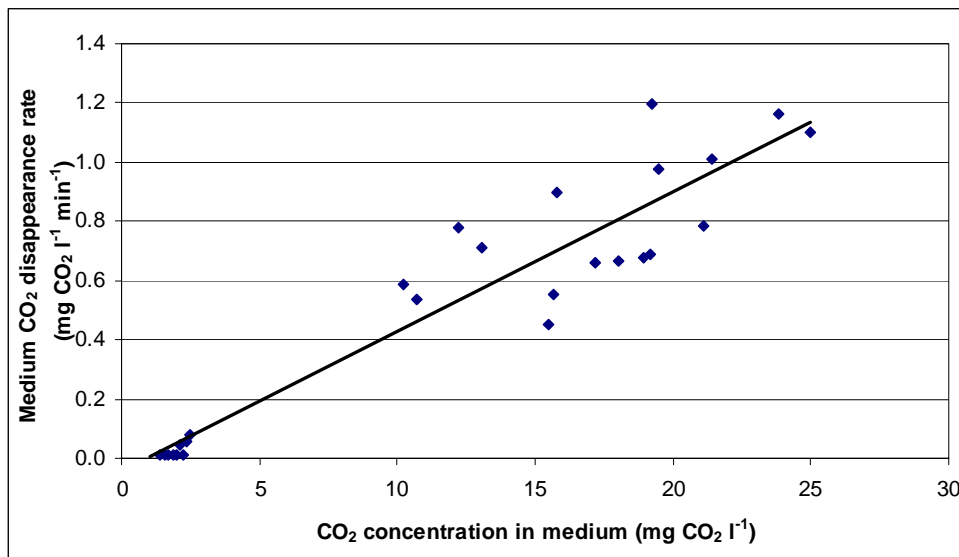
Figure 72. Relationship between CO_2 concentration in the culture medium and night-time rate of dissolved inorganic carbon (DIC) disappearance from the medium (degassing) for M09 and M10.

97

From these experiments we have now demonstrated that the effects of culture pH noted in the chemostat cultures also scale up to large outdoor cultures: at higher pH the losses of CO_2 from the culture medium are minimized.

Coal Reactor Performance

An initial test was performed with the coal reactor to determine the concentration of combustion gases produced. The combustion gases were injected into a PBR growing *H. pluvialis*. The gas was injected into the PBR in response to increases in pH caused by photosynthetic CO_2 uptake. Measurements of gas component concentrations were made before injection into the PBR and of the exhaust gas exiting the PBR.

Typical concentrations of gas components produced by the combustion of coal and injected into the PBR were CO_2 = 3.2 %, NO_X = 275 ppm, and SO_X = 325 ppm (Figure 73). The rate of gas flow into the PBR was 70 SCFH. Typical concentrations of gas components exiting into the PBR reactor were CO_2 = 0.1 %, NO_X = 2 ppm and SO_X = 1 ppm. The flow rate of gas out of the PBR was 720 SCFH. Note that the volume of combustion gas into the PBR is 70 SCFH but the exhaust gas is made up of that volume plus the air volume used in the airlift for a total of 720 SCFH. Thus, we can calculate the actual volumes of each individual gas, in and out of the PBR by multiplying the measured concentration times the flow rate. The results are shown in Table 16 and show that the microalgal culture was able to capture nearly 70% of the available CO_2 and over 90% of the NO_X and SO_X components.
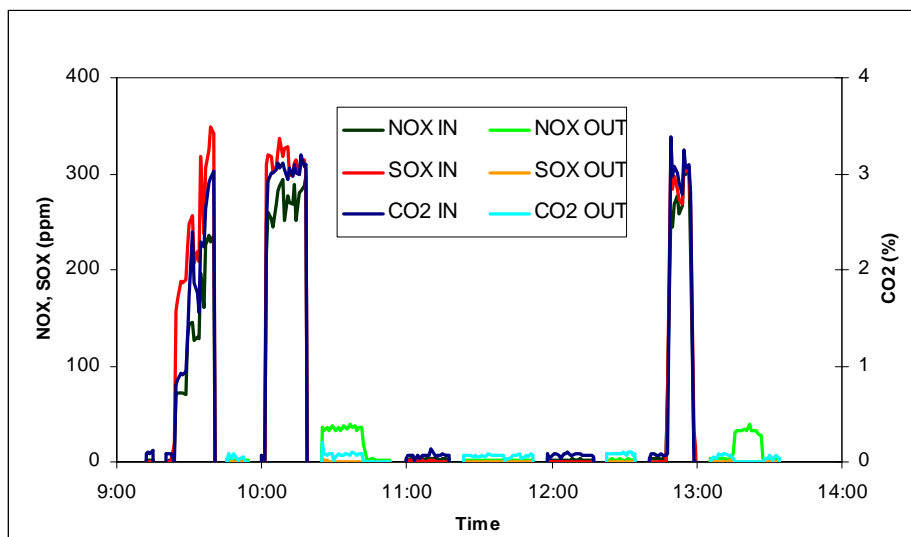
Figure 73. Gas analysis of coal combustion gases before (IN) and after (OUT) passage through the pilot scale photobioreactor.

98

Table 16. Measured Concentrations and Mass Flow Balance of CO_2, NO_X and SO_X Introduced into and Exiting the Photobioreactor

CO_2	3.2%	0.1%	2.24	SCFH	0.72	SCFH	68%
NOx	275 ppm	2 ppm	0.01925	SCFH	0.00144	SCFH	93%
SOx	325 ppm	1 ppm	0.02275	SCFH	0.00072	SCFH	97%

<u>Pilot Scale Photobioreactor Performance, CO_2 versus Coal Combustion Gases</u>

Our objective in these series of experiments was to determine whether any deleterious effects would be observed in culture performance at pilot scale when coal combustion gases were used directly as the source of carbon for the cultures.

We scaled up 6 different strains of microalgae for these experiments. In some cases we were able to run experiments in parallel, i.e., two cultures of the same strain growing at the same time, one receiving CO_2 and the other receiving coal combustion gases (CCG). In some cases, the same culture was exposed to CO_2 for a period of time before being exposed to coal combustion gases.

Experiments with strain AQ0008 (*Haematococcus pluvialis*)

We grew two cultures of AQ0008 which were exposed to coal combustion gases. One culture (AQ0008-041207) was grown initially for 4 days with CO_2, then it was diluted with fresh medium and switched over to CCG for 4 more days.

Figure 74 (top panel) shows the calculated estimates of CO_2 disappearance from the medium on the different days. The rates measured during the nighttime is ascribed to degassing of CO_2 from the culture while the rates measured during the daylight hours is the sum of degassing plus that assimilated through algal photosynthesis. The figure clearly indicates that the rates measured while the culture was grown on CO_2 are higher, both during the day and night hours. While one may conclude that, somehow, coal combustion gases would the cause of lower rates the effect might be indirect. As can be seen in the bottom panel of Figure 74, the use of coal combustion gases is associated with lower concentrations of dissolved CO_2 in the medium. Lower CO_2 concentrations in the medium are the result of lower alkalinity measured when the culture was exposed to CCG (Figure 75).

Another culture of the same strain (AQ0008-041111) was grown for four days exposed to CCG. Figure 76 (top panel) shows the calculated estimates of CO_2 disappearance from the medium on the different days. As in the previous experiment, the rates measured during the nighttime is ascribed to degassing of CO_2 from the culture while the rates measured during the daylight hours is the sum of degassing plus that assimilated through algal photosynthesis. The rates measured while the culture was grown on CCG are similar to those obtained in the previous experiment. As was also the case in that previous experiment, there is a clear dependency of the CO_2 disappearance rates on the amount of dissolved CO_2 in the medium. Also, as was observed before, the alkalinity and, thus, the concentration of dissolved CO_2 in the medium decreased following exposure of the culture to CCG (Figure 77).

99
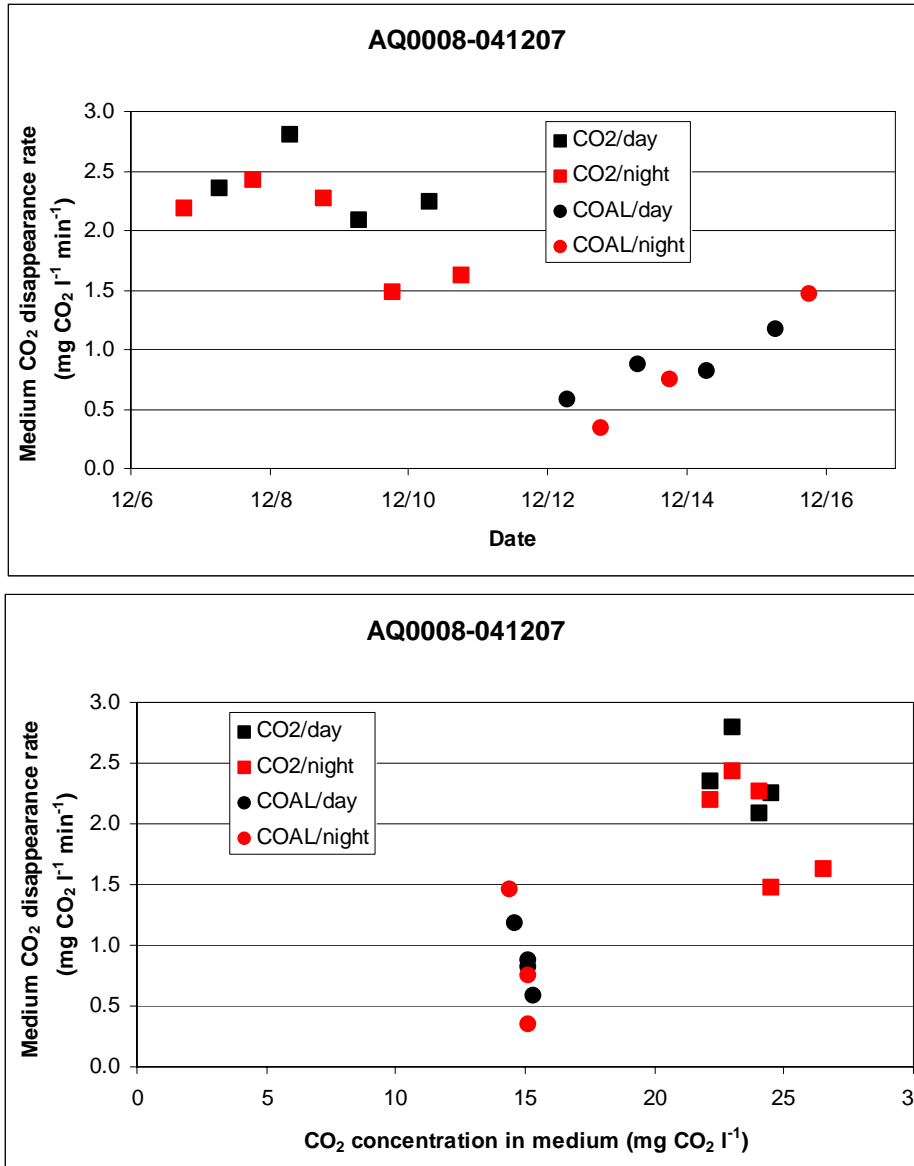
Figure 74. Rate of CO_2 disappearance from the cultures during daylight and nighttime on different days (top panel), relationship between the concentration of dissolved CO_2 in the medium and CO_2 disappearance rate (bottom panel).
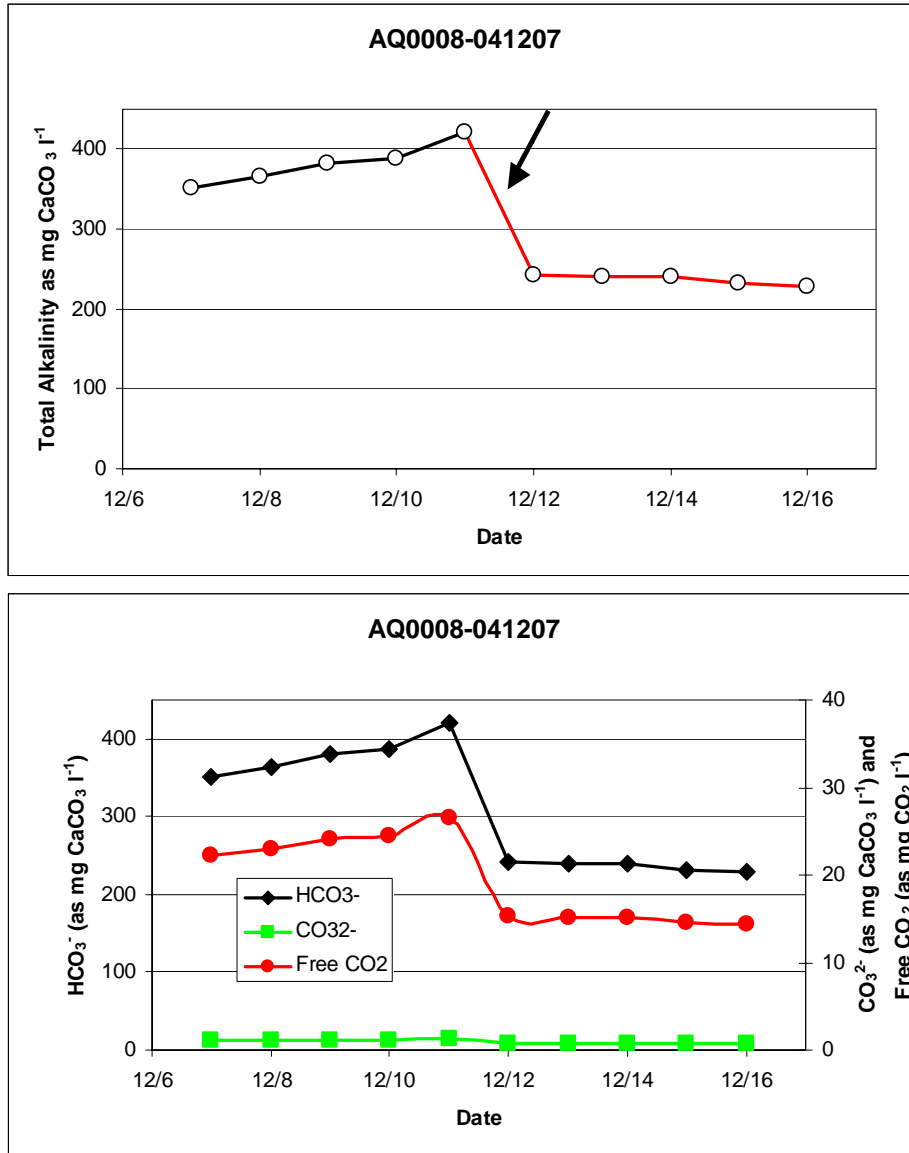
Figure 75. Changes in total alkalinity during CO_2 and coal gases exposure (black and red line respectively (top panel) and dissolved inorganic carbon species (bottom) in the medium. Arrow indicates the day when the culture was diluted with fresh medium.
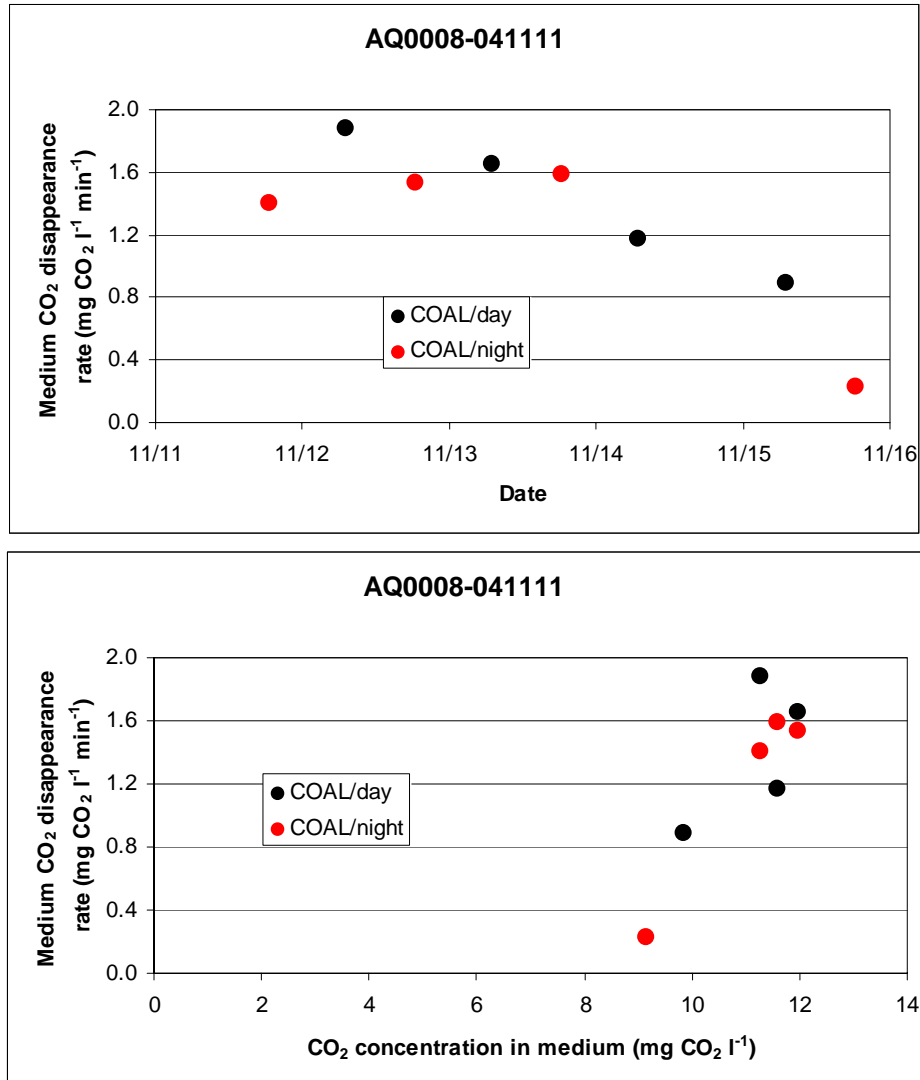
Figure 76. Rate of CO_2 disappearance from the cultures during daylight and nighttime on different days (top panel) and relationship between the concentration of dissolved CO_2 in the medium and CO_2 disappearance rate (bottom panel).
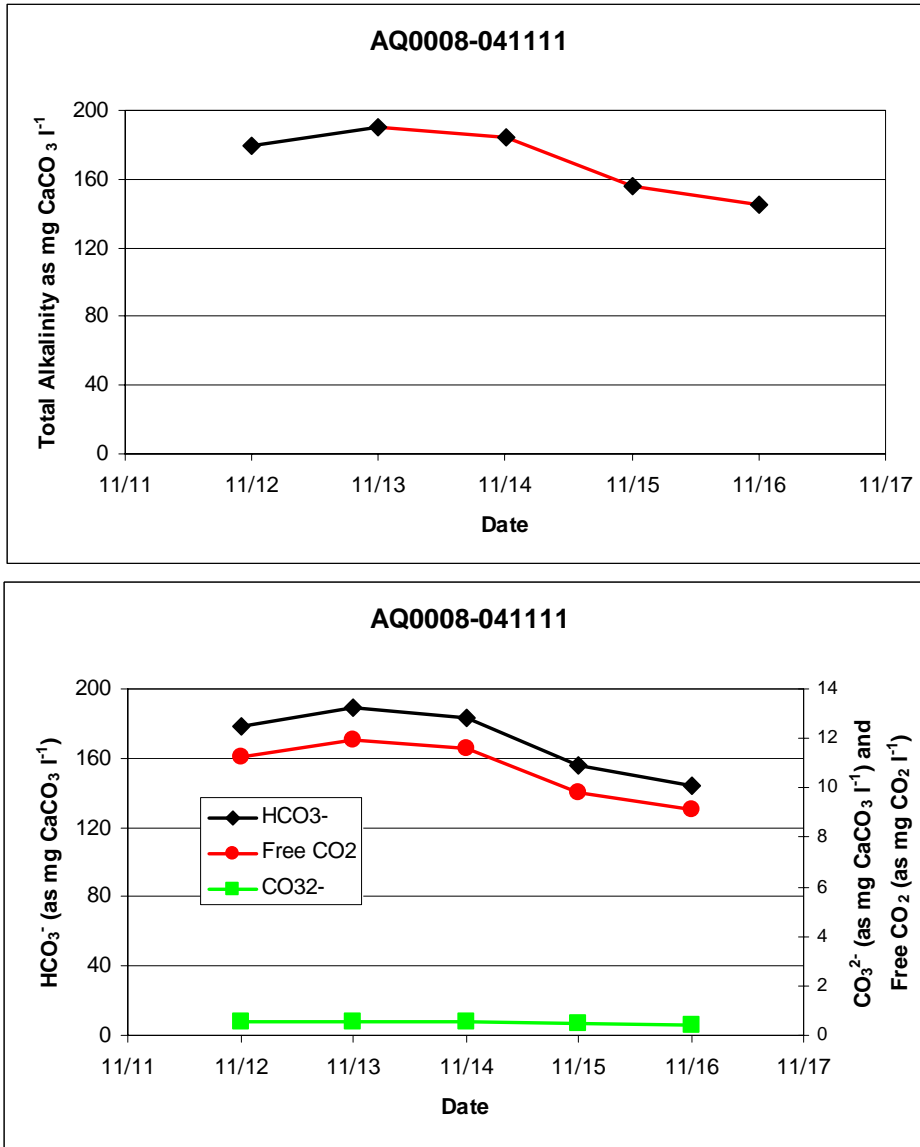
Figure 77. Changes in total alkalinity during CO_2 and coal gases exposure (black and red line respectively (top panel) and dissolved inorganic carbon species (bottom) in the medium. Arrow indicates the day when the culture was diluted with fresh medium

Experiments with strain AQ0011 (Unidentified Chlorophyte)

We grew three cultures of strain AQ0011 at pilot scale. First, we grew culture AQ0011-040217 for a total of 33 days and was exposed only to CO_2. As was found earlier, growth during exposure to CO_2 resulted in continued increases in the alkalinity and concentration of dissolved inorganic carbon species in the medium (Figure 78). Only on days when the culture was diluted with fresh medium did the alkalinity decrease by dilution.
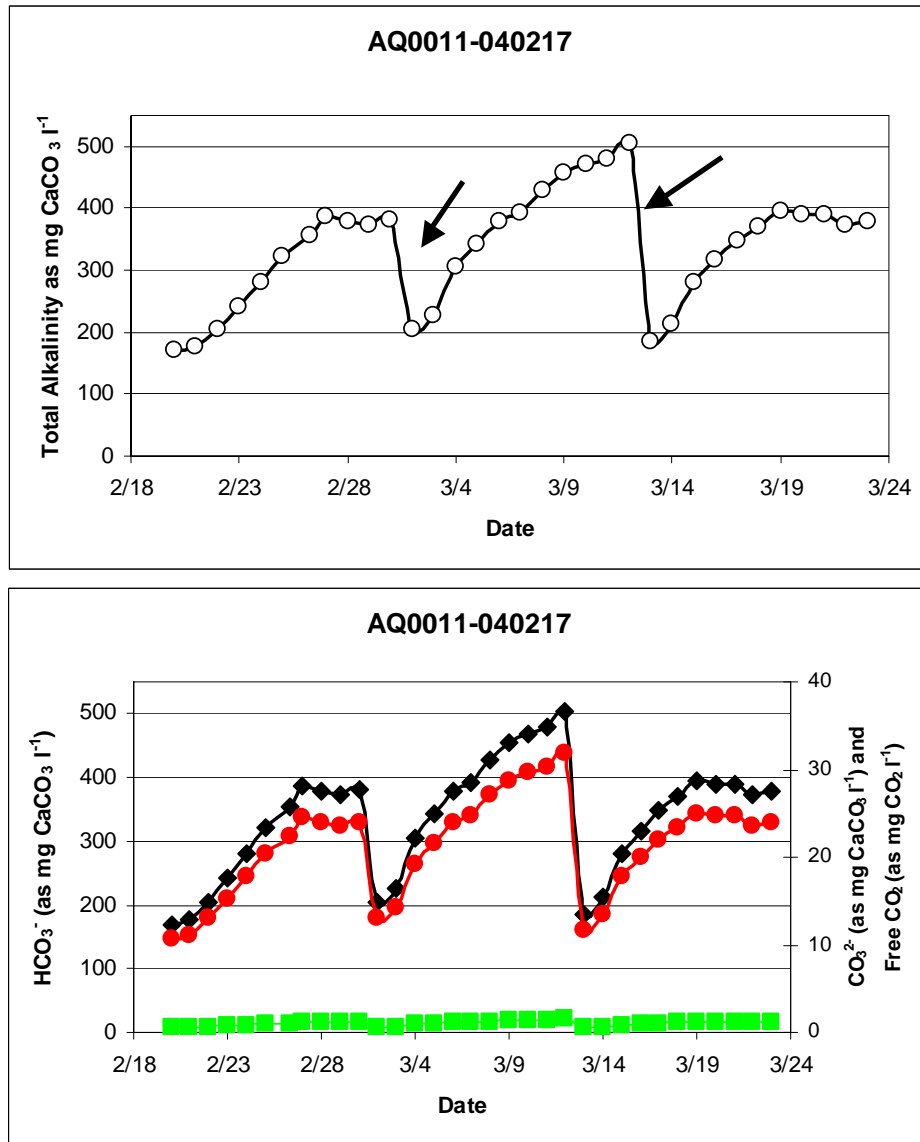
Figure 78. Changes in total alkalinity during CO_2 exposure (top panel) and dissolved inorganic carbon species (bottom panel) in the medium. Arrows in the top panel indicates the day when the culture was diluted with fresh medium.

Figure 79 (top panel) shows the calculated estimates of CO_2 disappearance from the medium on the different days. As in the previous experiment, the rates measured during the nighttime is ascribed to degassing of CO_2 from the culture while the rates measured during the daylight hours is the sum of degassing plus that assimilated through algal photosynthesis. The bottom panel shows clearly the dependence of the CO_2 loss rate on the concentration of CO_2 in the medium.
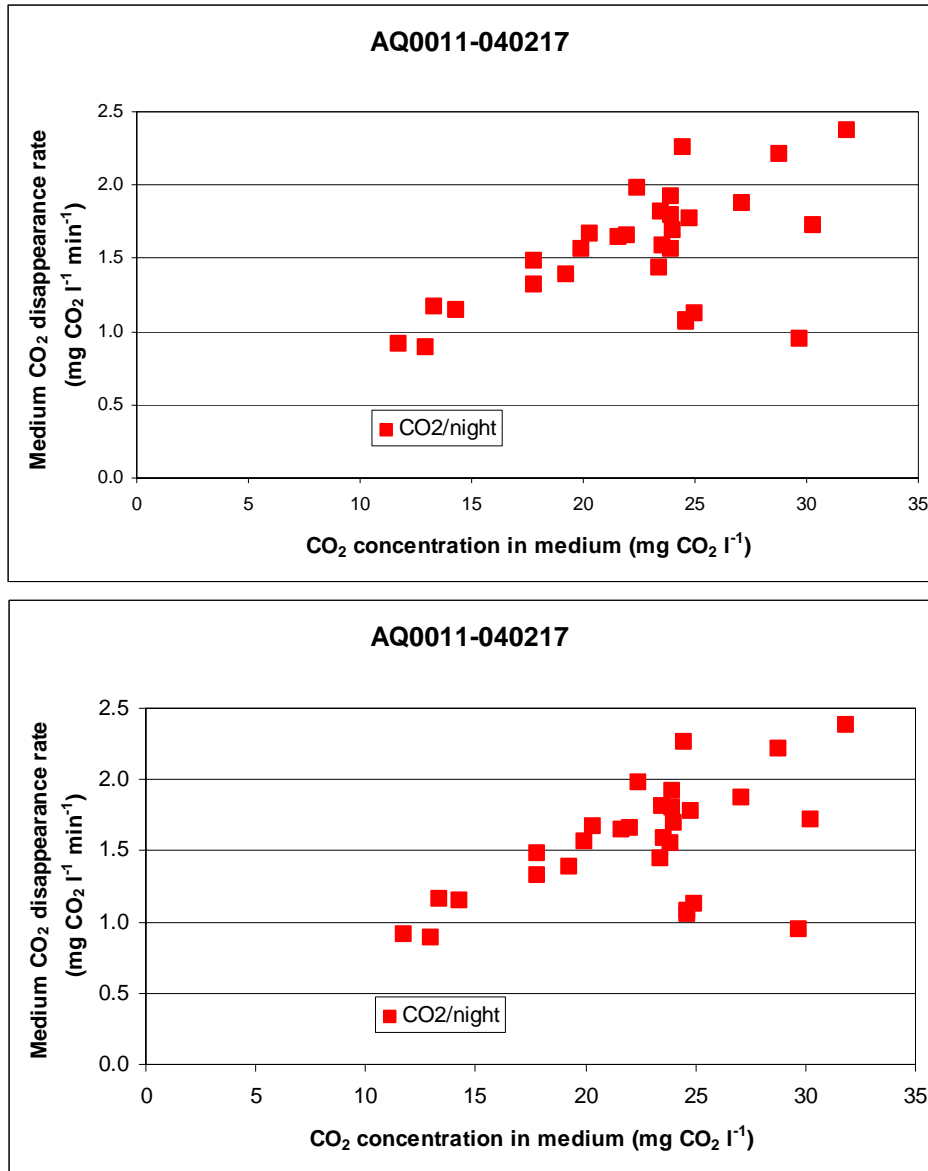
Figure 79. Rate of CO_2 disappearance from the cultures during daylight and nighttime on different days (top panel) and relationship between the concentration of dissolved CO_2 in the medium and CO_2 disappearance rate (bottom panel).

Two more cultures of strain AQ0011 were grown in parallel, one was exposed to CO_2 and the other to CCG. As was shown in previous experiments (above), the culture exposed to CO_2 showed large increases in alkalinity (Figure 80) and dissolved inorganic carbon species (not shown) as opposed to the culture exposed to CCG.
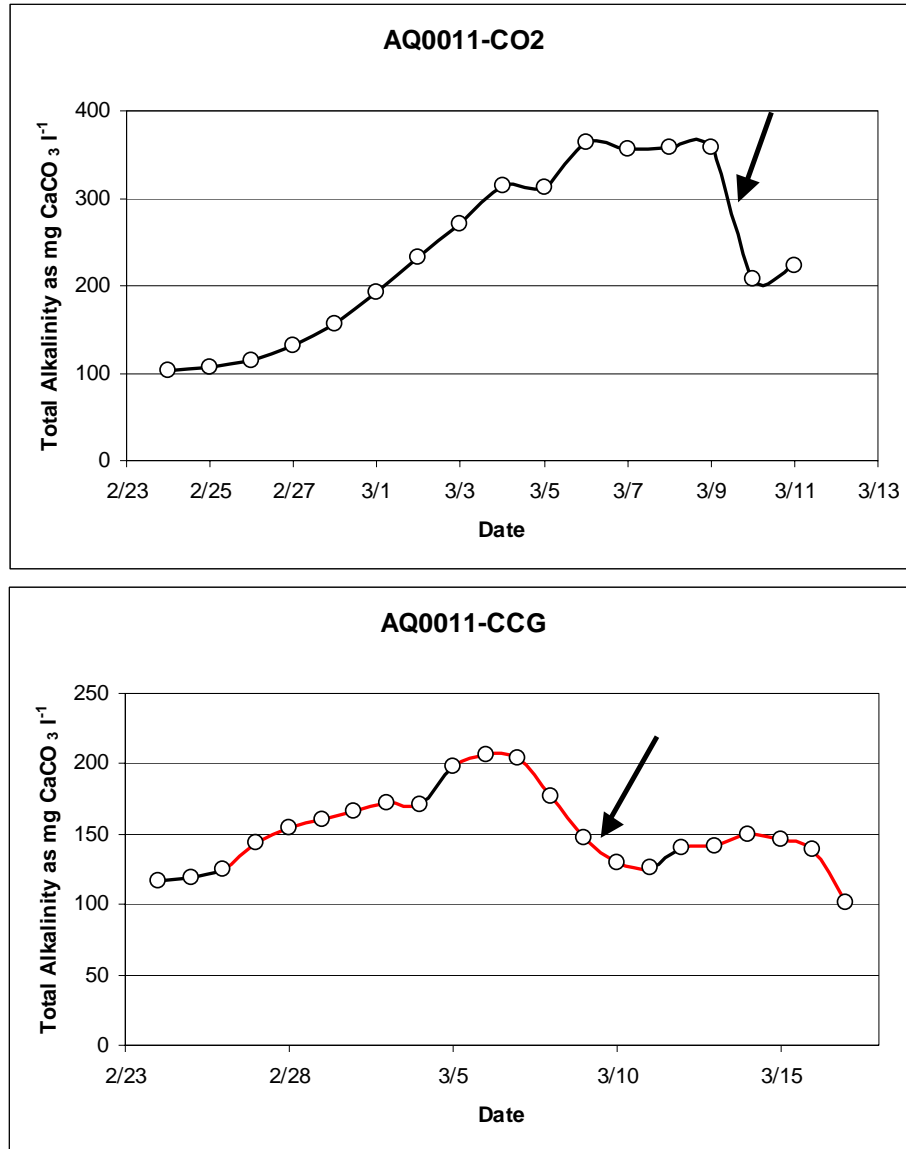
Figure 80. Changes in medium alkalinity in cultures of strain AQ0011 when grown exposed to CO_2 (top panel) or CCG (bottom panel). The black arrow indicates dilution of the culture with fresh medium.

As in the previous experiment, the rates measured during the nighttime is ascribed to degassing of CO_2 from the culture while the rates measured during the daylight hours is the sum of degassing plus that assimilated through algal photosynthesis. The lower concentration of CO_2 in the culture exposed to CCG is similarly associated with lower rates of CO_2 loss from the medium, whether via degassing (night values) of photosynthesis. Interestingly, in this experiment we can see that the slope of the relationship between degassing and CO_2 concentration in the medium is different, dependent on whether the culture was exposed to CO_2 or CCG (Figure 81).
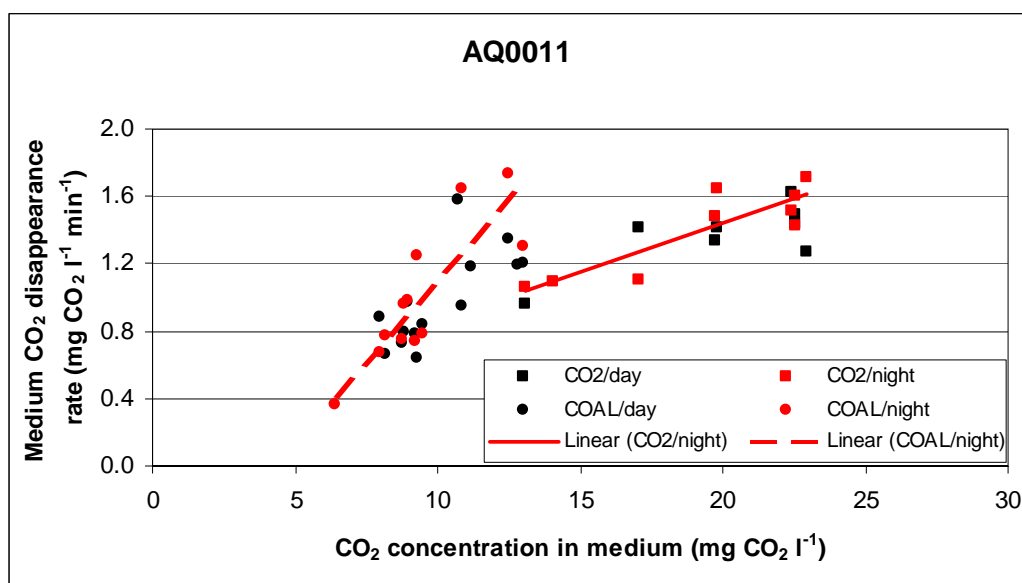
Figure 81. Dependency of CO_2 disappearance rates on medium CO_2 concentration for two cultures of strain AQ0011.

Experiments with strain AQ0012 (Unidentified Cyanobacterium)

We grew two cultures of strain AQ0012 at pilot scale. First, we show the results obtained from a culture that was only exposed to CO_2 during growth (AQ0012-050209). We found again that growth on CO_2 resulted in increasing alkalinity in the medium as well as dissolved inorganic carbon species. As in previous experiments, the rate of CO_2 disappearance from the medium was found to be dependant on the concentration of CO_2 in the medium (Figure 82).

Next, we show the results obtained from another culture of Strain AQ0012 that was initially grown on CO_2 but later switched to CCG and back to CO_2 (AQ0012-050130). As in previous experiments, only during periods on CO_2 exposure did the alkalinity and dissolved inorganic carbon species increase in the medium. However, in this case, we did not find a clear relationship between CO_2 disappearance rate and CO_2 concentration in the medium (Figure 83).
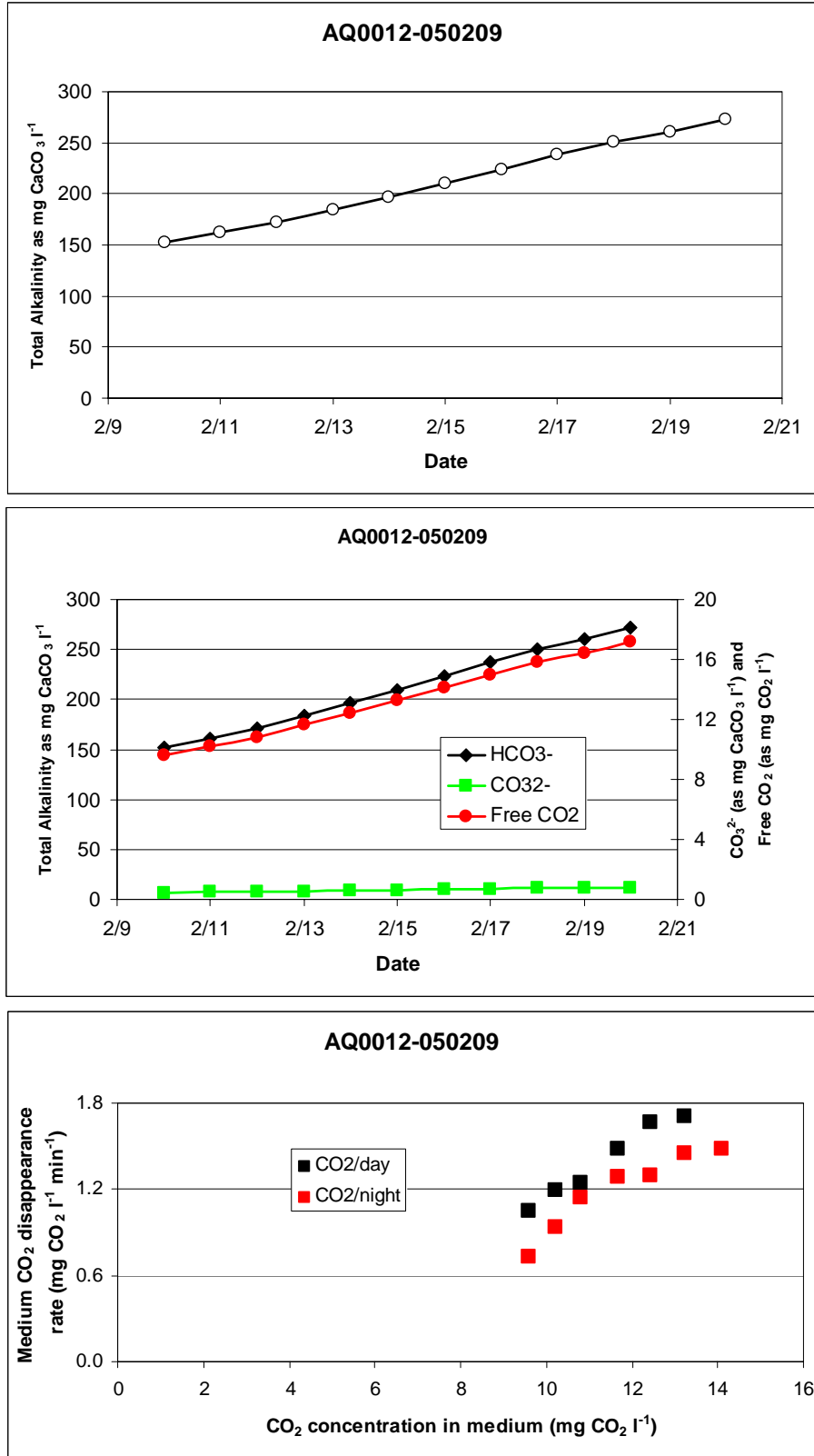
Figure 82. Changes in alkalinity (top panel), dissolved inorganic carbon (middle panel), and dependency of CO_2 disappearance rates on the concentration of CO_2 in the medium (bottom panel) for a culture of strain AQ0012 grown on CO_2.
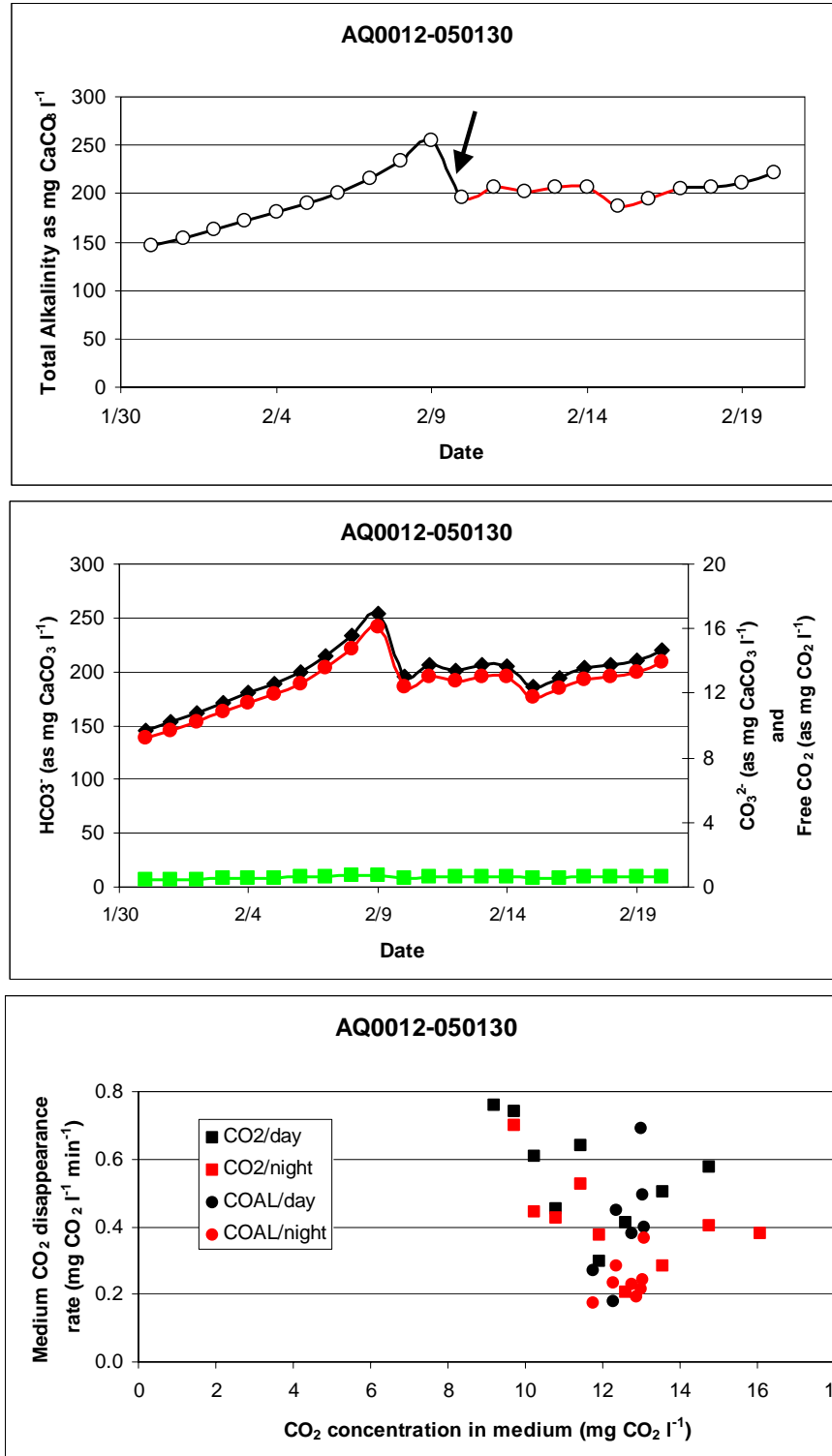
Figure 83. Changes in alkalinity (top panel), dissolved inorganic carbon (middle panel), and dependency of CO_2 disappearance rates on the concentration of CO_2 in the medium (bottom panel) for a culture of strain AQ0012 grown on CO_2 and CCG. Periods during which the culture was exposed to CO_2 and CCG are indicated by black and red lines in the top panel, respectively. The arrow indicates when the culture was diluted with fresh medium.

Experiments with strain AQ0024 (*Scenedesmus sp.*)

Two cultures of strain AQ0024 were grown at pilot scale. Culture AQ0024-050318 was grown solely on CO_2. After a few days of growth, part of the culture was harvested to start a second culture which was exposed to CCG (AQ0024-050323). As can be expected from the experiments reported earlier, a large increase in alkalinity was measured in the CO_2 culture but not in the CCG culture (Figure 84).
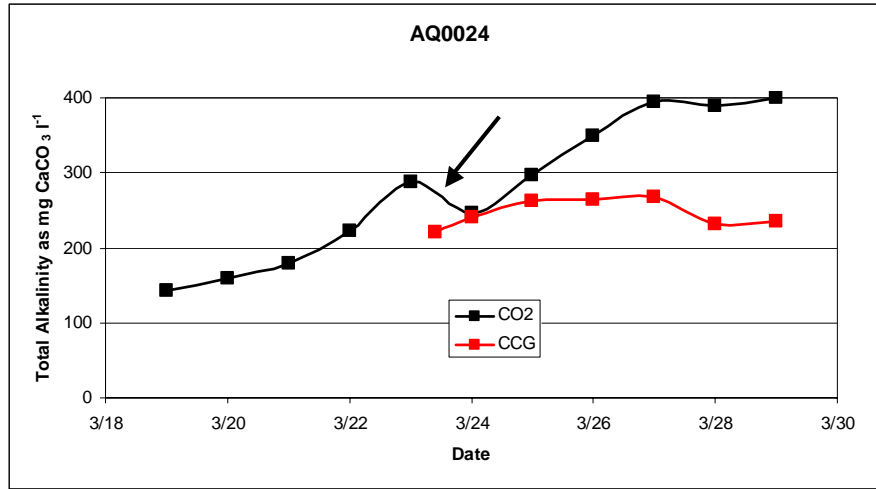
Figure 84. Changes in alkalinity in two cultures of strain AQ0024 when grown on CO_2 versus CCG. The black arrow indicates when the culture was diluted with fresh medium.

As in previous experiments, reduced medium alkalinity resulted in reduced concentrations of dissolved inorganic carbon species (not shown). Lower CO_2 in the medium, as in previous experiments, was also correlated with lower rates of CO_2 disappearance (Figure 85).
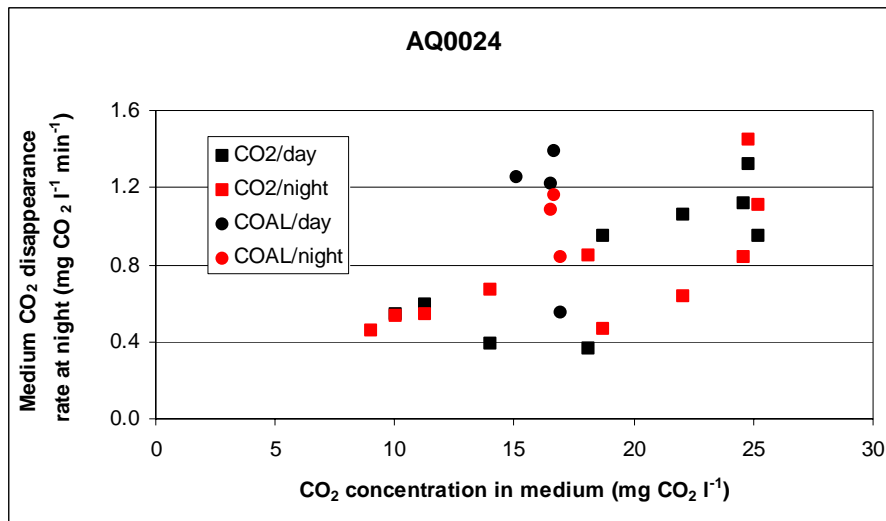
Figure 85 Rates of CO_2 disappearance from the medium for two cultures of strain AQ0024 whether grown on CO_2 or CCG during day and night times.

Experiments with strain AQ0033 (*Porphyridium sp.*)

We grew one culture of strain AQ0033 (AQ0033-040901) for 6 weeks at pilot scale and exposed it to CO_2 first and then to CCG. During the growth period on CCG we had technical problems with the coal combustor and, on four occasions, the culture was put back on CO_2. The results obtained during the switches back and forth between CO_2 and CCG gave us the opportunity to confirm again our previous results. Whenever the culture was exposed to CO_2, the alkalinity and dissolved inorganic carbon species increased, but not during exposure to CCG (Figure 86).
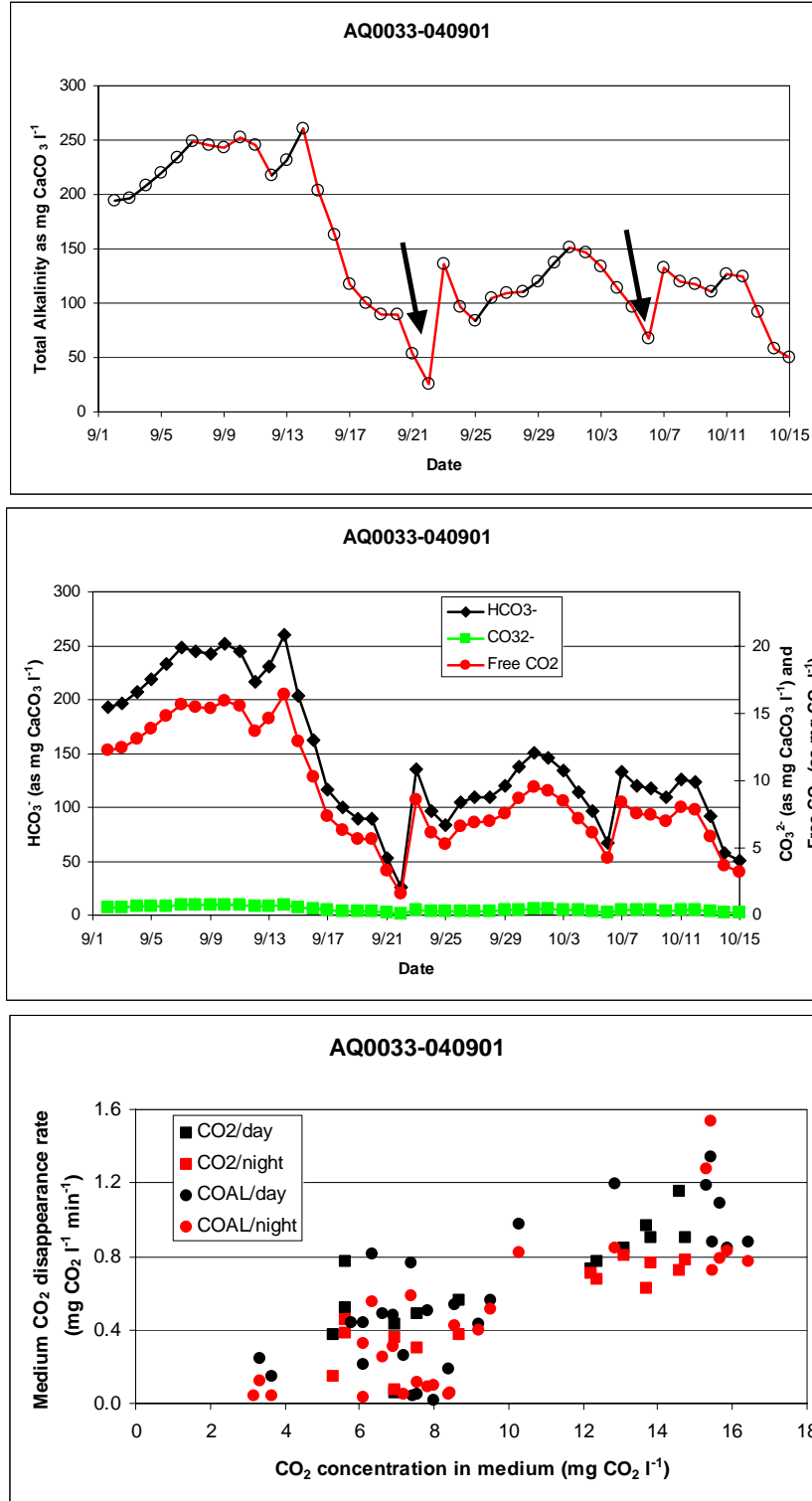
Figure 86. Changes in alkalinity (top panel), dissolved inorganic carbon (middle panel), and dependency of CO_2 disappearance rates on the concentration of CO_2 in the medium (bottom panel) for a culture of strain AQ0033 grown on CO_2 and CCG. Periods during which the culture was exposed to CO_2 and CCG are indicated by black and red lines in the top panel, respectively. The arrow indicates when the culture was diluted with fresh medium.

Experiments with strain AQ0059 (*Chlorella sp.*)

We grew one scale up culture of strain AQ0059 on CO_2. We did not have an opportunity to grow it while exposed to CCG. As was found earlier, growth during exposure to CO_2 resulted in continued increases in the alkalinity and concentration of dissolved inorganic carbon species in the medium. Similarly to previous experiments, the rates of CO_2 disappearance from the medium, whether degassing or photosynthetic in nature, correlate with the concentration of dissolved CO_2 in the medium (Figure 87).
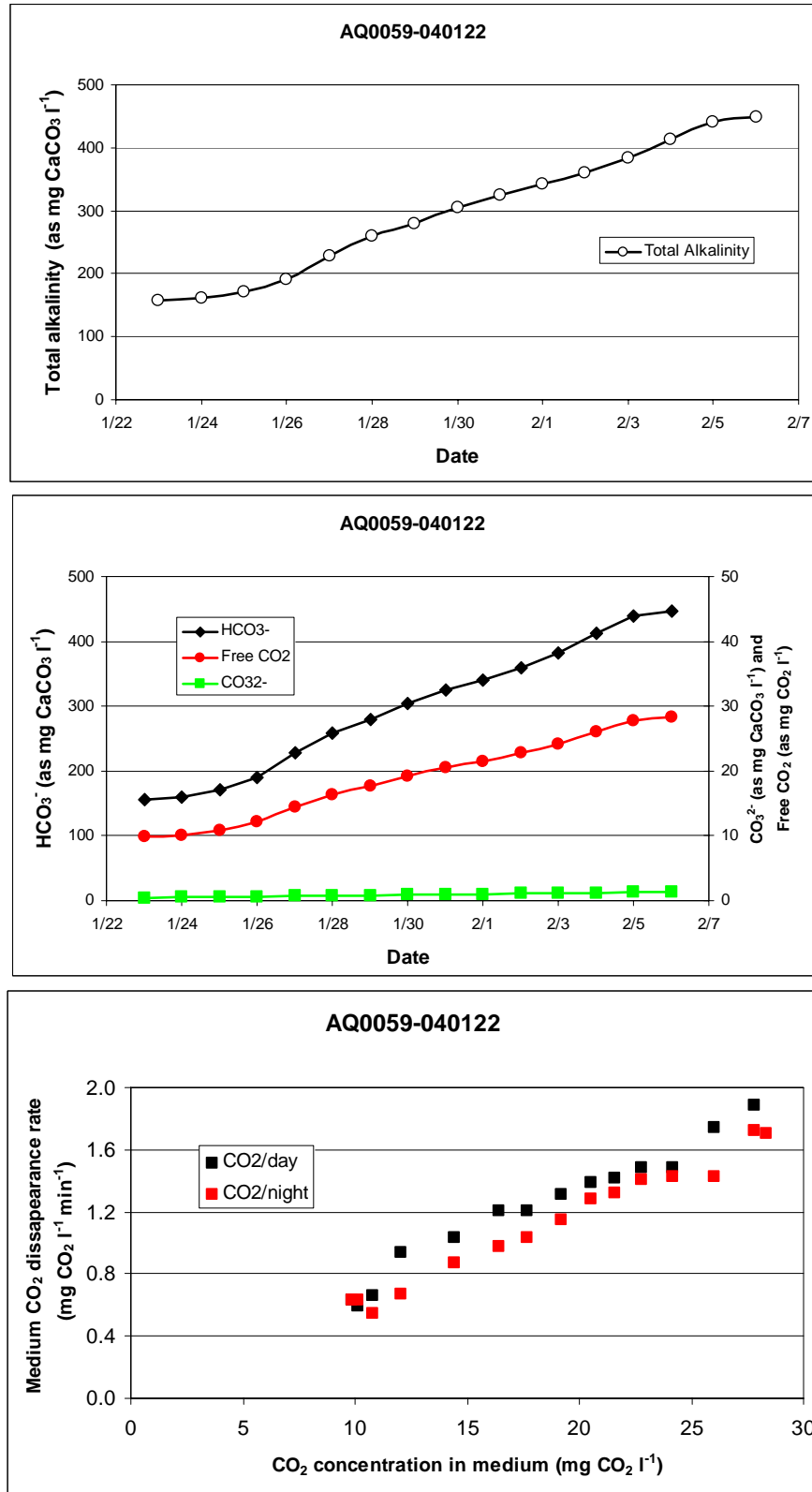
Figure 87. Changes in alkalinity (top panel), dissolved inorganic carbon (middle panel), and dependency of CO_2 disappearance rates on the concentration of CO_2 in the medium (bottom panel) for a culture of strain AQ0059 grown on CO_2.

114

Experiments with strain AQ0073 (*Botryococcus braunii*)

Here we present the results obtained from a pilot scale culture of strain AQ0073 which was grown on CO_2 for 12 days and then switched to CCG for 14 days (AQ0073-041014). As opposed to the experiments reported on above, AQ0073 was grown at pH 8.0.

As was found earlier, growth during exposure to CO_2 resulted in continued increases in the alkalinity and concentration of dissolved inorganic carbon species in the medium. Once the source of inorganic carbon for the culture was switched to CCG, the alkalinity decreased continuously. The changes in dissolved inorganic carbon species paralleled those of the alkalinity (Figure 88).
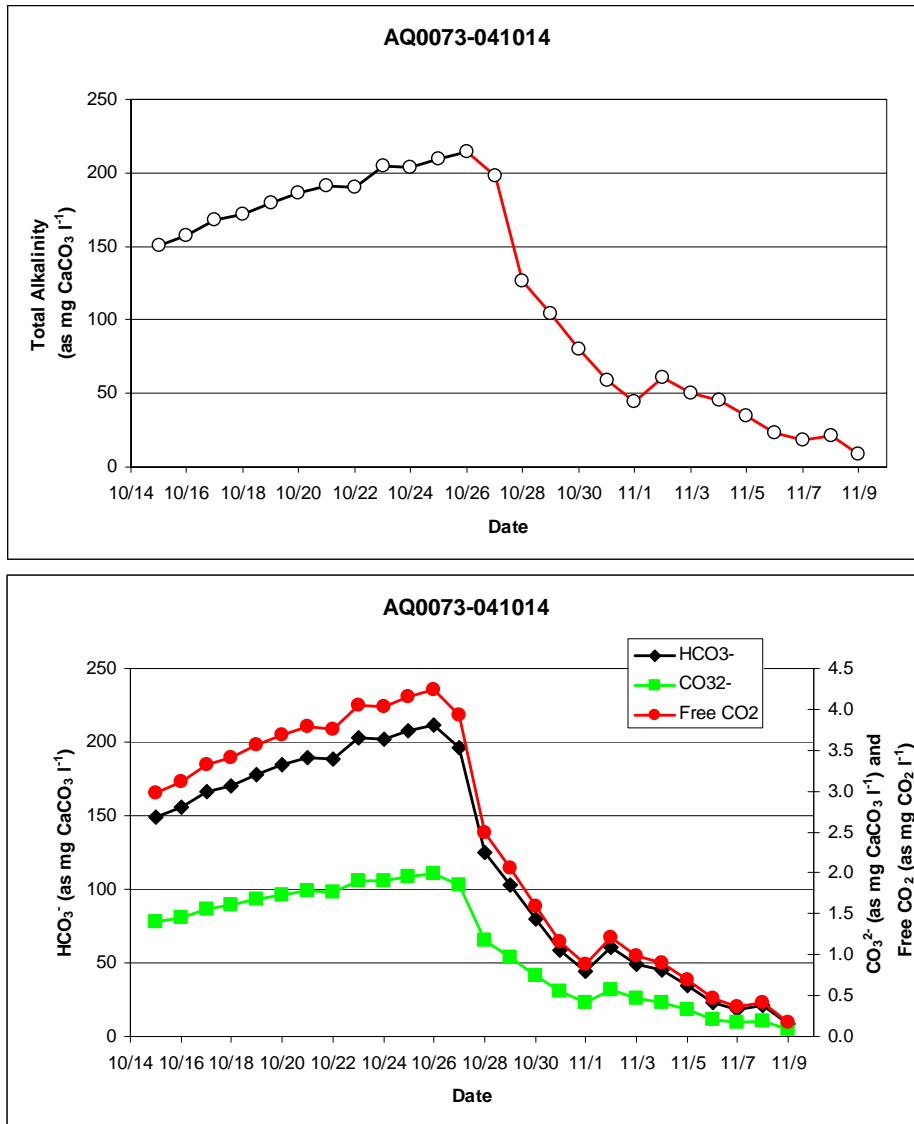
Figure 88. Changes in alkalinity (top panel) and dissolved inorganic carbon (bottom panel) for a culture of strain AQ0073 grown on CO_2 and CCG. Periods during which the culture was exposed to CO_2 and CCG are indicated by black and red lines in the top panel, respectively

115

Figure 89 (top panel) shows the calculated estimates of CO_2 disappearance from the medium on the different days. The rates measured during the nighttime is ascribed to degassing of CO_2 from the culture while the rates measured during the daylight hours is the sum of degassing plus that assimilated through algal photosynthesis. As can be seen in the bottom panel of Figure 89, the use of coal combustion gases is associated with lower concentrations of dissolved CO_2 in the medium. Similarly to previous experiments, the rates of CO_2 disappearance from the medium, whether degassing or photosynthetic in nature, correlate with the concentration of dissolved CO_2 in the medium. The combination of lowered alkalinity (associated with the use of CCG) and high pH (8.0) combined to produce some of the lowest concentrations of dissolved CO_2 of this study (Figure 89).
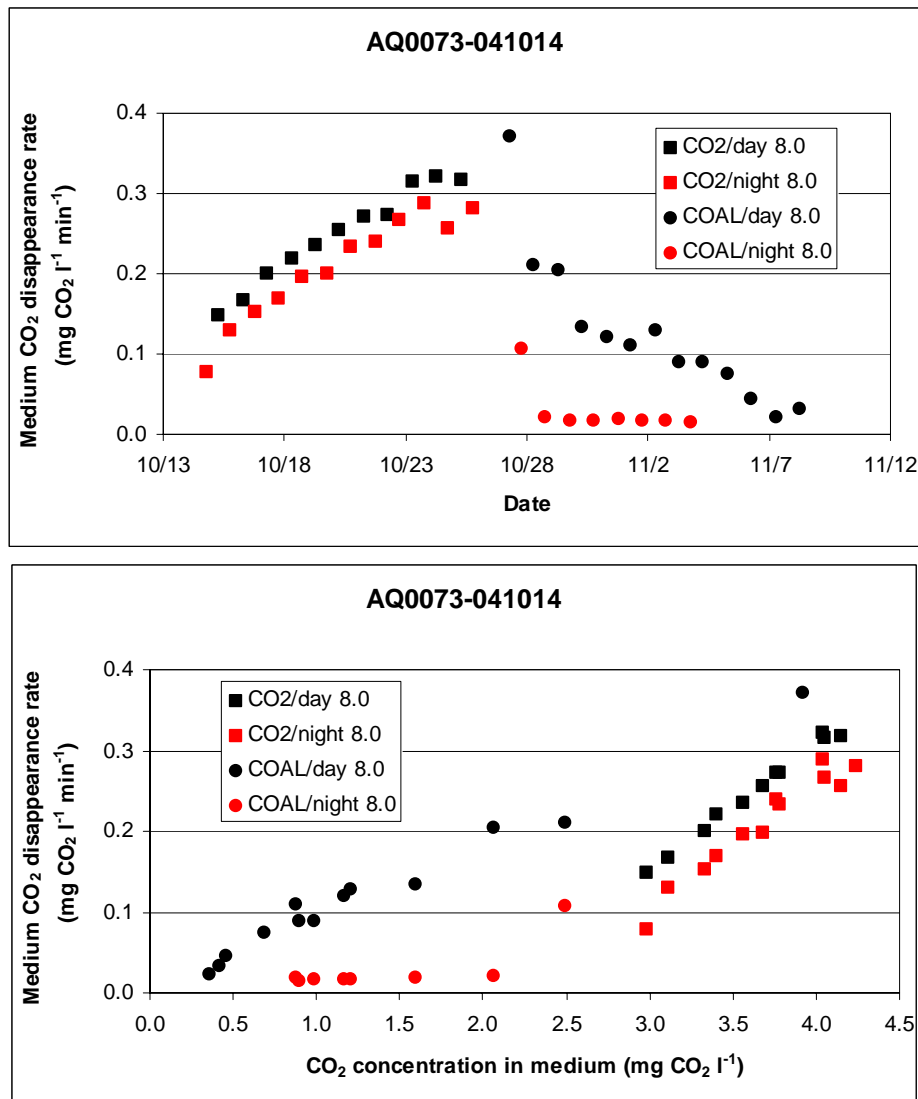
Figure 89. Rate of CO_2 disappearance from the cultures during daylight and nighttime on different days (top panel) and relationship between the concentration of dissolved CO_2 in the medium and CO_2 disappearance rate (bottom panel).

116

Summary of microalgal CO_2 capture rates at pilot scale in outdoor photobioreactors

Here we have reported results on experiments carried out in pilot scale outdoor photobioreactors. We have grown seven strains of microalgae in the presence of CO_2 and coal combustion gases. Table 17 summarizes the results as the averages of the CO_2 disappearance rates for each experiment obtained during day light hours (degassing plus microalgal uptake) and night time (degassing). The difference between those values represents the amount of CO_2 captured by the microalgae.

The productivity of outdoor microalgal cultures can be quite variable as they depend, for example, on the availability of sunlight. This is reflected in the daily values for carbon capture presented above. Even with all that variability, the data from these experiments reflect what was learned in Task 2, that a large fraction of the CO_2 that is available in the culture medium will simply escape (degassing) and will not be captured by the microalgae.

The data also indicate that the use of coal combustion gases directly by microalgal cultures does not appear to pose a physiological impediment to the algae for capturing CO_2. However, use of coal combustion gases does lower the alkalinity of the medium, presumably because of the presence of acid gases (NO_X and SO_X). For any one culture pH, lower alkalinity results in lower dissolved inorganic carbon in the medium. While our experiments were not specifically designed to test whether low carbon concentration in the medium would limit the growth of the microalgal strains we tested, it could cause lowered productivity and lowered carbon capture rates. If future work determines this to be a detriment to the microalgal cultures, the acid gases produced by coal combustion would need to be scrubbed from the flue gas in an industrial application.

Table 17. Summary of CO_2 Disappearance Rates at Pilot Scale in Outdoor Photobioreactors (as mg CO_2 l^{-1} min^{-1}).

Culture ID	CO_2/Day	Night	Diff/Photo	CCG/Day	Night	Diff/Photos
AQ0008-041207	2.37	1.99	0.28	0.86	0.85	0.01
AQ0008-041111	N/A	N/A	N/A	1.40	1.19	0.21
AQ0011-040217	1.65	1.55	0.10	N/A	N/A	N/A
AQ0011-050224-a	1.37	1.41	-.04	N/A	N/A	N/A
AQ0011-050224-b	N/A	N/A	N/A	0.98	1.00	-0.02
AQ0012-050209	1.39	1.19	0.20	N/A	N/A	N/A
AQ0012-050130	0.56	0.42	0.14	0.41	0.24	0.17
AQ0024-050318	1.11	0.90	0.21	N/A	N/A	N/A
AQ0024-050323	N/A	N/A	N/A	1.05	1.03	0.02
AQ0033-040901	0.68	0.51	0.16	0.58	0.45	0.13
AQ0059-040122	1.21	1.12	0.09	N/A	N/A	N/A
AQ0073-041014	0.25	0.21	0.04	0.15	0.03	0.12

4.3.2   Subtask 3.2 – Full Scale Production Runs

4.3.2.1 Initial Growth Rates

During the initial batch grow out period of photobioreactor cultures, maximum growth rates are observed as the cells' growth is not yet limiting. We pooled the growth data grown in full scale photobioreactors (up to 25,000 liters) during this initial phase of culture growth. A total of 18 cultures were grown in full scale MGMs representing 6 different strains of microalgae. The growth rates of the cultures were calculated from the daily changes in fluorescence-based biomass estimates (Figure 90).
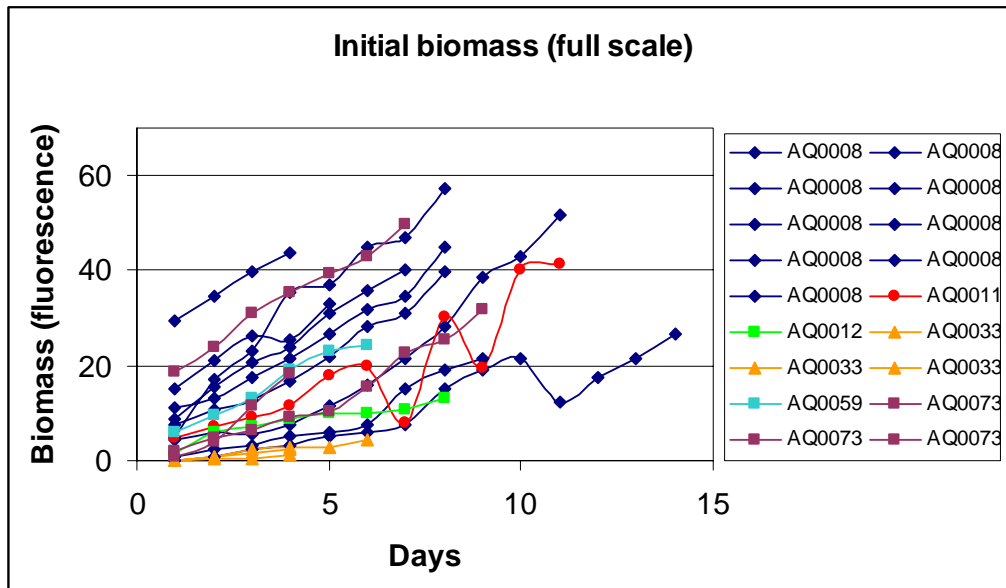
Figure 90. Daily biomass estimates.

For the 6 strains grown in full scale MGMs, the maximum daily growth rates ranged between 0.16 and 1.53 d^{-1} while average growth rates for each culture ranged between 0.13 and 1.00 d^{-1} (Figure 91).
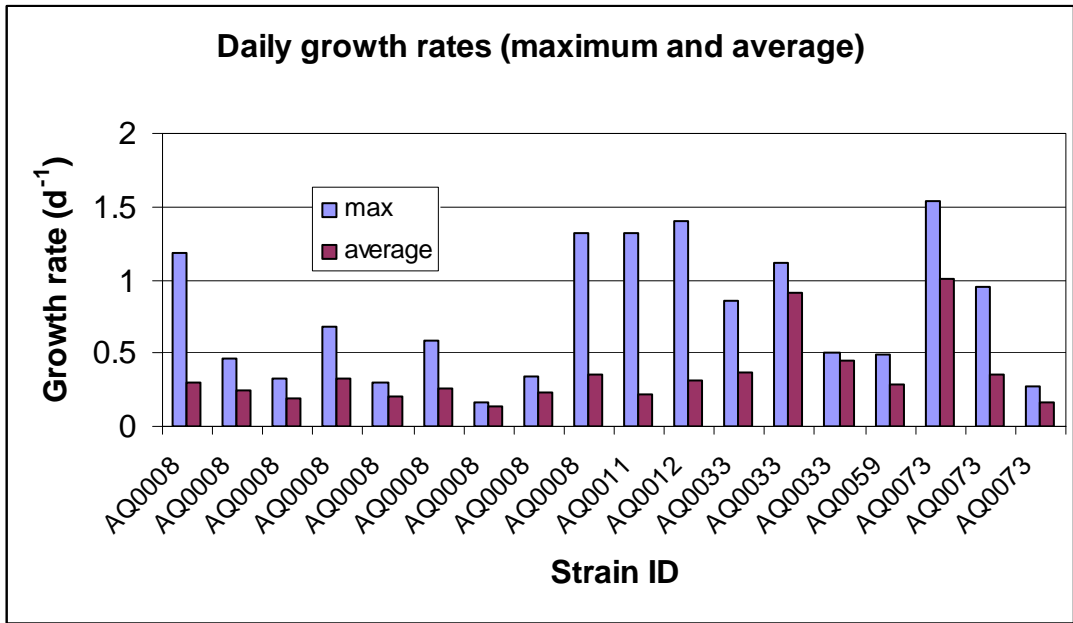
Figure 91. Growth rates measured in 18 individual pilot scale cultures.

If we average the obtained growth rates for all cultures representing any one strain we find the following:

Strain AQ0008	0.25 d^{-1}
Strain AQ0011	0.21 d^{-1}
Strain AQ0012	0.31 d^{-1}
Strain AQ0033	0.58 d^{-1}
Strain AQ0059	0.28 d^{-1}
Strain AQ0073	0.51 d^{-1}

We consider these rates only to be indicative of potential growth and, thus carbon capture potential into microalgal biomass. It must be kept in mind that in outdoor industrial applications of microalgal photosynthesis growth is always limited, usually by solar flux.

Next we consider the biomass productivities obtained during the same culture start up period. We established fluorescence vs. biomass relationships for the strains, above. Figure 92 shows the biomass (dry weight) estimates for the same cultures.
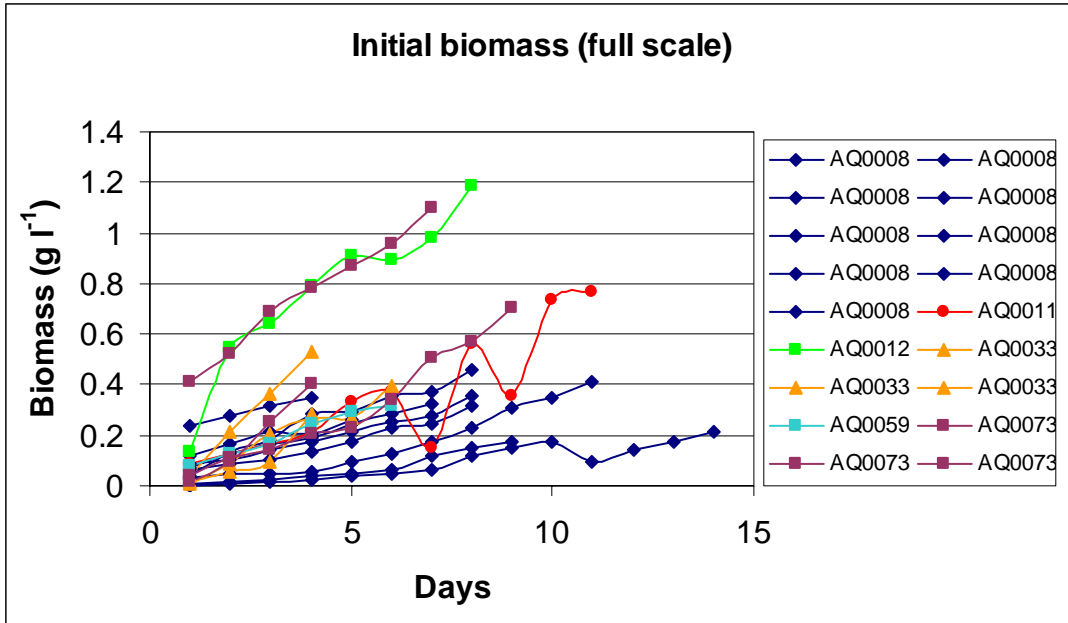
Figure 92. Biomass estimates (g l^{-1}) during the initial ramp up phase.

From these values we calculated the actual biomass production rates for this period (Figure 93). Cultures of strains AQ0011 and AQ0012 were the most productive cultures.
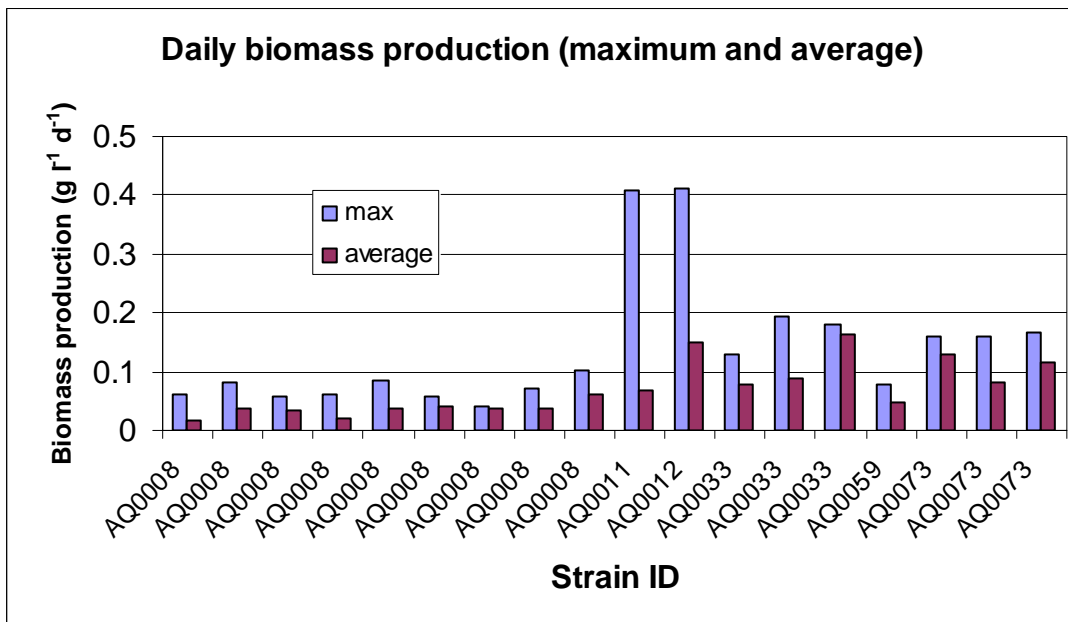
Figure 93. Daily biomass productivities during the ramp up phase.

4.3.2.2 Photosynthetic Carbon Uptake

Effects of Culture pH

For our first experiment at full scale we tested the effects of pH and gas composition on the CO_2 capture capacity of *Haematococcus pluvialis* (AQ0008) cultures grown in our commercial scale MGM photobioreactors (25,000 liters). Two cultures were grown in parallel, one was fed pure CO_2 as the microalgal carbon source and pH control (AQ0008-030903), the second one was fed the stack gases from the propane combustor (AQ0008-030927). Gas additions, whether pure CO_2 or stack gases, were added to the MGM cultures on demand, i.e., when the pH of the cultures indicated lowering of the concentration of CO_2 in the medium. Both photobioreactors were started at a nominal pH of 7.5, i.e., the controlling set points were 7.4 and 7.6. After several days, the pH was changed to 8.5, the set points were 8.4 and 8.6.

During this experiment we also used a gas analyzer consisting of a IMR400 gas dryer and a IMR5000 analyzer to measure the concentration of NOx, and CO_2 in the gas stream from the propane combustor before and after the gas was introduced into the photobioreactor. From these values, we have estimated the relative capture efficiency of the microalgal culture.

Figure 94 shows the pH values measured during the duration of the experiment in both photobioreactors. Both photobioreactors were started at a nominal pH of 7.5, i.e., the controlling set points were 7.4 and 7.6. After several days, the pH was changed to 8.5, the set points were 8.4 and 8.6. Figure 95 shows the cell concentrations and fluorescence-based biomass estimates obtained during the experimental period for these two photobioreactors.

Growth rates were calculated from the changes in cell concentration (Figure 95) and averaged for the each photobioreactor for the periods when the reactors were maintained at either 7.5 or 8.5 pH. For AQ0008-030903 (running on CO_2) the average growth rates were 0.28 d^{-1} and 0.10 d^{-1} at pH 7.5 and 8.5 respectively. For AQ0008-030927 (running on propane combustion gases) the average growth rates were 0.25 d^{-1} and 0.12 d^{-1} at pH 7.5 and 8.5 respectively.

The results of alkalinity measurements in these cultures indicate that, unlike those cultures exposed to coal combustion gases, propane combustion gases do not appear to be related to a decrease in alkalinity. Figure 96 shows the alkalinity measurements and calculated dissolved inorganic carbon concentrations for culture AQ0008-030927. The only occasions when the alkalinity dropped were on those days when the culture was diluted with fresh medium (top panel). The change in culture pH did, however, have a large effect on the relative abundance of dissolved CO_2 and CO_3^{2-} (bottom panel).
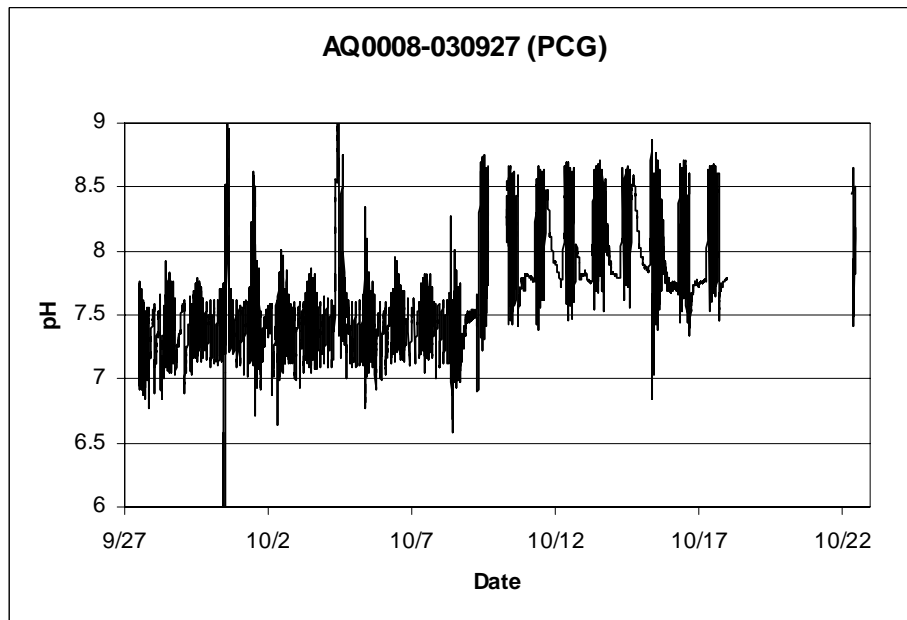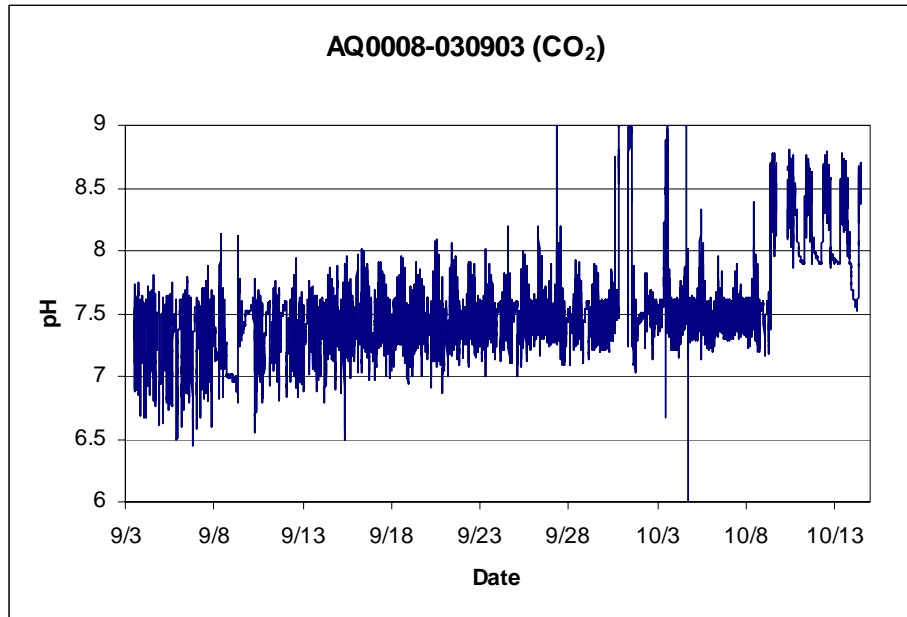
Figure 94. pH traces obtained from AQ0008-030903, a full scale photobioreactor fed CO_2, and AQ0008-030927, a full scale photobioreactor fed propane combustion gases.
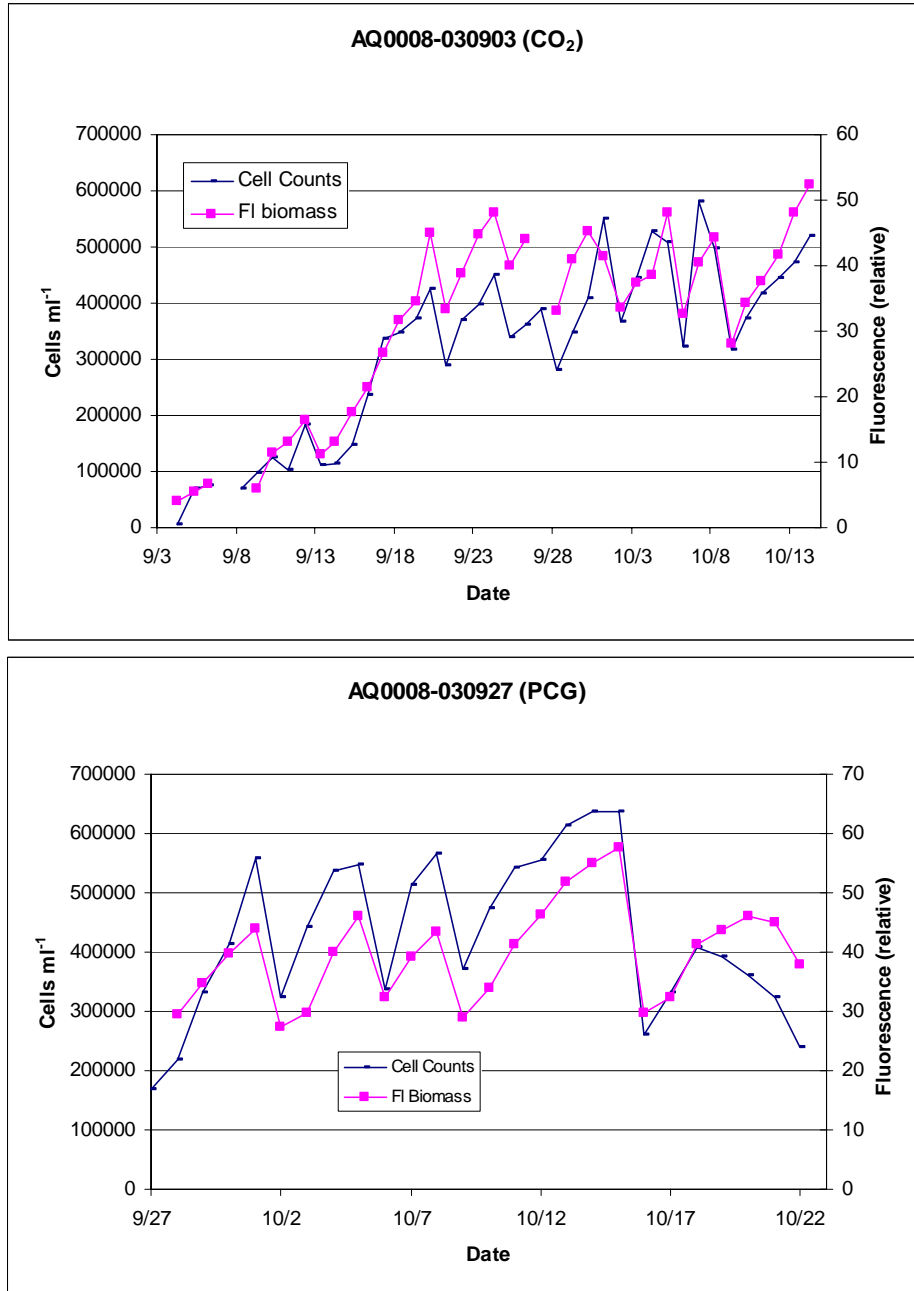
Figure 95. Cell concentration and fluorescence-based estimates of daily biomass for AQ0008-030903 and AQ0008-030927.
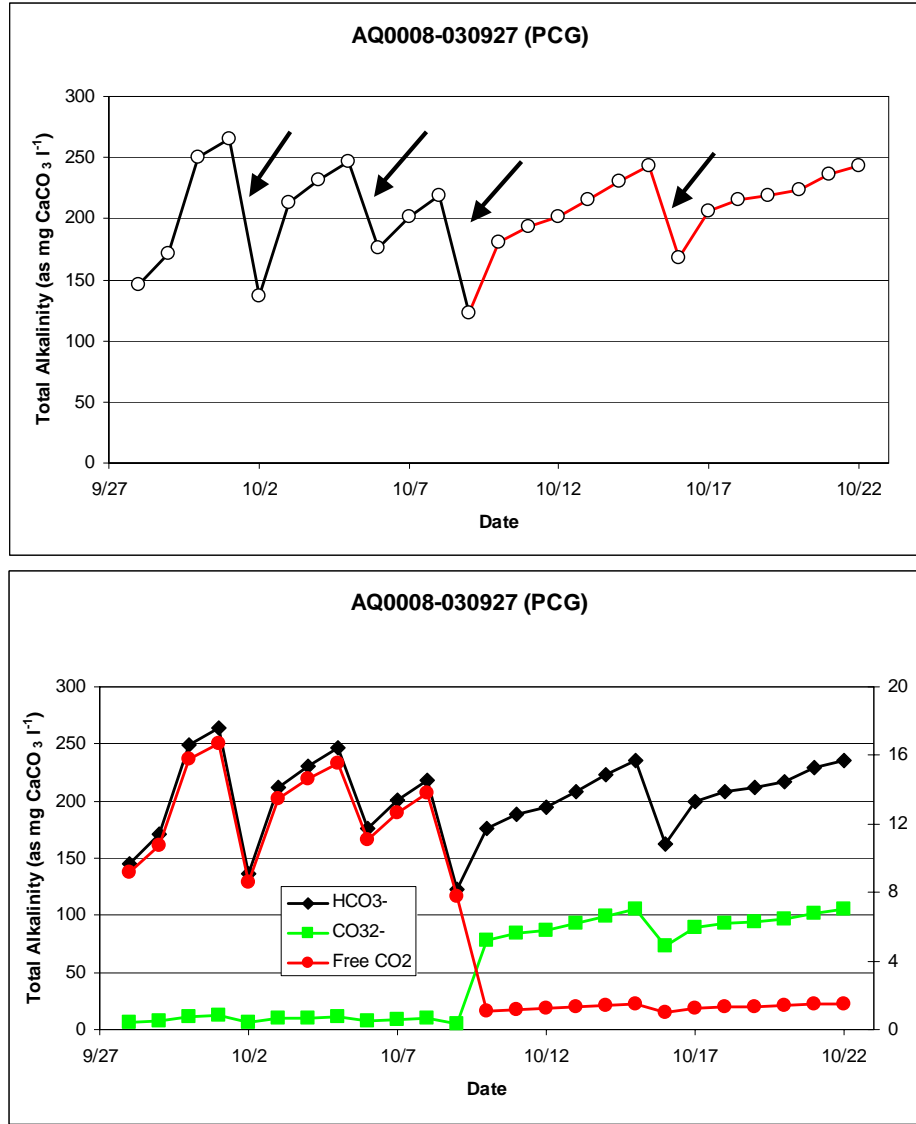
Figure 96. Top panel: results of alkalinity measurements on culture AQ0008-030927. The black line indicates the period during which the culture was grown at 7.5 pH. The red line indicates the period during which the culture was grown at 8.5 pH. Bottom panel: calculated concentrations of dissolved inorganic carbon species in the medium.

The calculated rates of CO_2 disappearance from the medium are shown in Figure 97. As was the case in the pilot scale experiments (Subtask 3.1), it is clearly seen that the rates are larger when the culture pH is maintained at 7.5 than when maintained at 8.5 in both photobioreactors. These results reflected those obtained in our chemostat scale experiments reported on earlier. We have then averaged the CO_2 disappearance rate over each day and night period, eliminating those during which culture dilutions took place. We have further averaged the day and night values for each pH condition for each photobioreactor. Finally, we subtracted the disappearance rates obtained during the night periods from those obtained for the daylight periods to calculate average photosynthetic rates. The results are shown in Table 18 and indicate that while the
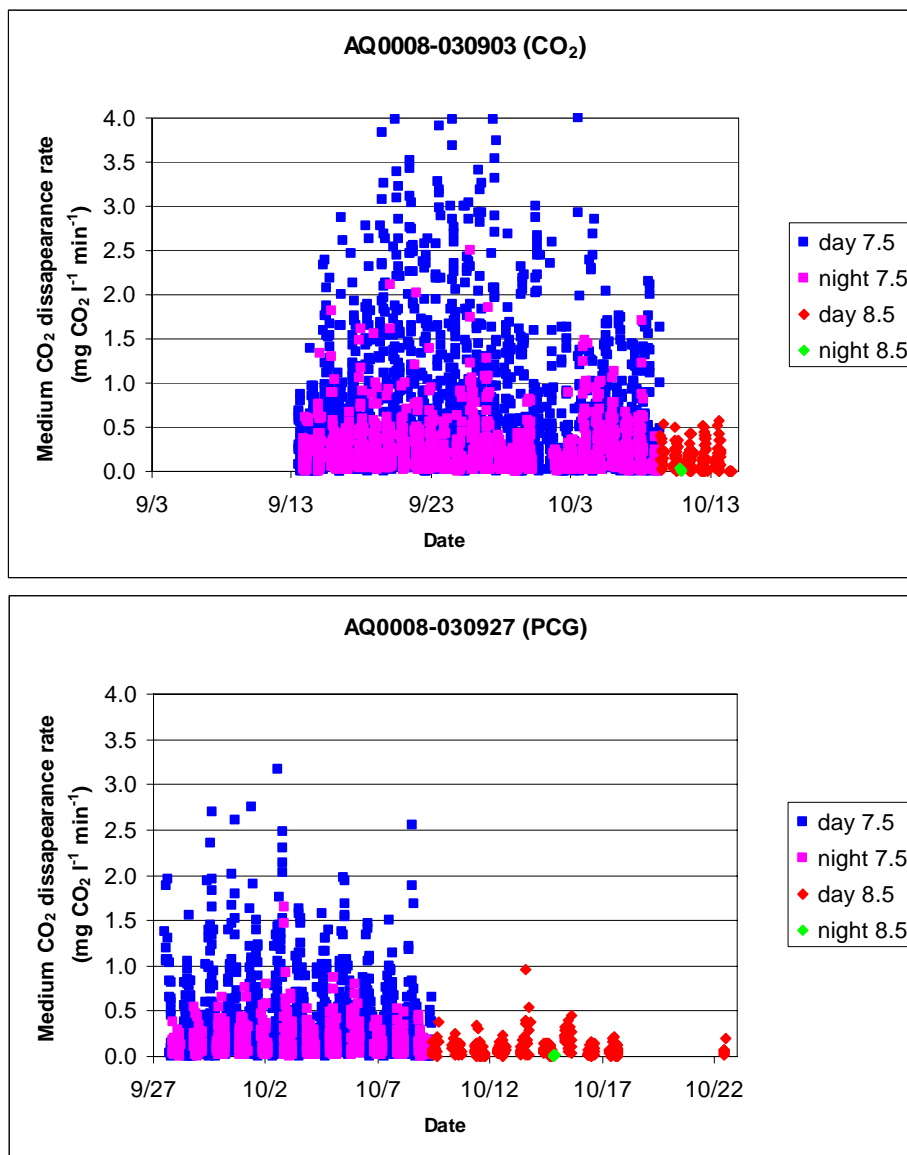
Figure 97. Rates of dissolved inorganic carbon (DIC) disappearance from the medium (photosynthesis and/or degassing) for M14 and M13. The different symbols indicate the different conditions under which these data were obtained (night vs. day, Ph 7.5 vs. pH 8.5).

Table 18. Average Rates of DIC Disappearance from the Medium (mg CO_2 l^{-1} min^{-1}) for AQ0008-030903 (fed pure CO_2) and AQ0008-030927 (fed propane combustion gases) at Either 7.5 or 8.5 pH and Either During the Day or Night Periods. The difference is assumed to be the photosynthetic rate.

pH	7.5			8.5		
Period	Day	Night	Difference	Day	Night	Difference
AQ0008-030903	0.58	0.24	0.34	0.13	0.02	0.11
AQ0008-030927	0.44	0.17	0.27	0.09	0.01	0.07

photosynthetic rates are higher for cultures maintained at 7.5 pH, the amount of CO_2 that is lost to the atmosphere from the medium is about 10 times higher at 7.5 pH than at 8.5 pH. These results agree well with those obtained in the pilot scale photobioreactors and in previous chemostat-scale experiments.

Finally, we have considered the effect of CO_2 concentration in the culture medium on CO_2 degassing rate during the night periods (i.e., in the absence of photosynthesis). The results are shown in Figure 98 superimposed on the results obtained from the pilot scale photobioreactors (M09 and M10, Figure 72). As was the case for the pilot scale experiment, more CO_2 is lost from the medium at higher CO_2 concentrations. Interestingly, at any CO_2 concentration in the medium the rate of degassing is lower for the full scale photobioreactors which translates into higher carbon capture efficiency.
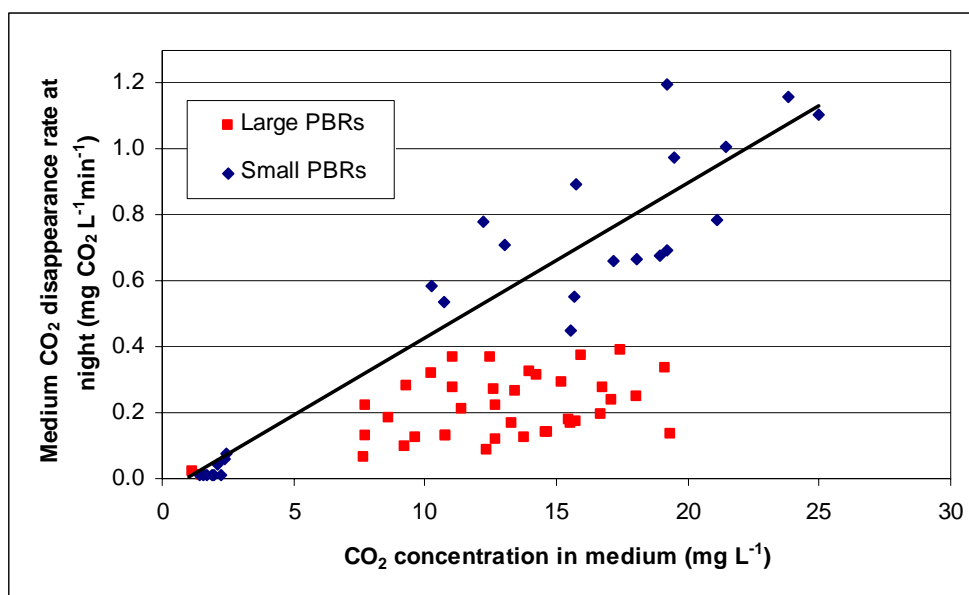
Figure 98. Relationship between CO_2 concentration in the culture medium and night-time rate of dissolved inorganic carbon (DIC) disappearance from the medium (degassing) for AQ0008-030927 and AQ0008-030903 (full scale photobioreactor-25000L-, red squares) superimposed on the values obtained for M09 and M10 (pilot scale-2000L-blue diamonds, Figure 72).

Due to technical issues, we were able to obtained a limited amount of data on individual gas concentrations in the gas stream, before and after passage through the photobioreactor. These measurements were carried out on the photobioreactor being fed propane combustion gases. Figure 99 shows an example of the gas concentration data obtained for a 24 hour period. As was noted earlier, the propane combustor produces combustion gases on demand, i.e., when the pH of the culture is rises above 7.6 in this example. The periods during which the combustor is active can be identified by the rapid decreases in pH resulting from the injection of CO_2 into the photobioreactor. During periods of no combustion, the gas concentrations measured reflect ambient air composition.
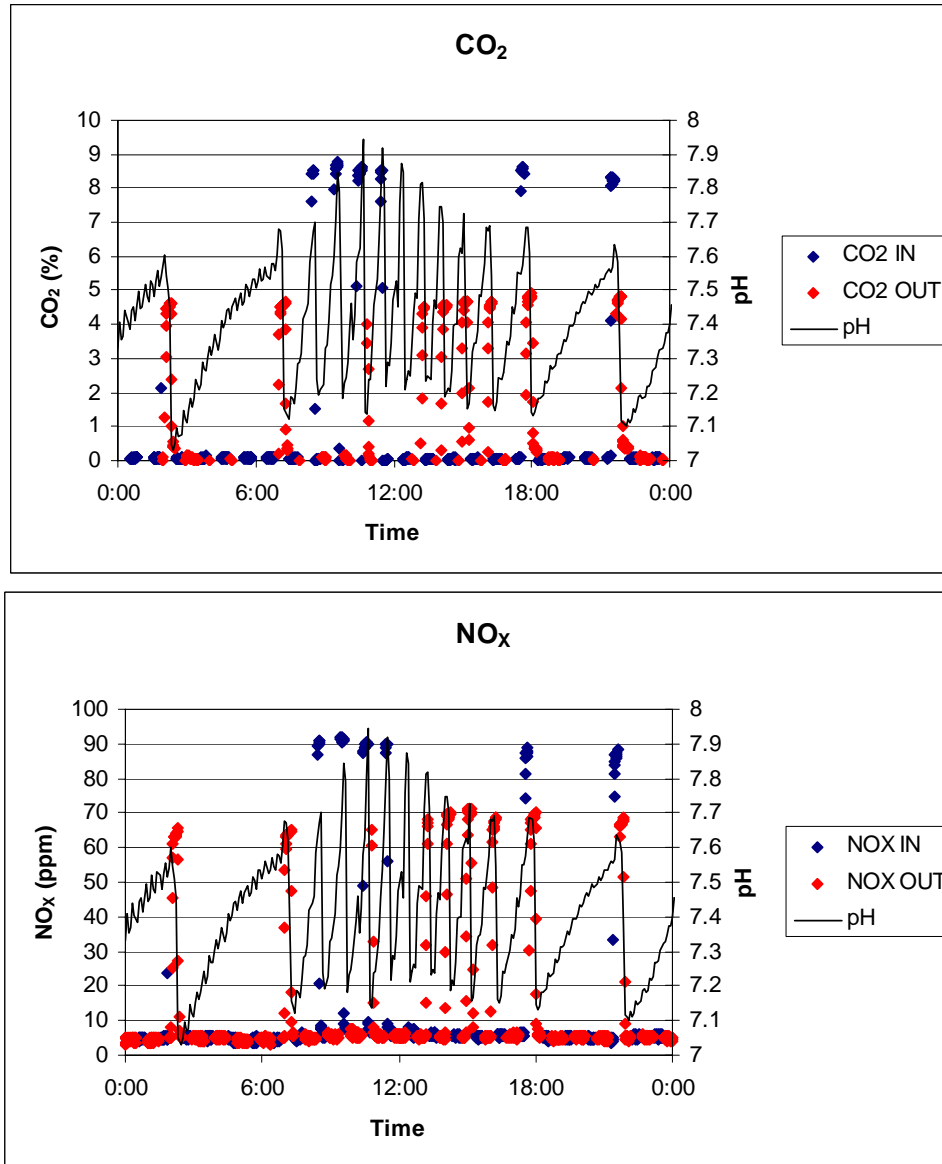
Figure 99. Sample concentrations of CO_2 and NO_X in the gas stream supplied from the propane combustor into the photobioreactor (IN) and in the gas stream leaving the photobioreactor (OUT) for a 24 h period.

Figure 100 shows the CO_2 and NO_X gas concentrations measured during several days of photobioreactor operation. The data indicates that the concentration of CO_2 in the combustor exhaust is about 8.7% (v:v) but only about 4.8% in the photobioreactor's exhaust when the combustor is running. Similarly, the concentration of NO_X is about 91 ppm in the combustor exhaust but only about 75 ppm in the photobioreactor's exhaust. This means that about 45% of the CO_2 and about 18% of the NO_X is scrubbed from the flue gas by passage through the photobioreactor.
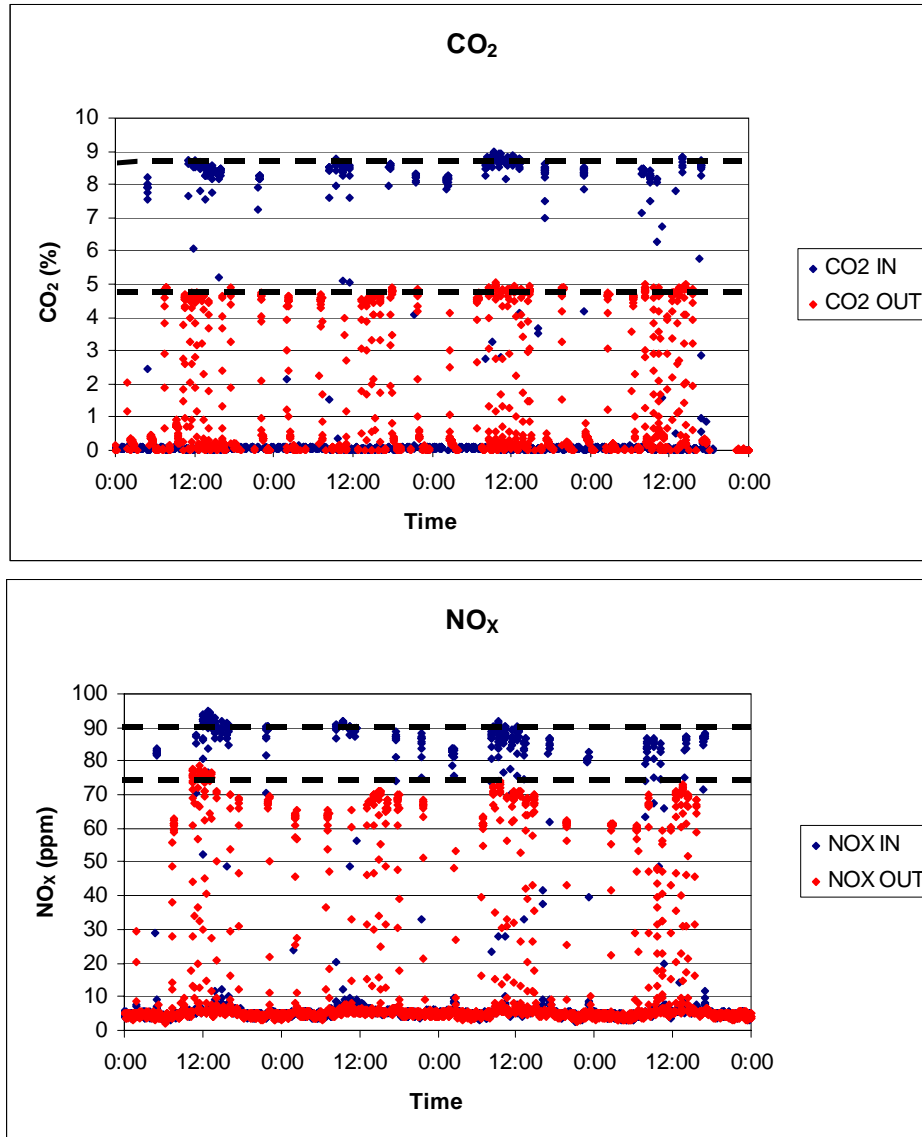
Figure 100. Concentration of CO_2 and NO_X in the gas stream supplied from the propane combustor into the photobioreactor (IN) and in the gas stream leaving the photobioreactor (OUT) for a 4-day period.

Performance of full scale photobioreactors: CO2 vs propane combustion gases

Our objective in these series of experiments was to determine whether any deleterious effects would be observed in culture performance at full scale when propane combustion gases (PCG) were used directly as the source of carbon for the cultures. We scaled up 6 different strains of microalgae for these experiments. In most cases the same culture was exposed to CO_2 for a period of time before being exposed to PCG.

Experiments with strain AQ0008 (*Haematococcus pluvialis*)

We performed a second direct comparison of microalgal performance in full scale photobioreactors being fed either pure CO_2 or actual combustion gases from a propane combustor utilizing strain AQ0008. Culture AQ0008-031025 was allowed to grow for 12 days and was then used to start a second full scale culture, AQ0008-031107. While the former was allowed to continue growing using CO_2, following dilution with fresh medium, the latter was grown with PCG. On both cultures, the pH was changed for several days at a time between 7.5 and 8.5.

Figure 101 shows the pH values measured during the duration of the experiment in both photobioreactors. AQ0008-031107 was fed propane combustion gases while AQ0008-031025 was fed pure CO_2 both on demand. As is shown in the figure, AQ0008-031025 was started with pH set points around 7.5 (7.4-7.6) while AQ0008-031107 was started with set points around 8.5 (8.4-8.6). The set points were switched as the experiment progressed.
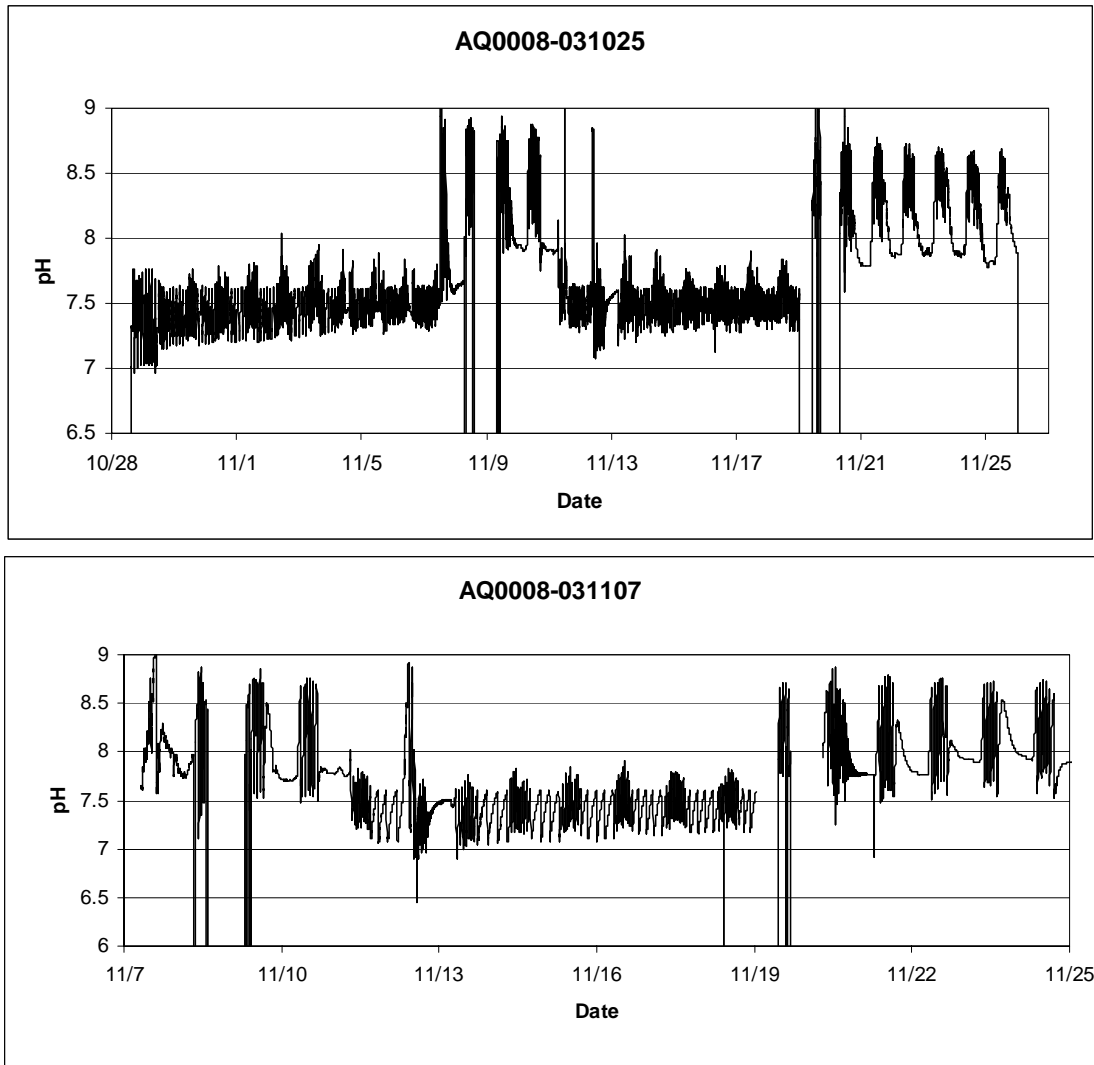
Figure 101. pH traces obtained for AQ0008-031025 (fed CO_2) and AQ0008-031107 (fed PCG).

The cultures in both PBRs accumulated biomass consistently (Figure 102); no deleterious effects were noted in AQ0008-031107, the photobioreactor fed propane combustion gases. Growth rates were calculated from the changes in cell concentration and averaged for the each photobioreactor for the periods when the PBRs were maintained at either 7.5 or 8.5 pH. For AQ0008-031025 (running on CO_2) the average growth rates were 0.26 d^{-1} and 0.29 d^{-1} at pH 7.5 and 8.5 respectively. For AQ0008-031107 (running on propane combustion gases) the average growth rates were 0.21 d^{-1} and 0.29 d^{-1} at pH 7.5 and 8.5 respectively.
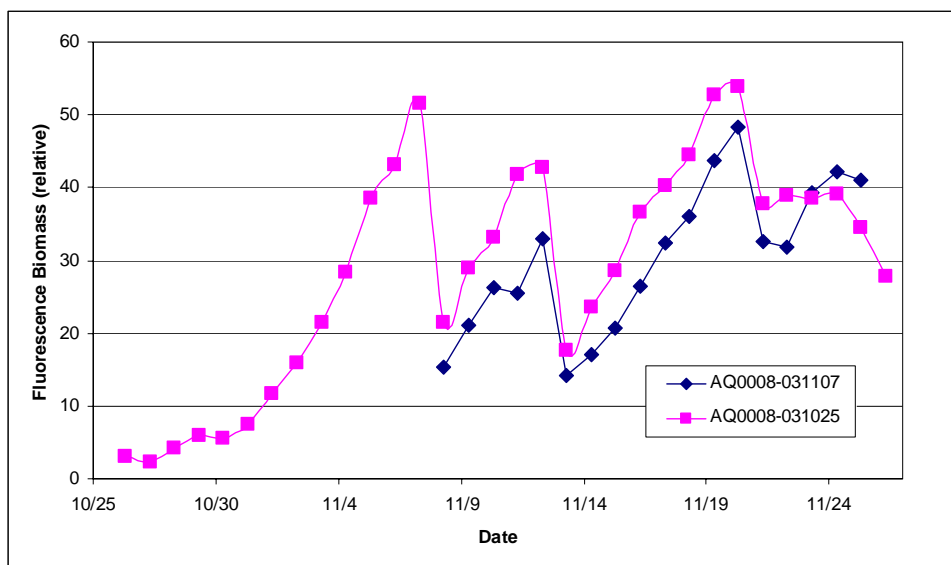
Figure 102. Fluorescence-based estimates of daily biomass for AQ0008-031025 (fed CO_2) and AQ0008-031107 (fed PCG).

The results of alkalinity measurements in these cultures indicate that, unlike those cultures exposed to coal combustion gases, propane combustion gases do not appear to be related to a decrease in alkalinity. Figure 103 and Figure 104 show the alkalinity measurements and calculated dissolved inorganic carbon concentrations for cultures AQ0008-031025 and Q0008-031107 respectively. The only occasions when the alkalinity dropped were on those days when the culture was diluted with fresh medium (top panels). The change in culture pH did, however, have a large effect on the relative abundance of dissolved CO_2 and CO_3^{2-} (bottom panels).

The calculated rates of CO_2 disappearance from the medium are shown in Figure 105. As was the case in the previous experiments, it is clearly seen that the rates are larger when the culture pH is maintained at 7.5 than when maintained at 8.5 in both PBRs. These results reflected those obtained in our chemostat scale experiments reported on earlier.
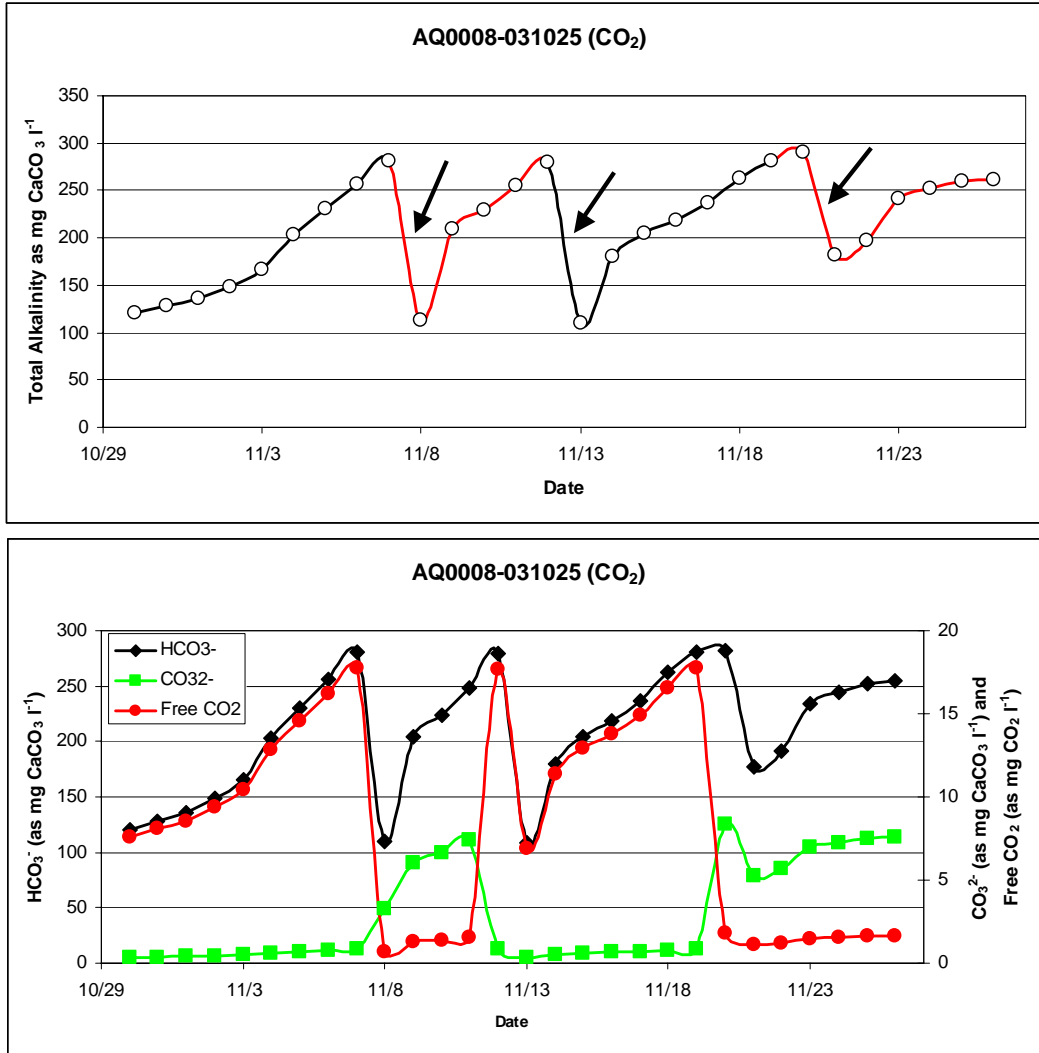
Figure 103. Top panel: results of alkalinity measurements on culture AQ0008-031025. The black line indicates the period during which the culture was grown at 7.5 pH. The red line indicates the period during which the culture was grown at 8.5 pH. Bottom panel: calculated concentrations of dissolved inorganic carbon species in the medium.
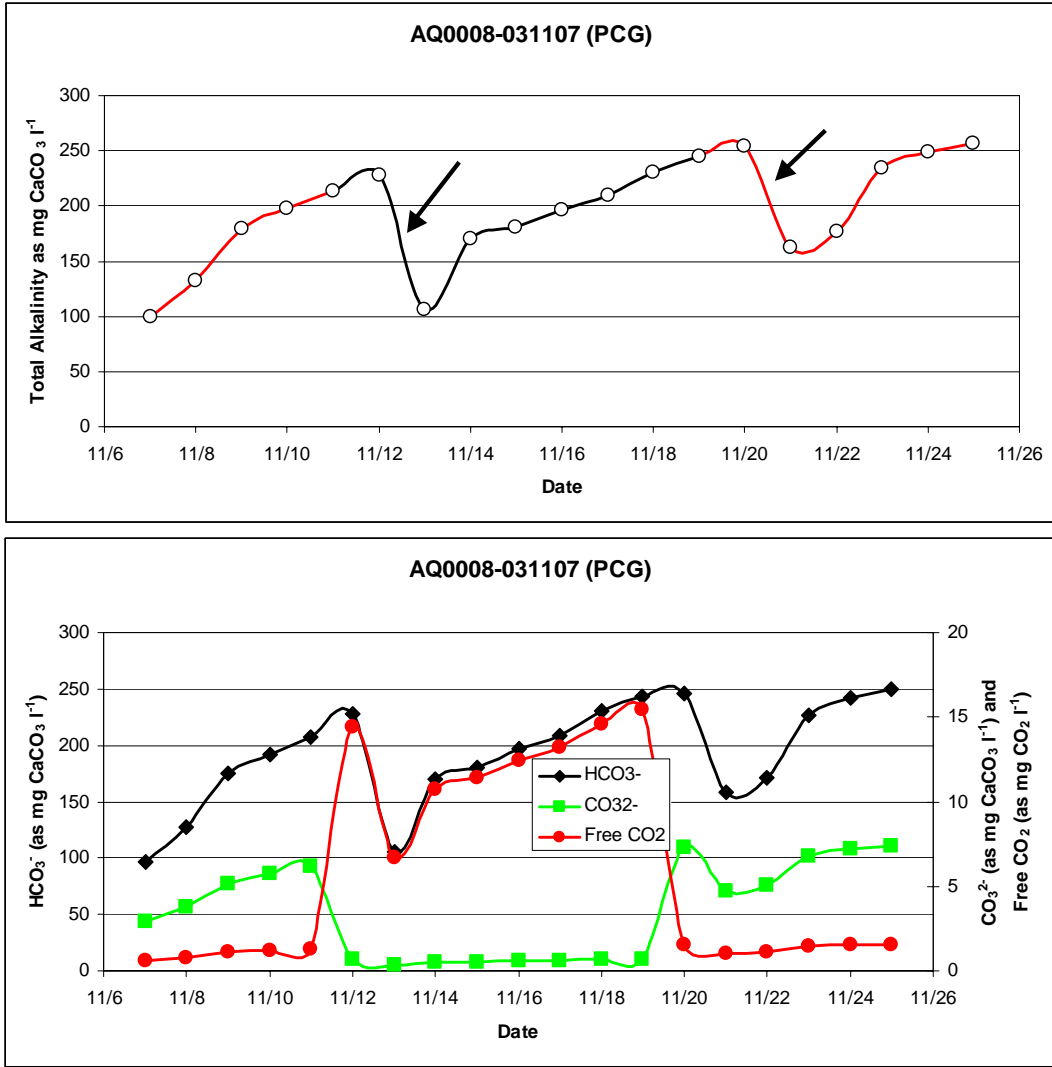
Figure 104. Top panel: results of alkalinity measurements on culture AQ0008-031107. The black line indicates the period during which the culture was grown at 7.5 pH. The red line indicates the period during which the culture was grown at 8.5 pH. Bottom panel: calculated concentrations of dissolved inorganic carbon species in the medium.
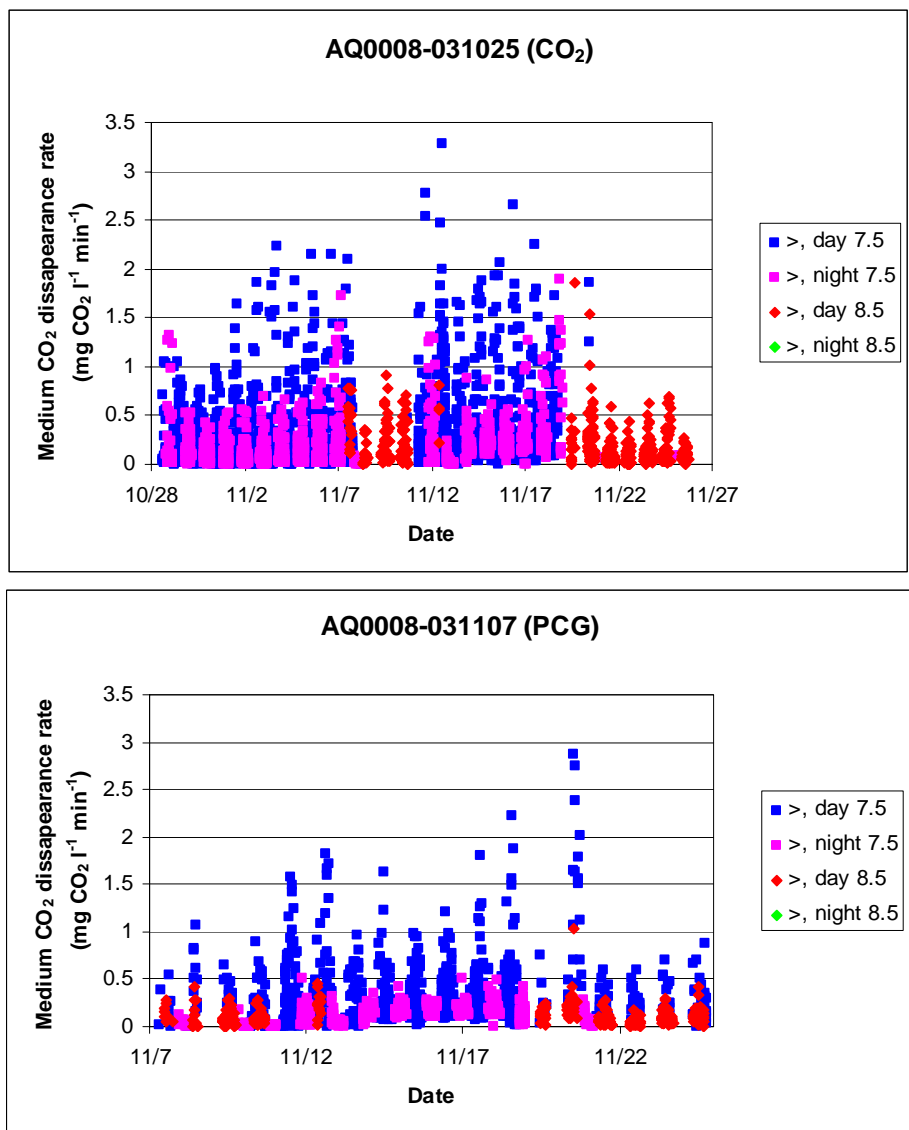
Figure 105. Rates of dissolved inorganic carbon (DIC) disappearance from the medium (photosynthesis and/or degassing) for AQ0008-031025 and AQ0008-031107. The different symbols indicate the different conditions under which these data were obtained (night vs. day, pH 7.5 vs. pH 8.5).

We have then averaged the CO_2 disappearance rate over each day and night period, eliminating those during which culture dilutions took place. We have further averaged the day and night values for each pH condition for each PBR. Finally, we subtracted the disappearance rates obtained during the night periods from those obtained for the daylight periods to calculate average photosynthetic rates. The results are shown in Table 19 and indicate that while the photosynthetic rates are higher for cultures maintained at 7.5 pH, the amount of CO_2 that is lost to the atmosphere from the medium is about 10 times higher at 7.5 pH than at 8.5 pH. These results agree well with those obtained, reported previously, in the pilot scale PBRs and in chemostat-scale experiments.

Table 19. Average Rates of DIC Disappearance from the Medium (mg CO_2 l^{-1} min^{-1}) for AQ0008-031025 (fed pure CO_2) and AQ0008-031107 (fed propane combustion gases) at Either 7.5 or 8.5 pH and Either During the Day or Night Periods. The difference is assumed to be the photosynthetic rate.

pH	7.5			8.5		
Period	Day	Night	Difference	Day	Night	Difference
AQ0008-031025	0.41	0.21	0.19	0.17	N/A	>0.17
AQ0008-031107	0.35	0.15	0.20	0.11	N/A	>0.11

Finally, we have considered the effect of CO_2 concentration in the culture medium on CO_2 degassing rate during the night periods (i.e., in the absence of photosynthesis). The results are shown in Figure 106 and indicate a dependency of degassing of CO_2 from the medium on the concentration of CO_2 in the medium. The same results were obtained from the commercial scale photobioreactors reported on previously (Figure 98). In all cases, and as was the case for the first pilot scale experiment (Figure 72), more CO_2 is lost from the medium at higher CO_2 concentrations.
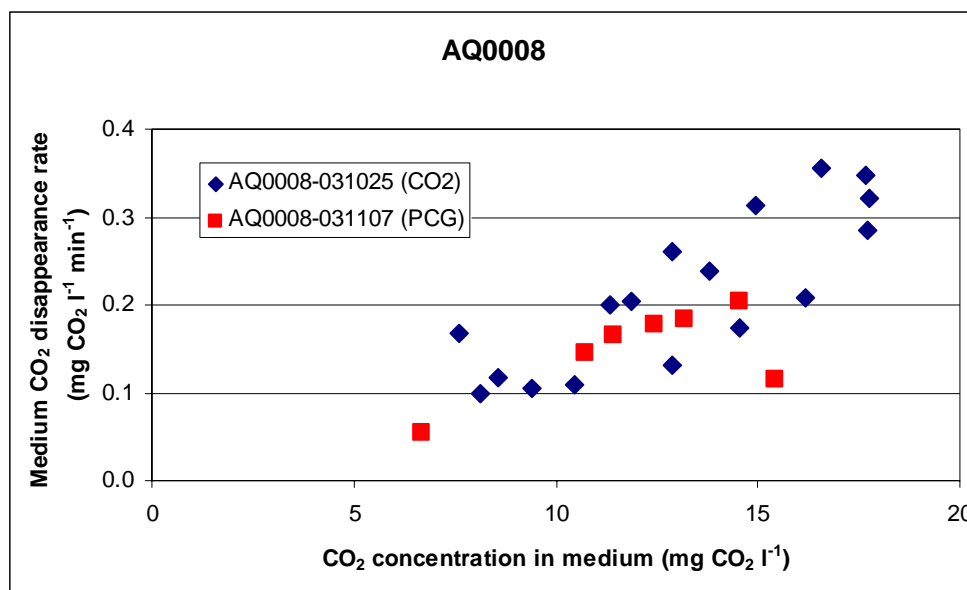
Figure 106. Relationship between CO_2 concentration in the culture medium and night-time rate of dissolved inorganic carbon (DIC) disappearance from the medium (degassing) for both cultures.

Gas analysis data

Figure 107 shows the gas concentrations measured for >2 weeks of photobioreactor operation (AQ0008-031107, propane combustion gases). The top panel shows the concentrations of CO_2 (%) measured at the inlet and outlet of the PBR. The bottom panel shows the

concentrations of NO_X measured at the inlet and outlet of the photobioreactor. The data indicate that the concentration of CO_2 in the combustor exhaust is about 8% (v:v) but only about 4.5% in the photobioreactor's exhaust when the coal combustor is running. Similarly, the concentration of NO_X is about 85 ppm in the combustor exhaust but only about 72 ppm in the photobioreactor's exhaust. This means that about 44% of the CO_2 and about 15% of the NO_X is scrubbed from the flue gas by passage through the photobioreactor. The results confirm those obtained earlier (Figure 100) where we estimated that 45% of the CO_2 and 18% of the NO_X were scrubbed during passage of the propane combustion gases through the culture.
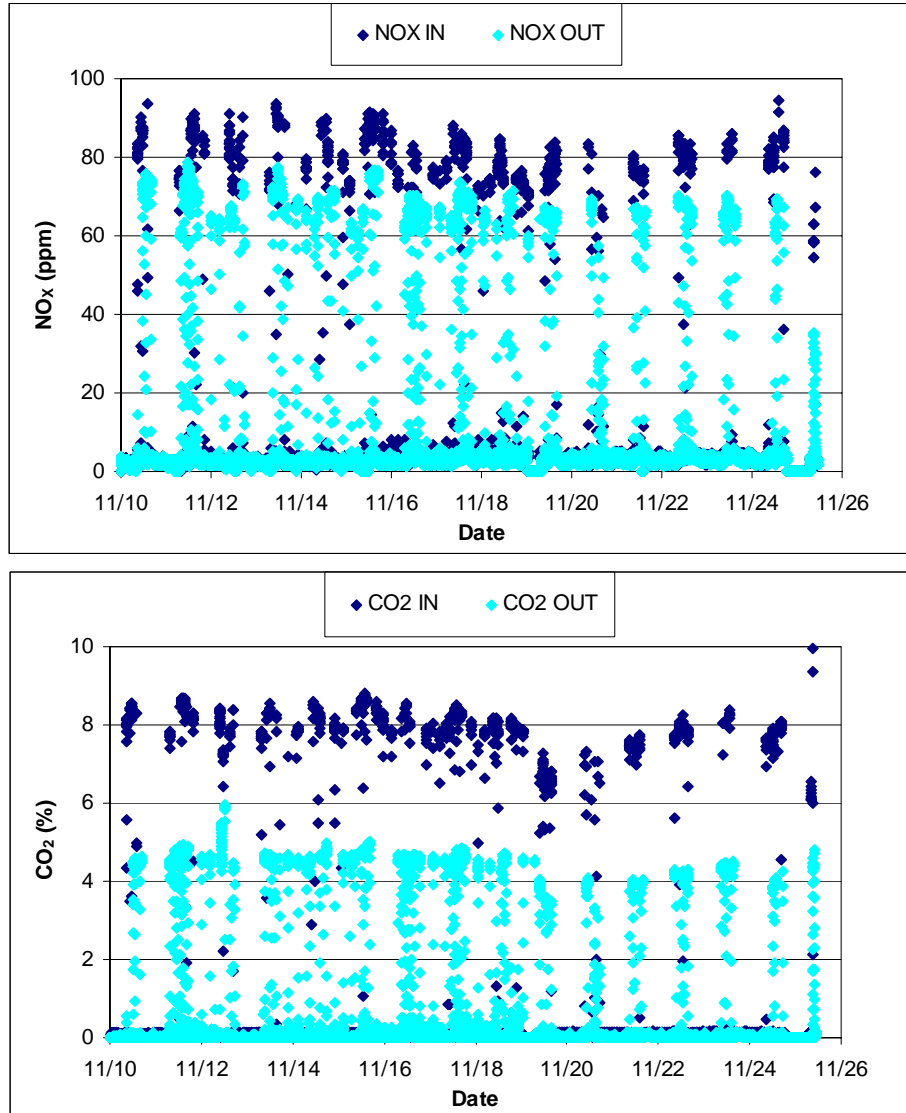
Figure 107. Concentration of CO_2 and NO_X in the gas stream supplied from the propane combustor into the photobioreactor (IN) and in the gas stream leaving the photobioreactor (OUT) for a > 2 week period.

135

Experiments with strain AQ0011 (Unidentified Chlorophyte)

We grew one cultures of strain AQ0011 at full scale. Culture AQ0011-040323 was grown for 4 weeks at 7.5 pH. During 7 days, the culture was grown on CO_2 and the rest of the time it received PCG. As was found earlier with strain AQ0008, growth during exposure to CO_2 and PCG resulted in continued increases in the alkalinity and dissolved inorganic carbon species (Figure 108).
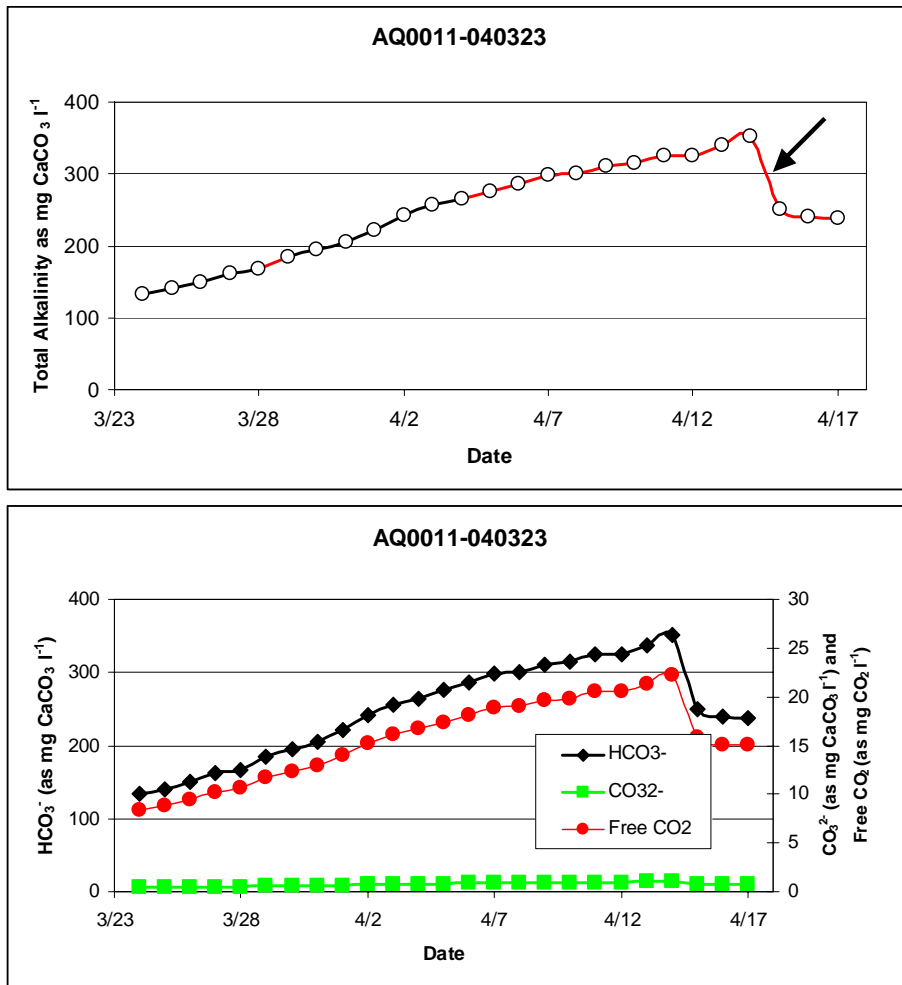
Figure 108. Changes in total alkalinity during growth (top panel) and dissolved inorganic carbon species (bottom panel) in the medium. Black lines in top panel indicate growth on CO_2 and red lines indicate growth on PCG. Arrows in the top panel indicates the day when the culture was diluted with fresh medium.

The calculated rates of CO_2 disappearance from the medium are shown in Figure 109. As in previous experiments, the rates measured during the nighttime are ascribed to degassing of CO_2 from the culture while the rates measured during the daylight hours is the sum of degassing plus that assimilated through algal photosynthesis. As can be seen in the bottom panel of

136
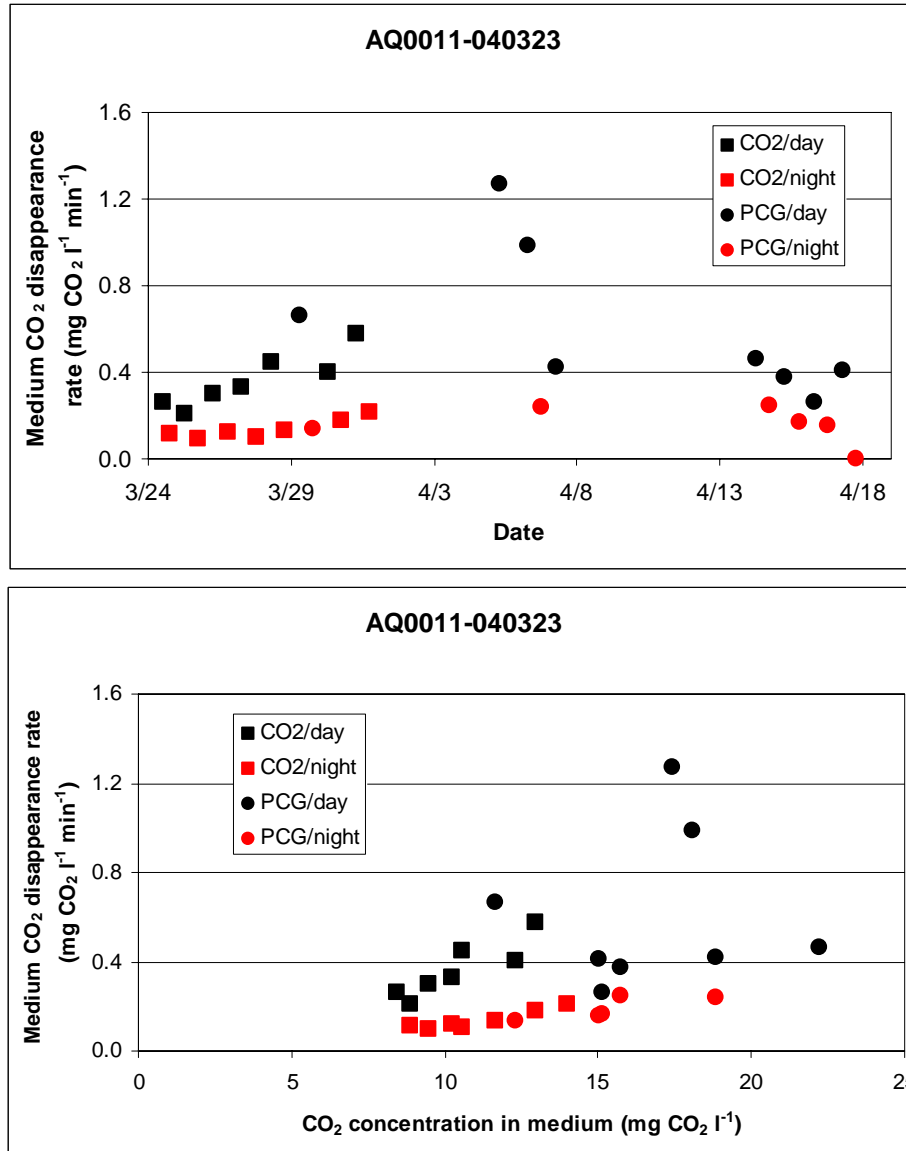
Figure 109. Rate of CO_2 disappearance from the cultures during daylight and nighttime on different days (top panel) and relationship between the concentration of dissolved CO_2 in the medium and CO_2 disappearance rate (bottom panel).

Figure 109, and as opposed to the coal combustion gas experiments conducted on pilot scale photobioreactors, the use of PCG is not associated with lower concentrations of dissolved CO_2 in the medium. However, and similarly to previous experiments, the rates of CO_2 disappearance from the medium, whether degassing or photosynthetic in nature, correlate with the concentration of dissolved CO_2 in the medium.

Experiments with strain AQ0012 (Unidentified Cyanobacterium)

We grew two cultures of strain AQ0012 at full scale. Both cultures (AQ0012-040424 and –050220) were sequentially grown on CO_2 and PCG. We found again, in both cultures, that growth on CO_2 resulted in increasing alkalinity in the medium as well as dissolved inorganic carbon species. The same results were obtained when the cultures were grown on PCG (Figure **110** and Figure 111).
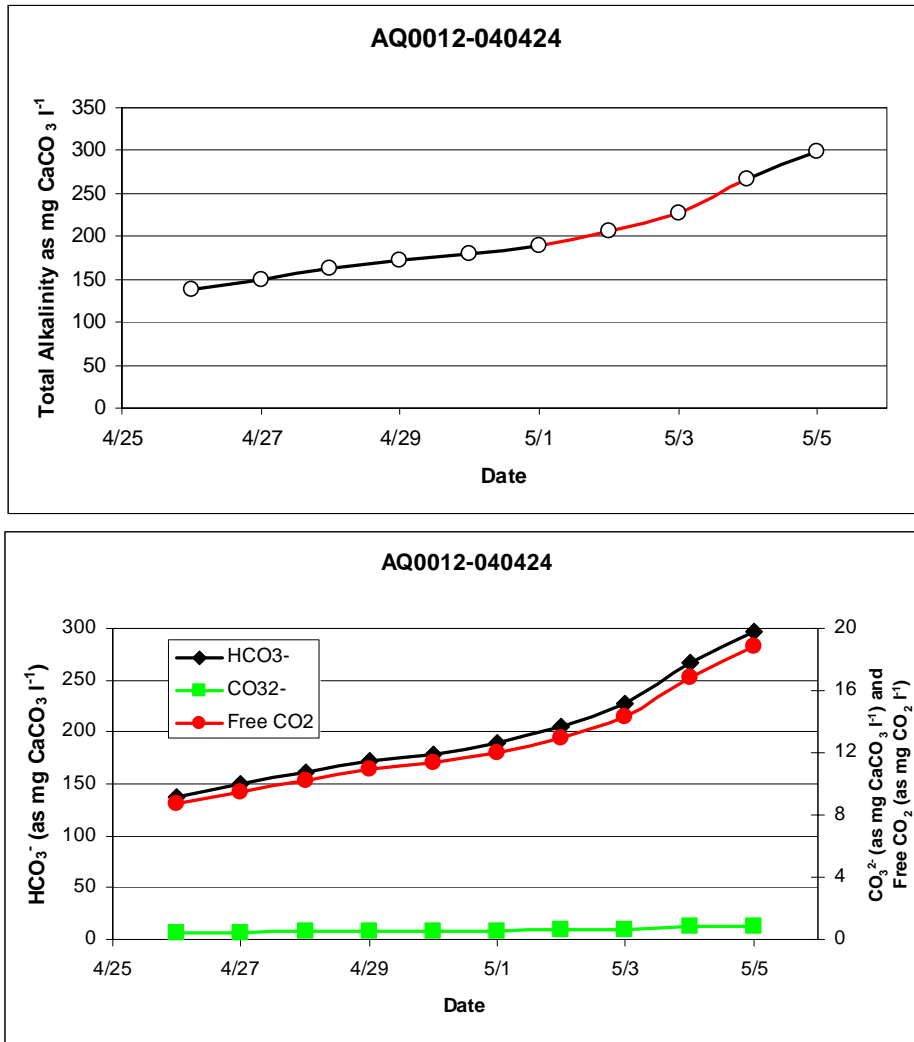
Figure 110. Changes in alkalinity (top panel) and dissolved inorganic carbon (bottom panel) for culture AQ0012-040424 grown on CO_2 and PCG. Periods during which the culture was exposed to CO_2 and PCG are indicated by black and red lines in the top panel, respectively.
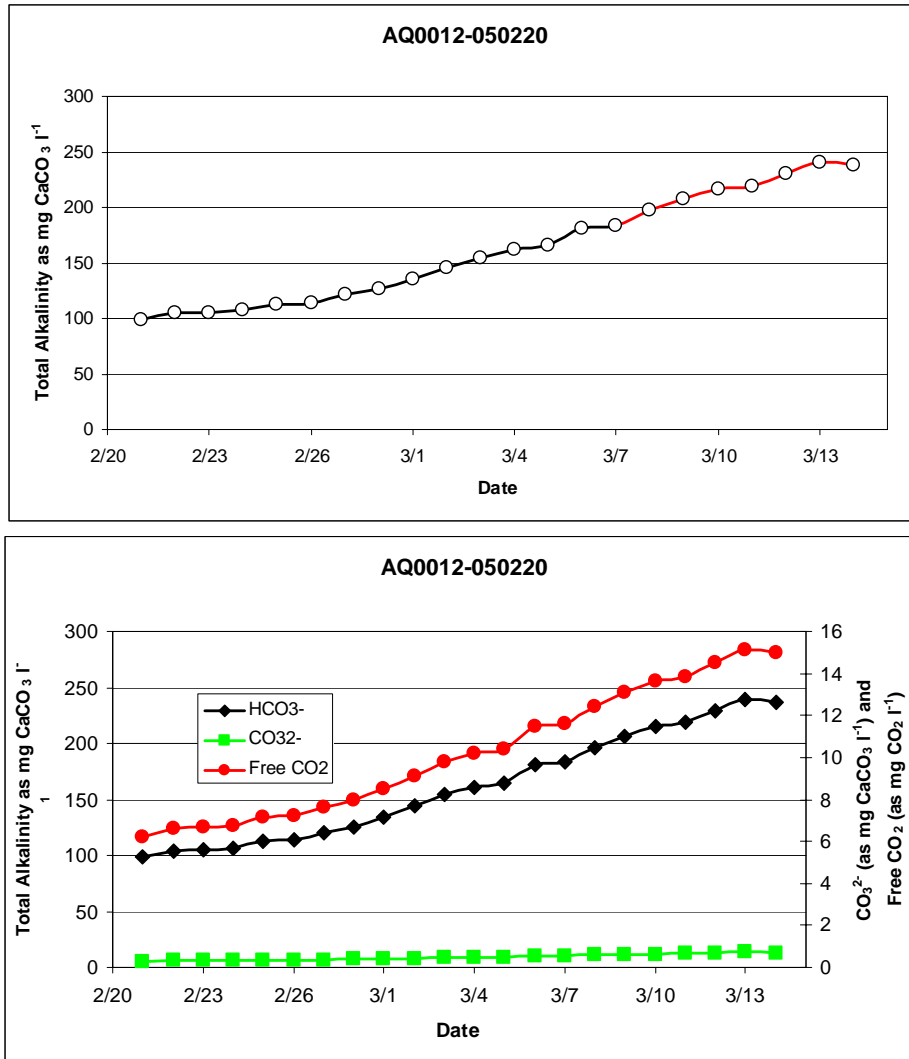
Figure 111. Changes in alkalinity (top panel) and dissolved inorganic carbon (bottom panel) for culture AQ0012-050220 grown on CO_2 and PCG. Periods during which the culture was exposed to CO_2 and PCG are indicated by black and red lines in the top panel, respectively.

Since growth on PCG does not result in decreases in alkalinity nor in dissolved inorganic carbon species, the range of medium CO_2 concentrations that the cultures were exposed to were smaller than in the coal combustion experiments. Still, a relationship exists between medium CO_2 concentration and CO_2 loss rates (Figure 112).
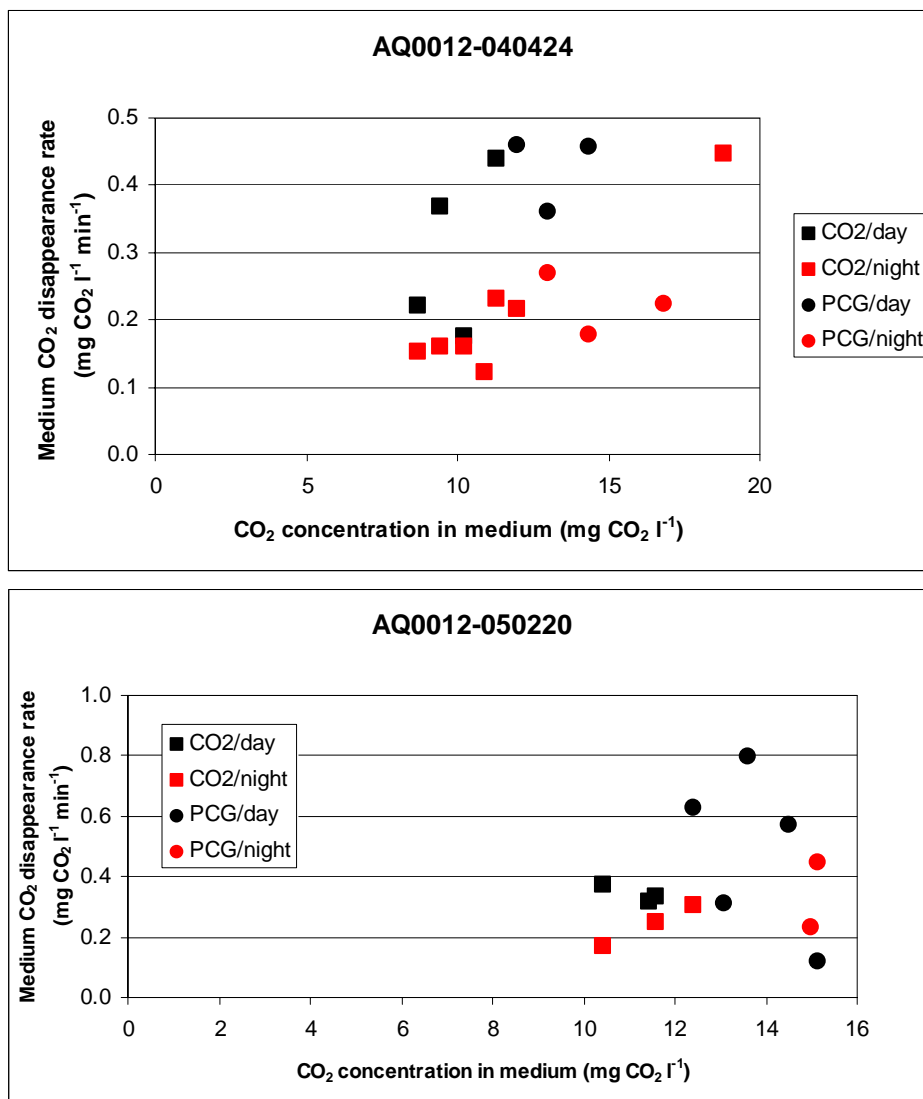
Figure 112. Rates of CO_2 disappearance from the medium for two cultures of strain AQ0012 whether grown on CO_2 or PCG during day and night times

Experiments with strain AQ0033 (*Porphyridium sp.*)

We grew one culture of strain AQ0033 (AQ0033-041213) for 5 weeks at full scale and exposed it to CO_2 first and then to PCG for two different periods. The results obtained during the switches back and forth between CO_2 and PCG gave us the opportunity to confirm again our previous results. Whenever the culture was exposed to CO_2 and to PCG the alkalinity and dissolved inorganic carbon species increased (Figure 113).
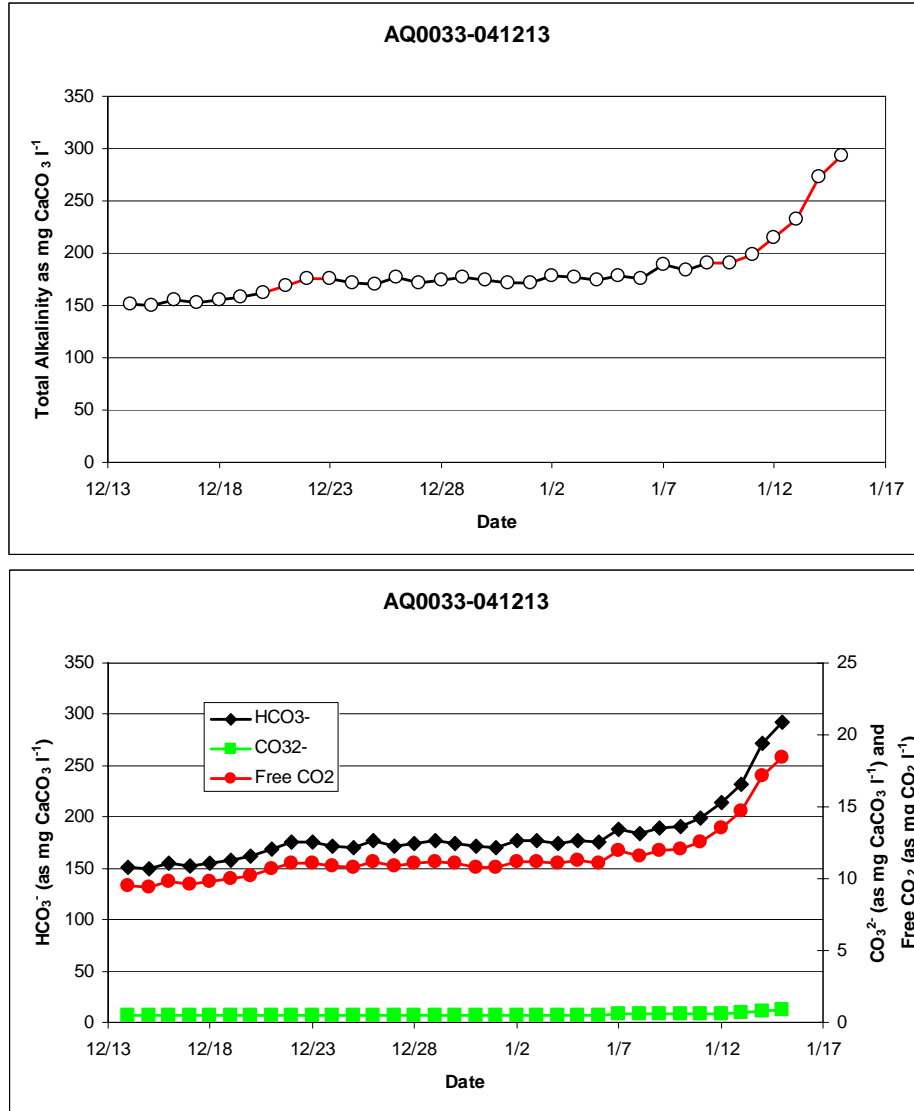
Figure 113. Changes in alkalinity (top panel) and dissolved inorganic carbon (bottom panel) for a culture of strain AQ0033 grown on CO_2 and PCG. Periods during which the culture was exposed to CO_2 and PCG are indicated by black and red lines in the top panel, respectively.

As was the case in the previous experiments, since growth on PCG does not result in decreases in alkalinity nor in dissolved inorganic carbon species, the range of medium CO_2 concentrations that the cultures were exposed to were smaller than in the coal combustion experiments. Still, a relationship exists between medium CO_2 concentration and CO_2 loss rates (Figure 114).
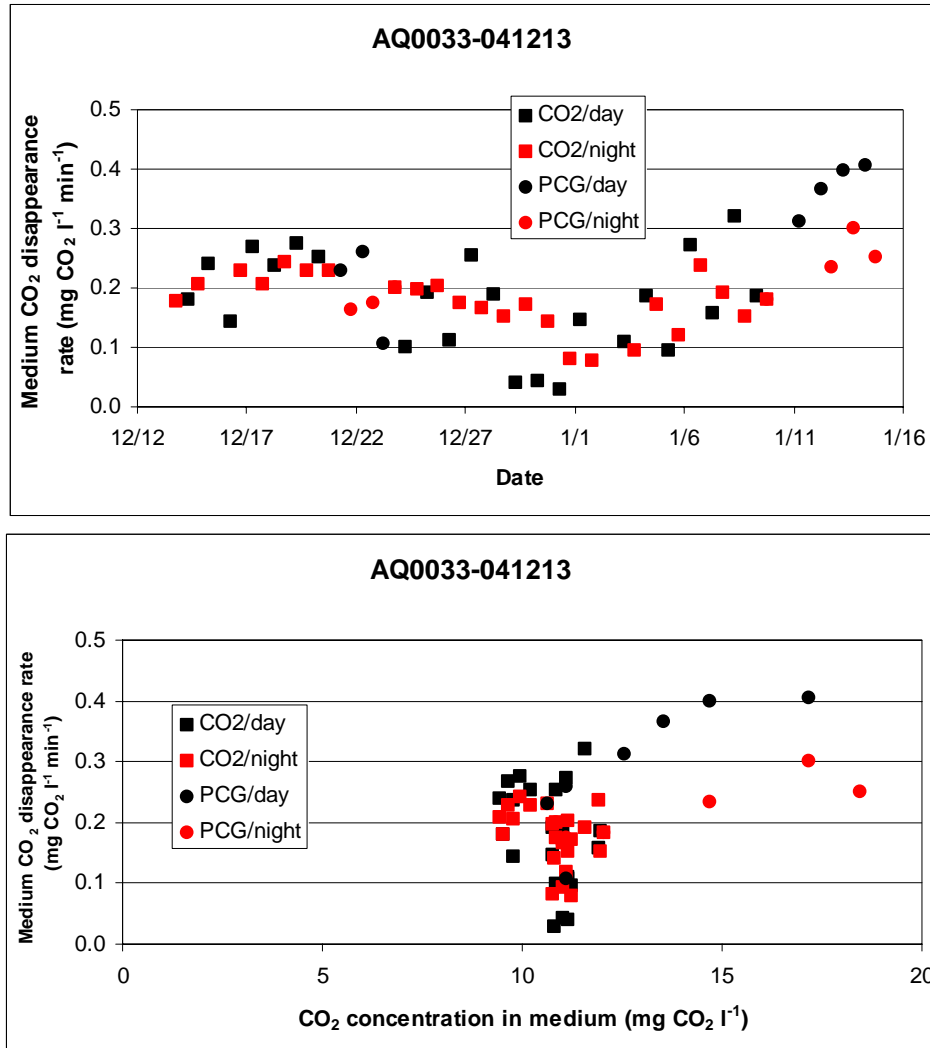
Figure 114. Rates of CO_2 disappearance from the medium for a culture of strain AQ0033 whether grown on CO_2 or PCG during day and night times. Top panel: timeline of CO_2 loss rates. Bottom panel: relationship between medium CO_2 concentration and CO_2 disappearance rate.

Experiments with strain AQ0059 (*Chorella sp.*)

Here we present the results obtained from a pilot scale culture of strain AQ0059 which was grown on CO_2 for 4 days, then switched to PCG for 23 days, and then switched back to CO_2 for 6 days (AQ0059-040206).

As can be expected from the experiments reported earlier, a large increase in alkalinity was measured in the culture whether grown on CO_2 or PCG. The two occasions when the alkalinity in the medium dropped it was caused by dilution of the culture with fresh growth medium (Figure 115).
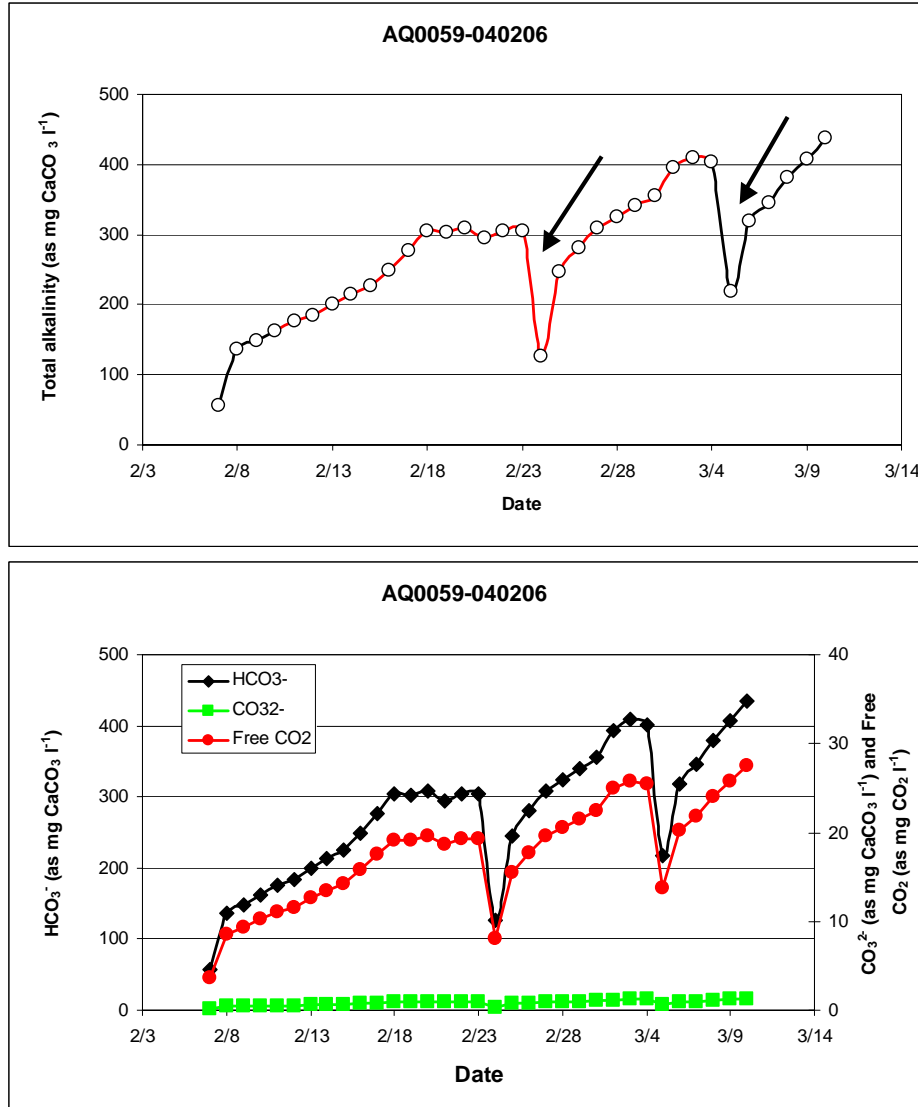
Figure 115. Changes in alkalinity in a culture of strain AQ0059 when grown on CO_2 and PCG. The black arrow indicates the days when the culture was diluted with fresh medium.

During this experiment we encountered technical difficulties which the computer that stored the pH data from our automated monitoring and control system. Thus, we have a limited data set of CO_2 disappearance rates (Figure 116). The limited amount of data does, however, corroborate the relationship between medium CO_2 concentration and CO_2 loss rates from the medium.
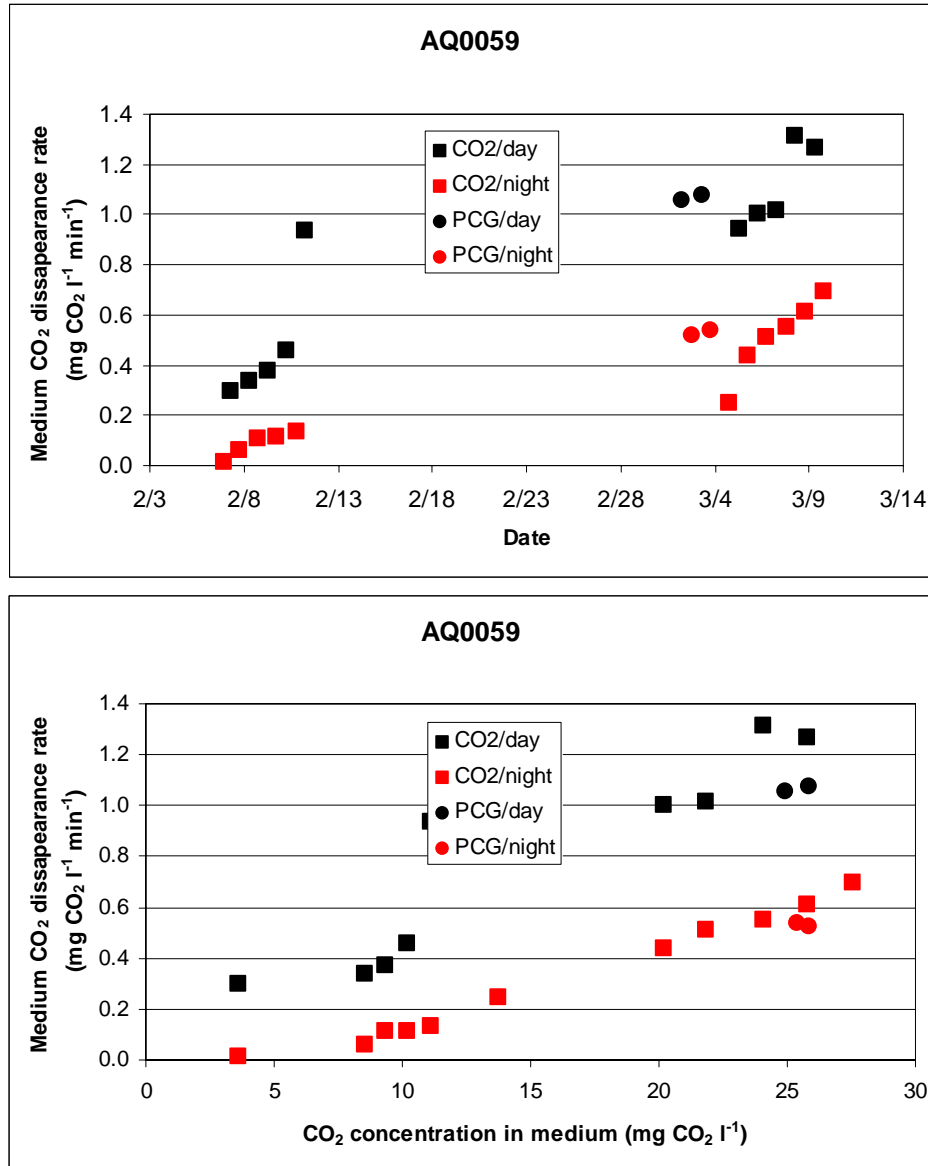
Figure 116. Rates of CO_2 disappearance from the medium for a culture of strain AQ0059 whether grown on CO_2 or PCG during day and night times. Top panel: timeline of CO_2 loss rates. Bottom panel: relationship between medium CO_2 concentration and CO_2 disappearance rate. A computer malfunction limited the amount of data available.

Experiments with strain AQ0073 (*Botryococcus braunii*)

We grew two different cultures of strain AQ0073 for exposure to PCG. Culture AQ0073-041109 was grown at 8.0 pH and exposed to CO_2 for the first 4 days and, then, switched to PCG (Figure 117). Culture AQ0073-050126 was grown at 7.5 pH and exposed to CO_2 for the first 6 days and, then, switched to PCG (Figure 118). In both cultures, the alkalinity increased over
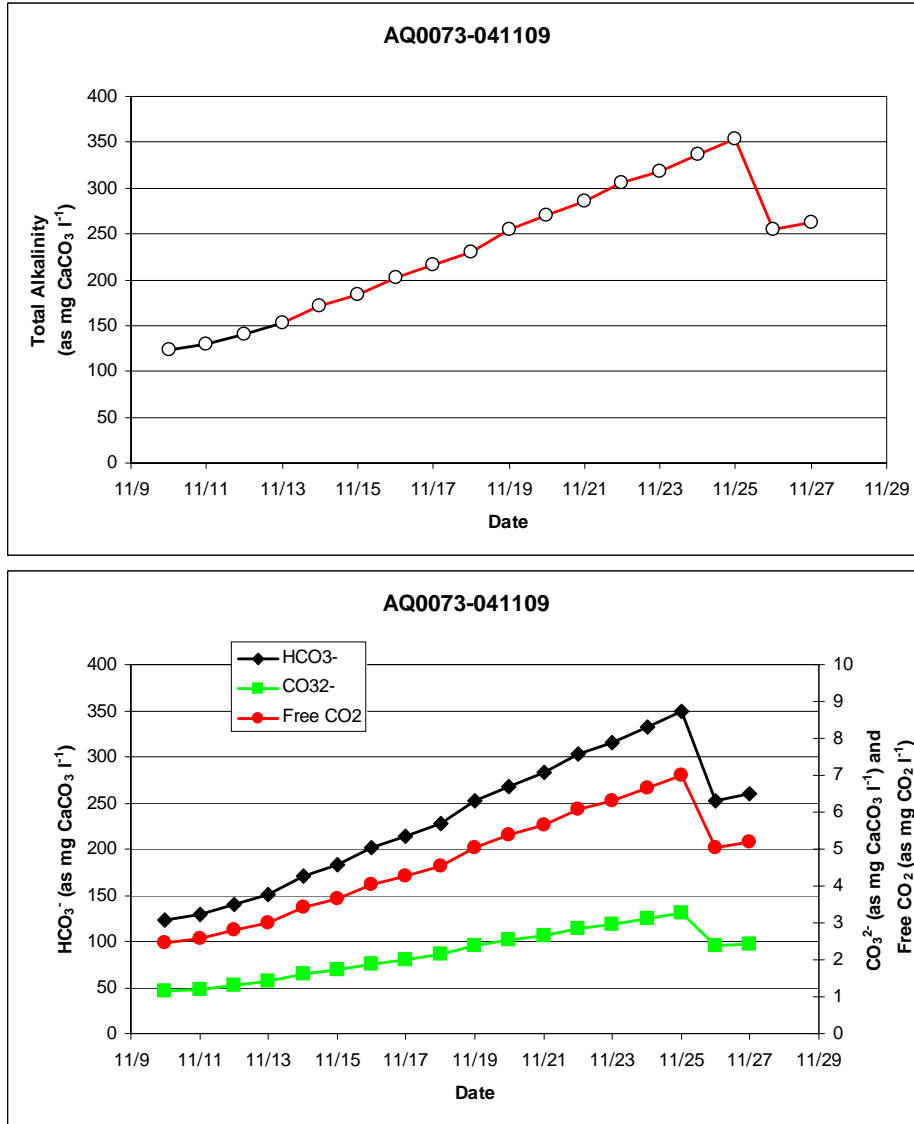
Figure 117. Changes in alkalinity in a culture of strain AQ0073 when grown on CO_2 and PCG at 8.0 pH. The black arrow indicates the days when the culture was diluted with fresh medium.
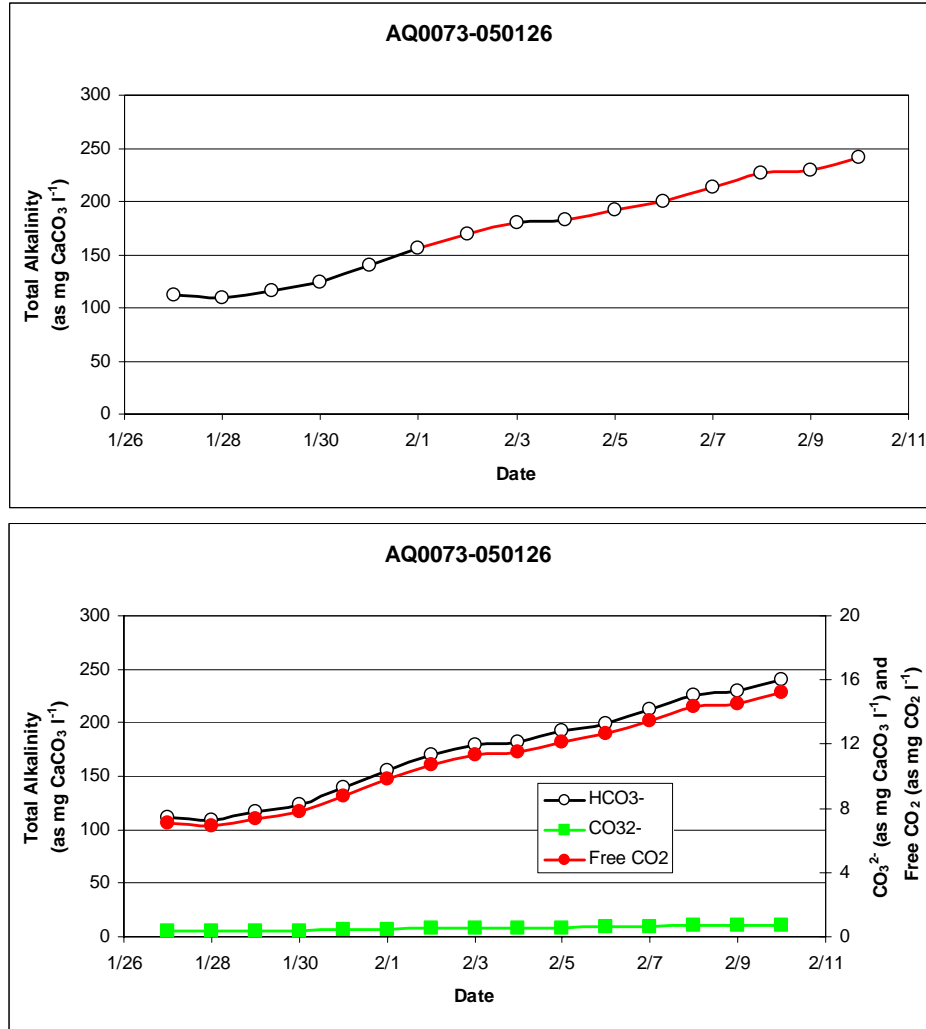
Figure 118. Changes in alkalinity in a culture of strain AQ0073 when grown on CO_2 and PCG at 7.5 pH.

time. The alkalinity in culture AQ0073-041109, grown at 8.0 pH, increased faster than in the culture grown at 7.5 pH. However, the concentration of dissolved CO_2 in the medium was higher in culture AQ0073-050126, grown at 7.5 pH.

The calculated rates of CO_2 disappearance from the medium for both cultures are presented in Figure 119 and Figure 120. As can be expected based on the previous experiments, the rates measured were related to the concentration of dissolved CO_2 in the medium.
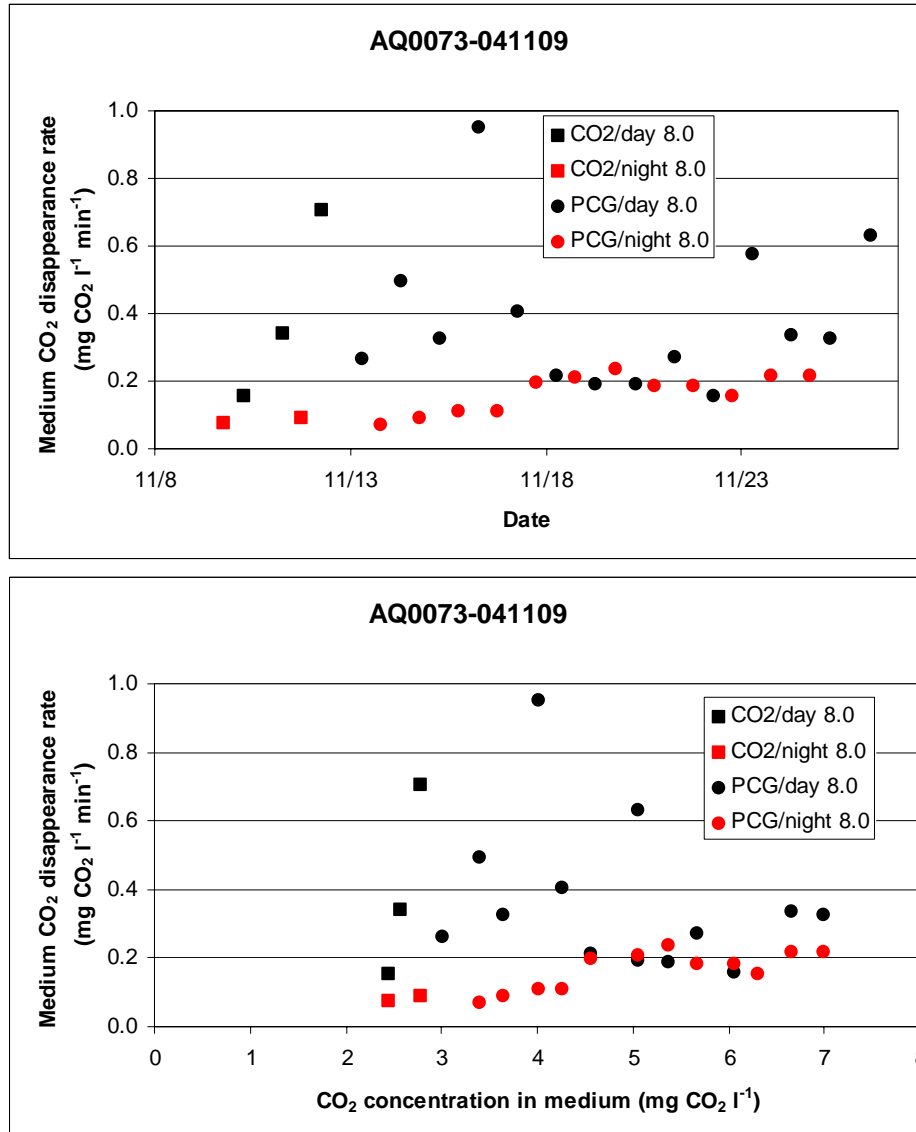
Figure 119. Rate of CO_2 disappearance from culture AQ0073-041109, grown at 8.0 pH during daylight and nighttime on different days (top panel) and relationship between the concentration of dissolved CO_2 in the medium and CO_2 disappearance rate (bottom panel).
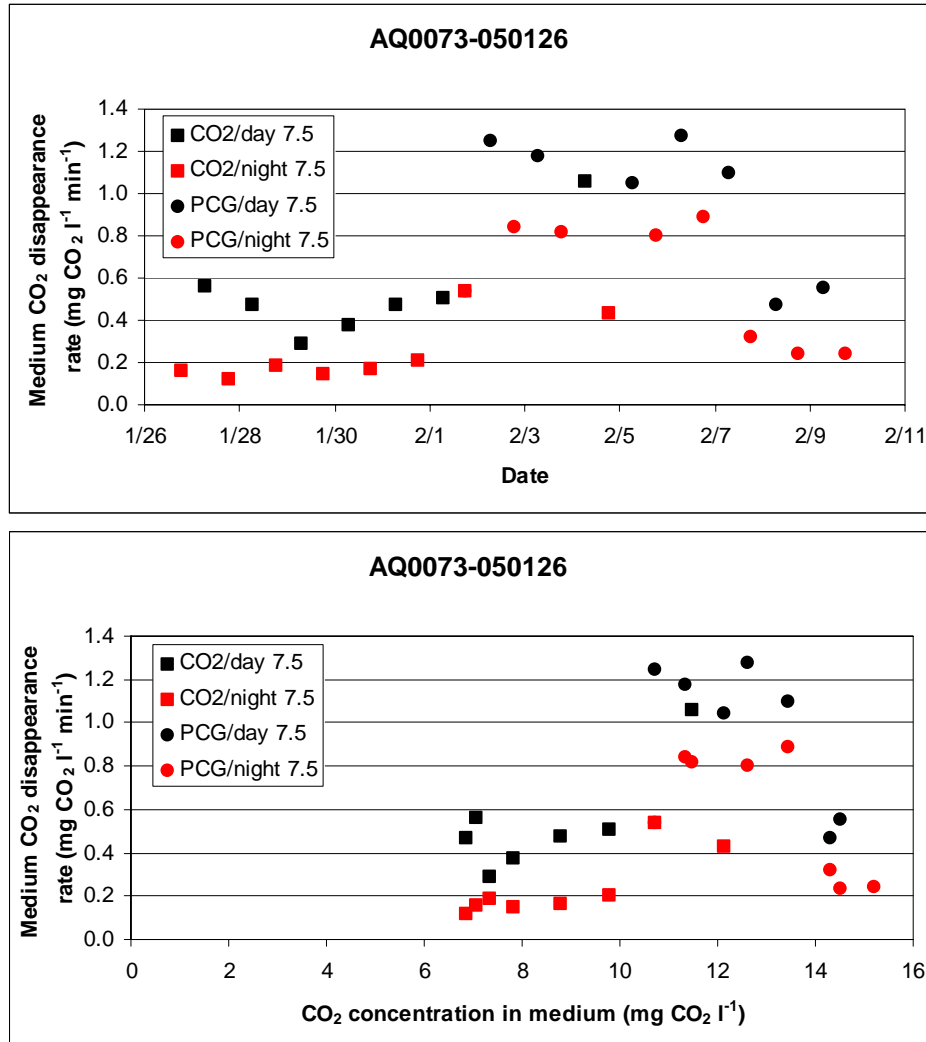
Figure 120. Rate of CO_2 disappearance from culture AQ0073-050126, grown at 7.5 pH during daylight and nighttime on different days (top panel) and relationship between the concentration of dissolved CO_2 in the medium and CO_2 disappearance rate (bottom panel).

Summary of microalgal CO_2 capture rates at full scale in outdoor photobioreactors

Here we have reported results on experiments carried out in full scale outdoor photobioreactors. We have grown six strains of microalgae in the presence of CO_2 and propane combustion gases. Table 20 summarizes the results as the averages of the CO_2 disappearance rates for each experiment obtained during daylight hours (degassing plus microalgal uptake) and night time (degassing). The difference between those values represents the amount of CO_2 captured by the microalgae.

The productivity of outdoor microalgal cultures can be quite variable (see figures above) as they depend, for example, on the availability of sunlight. This is reflected in the daily values

148

for carbon capture presented above. Even with all that variability, the data from these experiments reflect what was learned in Task 2, that a large fraction of the CO_2 that is available in the culture medium will simply escape (degassing) and will not be captured by the microalgae. We did find out that degassing does appear to be somewhat less in full scale photobioreactors (e.g., Figure 98).

The data also indicate that the use of propane combustion gases directly by microalgal cultures does not appear to pose a physiological impediment to the algae for capturing CO_2. As opposed to coal combustion gases (mainly CO_2, NO_X and SO_X), propane combustion gases (CO_2 and NO_X but no SO_X)do not lower the alkalinity of the medium.

Table 20. Summary of CO_2 Disappearance Rates at Full Scale in Outdoor Photobioreactors (as mg CO_2 l^{-1} min^{-1}).

Culture ID/pH	CO_2/Day	Night	Diff/Photos	PCG/Day	Night	Diff/Photos
AQ0008-030903/7.5	0.58	0.24	0.34	N/A	N/A	N/A
AQ0008-030903/8.5	0.13	0.02	0.11	N/A	N/A	N/A
AQ0008-030927/7.5	N/A	N/A	N/A	0.44	0.17	0.27
AQ0008-030927/8.0	N/A	N/A	N/A	0.09	0.01	0.07
AQ0008-0310205/7.5	0.41	0.21	0.19	N/A	N/A	N/A
AQ0008-0310205/8.5	0.17	N/A	>0.17	N/A	N/A	N/A
AQ0008-031107/7.5	N/A	N/A	N/A	0.35	0.15	0.20
AQ0008-031107/8.5	N/A	N/A	N/A	0.11	N/A	>0.11
AQ0011-040323/7.5	0.36	0.12	0.24	0.63	0.19	0.44
AQ0012-040424/7.5	0.38	0.21	0.17	0.43	0.22	0.20
AQ0012-050220/7.5	0.34	0.24	0.10	0.49	0.34	0.15
AQ0033-041213/7.5	0.17	0.18	0.00	0.30	0.21	0.08
AQ0059-040206/7.5	0.79	0.32	0.48	1.07	0.53	0.54
AQ0073-041109/8.0	0.40	0.08	0.32	0.38	0.16	0.22
AQ0073-050126/7.5	0.53	0.24	0.29	0.98	0.59	0.39

4.3.3   Carbon Uptake into Inorganic species

4.3.3.1 Model Showing the Dependence of Alkalinity on Microalgal Growth

Our first step consisted in utilizing the stoichiometric equation to estimate the expected change in alkalinity, dissolved inorganic carbon (DIC) species and nutrient concentrations (NO_3^-, $H_2PO_4^-$)caused by photosynthetic growth equivalent to 1 mM of carbon.

$$106CO_2 + 16NO_3^- + H_2PO_4^- + 122H_2O + 17H^+ \xrightarrow{\quad photosynthesis \quad} \{C_{106}H_{263}O_{110}N_{16}P_1\} + 138O_2$$

The results are summarized in Table 21 and show decreases in nutrient concentrations as well as in total dissolved inorganic carbon, but an increase in pH, $CO_3^=$ and alkalinity. If we run the model in 0.1 mM of carbon uptake steps we can represent the results in graphical form showing the changes in dissolved inorganic carbon (DIC) species (Figure 121).

Table 21. Estimated Changes in Chemical Composition of Nutrient Medium Following Photosynthetic Growth Equivalent to 1 mM C

	Concentration in fresh medium	Concentration in medium after growth equivalent to 1mM carbon
$H_2PO_4^-$ (uM)	20.00	10.57
NO_3^- (uM)	320.00	169.06
pH	7.50	10.04
Alkalinity (mEq/l)	2.30	2.47
HCO_3^- (mM)	2.25	0.26
$CO_3^=$ (mM)	0.027	1.104
Free CO2 (nM)	0.094	0.000
Total Dissolved Inorganic C (mM)	2.37	1.37
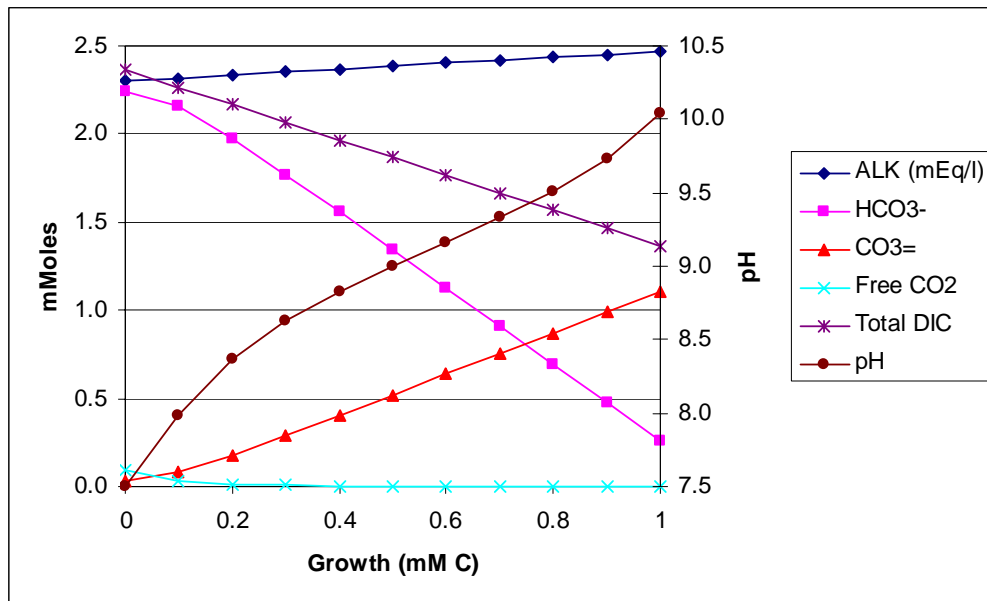
Figure 121. Modeled changes in medium concentration of alkalinity, HCO_3^-, $CO_3^=$, free CO_2 and total DIC as well as pH following photosynthetic growth of microalgae.

        In reality, our cultures are run as pH-stats, that is, we control the pH of the cultures with on-demand injections of CO_2. Thus, we extended that analysis to a long-term model culture assuming pH control of the culture (accomplished with on-demand CO_2 additions to the medium) and assuming reasonable growth rates as obtained from our experimental cultures. In this exercise, it was assumed that the pH of the cultures was controlled between 7.5 and 8.5: CO_2 is injected when the culture reaches a pH value above 8.5 and the injection stops when the culture's pH reaches 7.5.

The results are shown in Figure 122 and indicate that not only the alkalinity increases over time but also the total DIC concentration. Therefore, according to our model calculations, CO_2 injected into the culture and dissolved in the medium will be used in photosynthesis plus it will accumulate as DIC in the medium. This has the effect of enhancing the CO_2 capture and sequestration capacity of the microalgal culture.
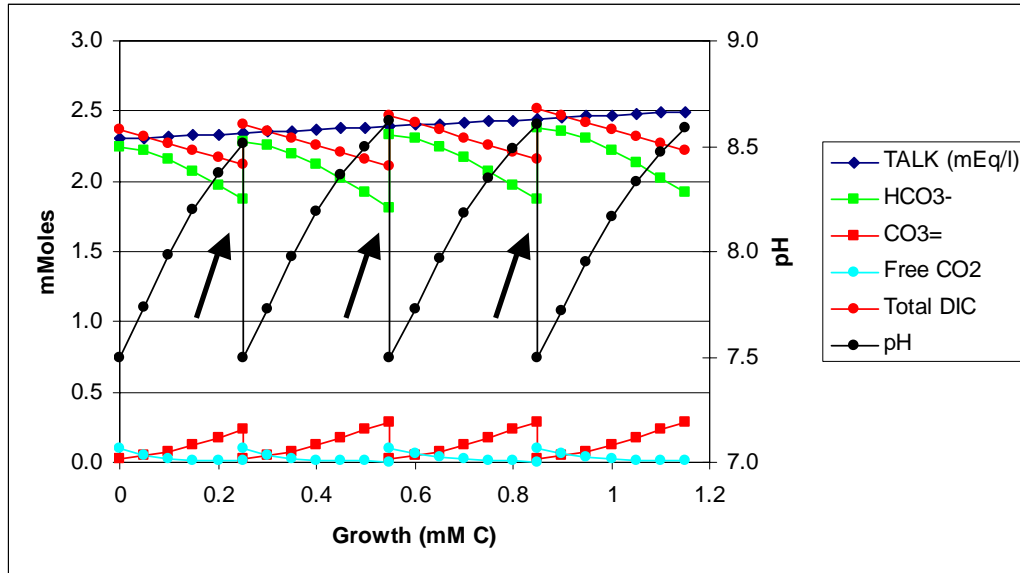
Figure 122. Modeled changes in medium concentration of alkalinity, HCO_3^-, $CO_3^=$, free CO_2 and total DIC as well as pH following photosynthetic growth of microalgae but assuming pH control effected by automatic injections of CO_2. The arrows indicate injection of CO_2 into the model culture after the culture's pH reaches >8.5.

Finally, we tested the hypothesis that a growing microalgal culture utilizing NO_3^- and $H_2PO_4^-$ as its source of nitrogen and phosphorus would accumulate carbon in biomass as well as DIC in the medium on a 25,000 liter culture of *H. pluvialis*. Figure 123 shows the estimates of microalgal biomass in the culture, calculated from the cell concentration values. The changes in alkalinity estimated from the calculated assimilation of CO_2 by the biomass as well as the actual measured values are shown in Figure 124. The data indicates that both sets of values respond similarly to CO_2 assimilation (and the concomitant assimilation of NO_3^- and $H_2PO_4^-$) by the biomass. Indeed, the two sets of data are highly correlated (Figure 125), validating our modeling approach.
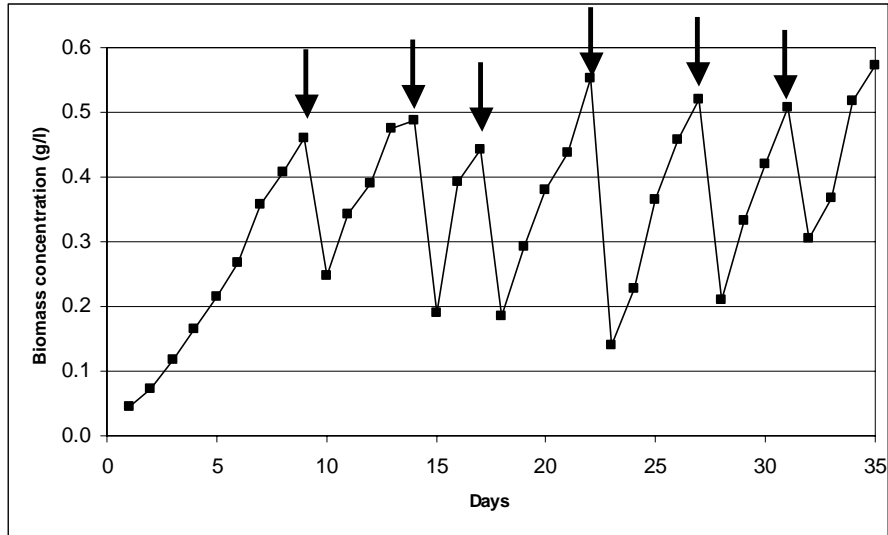
Figure 123. Changes in biomass concentration (estimated from cell concentration measurements) in a growing culture of *H. pluvialis* in a 25,000 liter photobioreactor. The arrows indicate the days on which the culture was diluted with fresh medium.
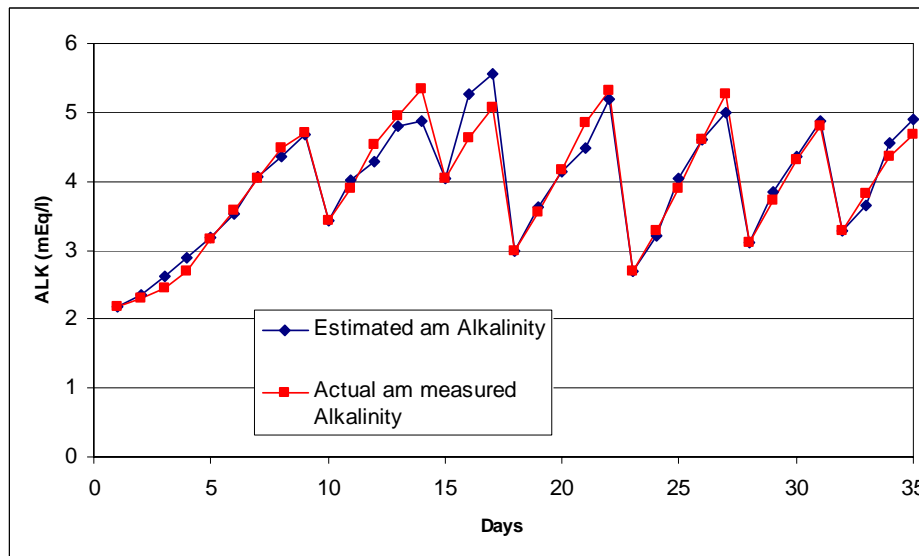
Figure 124. Measured and estimated alkalinity concentrations in a growing culture of *H. pluvialis*. On the days following culture dilutions (see MRFigure XX), the estimated alkalinity was made equal to the measured alkalinity.
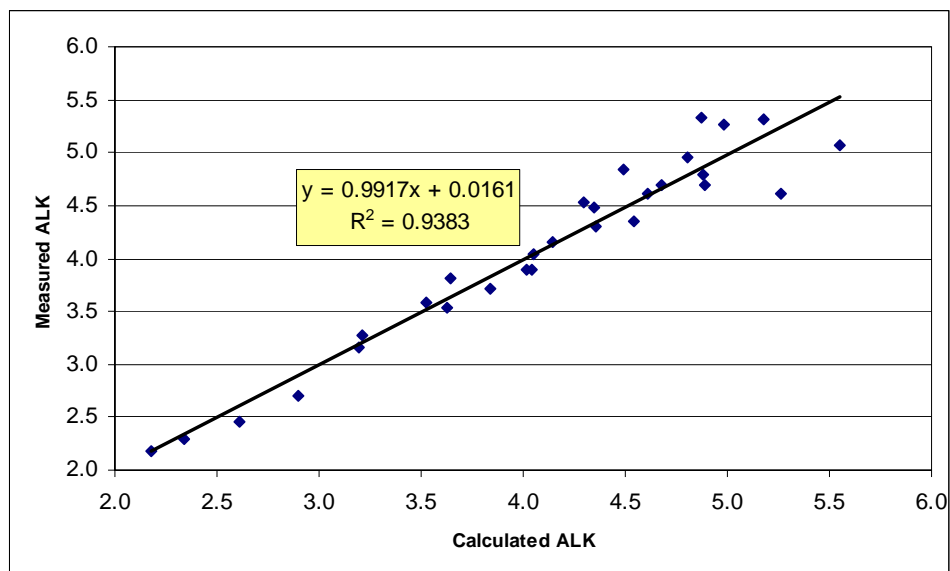
Figure 125. Comparison between modeled alkalinity, estimated from biomass assimilation of CO_2 over the previous 24 hours and actual measured alkalinity. The data points obtained in *am* samples following culture dilution were not considered in this analysis since they are arbitrarily made equal.

4.3.3.2 Carbon Sequestration into Dissolved Inorganic Carbon Species

The stoichiometry of microalgal growth (previous section) predicts that for each mole of CO_2 captured by the microalgal biomass, $17/106 = 0.16$ moles of alkalinity are produced in the culture's medium (when the algae are grown on NO_3^- and $H_2PO_4^-$). The increase in alkalinity would be reflected in increases in DIC; at our standard culture pH this is further reflected in increases in HCO_3^-.

If we review the data obtained in the pilot and full scale photobioreactor experiments (sections 4.3.1 and 4.3.2), it is clear that alkalinity and DIC species increase as a result of photosynthetic microalgal growth in cultures feed pure CO_2. The same observation was made on cultures feed propane combustion gases (mainly about 8.5% CO_2 and 90 ppm NO_X). However, in cultures feed coal combustion gases (about 3% CO_2, 275 ppm NO_X and 325 ppm SO_X, Table **16**) the opposite was observed. Utilization of coal combustion gases to provide CO_2 to the cultures results in larger amounts of acid gases introduced into the culture which results in larger losses of alkalinity and dissolved inorganic carbon species.

For CO_2 and PCG cultures, then, microalgal photosynthesis does not only capture CO_2 into biomass but into the medium as well. We had previously shown that increases in culture medium alkalinity and DIC could be used to drive reactions resulting in the calcification of dissolved inorganic carbon (Section 4.2.2.3). We have now scaled those observations to industrial scale outdoor cultures of microalgae. We expect that future research will exploit the inorganic carbon sequestration capacity of microalgal cultures.

153

4.3.4 Subtask 3.3 – Algae Separation and Final Product

Harvesting microalgal biomass has been identified as one of the most expensive processes in microalgal biomass production (Molina-Grima et al, 2003) and, thus, in microalgal-based carbon sequestration. Of the different available methodologies, centrifugation has been identified as the most efficient. We expected that cells of different morphology, size and density may affect significantly the efficiency and thus the costs associated with biomass centrifugation. Here, we present results of experiments designed to investigate the possible costs associated with harvesting a large number of microalgal strains. We chose strains of very different size and morphology, from 4 μm diameter coccoid cells to large filamentous ones. First, we report on pilot scale studies conducted using a benchtop centrifuge. Also under Pilot Studies we report on small scale experiments carried out a small and simple lamellar settler. Finally, we report on full scale centrifugation experiments using a commercial centrifuge.

4.3.4.1 Pilot Studies

Bench-top Centrifugation Experiments

We have carried out a set of bench scale centrifugation tests to determine the settling characteristics of different species of microalgae. These tests are designed to make relative estimates of centrifugation capacity needed for different species of microalgae. It is expected that different species of microalgae will be more or less difficult to separate from the growth medium by centrifugation because of different physical characteristics such a density and particle size. This information will then be used in our economic model to support our cost estimates of algal biomass harvesting and separation from the growth medium.

We have tested 22 different microalgal strains. Figure 126 shows examples of data obtained from four different strains of microalgae. The data obtained was fit to a model of the form:
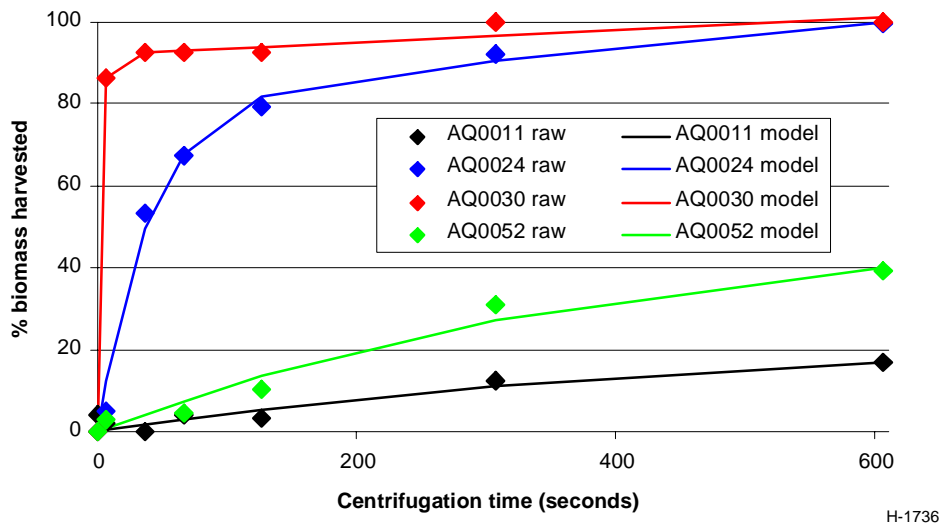
Figure 126. Four data sets obtained from four morphologically different strains of microalgae (see also Figure 127).
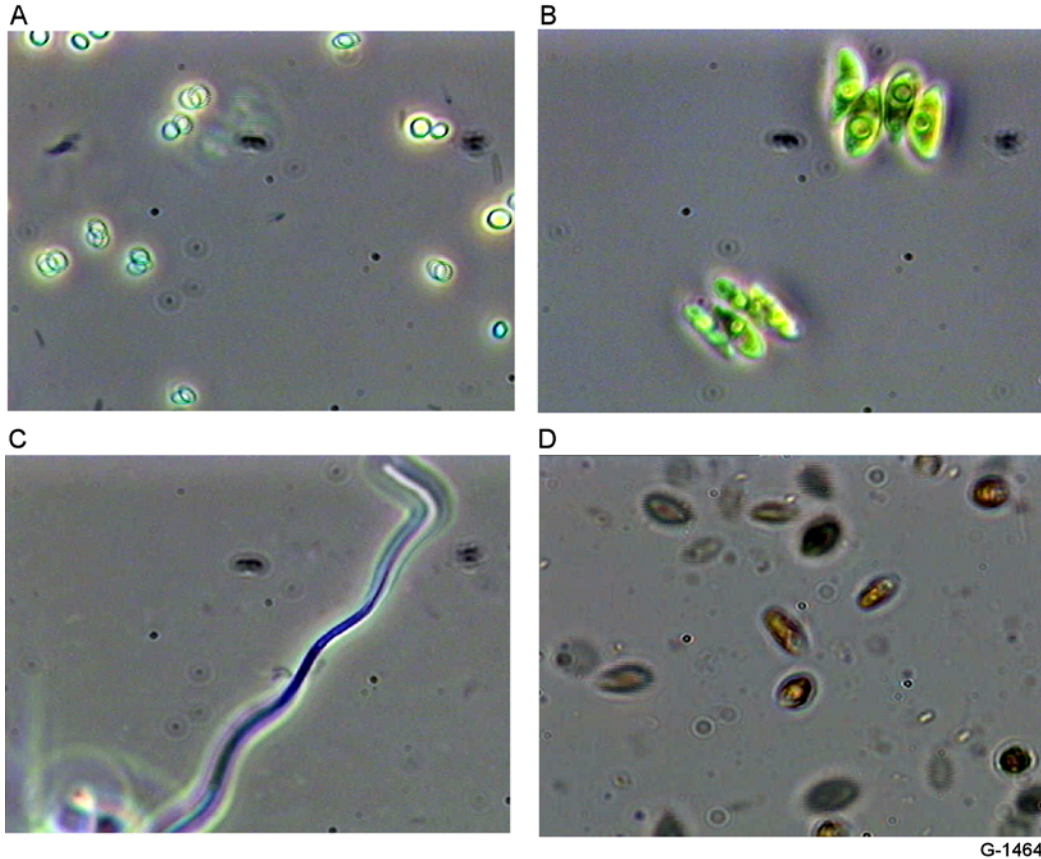
Figure 127. Microphotographs (400x) of strains AQ0011 (A), AQ0024 (B), AQ0030 (C) and AQ0052 (D) showing differences in size and morphology.

$$\%\text{Harvest} = \%\text{Harvest}_{\text{max}} * \left(1 - e^{\left(\frac{-a*\text{time}}{\%\text{Harvest}_{\text{max}}} \right)} \right) * \left(e^{\left(\frac{-b*\text{time}}{\%\text{Harvest}_{\text{max}}} \right)} \right) \qquad (16)$$

where:

%Harvest   is the fraction of biomass harvested from the medium after a specific amount of time,

$\%\text{Harvest}_{\text{max}}$ is the maximum harvestable biomass (up to 100%),

a is the harvest efficiency factor (larger for easier to harvest strain),

b is a modifier that reflects the fact that since microalgal populations are heterogeneous (e.g., some cells are larger than others) it is expected that larger cells will harvest faster than smaller cells of the same population, thus affecting the efficiency of the process, and

time   is the amount of time for which the specific sample was centrifuged.

For example, for the data shown in Figure 126 the calculated efficiency factors (*a*) are 0.046, 0.120, 2.046, and 39.3 for AQ0011 (3 um coccoid cells), AQ0052 (3 x 6 um ovoid cells),

155

AQ0024 (4-cell chain forming ovoid cells 4 x 8 um), and AQ0030 (a filamentous Cyanobacterium) respectively (Figure 127). Our calculated centrifugation efficiency factors thus reflect the differences in cell size and morphology. Figure 128 summarizes the centrifugation harvest efficiencies obtained for 22 strains tested. These values will be used in our economic model to estimate the costs, in capital equipment as well as running costs (manpower, supplies, utilities), of processing biomass from different microalgal strains.
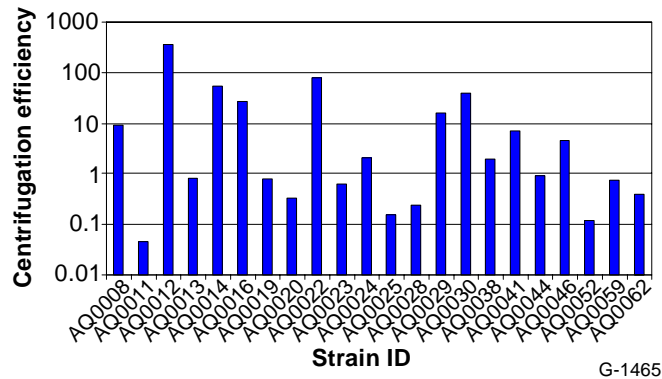
Figure 128. Summary of centrifugation efficiency factors obtained for 22 microalgal strains.

Using Eq. (17), we estimated the % biomass that would be harvested under our standard conditions within a standard 30 second period. The results are shown in Figure 129 and range from less than 2% for AQ0011 (a very small coccoid organism) to 100% for filamentous forms like AQ0012 and AQ0016.

We are most familiar with the costs associated with the harvesting/centrifugation of *Haematoccocus pluvialis* (AQ0008), a green microalga that we produce commercially. For our cost modeling efforts (Task 5) we will relate the centrifugation costs of other microalgal strains to those of *Haematococcus* as shown in Figure 129.
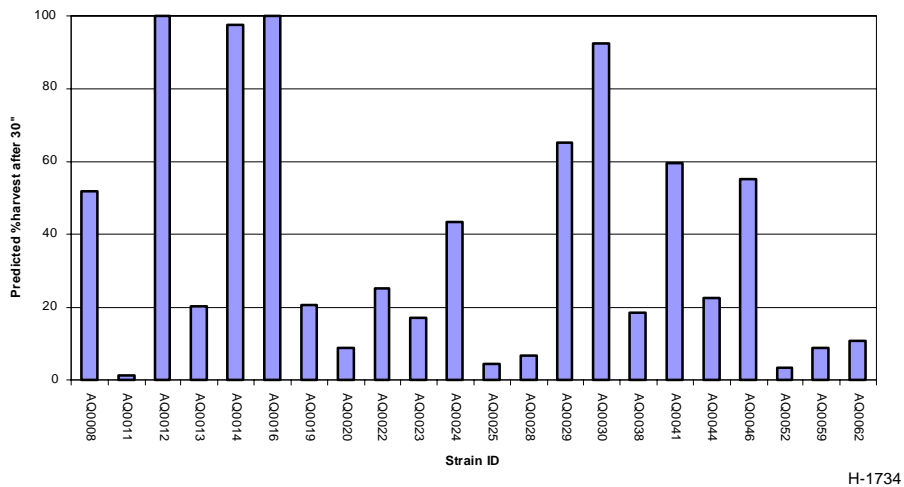
Figure 129. Calculated percent biomass harvested in a standard 30 second period for the different microalgal strains.

156

<u>Lamellar Settler</u>

Our fist experiment consisted of using non-stressed *H. pluvialis* cells using the lamellar settler in the horizontal position. These cells were used to obtain data for a worst-case scenario, i.e., cells that are not specially dense and that can swim. The fluorescence-based biomass estimate of the culture fed into the lamellar settler was 420 (relative units) while the outflow was 306. Thus, the biomass harvest efficiency was only 27%.

The next tests were conducted using stressed *H. pluvialis* cells. These cells do not have the ability to swim and have a settling velocity of about 0.5 cm min^{-1}. We run the culture through the lamellar settler while placed in the horizontal and at 16° and 30° from the horizontal.

When the lamellar settler was placed horizontally, a maximum of 90% of the biomass was harvested. By placing the settler at 16° and 30° we were able to harvest 96% and 94% of the biomass respectively. The photographs in Figure 130 present views of the inlet and outlet sections of the settler showing the difference in biomass concentration as the settler fills up with culture. Figure 131 consists of two photographs of the bottom of the lamellar settler showing the sedimentation pattern of the cells.

In summary, our tests show that the relatively cheaper lamellar settler technology may be used successfully to harvest microalgal cells but only if the cells are substantially heavier than the growth medium, as is the case for stressed *H. pluvialis* cells.
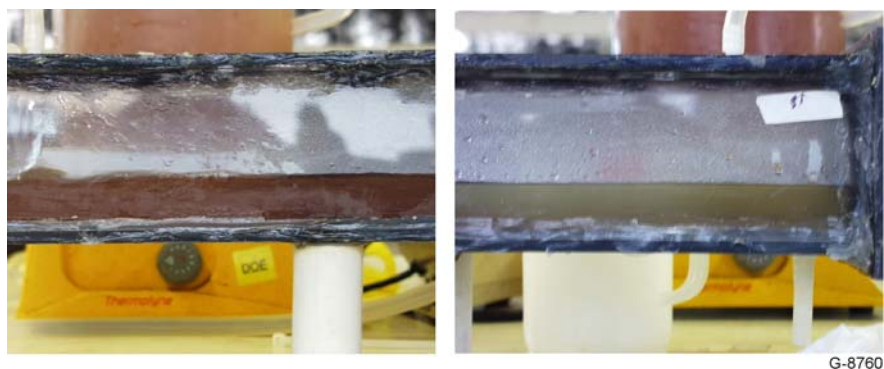
Figure 130. Inlet (left) and outlet (right) sections of the lamellar settler. It can be easily seen that the cells concentration diminishes quickly as the model lamellar settler unit fills up with the microalgal culture.

Figure 131. Photographs of the bottom of the unit after draining showing the pattern of settled cysts near the inlet (top) and outlet (bottom) ports.

4.3.4.2 <u>Full Scale Centrifugation Experiments</u>

Five different microalgal cultures, with very different cellular morphologies were processed with our commercial centrifuge (AQ0011, small cocoid, single cells of 3-4 μm diameter; AQ0012, thin-3 μm- filaments, up to several 100's μm long; AQ0015, thick-13 μm-filaments, up to several mm long; AQ0024, colonial, 15 x 6 μm oblong cells; and AQ0073, colonial, 8-10 μm diameter cells. See Figure 132).

Figure 132. Microphotographs (400x) of strains AQ0012 (left), AQ0015 (center) and AQ00733 (right) showing differences in size and morphology. For micrographs of AQ0011 and AQ0024 see Figure 127.

The feed flow from the culture into the centrifuge was adjusted to insure that a minimum of 90% of the biomass was harvested in one pass. Once the flow rates were adjusted they were measured by timing the fill up of a standard volume. The results are shown in Figure 133.
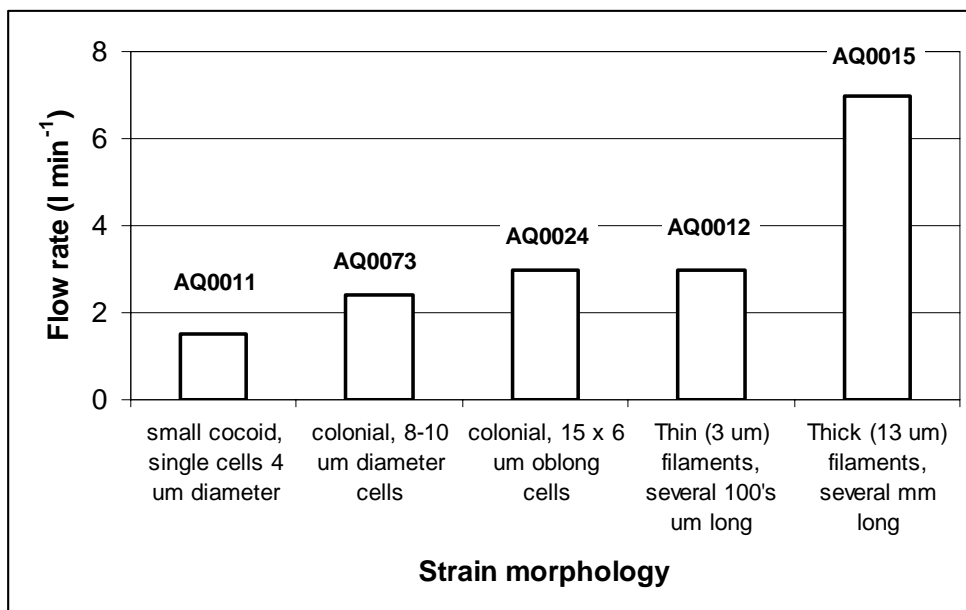
Figure 133. Maximum flow rates into the centrifuge that permit capture of 90% of the culture biomass.

The measured flow rates ranged between 1.5 and 7 liters min^{-1}. Clearly, strain morphology has a significant effect on centrifugation efficiency which will affect the costs associated with the individual strains. This will be discussed further in Task 5.

4.4   Task 4 - Carbon Sequestration System Design

To evaluate the potential for application of photosynthetic sequestration of CO_2 to industrial- scale combustion systems, we have conducted a system-level design study. This task consists of two sub-tasks: Task 4.1 Component Design and Development; and Task 4.2 System Integration. In Task 4.1 we identified an innovative photobioreactor concept and conducted design and feasibility analyses. In Task 4.2, the results of experiments were applied to determine relationships for a process model based on the MGM system that was then employed to identify harvesting scenarios that optimized carbon capture and revenues.

4.4.1   Subtask 4.1 - Component Design and Development

In this sub-task we will develop design concepts for key components of the industrial scale photosynthetic sequestration of CO_2. As the proposed system depends on the solar energy to photo-synthetically convert CO_2 to products compounds, optimization of the photobioreactor is an important part of this task. We are aware of the vast amount of work conducted in solar energy R&D programs sponsored by DOE and other agencies.

159

This task consists of two sub-tasks: Task 4.1-Component Design and Development; and Task 4.2-System Integration. Process simulations have been performed for conventional coal-fired and gas turbine power stations and natural gas boilers.

4.4.1.1 <u>Photobioreactor Design Concept</u>

Microalgae utilize solar radiation to convert CO_2 into organic substances and oxygen. This photosynthetic reaction requires solar spectra typically between 400 nm and 700 nm. This is called photosynthetically active radiation (PAR). Solar spectra outside of the PAR wavelength regime are not utilized by microalgae. Figure 134 shows solar spectral data for AM1.5, a typical terrestrial condition in the United States. The portion of the spectra used by microalgae is indicated in the figure. The solar spectral energy between 400 nm and 700 nm is 424 W/m^2, which is 44% of the total solar spectral energy of 962 W/m^2. It is important to note that only a fraction of the solar energy, less than half of the solar energy, is within the spectral range for photosynthetic processing by microalgae.
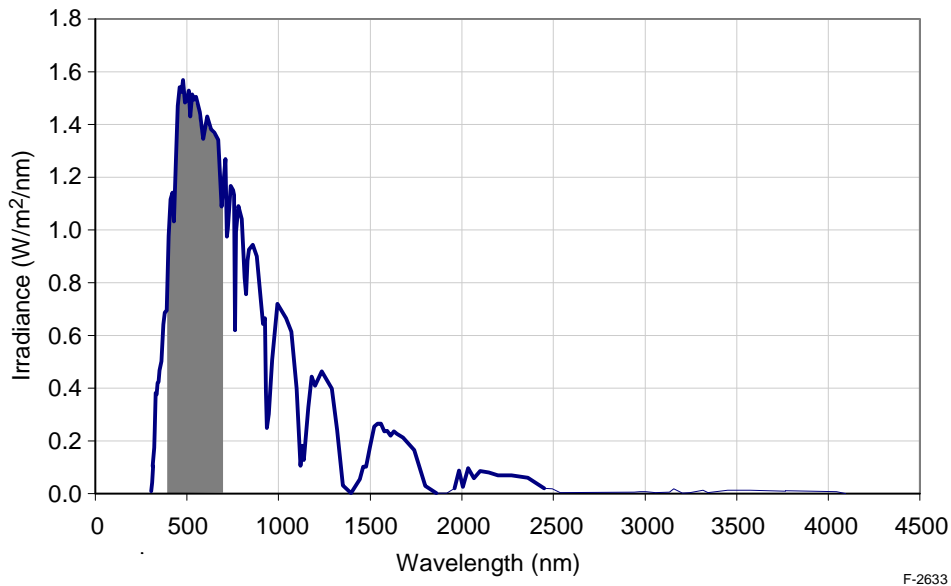
Figure 134. Solar spectral irradiance.

Our strategy for developing an efficient photobioreactor is as follows: (a) design the photobioreactor which maximizes availability of the PAR spectra for microalgae; and (b) develop innovative ways to utilize the solar radiation outside of PAR spectra for generating products that potentially offset the sequestration cost.

Item (a) is the standard method, and researchers have tackled this problem. We are aware that (b) has been discussed in literature (NEDO, 2000) but has not been practiced in the past. PSI has been working on this very issue in the past for a program supported by NASA/KSC (Nakamura, 2001). In this program we have demonstrated separation of PAR from the solar spectra and directed it to a location 10 m away from the solar collector, while the longer wavelength spectra outside of the PAR was converted to electrical power by low-bandgap

Photovoltaic cells. Figure 135 shows a schematic of the concept. In this concept, the solar radiation from the concentrator is directed to a selective spectral reflector which reflects only the PAR spectra while the longer wavelength components are transmitted to the PV cells.
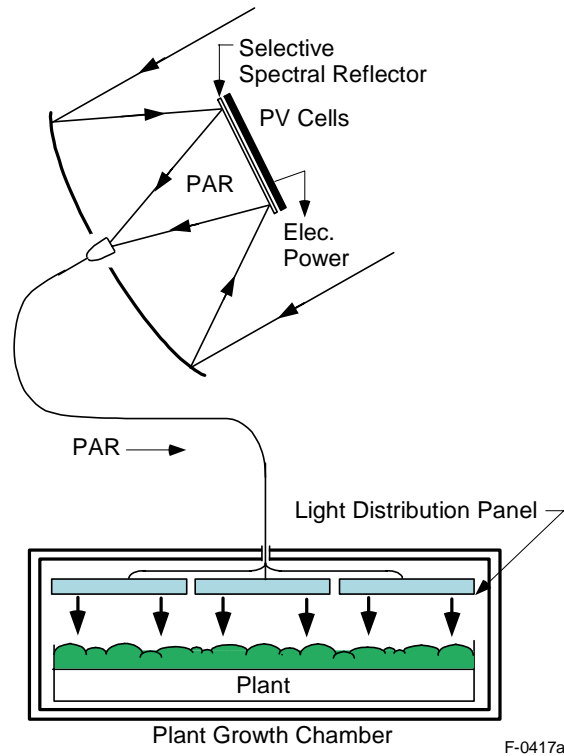
Figure 135. Concept for utilizing solar spectra not used for photosynthetic process.

In the past, PSI conducted a series of experiments for electrical power generation utilizing the GaSb cell, one of the low-bandgap PV cells. The project has been conducted with PSI's IRAD fund and with NASA/KSC's SBIR fund. The objective of the test project is to demonstrate, for the first time, the potential of using solar IR spectra that would not be utilized in space-based solar plant lighting. The test results showed that it is possible to convert the solar IR spectra into electric power at efficiencies theoretically predicted, e.g., 15.5% for the GaSb cell, while the PAR spectra are transmitted to the plant growth facility. Figure 136 shows a photograph of the experimental facility. As shown in the photo, a 20-in. parabolic mirror reflects the solar radiation to the PV cell module near the focal point of the mirror. The cold mirror (Coherent 35-6907) installed at the PV cell module reflects the PAR to the aperture of a 10-m lightguide which transmits the light to the inside of the building. Emission of the PAR from the other end of the lightguide in the building is visible.

H-1741
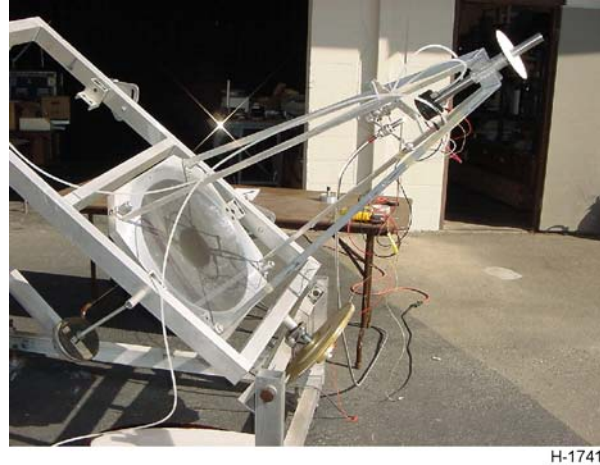
Figure 136. Experimental facility for GaSb cell performance tests with the IR solar spectra.

The experimental results reviewed above demonstrated that full utilizations of solar spectra is possible for two distinct purposes: CO_2 sequestration; and electric power generation. We consider this result is potentially very important in reducing the cost of CO_2 sequestration. Note that the electric power is generated at no penalty to photosynthesis of microalgae. The area required for photosynthetic process by microalgae is a key cost driving factor. Therefore, we need to develop a photobioreactor design which makes efficient use of solar light.

We are investing possibilities for developing an efficient photobioreactor which:
(a) maximizes availability of the PAR spectra for microalgae; and (b) utilizes the solar radiation outside of PAR spectra for generating products that potentially offset the sequestration cost.

We have been looking into possibilities of implementing method (b). We have developed several design concepts for microalgae growth and photovoltaic power generation. Figure 137 shows a schematic of the concept. In this concept, the solar radiation is directed to a selective spectral reflector which reflects only the non-PAR spectra to the PV cells while the PAR components are transmitted to the photobioreactor.
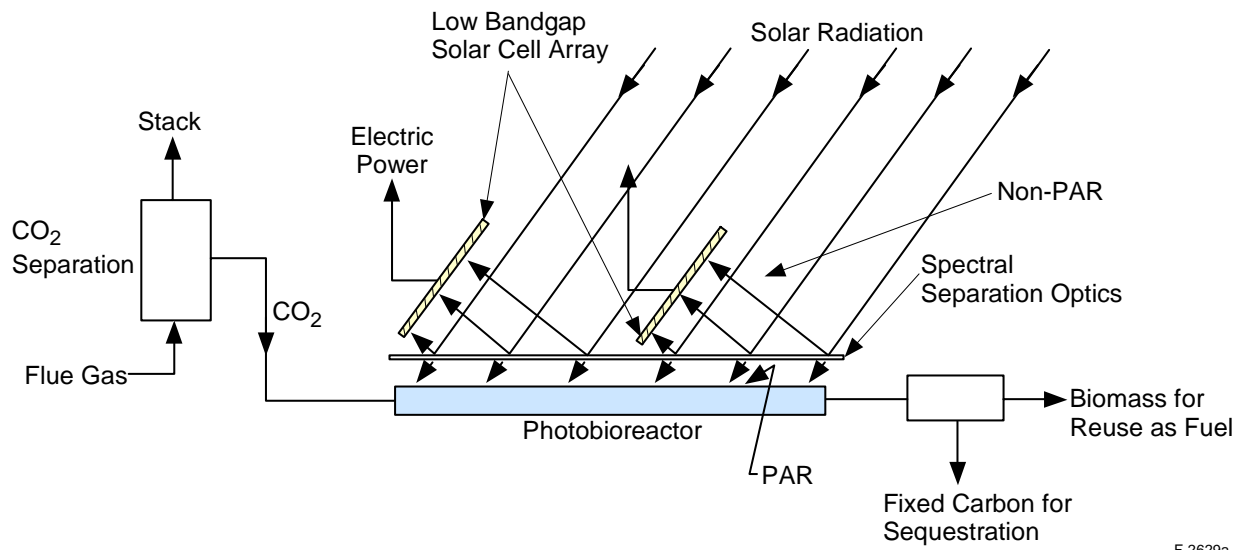
Figure 137. Concept for utilizing solar spectra not used for photosynthetic process.

4.4.1.2 Photobioreactor for CO_2 Sequestration and PV Power Generation

One of the important requirements for bio-fixation of CO_2 is to reduce the cost of the process. Aquasearch Inc. came up with producing high commercial value byproducts (pigments, diet supplements) to offset the sequestration cost. We discussed a method of utilizing the photosynthetically active radiation (PAR) for microalgae and non-PAR for photovoltaic electric power generation. The objective of the concept discussed in this report is to generate electric power utilizing the non-PAR spectra not useful for microalgae. By this method, biofixation of CO_2 is not disturbed by PV power generation. We will be using the solar spectra, which would otherwise be wasted, for useful purpose.

The photosynthesis reaction of microorganisms utilizes solar spectra between 400 and 700 nm, although the absorbance characteristic of species may vary. Figure 138 shows absorbance spectra of three species of planktonic algae (Kirk, 1983). These spectra, called photosynthetically active radiation (PAR), are only a portion of the incident solar energy on earth.
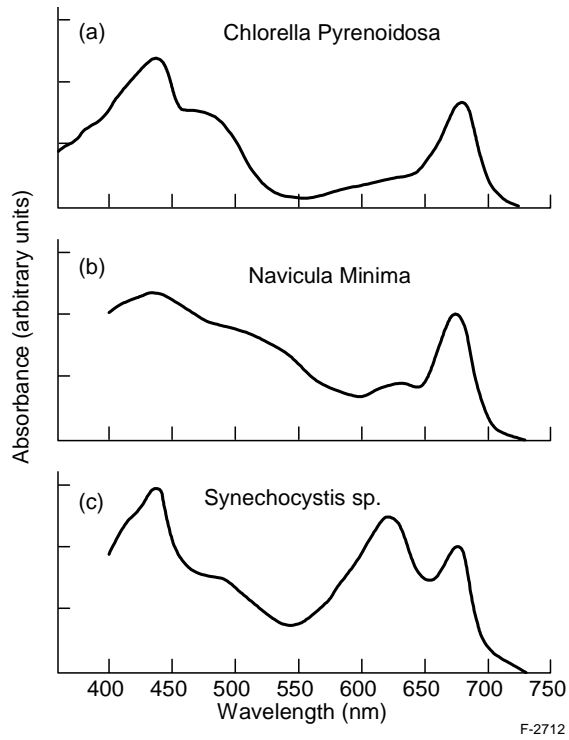
Figure 138. Absorbance spectra of three species of planktonic algae.

In the past PSI has demonstrated separation of PAR from solar spectra using dichroic optics (cold mirror). Figure 139 shows the decomposed AM1.5 spectra (Nakamura, Fraas, Avery, 2002).
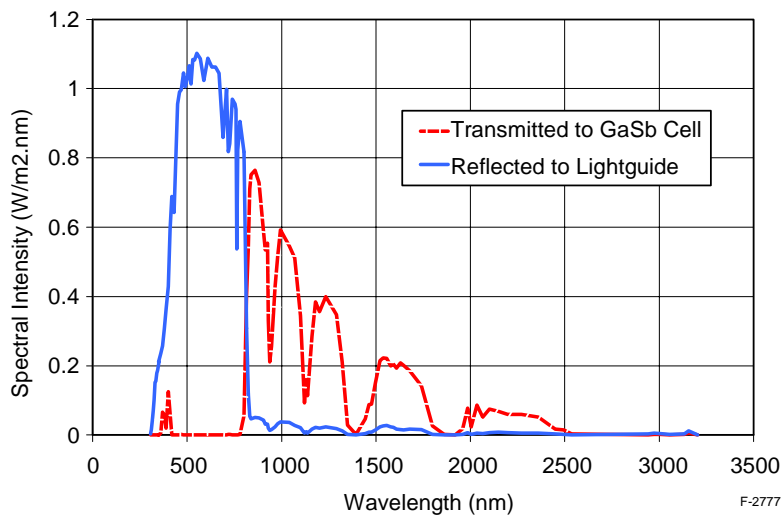
Figure 139. AM1.5 Solar Spectra (direct) separated by the Cold Mirror (Coherent 35-6907).

Conversion of the non-PAR solar spectra to electric power can be accomplished by using low bandgap photovoltaic cells. Candidate photovoltaic cells include crystalline Si (cr-Si λ_{bg} =1.11 μm), crystalline Ge (cr-Ge λ_{bg} =1.9 μm), crystalline InGaAs (cr-InGaAs λ_{bg}= 1.55 μm), and crystalline GaSb (cr-GaSb λ_{bg} =1.8 μm), and thin film copper-indium-gallium-diselenide (CIGS λ_{bg} =1.8 μm). Table 22 shows a list of the five listed PV cells, with effective wavelengths given in the second row. For the cr-Si cell, the solar spectra $\lambda < 400$ nm or the spectra 700 nm $< \lambda < 1.11$ μm can be utilized for electric power generation. The cr-InGaAs cell has an effective wavelength up to 1.55 μm and can utilize a broader solar wavelength regime ($\lambda < 400$ nm and 700 nm $< \lambda < 1.55$ μm). The cr-GaSb cell has an even broader regime, converting solar spectra up to 1.8 μm ($\lambda < 400$ nm and 700 nm $< \lambda < 1.8$ μm), and cr-Ge even broader ($\lambda < 400$ nm and 700 nm $< \lambda < 1.9$ μm). The thin film CIGS cell has a spectral range close to that of cr-Si, but this amorphous material is more economical.

Table 22. Characteristics of Low-Bandgap Photovoltaic Cells

	cr-Si	cr-InGaAs	cr-GaSb	cr-Ge	CIGS
Bandgap Energy Eq (eV)	1.12	0.8	0.72	0.66	1.10
Effective Wavelength (μm)	<1.11	<1.55	<1.8	<1.9	<1.14

4.4.1.3 Large Scale Photobioreactor

The photobioreactor with PV cells to be used for the CO_2 sequestration must be in a large scale and low cost. A photobioreactor design concept is shown in Figure 140. In this design, microalgae flows in the transparent tube placed at the focal point of the cylindrical reflector. The reflector is aligned in the east-west direction so that the focus of the sun is always on the photobioreactor tube.
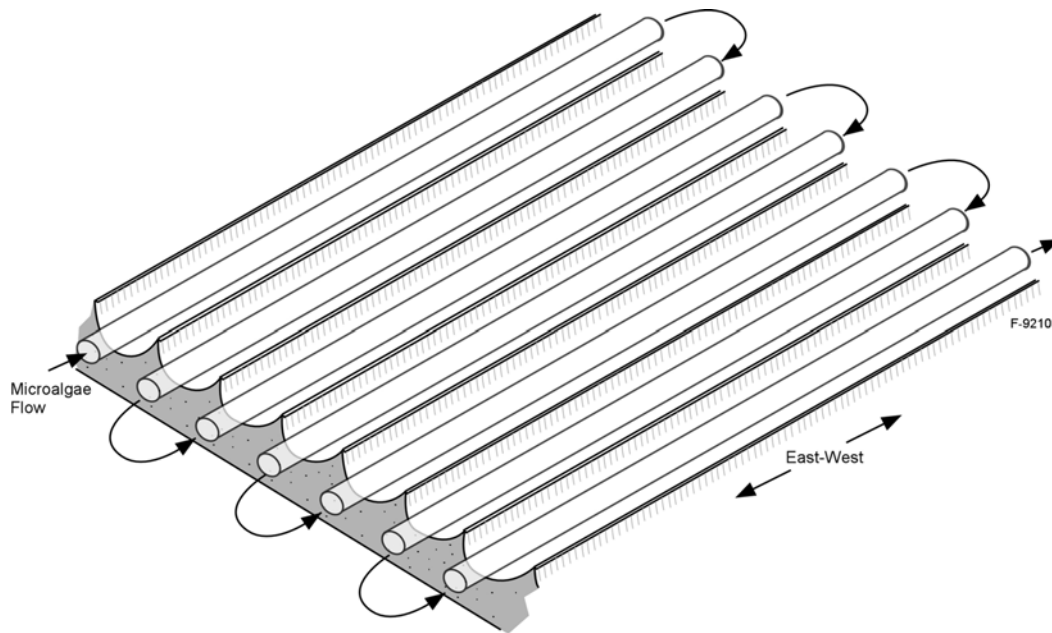
Figure 140. Large scale photobioreactor for CO_2 sequestration and PV power generation.

165

4.4.1.4 Construction of Photobioreactor and PV Cells

Construction of the photobioreactor is described in Figure 141. The cylindrical reflector is mould on the ground, likely to be made of concrete. PV cell panel (made of thin film amorphous silicon, for example) is placed on the cylindrical reflector surface. The PV cell panel is covered with a transparent membrane which has dichroic coating. The coating characteristic is the same as the "cold mirror" we have used in our previous solar spectra splitting experiment. The dichroic membrane reflects the PAR spectra to the photobioreactor tube, while the non-PAR spectra reaches the PV cell panel.

As the cylindrical reflector is aligned in the east-west direction, it does not require daily solar tracking. However, it does require seasonal adjustment. This can be achieved by moving the photobioreactor tube as shown in Figure 141. In this figure adjustment of the photobioreactor tube for Hawaii (20 deg north) location is depicted. At Summer Solstice, the Sun is almost directly above (93.5 deg), while at Winter Solstice, the Sun is at 46.5 deg. The photobioreactor tube must be moved between the two extreme locations. However, this seasonal movement of the photobioreactor tube can be made with a simple mechanical device at a minimum power requirement. Note that moving the photobioreactor tube, rather than tilting the cylindrical reflector, is cost effective method for a large scale photobioreactor plant.
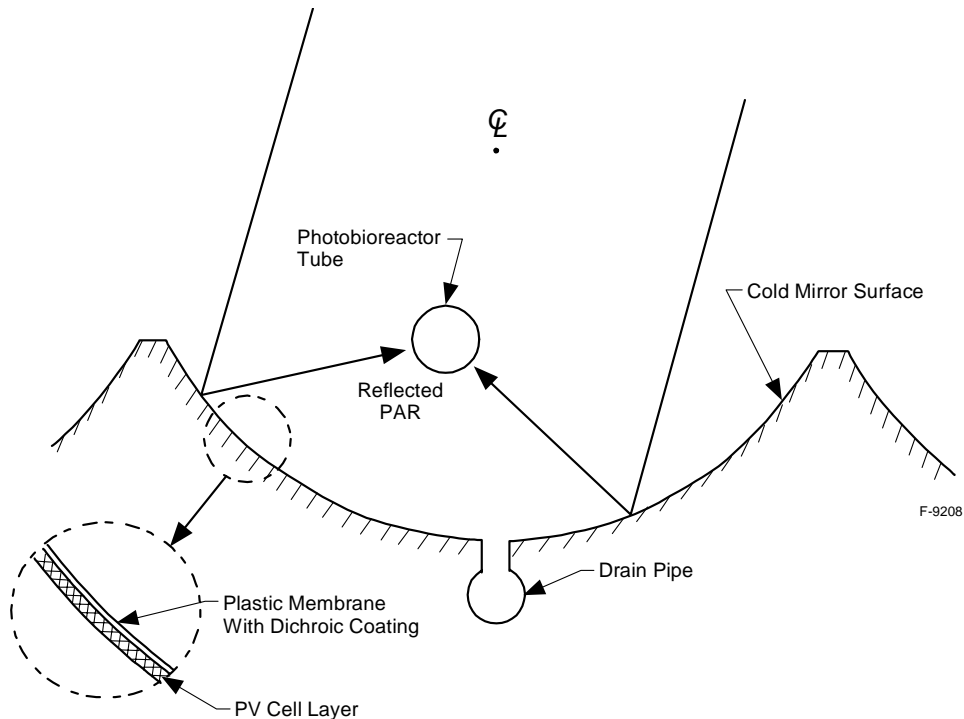
Figure 141. Construction of the cylindrical reflector and the photobioreactor tube.

4.4.1.5 <u>Potential Cost Benefit</u>

It is instructive to estimate how much potential cost benefit this concept will bring. For this purpose we will conduct rough order of magnitude calculation. The typical silicon PV module currently on the market will have efficiencies between 7 – 14%. For the non-PAR solar spectra, the equivalent efficiency will be 1/3 of the full solar spectra. This means that the full spectra equivalent efficiency is 3 – 5%. Based on $800W/m^2$ average solar insolation for 8 hours per day, the electric power generated will be 192 -320 Wh/m^2 per day, or rounding the digit, 0.2~0.3 kWh/m^2 per day. Using the electricity cost at 4¢/kWh, this translates to 0.8 ~1.2¢/m^2 per day. We may use 1 ¢/m^2 per day for the electric generation cost benefit.

The typical PV modules currently on the market will cost between $3 and $6 per Watt, with efficiencies ranging from about 7% to 14% (AM1.5: the AM0 efficiencies could be marginally higher), depending on the technology. This on average amounts to around $400-$500 per square meter. For most of these technologies, the product life is 10 ~ 20 years.

The example discussed above is for a typical PV module taking advantage of the whole solar spectra. Nevertheless, we may use the cost figure as our reference. Using the cost benefit for the electric power by-product as 1 ¢/m^2 per day, we come up with the cumulative electricity generation cost benefit for 10 years will be $36.5/$m^2$ ($0.01 per day × 365 days ×10 years). This is less than 10% of the capital cost expected for a typical PV module. Thus, in order for the electricity byproduct to pay for a part of the CO_2 sequestration cost, the PV module discussed in Figure 10 shall become 10% of the typical PV module cost available to date. In addition to the const of PV cells, optical components such as selective beam splitter must be included in the cost calculation.

Based on the foregoing discussion we may conclude that the cost benefit associated with simultaneous CO_2 sequestration and electricity generation is not likely given the state of the art PV cost. However, if the cost of the PV cells fall below 10% of the current cost, then electric power generation using non-PAR solar spectra will work towards lowering the CO_2 sequestration cost.

4.4.2   <u>Subtask 4.2 – System Integration</u>

The primary goals of photosynthetic sequestration of anthropogenic CO_2 are to optimize carbon capture and to maximize revenues from the sale of the microalgae product. In the case of *Haematococcus pluvialis* production, these goals are generally compatible and can be attained by a number of strategies. For example, carbon capture efficiency could be improved by redesigning the system to recycle vented CO_2 or microalgae yield could be increased by modifying the media or changing the harvesting strategy. A system model is an essential tool to quantify performance and to evaluate the consequences of different operating scenarios. For this Subtask, a process model of the current microalgae production process based on the MGM was developed. This model was then applied to investigate harvesting strategies that would maximize microalgae yield. Optimizing the harvesting strategy can be accomplished with minimal effort, without radical modifications to the process (e.g., vented CO_2 gas recycling)--the consequences of which would be difficult to predict without extensive additional experimentation.

Operational data were analyzed to develop the constituent relationships of the process model. The distribution of CO_2 introduced into the photobioreactor among the different pools (e.g., biomass, DIC; vented gas) was of particular importance and additional testing was conducted to close the carbon mass balance. The results of these tests and the corresponding carbon balance are reported first, followed by the derivation of functional relationships used by the process model. Model verification results are then presented along with a sensitivity analyses. Finally, the model is applied to optimize the microalgae harvesting strategy.

4.4.2.1 <u>Carbon Venting Rates</u>

Table 23 summarizes the measured flow rates of gas vented from the photobioreactor and the corresponding carbon concentrations in that gas determined following the procedures described in Section 3.4.2.

Table 23. Vent Flow Rate and Vented Carbon Concentrations

Time	Vent Flow Rate (L/min)	Vented Carbon Concentration (g/L)
14:52	580.78	1.46E-03
15:00	554.08	2.41E-03
15:09	554.08	2.28E-03
15:14	580.78	2.39E-03
15:20	554.08	2.59E-03
15:25	580.78	1.34E-03
15:30	580.78	1.33E-03
15:35	580.78	1.47E-03
15:40	580.78	7.81E-04
15:45	580.78	7.77E-04

Gas flow rate varied between 554.08 L/min and 580.78 L/min and the vented carbon concentration ranged from 7.77 x 10^{-4} g/L to 2.59 x 10^{-3} g/L over the 53 minute duration of the experiment. The vent flow rate was observed to be relatively steady; the two values in the Table correspond to the smallest change in pressure drop that could be resolved with the Magnehelic differential pressure gauge. The mass flow rate of carbon vented out of the photobioreactor was calculated from data in Table 23 and is presented in Table 24.

The mass flow rate of carbon vented out of the photobioreactor increased from 0.845 g/min at 14:52 to 1.434 g/min at 15:20 and then decreased to 0.452 g/min at 15:45. CO_2 was injected into the MGM media at a constant rate of 11.80 L/min between 14:54 and 15:05. This sparging resulted in an increase in the mass flow rate of vented carbon that persisted for about 20 minutes after the CO_2 injection was terminated.

168

Table 24. Mass Flow Rate of Vented Carbon from MGM

Time	Mass Flow Rate of Vented Carbon (g/min)
14:52	0.845
15:00	1.336
15:09	1.266
15:14	1.390
15:20	1.434
15:25	0.776
15:30	0.770
15:35	0.856
15:40	0.454
15:45	0.452

The discrete carbon flow rate data were integrated numerically using Matlab to determine the total mass of carbon vented from the photobioreactor over the entire duration of the experiment. This quantity was divided by the total mass of carbon entering the photobioreactor via the CO_2 and air injections over the duration of the experiment to estimate the percentage of carbon vented. The carbon loss during the experiment was 41.4%. This value was used in the carbon mass balance equation to represent the fraction of CO_2 entering the MGM during the day that is eventually vented. It was also assumed that all the carbon contained in the air injections is vented during the night, when photosynthesis ceases and there is no CO_2 sparging into the liquid media. There may be additional loss of carbon from the photobioreactor, which currently is not accounted for, since CO_2 outgassing from the media may occur at night and this carbon will be vented along with the CO_2 in the air injections. Additional experiments must be conducted to determine accurately the value of the carbon loss.

4.4.2.2 Carbon Assimilated by Biomass

Average dry cell mass, average %TOC on a dry mass basis, and the number of cells in the photobioreactor were used to calculate the daily mass of carbon bound in the biomass. Average dry cell mass determined from the data in Table 3.4.1 and the results of the %TOC analysis of these samples are presented in Table 25.

Table 25 indicates that the dry cell mass varied between 6.81×10^{-10} g and 1.01×10^{-9} g over the 6 days of sampling and %TOC ranged from 40.03% and 46.01% over this period. The average and standard deviation of the morning values for the dry cell masses were 7.95×10^{-10} g and 1.00×10^{-10} g, respectively. The average absolute error of the morning values for the dry cell masses was 1.29×10^{-13} g. The average and standard deviation of the morning values of %TOC were 43.05% and 1.96%, respectively. This value is reasonable compared to data in the literature that report typical dry mass %TOC of microalgae of approximately 50% (Becker, 1994).

Table 25. Dry Cell Mass and %TOC for *Haematococcus pluvialis* Samples

Date	Time	Dry Cell Mass (g)	Total Organic Carbon (%)
4/26/03	5:40	7.45E-10	40.03
4/26/03	18:45	8.85E-10	41.41
4/27/03	5:40	7.71E-10	42.17
4/27/03	18:30	7.64E-10	42.70
4/28/03	6:05	6.81E-10	43.18
4/28/03	18:50	9.91E-10	42.82
4/29/03	5:30	7.44E-10	43.15
4/29/03	18:45	8.05E-10	43.79
4/30/03	6:00	8.79E-10	43.74
4/30/03	19:00	1.01E-09	45.23
5/1/03	5:25	9.51E-10	46.01

The dry cell mass and %TOC were employed to estimate the mass of carbon per cell. The mass of carbon per cell over the six day period is plotted in Figure 142. The mass of carbon per cell is observed to vary between 2.98 x 10^{-10} g and 4.57 x 10^{-10} g, generally increasing during the day via photosynthesis and decreasing at night due to respiration. There appears to be an increasing trend over time.
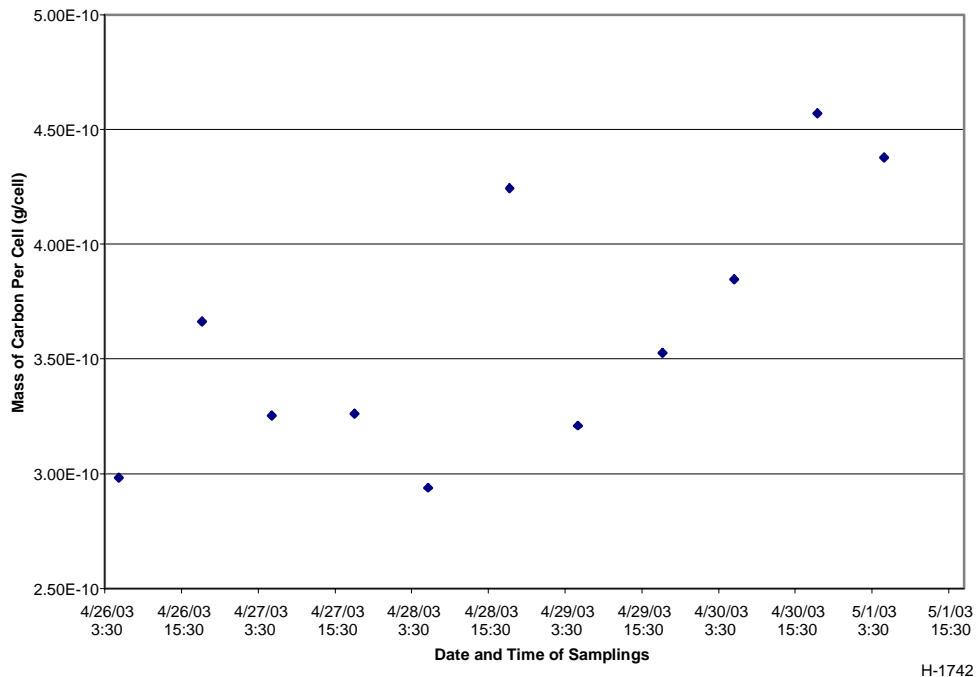
Figure 142. Mass of carbon per cell.

170

4.4.2.3 Carbon Mass Balance Calculations

        Using the results of the gas venting experiments, cell sample analysis, and the photobioreactor operational data, values of the different terms in the carbon mass balance equation (Eq. (4)) were calculated and are shown in Table 26. The data were from M13A-020423 which operated from April 23, 2003 to May 27, 2003. It should be noted that entries in Table 26 are not continuous; results are missing for a number of dates since the daily data set provided by Mera Pharmaceuticals was incomplete. Data were not provided for the period around the harvesting dates of May 1, 2003, May 6, 2003, May 9, 2003, May 14, 2003, May 19, 2003, May 23, 2003, and May 27, 2003. When the photobioreactor is harvested, a portion of the liquid media (about 50%) and the cells contained therein is extracted and transferred to the open ponds. Fresh media is then added to compensate for the amount removed.

        Table 26 indicates that the daily mass flow rates of carbon injected into and vented out of the photobioreactor varied between 898.34 g/day and 1914.77 g/day and between 441.25 g/day and 832.19 g/day, respectively. The respective ranges of the changes in dissolved inorganic carbon, carbon bound in biomass, and carbon in the headspace were 12.80 g/day to 189.21 g/day, 69.64 g/day to 676.68 g/day, and 16.56 g/day to 689.17 g/day.

Table 26. Carbon Mass Balance for Photobioreactor

Date	Carbon Injected into MGM (g/day)	Carbon Vented Out of MGM (g/day)	DIC (g/day)	Carbon Bound in Biomass (g/day)	Carbon in Gas Space (g/day)
4/26/03	899.61	443.56	70.89	218.86	166.30
4/27/03	898.34	441.25	58.34	341.92	56.83
4/28/03	1051.91	499.30	65.77	408.74	78.10
4/29/03	1011.39	478.98	51.21	69.64	411.56
5/3/03	962.70	465.43	12.80	210.90	273.57
5/4/03	1107.51	520.48	189.21	381.25	16.56
5/7/03	1628.55	686.29	115.98	540.11	286.16
5/8/03	1691.50	742.69	169.60	349.94	429.28
5/10/03	1488.99	668.02	94.87	480.92	245.18
5/11/03	1526.21	673.93	112.90	381.29	358.08
5/12/03	1684.59	745.34	71.50	256.54	611.20
5/13/03	1784.24	782.69	44.97	326.89	629.69
5/15/03	1376.35	628.38	72.97	415.10	259.90
5/16/03	1588.86	706.96	134.41	614.64	132.84
5/17/03	1715.64	750.62	29.03	381.69	554.31
5/18/03	1914.07	816.54	125.51	282.84	689.17
5/21/03	1558.77	691.16	92.91	375.37	399.32
5/22/03	1785.67	782.66	135.44	393.48	474.09
5/25/03	1914.77	832.19	68.11	676.68	337.78
5/26/03	1770.71	776.55	124.56	257.20	612.40

The percentage of injected carbon that is assimilated into the biomass pool (i.e., the ratio of carbon bound in biomass divided by the mass of carbon injected) ranged from around 7% to 39% with a cumulative average of 25%. This suggests that additional research needs to be conducted to improve the carbon capture efficiency. One possibility may be a system where vented gases are recirculated back into the photobioreactor. The effect of recirculation on gas transfer from the sparged gas into the liquid media, microalgae growth, and other technical and economic factors will need to be investigated.

The results provide insight into the behavior of the photobioreactor. Since the daily rate of change of carbon bound in cell biomass ($\frac{d[C_{biomass}]}{dt}$) is observed generally to be significantly greater than the increase in the DIC pool in the media ($\frac{d[DIC]}{dt}$), it appears that CO_2 that is injected and dissolves into the liquid is being effectively assimilated by the cells.

The results in Table 26 indicate that carbon accumulates continuously in the liquid media (as DIC) and the headspace. The accumulation of DIC in the media is determined directly from data on pH and alkalinity. The accumulation of CO_2 in the headspace, however, is an inferred quantity and strongly reflects the measured daytime carbon venting rate, which is taken to be a fixed percentage of the CO_2 injection rate. At night, it was assumed that the carbon venting rate falls to exactly equal the rate on carbon entering the photobioreactor with the airlift injections; hence, CO_2 levels in the headspace at the end of the day are essentially maintained until the next morning.

It is possible that CO_2 venting losses exceed the amount of CO_2 entering the photobioreactor during the night, reducing or negating the calculated accumulation in the headspace. Under this scenario, CO_2 concentrations in the headspace may fall to levels comparable to the CO_2 concentration in air during the night, which would promote outgassing from the liquid media. Assuming that all of the CO_2 advected into the photobioreactor with the airlift injections is vented, the equation for the nighttime concentration of CO_2 in the headspace, y, as a function of time is:

$$y = y_{atm}\left[1 - e^{\left(-\frac{Q}{V_g}t\right)}\right] + y_0 e^{\left(-\frac{Q}{V_g}t\right)} - \left(\frac{V_l}{V_g}\right)[DIC]_t$$
$$+ \left(\frac{V_l}{V_g}\right)[DIC]_0 e^{\left(-\frac{Q}{V_g}t\right)} + \left(\frac{V_l Q}{V_g^2}\right) e^{\left(-\frac{Q}{V_g}t\right)} \int_0^t [DIC]_\tau e^{\left(\frac{Q}{V_g}\tau\right)} d\tau$$

(17)

where y_{atm} is the carbon dioxide concentration in air (mol/L), Q is the volumetric air flow rate into the photobioreactor (L/min), V_g is the volume of the headspace (L), t is the time (min), y_0 is the initial headspace CO_2 concentration (mol/L), V_l is the volume of the media (L), $[DIC]_t$ is the dissolved inorganic carbon concentration at time t (mol/L), $[DIC]_0$ is the initial dissolved inorganic carbon concentration (mol/L), and τ is the variable of integration.

172

Overnight headspace CO_2 concentration as a function of time was calculated using Eq. (18) for the two dates when nighttime alkalinity data needed to determine [DIC] was available: April 26, 2003 and April 27, 2003. These results are plotted in Figure 143 and Figure 144, respectively.

Figure 143 and Figure 144 indicate that CO_2 accumulated in the headspace during the day dissipates quickly to a level comparable to the concentration of CO_2 in air at night which was 1.70×10^{-5} mol/L. It is reasonable to conclude, therefore, that the net daily change in carbon in the headspace was zero because accumulated CO_2 is vented out of the MGM at night. The daily amounts of carbon vented from the MGM should then equal the sum of the values given in columns 3 and 6 of Table 26.
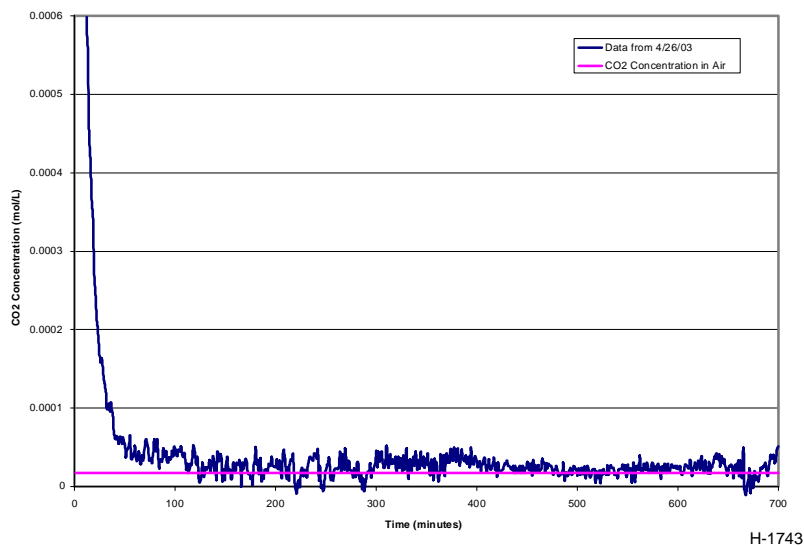
Figure 143. Nighttime headspace CO_2 concentration for 4/26/03.
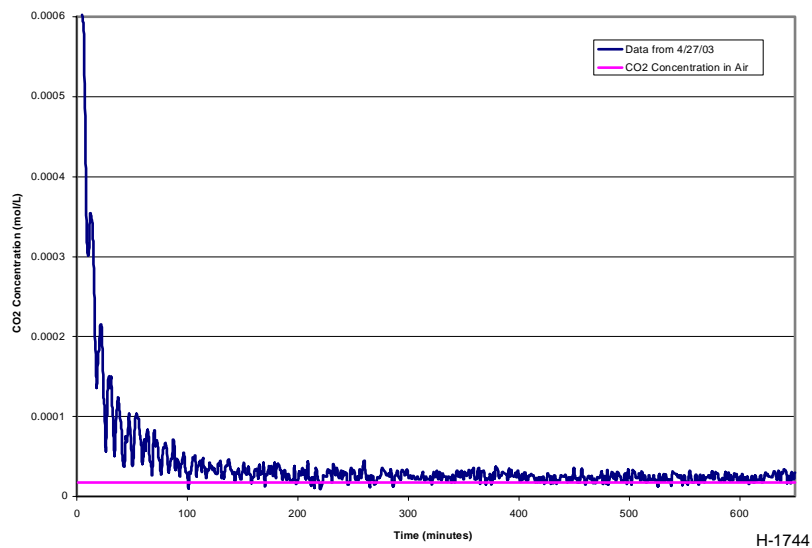
Figure 144. Nighttime headspace CO_2 concentration for 4/27/03.

173

4.4.2.4 Process Model Relationships

Relationships between different variables that appear in the carbon mass balance equation were derived and incorporated into the STELLA process model. The first relationship was for the daily mass flow rate of carbon injected into the MGM. The data and curvefit are plotted in Figure 145. The corresponding R^2 value of the linear curvefit is also included in the figure. Given the scatter in the data, a linear equation appears reasonable. The carbon injection rate responds to increasing pH due to carbon depletion in the media either by degassing of the carbon or photosynthetic utilization. Increasing carbon injection rates therefore indicate rising rates of depletion of carbon in the media.

Figure 146 plots the mass flow rate of carbon degassed from the media as a function of the daily rate of carbon injection into the photobioreactor. The carbon degassing rate is the amount of injected carbon that does not dissolve in the media over the course of a day and is the sum of the daily carbon venting rate and the change in carbon concentration in the headspace (columns 3 and 6 in Table 26). A linear curvefit to the data and the corresponding R^2 value are shown in the figure. Using this relationship, the partitioning of the injected carbon between the media phase, where the carbon is available for cell growth, and the gas phase, where carbon will eventually be vented, can be determined.
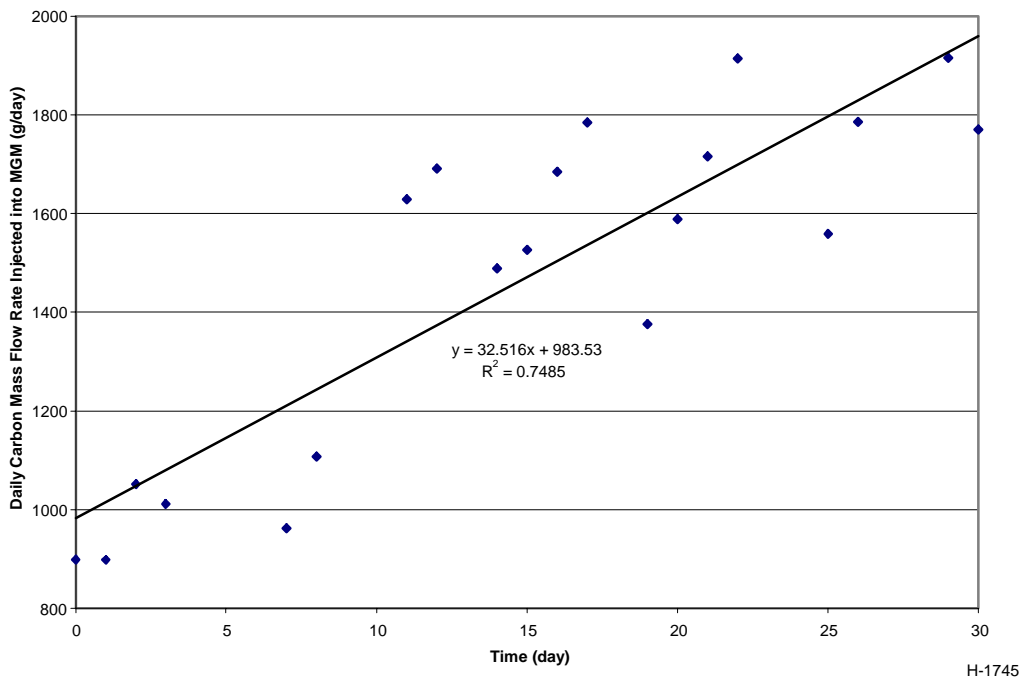
Figure 145. Daily carbon mass flow rate injected into the MGM over time.

174

The chart shows:
- Y-axis: Daily Carbon Mass Flow Rate Degassed Out of Media (g/day), ranging from 400 to 1600
- X-axis: Daily Carbon Mass Flow Rate Injected into MGM (g/day), ranging from 800 to 2000
- Equation: $y = 0.7955x - 160.11$
- $R^2 = 0.7939$
- H-1746
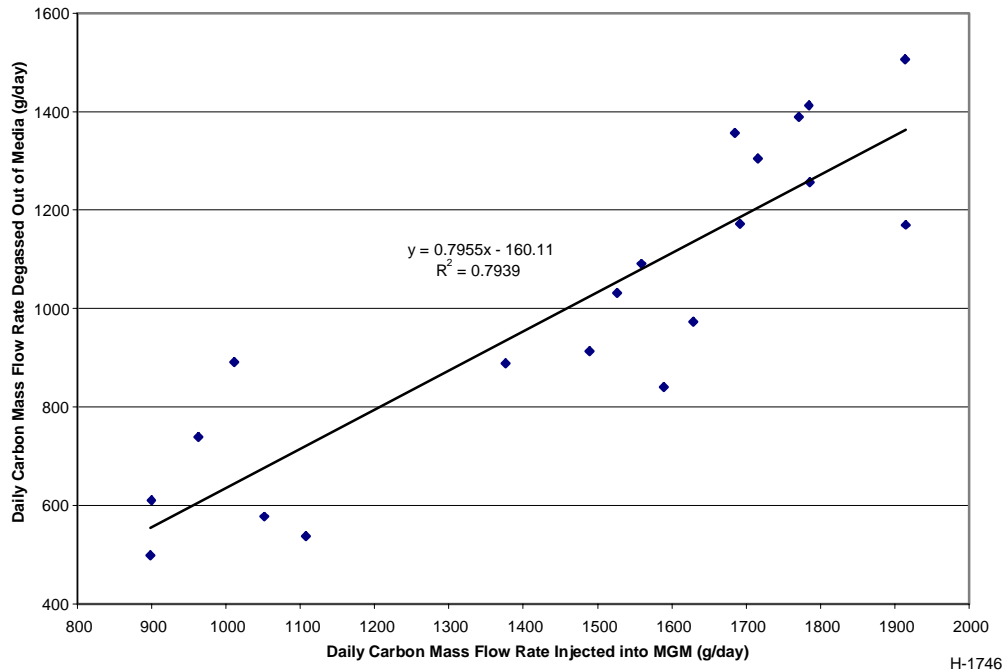
Figure 146.   Daily carbon mass flow rate degassed out of the media vs. daily carbon mass flow rate injected into the MGM.

Figure 147 presents data on the daily change in the mass of carbon bound in biomass as a function of the daily change in the mass of total carbon in the media. The total carbon in the media is the sum of carbon bound in biomass and in the DIC pool. Again, the data suggest a linear relationship between these two quantities and a curvefit and corresponding value of R^2 are included in the figure. Using this relationship, the daily change in carbon bound in biomass can be estimated from the daily change in total carbon in the media, which is the difference between the daily carbon injection rate and the daily degassing rate. Note that the daily degassing rate can be determined by the equation given in Figure 146 from the carbon injection rate.

Finally, a relationship was derived for the daily specific growth rate as a function of the daily rate of carbon assimilation into the cell biomass pool. The daily specific growth rate is the number of cell divisions that occur per cell per day. The relationship quantifies how the rate of carbon assimilation by cells affects cell division. Data plotted in Figure 148 indicates that rate of cell division increases linearly with the amount of carbon captured by the biomass pool. The best fit curve and the corresponding R^2 value are included in the figure. The curvefit provides a means to estimate the increase in the cell population in the photobioreactor given the amount of carbon bound in the biomass in a day.

Taken together, the above relationships can be used to calculate the number of cells in the photobioreactor at any time and the fate of injected carbon (dissolved, degassed, or bound in biomass) given the initial cell population and carbon injection rates (within the range of conditions of the data used to derive the relationships).
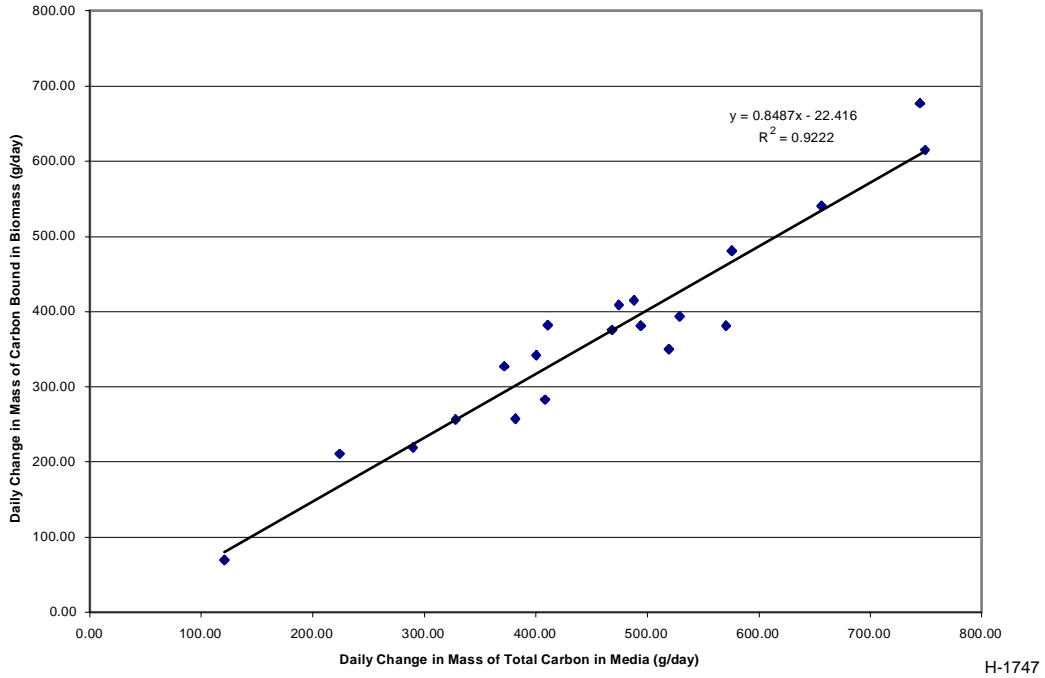
Figure 147.   Daily change in the mass of carbon bound in biomass vs. daily change in the mass of total carbon in the media.
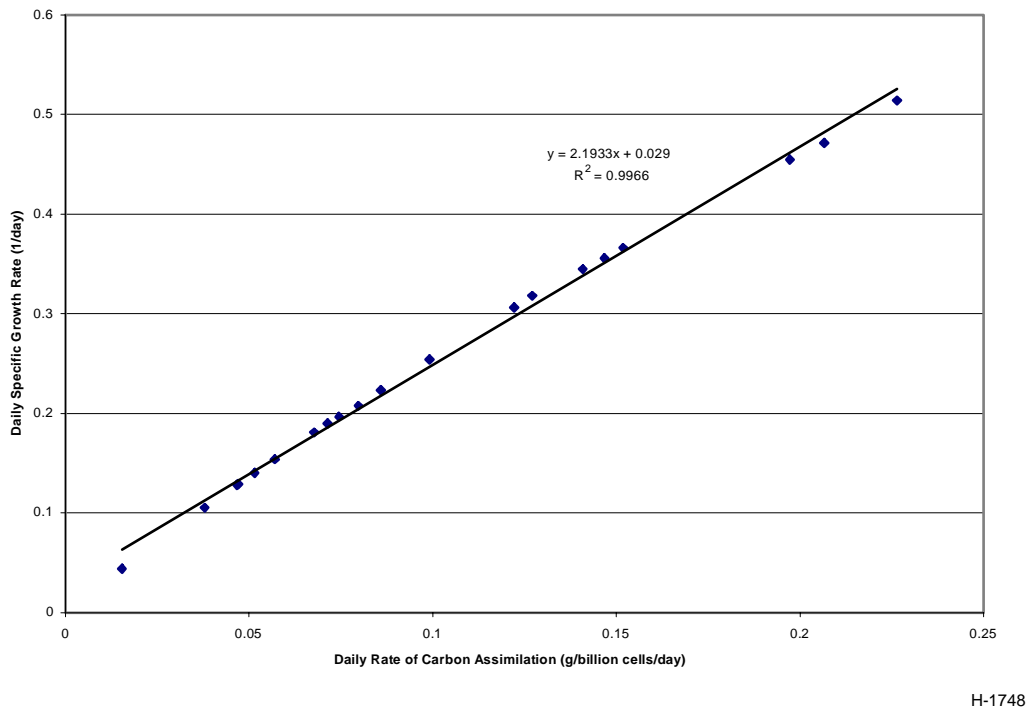
Figure 148. Daily specific growth rate vs. daily rate of carbon assimilation.

176

4.4.2.5 STELLA Process Model

A schematic drawing that summarizes the primary features of the *Haematococcus pluvialis* production process model that utilizes the STELLA software is shown in Figure 149. This model integrates the carbon mass balance, *Haematococcus pluvialis* population dynamics, and the harvesting strategy using the relationships that were developed and the photobioreactor operational data.
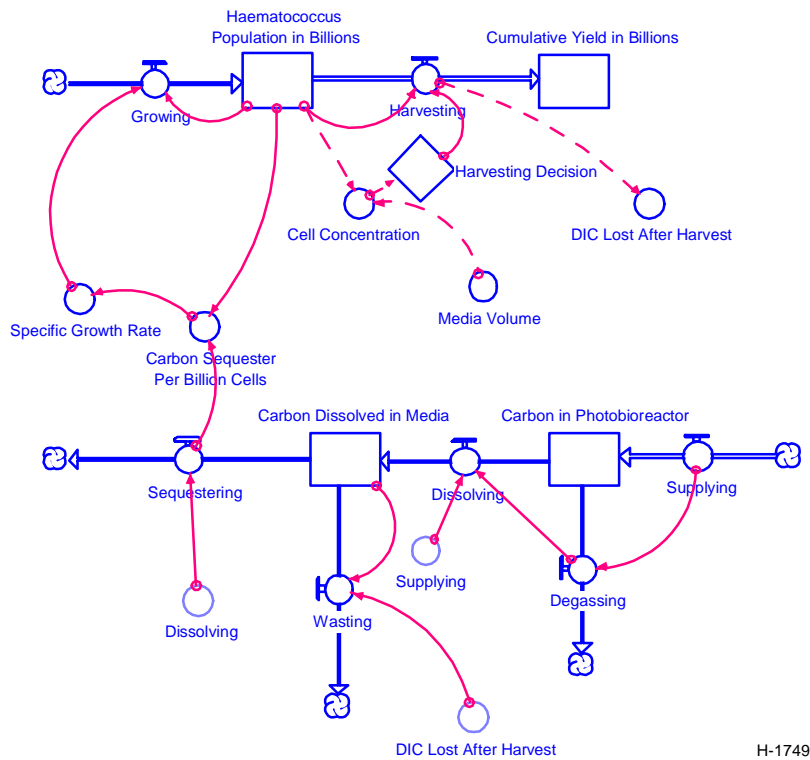
Figure 149. Schematic drawing of the STELLA process model.

4.4.2.6 Verification of the STELLA Model

The STELLA process model was verified by comparison with data from M10A-040810, a different photobioreactor than the one used to develop the functional relationships between variables used by the model. Table 27 compares simulated population size and the data for M10A-040810. The results in Table 27 are plotted in Figure 150. The corresponding estimated percent errors of the simulations are given in Table 28.

The percent error ranged from 5.44 % to 34.85% with no clear trend with regard to underpredictions and overpredictions. The average percent error for all five dates tested was 14.51%. This value appears to be biased by the single large error for 8/30/04. The model appears to simulate the photobioreactor operation reasonably well.

177

Table 27. Comparison of Model Results and Data for MGM M10-040810

Date	Simulated Population Size (cells)	Population Size from Data Set (cells)
8/29/04	4.86E+12	5.44E+12
8/30/04	5.70E+12	4.23E+12
8/31/04	4.58E+12	5.12E+12
9/1/04	3.47E+12	3.9E+12
9/2/04	4.49E+12	4.75E+12
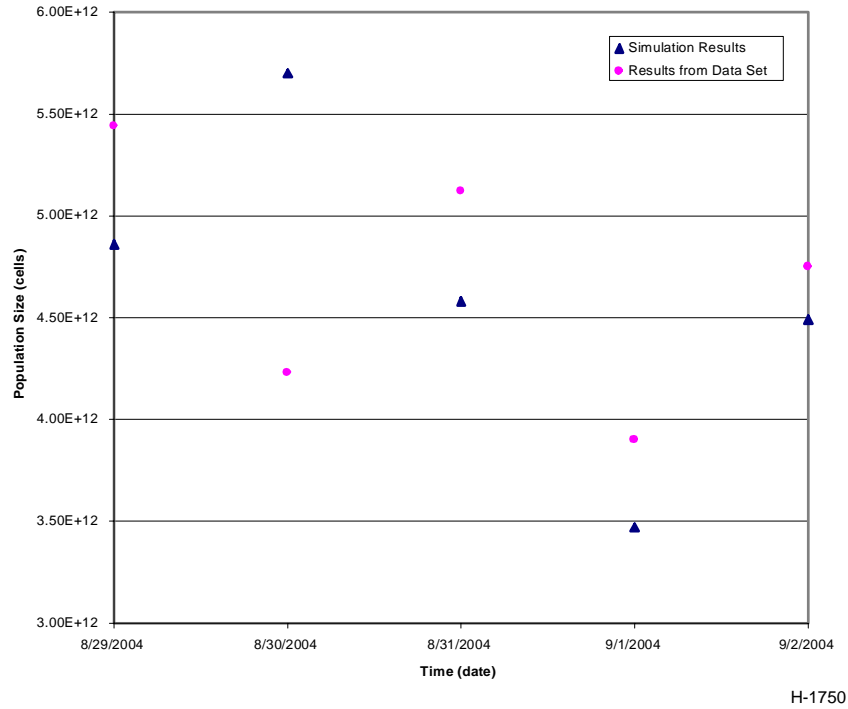
Figure 150. Comparison of model results and data for MGM M10-040810.

Table 28. Percent Error of Model Predictions of Cell Population for M10-040810

Date	Percent Error (%)
8/29/04	10.57
8/30/04	34.85
8/31/04	10.60
9/1/04	11.12
9/2/04	5.44

4.4.2.7 Sensitivity Analysis

In the present investigation, harvesting strategy is based on two parameters: target cell concentration that must be achieved in the photobioreactor before harvesting can take place and the number of cells collected during a harvest. Optimizing the harvesting strategy involves varying these two parameters to achieve a maximum cumulative cell yield (i.e., sum of cells collected over all harvests for a given duration of operation). Sensitivity analyses were conducted using the STELLA software to facilitate the optimization and also to gain insight into the predicted behavior of the *Haematococcus pluvialis* production process

Mera Pharmaceuticals currently uses a target cell concentration at 521,000 cells/mL and harvesting quantity at 3.2 trillion cells. For the sensitivity analysis, target cell concentration was first varied from 300,000 cells/mL to 700,000 cells/mL in increments of 200,000 cells/mL while harvesting quantity was held fixed at 3.2 trillion cells. Harvesting quantity was next varied from 1 trillion cells to 5 trillion cells in increments of 2 trillion cells with target cell concentration fixed at 521,000 cells/mL. Results obtained using the sensitivity analysis function of STELLA are presented in Table 29 and Table 30.

Table 29. Target Cell Concentration and Cumulative Yield from the Sensitivity Analyses

Target Cell Concentration (cells/mL)	Cumulative Yield (in billions of cells)
300,000	29,849
500,000	31,623
700,000	33,220

Table 30. Harvesting Quantity and Cumulative Yield from the Sensitivity Analyses

Harvesting Quantity (in billions of cells)	Cumulative Yield (in billions of cells)
1,000	31,623
3,000	30,813
5,000	30,031

Table 29 indicates that cumulative yield increases with target cell concentration. The cumulative yield grew by about 3.4 trillion cells as target cell concentration increased from 300,000 cells/mL to 700,000 cells/mL.

Table 30 indicates that cumulative yield decreases with increasing harvesting quantity. The cumulative yield decreased by about 1.6 trillion cells as harvesting quantity increased from 1 trillion cells to 5 trillion cells.

These results provide guidance on how best to optimize harvesting strategy. It appears that maximum cumulative yield (which corresponds to the maximum carbon sequestration) may be approached by increasing the target cell concentration and decreasing the harvesting quantity.

4.4.2.8 Model Simulations

The STELLA process model was used to investigate different harvesting scenarios. In each of these scenarios, initial cell count, carbon injection rates, and the total number of days until the final harvest were the same. Only the harvesting criteria were different. Table 31 provides the target cell concentration in the photobioreactor (which must be attained before each harvesting), the harvesting cell quantity, and the corresponding cumulative cell yield for six scenarios.

Table 31. Target Cell Concentration, Harvest Quantity, and
Maximum Cumulative Yield for Six Scenarios

Scenario	Target Cell Concentration (cell/mL)	Harvested Quantity (in billions of cells)	Cumulative Yield (in billions of cells)
1	521,000	3200	30,943
2	300,000	1000	29,849
3	400,000	1000	30,756
4	500,000	1000	31,623
5	600,000	1000	32,436
6	700,000	1000	33,220

Table 31 indicates that cumulative yield increases as the target cell concentration was increased while holding harvesting quantity constant at 1×10^{12} cells. This result primarily reflects the larger number of cells in the MGM at the time of the final harvest, which is included in the cumulative yield. The maximum cumulative yield of 3.32×10^{13} cells occurs in scenario 6 that had the highest target cell concentration and the lowest harvesting quantity among the different scenarios tested, which is consistent with the results from the sensitivity analyses. While this yield exceeds the yield for the current harvesting strategy, scenario 1, by over 3×10^{12} cells, it may not be feasible under the current facilities and labor force limitations at Mera Pharmaceuticals, Inc. Scenario 1 requires nine harvests spaced apart by several days to allow the concentration in the photobioreactor to recover, while scenario 6 requires 27 daily harvests. Daily harvesting of the photobioreactor would place a strain on the small labor force employed at the Mera Pharmaceuticals facility. Moreover, seven ponds are required to stress the *Haematococcus pluvialis* harvested from the photobioreactor without wasting any microalgal cells under scenario 6, while only five ponds are currently available at the Mera Pharmaceuticals facility.

A realistic harvesting scenario that provided a cumulative yield greater than the yield obtained with the current harvesting strategy was determined by additional model simulations. Scenarios were investigated with harvesting quantity held constant at the current value of 3.2×10^{12} cells and target cell concentration varied between 5×10^5 cells/mL and 5.5×10^5 cells/mL. A target cell concentration of 5.5×10^5 cells/mL was found to produce the maximum cumulative yield of 3.12×10^{13} cells, a relatively insignificant increase of 2.57×10^{11} cells (approximately 0.7%) over the yield for the current harvesting strategy. It appears, therefore, that the current harvesting strategy may represent the best possible scenario when real constraints imposed by the limited labor force and number of available open ponds are taken into consideration.

Nonetheless, the present results suggest that the process model can be a valuable tool to optimize carbon capture and revenue streams when planning new facilities.

4.5   Task 5 - Economic Analysis

4.5.1   Subtask 5.1 – Gas Separation Process

Economic analysis of technologies currently available to separate and capture CO_2 from fossil-fueled power plants is discussed in Section 4.1.2. Application of these carbon dioxide separation processes to flue gas depends on the concentration of CO_2 in the stream, on the presence of impurities in the gas, and on the pressure of the flue gas stream. Chemical adsorption may be preferred for cases in which the concentration of CO_2 is low and the pressure is near atmospheric. Physical adsorption is favored for higher total pressure and concentration of CO_2. Chemical adsorption using MEA is the most mature technology and looks to be the most economically viable in the near future.

A unit sized for a 25 MWe plant burning a bituminous coal would process 235,000 lb/hr of flue gas and produce 42,000 lb/hr of CO_2. Table 11 lists the major equipment and costs. The total major equipment cost is approximately $5M (1999 dollars). The total capital cost is on the order of $11M.

The processes discussed in Section 4.1.2 are currently demonstrated on a commercial scale, but for the production of CO_2 (from chemical plants or natural gas processing plants, for example). The cost of these technologies is too high for the reduction of greenhouse gases. Research into less expensive processes that are aimed at carbon emissions reductions is still in the early stages. The hope is that in the near future, less costly options will be available for fossil fuel-fired combustion sources. Some of the technologies now being developed include membranes, novel gas-liquid contactors, solid sorbents, and the formation of CO_2/water hydrates.

4.5.2   Subtask 5.2 – Photobioreactor Carbon Fixation Process

Here we have strived to determine the costs associated with the photobioreactor carbon fixation process of a microalgal-based carbon sequestration plant. We have, first, designed a microalgal facility at an economically significant scale (12 acres). Second, we have compiled the capital and recurring costs of a microalgal plant producing astaxanthin from *Haematococcus pluvialis* based on our experiences at the Mera Production facility. Using this as the framework we have also carried out cost analysis for microalgal plants that produce, for example, *Spirulina* biomass or *Nannochloropsis* lutein. Finally, we have estimated how changes in facility scale (i.e., size) would affect the cost estimates. The costs have been compared to expected revenues from the high value products produced from the carbon sequestration activity.

A detailed economic model was developed for the production of high value substances from microalgae. Using over 500 input variables, the model calculates capital and operating costs as well as land, labor and utility requirements. It also generates cash flow and balance sheets for the first 15 years of operation given market price and sales expectations. The

model has been ground truthed by running it for *Haematococcus pluvialis* and making sure it agrees with the reality of producing astaxanthin at Mera. The model was developed to be as flexible as possible and accommodating of any microalgae and type of processing that microalgae would require to produce the valuable end product. For example, the end product might be composed of simply dried biomass or it may require extraction and encapsulation to be sold as a human nutritional supplement. There is also flexibility in the types of growth units used; enclosed Mera Growth Modules (MGMs), open ponds or any combination of the two can be used.

4.5.2.1 <u>Microalgal Plant Design</u>

Our first activity under this subtask included the design of a microalgal facility of commercially significant scale that would produce a high value product, such as astaxanthin. The design parameters are based on Mera's experience in commercial production and historical data. This first design effort assumes no optimization concerning efficiency of CO_2 utilization, including gas dissolution into the growth medium or losses due to degassing from the medium.

The design parameters for this plant are

Total plant surface area:	12 ha
Culture surface area:	7 ha
Support systems:	5 ha
Productivity:	8 g C m^{-2} d^{-1}
Efficiency of CO2 utilization:	12%
Percent of culture area under cultivation:	81.6%

We can estimate that this plant would capture up to about 1.6 tons of CO_2 per day. Again, assuming no optimization in CO2 utilization efficiency (12% based on the results of Section 4.2.2.1.1), the plant would need to be fed by a combustion source generating about 13 tons CO_2 d^{-1}. This is approximately the amount of CO_2 generated when producing 1.7 MW of thermal power by burning bituminous coal. The same plant can be expected to produce about 8 kg of nutraceutical grade astaxanthin d^{-1}, which at a wholesale price of US$10,000 would generate about US $2.5 million month^{-1}.

As a first step in the design process, we have specified the mass flows of the different materials necessary to run Mera's actual plant in Kona Hawaii (Figure 151).

The plant under consideration is, however, significantly larger (about 30x more capacity). Such a plant is depicted in Figure 152. It should be noted that this plant's characteristics are specific to the production of a high value product, astaxanthin, from *Haematococcus*. Thus, the plant utilizes both enclosed photobioreactors (MGM), depicted green in the figure, and open pond systems, depicted red in the figure. Further work on this design will also generate alternate designs for similar sized plants to produce other types of materials which might utilize only open pond reactors (e.g., *Spirulina*) or only enclosed photobioreactors (e.g., *Nanochloropsis* for lutein production).

182
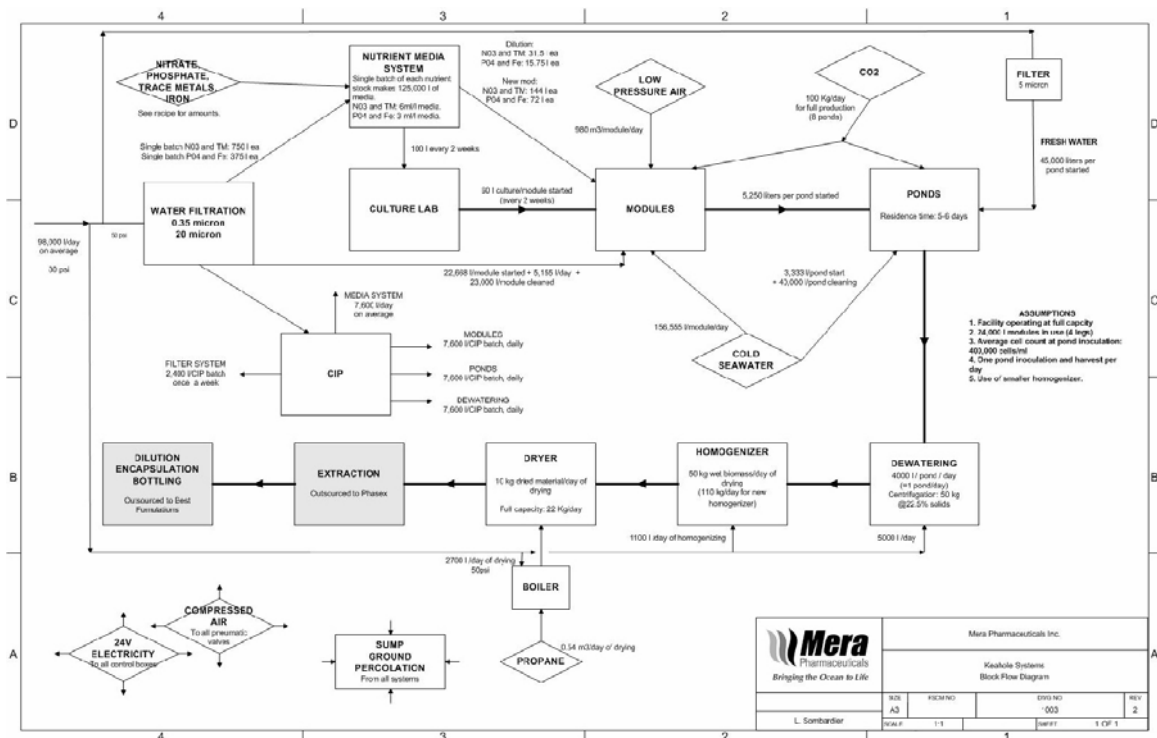
Figure 151. Mass flows of the different materials necessary to run Mera's present production plant in Kona, Hawaii, for the production of astaxanthin from *Haematococcus*.
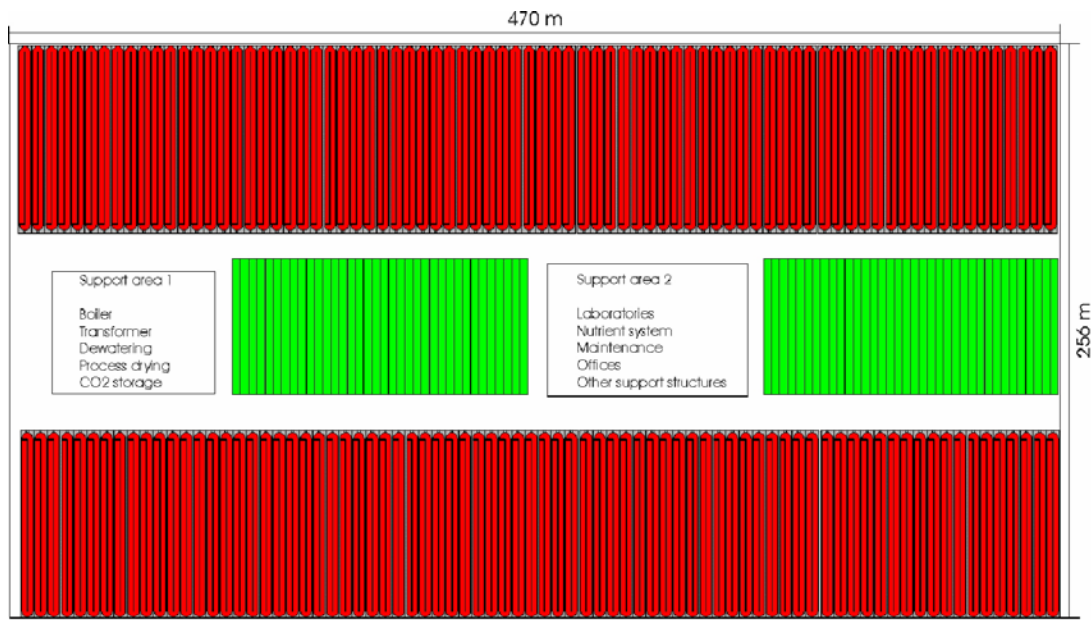
Figure 152. Conceptual design of an expanded microalgal facility (about 30x capacity of Mera's facility) for the production of astaxanthin from *Haematococcus*. Green areas represent cultivation units made up of enclosed photobioreactors. Red areas represent cultivation units made up of open pond systems.

183

4.5.2.2 <u>Capital and Recurring Costs of Microalgal Plant</u>

We have compiled the capital and recurring costs of a microalgal plant producing astaxanthin from *Haematococcus pluvialis* such as the one depicted in Figure 152. Similarly, we have carried out similar cost analysis for microalgal plants that produce other products such as *Spirulina* biomass and lutein from *Nannochloropsis*.

As a first step we have tabulated (e.g., Table 32 all the capital costs (e.g., equipment), recurring costs (materials and supplies), labor costs, utilities, etc). These costs have been included in a model that includes over 500 variables that are used to calculate monthly cost of goods, capital equipment requirements, land requirements and cash flow and balance sheets for 15 years of operation. The model is in the form of an EXCEL workbook with 9 separate worksheets: CULTURE PARAMETERS, OPERATIONS PARAMETERS, UTILITIES CALC SHEET, LABOR CALC SHEET, CAPITAL COSTS, ECONOMIC MODEL, PROFIT AND LOSS, CASH FLOW, and BALANCE SHEET. Full details for labor, utilities, and other operational costs are listed as well as capital costs. Furthermore, it includes a table compiling various microalgae products along with the corresponding microalgae's growth parameters, expected market price and estimated cost of sales parameters. The first five worksheets are used to update, by the user, the processes and associated costs for the different aspects of microalgal production. For example, the user may consider changing the parameters in the LABOR CALC SHEET and UTILITIES CALC SHEET depending on where the microalgal plant would be sited. The input is used in the ECONOMIC MODEL worksheet to estimate the total costs associated with the different aspects of the production of microalgal biomass in photobioreactors, including production of inoculum as well as harvesting, drying and processing costs. Finally, the last three sheets use the costs generated in the ECONOMIC MODEL worksheet plus information on the expected value of the microalgal biomass to generate Profit and Loss, Cash Flow, and Balance Sheet statements.

The model was run for promising alga such as *Haematococcus pluvialis*, *Spirulina*, *Dunaliella* and *Chlamydomonas*. However, it was designed to accept any other type of algae as long as reasonable assumptions can be made on the amount of biomass produced monthly by a minimal growth unit (module and/or pond), type of processing required, market price and sales information such as cost of sales, distribution costs and duration of ramp up to 100% sales.

Model output includes expected monthly expenses depending on the user's input with respect to desired product and quantity to be produced. Land requirements and initial capital costs are calculated. The number of years over which capital costs are depreciated is also a variable. Monthly expenses include direct supplies, utilities such as electricity, freshwater, saltwater, and CO_2, maintenance, direct labor as well as fringe benefits and overhead. Finally, outsourced activities such as extraction and encapsulation of high-value microalgal products are also listed under monthly expenses. These monthly expenses are then used to create a yearly cash flow sheet after determining revenues based on expected sales and cost of sales in the profit and loss sheet. Finally, a balance sheet valid for the first 15 years of operation is generated based on projections.

Table 32. Partial List of Infrastructure Equipment in Mera's Kona Microalgal Plant
Shown as an Example of the Large Database that We Have Put Together
to Use as Input into Our Economic Models

Part Number	Manufacturer	Type of Part	Number of parts in Kona	Purchase Price	Total Cost
2A147	AMETEK	Pressure Gauge	8	$4.66	$37.28
5HK69	Ametek	Pressure Gauge	3	$8.15	$24.45
38-06-61-010	AMIAD	Turboclean Filter	1	$1,539.30	$1,539.30
6KK47	APOLO	Isolation Valve	1	$7.92	$7.92
1113060	Asahi	Butterfly valve	1	$179.20	$179.20
1070005	ASAHI	Isolation valve	6	$11.30	$67.80
1101020	ASAHI/AMERICA	Isolation Valve	1	$157.00	$157.00
CHII-N1-2FE	CHALLENGER	transfer pump	1	$548.00	$548.00
TN4885JP	Chem-Tainer, Inc.	Chemical Storage Tank	4	$951.00	$3,804.00
TN7285JP	Chem-Tainer, Inc.	Chemical Storage Tank	3	$1,606.00	$4,818.00
TC8086CC	Chem-Tainer, Inc.	Storage Tank	1	$12,199.00	$12,199.00
OS	CLA-VAL	Pressure Regulator	1	$652.00	$652.00
250W	CLOW	Isolation Valve	2	$282.00	$564.00
38471	EG&G Rotron	Blower, air, low pressure	4	$2,918.00	$11,672.00
FEBCO 825Y RP	FEBCO	Isolation Valve	2	$40.05	$80.10
KC 1130	FINISH THOMPSON	Pump	1	$1,753.00	$1,753.00
VTPVS20V-B	FIP	3-way valve	2	$269.87	$539.74
VFXV105	FIP	Ball valve	11	$17.40	$191.40
VXPVS05E-B	FIP	Control valve, FIP type	2	$34.78	$69.56
1011-10	FLO CONTROL	Backflow Valve	1	$11.17	$11.17
1011-20	FLO CONTROL	Spring Check Valve	8	$15.53	$124.24
3/4 DN 20	FN	Isolation Valve	1	$11.74	$11.74
2" DN 50	FNW	Isolation valve	2	$40.05	$80.10
69050D331141	Gemu	valve, Gemu pneumatic	17	$426.00	$7,242.00
69080D301141	GEMU	Valve,Gemu pneumatic	2	$963.00	$1,926.00
HUR-170-HP	Harmsco	Filter	4	$2,500.00	$10,000.00
1078002	HARRINGTON	Labcock Valve	4	$11.40	$45.60
HCTB1200SACTV	Hayward	Ball valve	48	$250.40	$12,019.20
HCTB1200SACTV-4	Hayward	Ball valve	5	$602.40	$3,012.00
HCTB1100SACTV	HAYWARD	Isolation valve	3	$267.00	$801.00
2475N7.5	Ingersol Rand	Compressor, air	1	$2,273.00	$2,273.00
MP0101	Inland Machinery	portable S.S. tank	2	$3,600.00	$7,200.00
L423-44	LMI, Milton Roy	Metering Pump	4	$2,983.50	$11,934.00
U-07553-70	MASTERFLEX	Tubing Pump	1	$495.00	$495.00
11200-0100	NORTON	storage tank	2	$472.90	$945.80
CKM050V-PF	PLAST-O-MATIC	Backflow Valve	5	$82.10	$410.50
PRH300B-PV	Plast-O-Matic, Inc.	Pressure Regulator	1	$1,623.16	$1,623.16
3-2536-P0	Signet	Flow sensor	11	$224.40	$2,468.40
SS4P4T1	Swagelock	Pecock Valve	4	$45.90	$183.60
A/SA182	TAH Industries, Inc.	Static mixer	1	$450.00	$450.00
MBV200VST-PV	TRUE BLUE	Control valve	17	$77.38	$1,315.46
RF45	Water King	Water Softener	1	$1,582.00	$1,582.00
A88E1013	WATTS	Backflow Valve	2	$134.34	$268.68
25AUB-Z3	WATTS	Pressure Regulator	2	$85.30	$170.60

To illustrate the capabilities of the model, three different types of products were examined in this report: *Spirulina* biomass for the nutraceutical market, astaxanthin gelcaps for the nutraceutical market and *Haematococcus pluvialis* biomass for the feed market. In these model runs we assume that capital expenses are depreciated over 10 years, that the microalgal plant starts production in 2004 and that sales reach 100% of production within 3 years.

Example 1. Biomass from *Spirulina* for the nutraceutical market. We assume that

- *Spirulina* biomass represents 100% of the produced biomass (by weight),
- *Spirulina* will be sold into the high end nutraceutical market ($200/kg), and
- "cost of sales" represent 20, 15 and 10% of sales for years 1, 2, and 3.

Example 2. Astaxanthin from *Haematococcus* biomass for the nutraceutical market. Our basic assumptions are

- Astaxanthin represents 3% of the produced biomass (by weight),
- astaxanthin will be sold into the nutraceutical retail market ($70,000/kg),
- higher costs will be incurred by extraction, encapsulation and bottling of the astaxanthin, and
- higher "cost of sales" would be incurred over the first two years since this represents a new product unknown to the consumer.

Example 3. Astaxanthin from *Haematococcus* biomass for the feed market. Our assumptions are

- Astaxanthin represents 3% of the produced biomass (by weight),
- astaxanthin will be sold into the bulk feed ingredient market ($2,000/kg),
- lower costs will be incurred since there is no need for extraction, encapsulation and bottling of the astaxanthin, and
- lower "cost of sales" would be incurred over the first two years since this represents a product already known to the consumer.

The resulting Net Sales, Total Expenses, Net Cash Flow and Cumulative Cash Flow for the first 15 years of operation are shown in Figure 153. for the three scenarios. It is clear from those results that the model reflects changes in the assumptions in each case such as, for example, lowered production costs for *Spirulina* biomass and Feed astaxanthin and higher selling price for Nutraceutical astaxanthin. Figure 153. clearly indicates that out of these three very different products, the least viable option is the astaxanthin fish feed product. The two nutraceutical products are able to generate sufficient cash to cover all costs associated with the microalgal-based carbon sequestration scheme and, in the case of the nutraceutical astaxanthin, it has potential to generate significant profits.
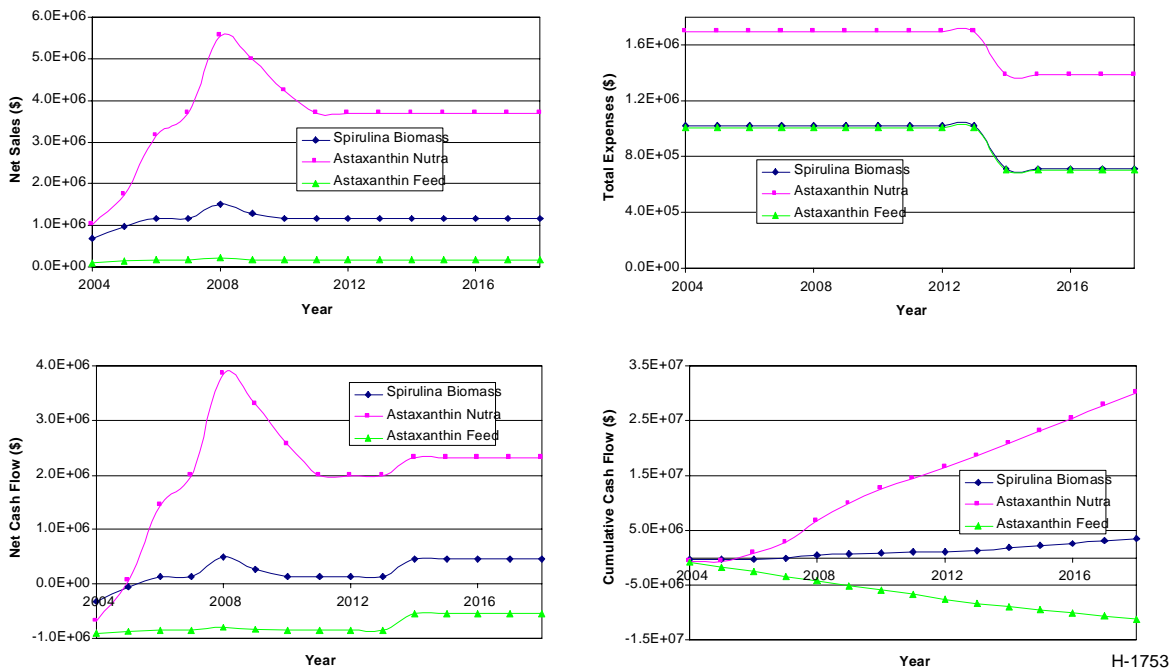
Figure 153. Resulting Net Sales, Total Expenses, Net Cash Flow and Cumulative Cash Flow for the first 15 years of operation for three microalgal scenarios: *Spirulina* biomass, nutraceutical astaxanthin and feed astaxanthin.

The results shown above assume no optimization of the microalgal cultivation processes involved and no experiments were conducted to optimize those processes. However, we did explore how changes in one characteristic of the cells could affect the costs. Specifically, we used the data obtained in section 4.3.4.2 to understand how centrifugation characteristics of the microalgae can affect total costs of capturing carbon while producing the biomass. In the case of *Haematococcus*, harvest costs represent 7.9 % of the total costs. We have calculated that in the case of AQ0011, a difficult strain to harvest because of its small size, the harvest costs would represent about 17.6 % of the total costs while for strain AQ0015, a very easy to harvest strain, the number would be only 3.3% of the total costs. The different harvest costs would affect the total costs as well. The total costs for strain AQ0011 would be about 11.8 % higher than for *Haematococcus* while the total costs for strain AQ0015 would be about 4.7 % lower.

One important advantage of a detailed economic model is the ability to identify areas of high cost and to plan for optimization in those areas. It can also help identify the best location for the algae plant. For example, in Hawaii, labor and utility costs are particularly high. Although there may be other reasons to place an algae facility in Hawaii, the model can help identify other locations which may have a positive impact on the feasibility of the project. It might not make sense to produce astaxanthin for fish feed in Hawaii but it might very well make good sense to do it elsewhere.

187

Sensitivity analyses have been carried out in particular for the astaxanthin market. We have looked at the effect of varying variables such as % biomass that consists of astaxanthin, kg biomass produced by a growth unit and price of kg of product on net returns and breakeven prices for the product. We have also examined the effect of diversification using markers for solvency, liquidity and profitability to determine the viability of the algae project.

Another useful way of looking at the economic viability of an algae facility is to perform a risk analysis on the model created. By assuming varying distribution patterns for parameters such as price of product, kg produced by a pond or growth unit, amount sold as raw biomass versus amount sold as nutraceutical, one can calculate probabilities of obtaining any given net return and thereby make a forecast of expected viability including the worst and best case scenarios. Figure 154 below shows a sensitivity chart and the impact of the main variables on net return. The highest impact is the form in which the product is sold; the closer the product is to being in finished retail form the better in terms margins made. The next most important economic factor is not necessarily the amount of biomass produced but rather the % of biomass that constitutes the product.
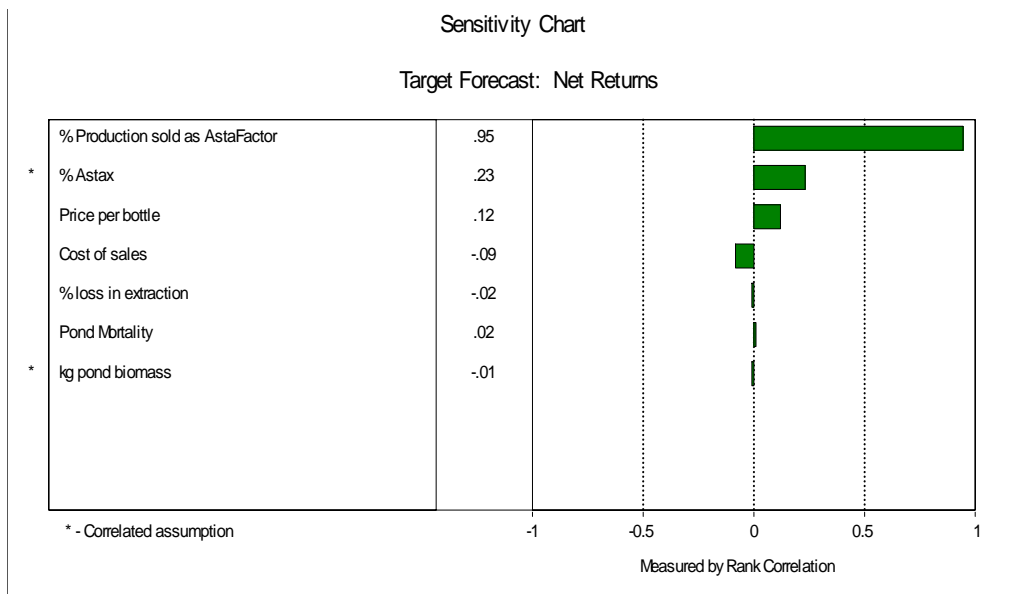
Figure 154. Risk analysis used to forecast economic viability of a microalgal-based carbon sequestration scheme.

4.5.3.3 Calculation of "Economies of Scale" Factors in Microalgal Plant Engineering

It is expected that as the size (scale) of the microalgal facility increases, the costs per unit biomass produced/costs per unit CO_2 sequestered will decrease. We have modeled the ESF (Economy of Scale Factor) by, first, determining the costs associated with what we consider to be the smallest size microalgal plant that is economically viable (smallest economical unit or SEU). Based on our experience and economic models at Mera's microalgal plant, and based on the capacity of the different units of material handling equipment used in these processes we can determine at what scale (e.g., 2x, 5x, 20x, 200x capacity of the smallest size plant) the change in

188

ESF becomes 0 (zero). Then, we have determined the estimated costs of several microalgal plants of intermediate size. Using these data we have formulated an equation that relates microalgal plant scale to ESF (Figure 155). In Figure 155, we show a number of possible scenarios. The different results are caused by assuming differences in the rate at which savings can be effected as plant size increases. We have also assumed that the maximum ESF that can be attained is 50% for this exercise. The equation's factors that ultimately fit our scale up cost estimates can now be used in conjunction with our economic models to determine the actual costs of any plant that may be size limited by, for example, land area available near a fuel combustion gases source (e.g., a power plant).
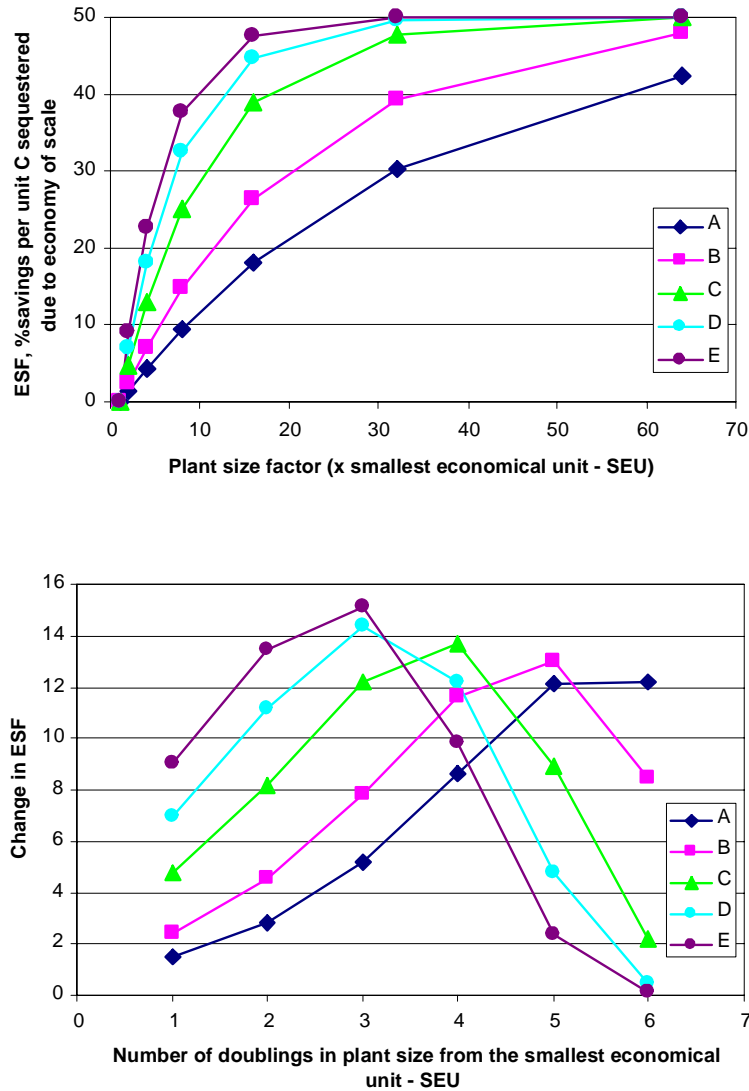
H-1754

Figure 155. Possible ESF results based on 5 different scenarios reflecting differences in the assumed rate at which savings can be effected (A→E = faster) as plant scale increases (top panel) and the resulting changes in ESF as plant size doubles (bottom panel). In this case, we have assumed that maximum attainable ESF is 50%. See text for details.

189

5. SUMMARY AND CONCLUSIONS

5.1   Supply of CO_2 from Power Plant Flue Gas to Photobioreactor

5.1.1 CO_2 Separation and Clean-Up Technologies

In the United States about two-thirds of the capacity in the utility power generation sector is based on fossil fuel combustion. Coal and natural gas are the primary fuels for power generation; fuel oil is important in specific regions. All fossil fuels amount to 71% of the electricity generating capacity. Fossil fuels represent an even larger segment of the non-utility power generation market (approximately 90%, if the use of biomass is included).

Concentrations of trace acid gas species such as NO_x and SO_2 depend on the composition of the fuel and on the air pollution control system employed. Natural gas-fired combustors have virtually no SO_2 in the flue gas, while coal-fired systems have hundred of parts per millions. The range of NO_x emissions given in Table 3 reflects the use of low NO_x burners and/or post-combustion NO_x control to remove some of the NO_x from the flue gas.

There are several technologies currently available to separate and capture CO_2 from fossil-fueled power plants including absorption from gas streams by contact with amine-based solvents, cold methanol or sorbents and passing the gas stream through special membranes. The optimum process for capturing CO_2 is largely influenced by the concentration or partial pressure of CO_2 in the flue gas; this depends, in turn, on the characteristics of the fuel and combustion system.

Application of these carbon dioxide separation processes to flue gas depends on the concentration of CO_2 in the stream, on the presence of impurities in the gas, and on the pressure of the flue gas stream. Chemical adsorption may be preferred for cases in which the concentration of CO_2 is low and the pressure is near atmospheric. Physical adsorption is favored for higher total pressure and concentration of CO_2.

Chemical adsorption using MEA is the most mature technology and looks to be the most economically viable in the near future. A unit sized for a 25 MWe plant burning a bituminous coal would process 235,000 lb/hr of flue gas and produce 42,000 lb/hr of CO_2. The total major equipment cost is approximately $5M (1999 dollars). The total capital cost is on the order of $11M.

5.1.2   Carbon Dioxide Dissolution Method

In the small, laboratory scale reactors, any introduced gases are effectively mixed instantaneously throughout the culture medium. This is not so in larger scale reactors, due to the physical configuration of the photobioreactor. In the current Aquasearch commercial reactor, there are two gas streams added to the photobioreactor. A large stream of transport air is added using multiple injectors arranged radially near the walls of the photobioreactor. Large (~1.25 cm (~ ½ in.)) diameter nozzles are used. This air is used to add momentum to the liquid and promote liquid circulation in the long tube that comprises the photobioreactor. In the current design, a high-volume, low-pressure flow of filtered ambient atmosphere is introduced in a 2-m vertical airlift section of the reactor in which fluid rises, creating the head pressure necessary for recirculation.

Slightly upstream of the air injection location, pure CO_2 is added through a small pipe with a sparger on the end to produce small bubbles. The CO_2 is introduced in a 2-m "down-flowing" section, where it rises against the fluid flow. This procedure dramatically improves the dissolution of CO_2. CO_2 is not added continuously, but rather is added when the pH of the liquid rises to a certain level. CO_2 is used both to provide carbon for growth of microalgae and to keep the pH in an optimum regime for growth.

In the commercial-scale photobioreactors, air is needed for circulating the liquid. In the smaller chemostats that are used to grow microalgae in the laboratory, CO_2 is sometimes used by itself, without adding any air to promote mixing. This can result in much higher carbon conversion (or efficiency of CO_2 utilization) than in the larger scale system. As far as the growth rate of microalgae is concerned, air has both advantages and disadvantages.

The chief advantage of the transport air is that it removes some of the dissolved oxygen in the water. Photosynthesis results in the production of O_2 by the microalgae. Under some conditions, the water can be supersaturated with oxygen. When this occurs, the rate of photo-synthesis (and growth) falls rapidly. The relatively large flow of air through the photobio-reactors strips out some of the dissolved oxygen and prevents high levels of supersaturation.

The chief disadvantage of the transport air addition is that is strips CO_2 as well as O_2 from the water. The removal of CO_2 lowers the efficiency of carbon utilization by 50% to 80%. Thus, in the commercial photobioreactors, the efficiency of CO_2 utilization (based on carbon production and CO_2 usage) is only 12.5%.

If we introduce a flue gas containing 5 to 10% CO_2 in the downflowing section where pure CO_2 is currently introduced, the 10 to 20-fold increase in flow rate could create a substantial back-pressure on the airlift-driven circulation. We may be able to solve this problem by simply increasing the flow rate of the airlift supply to overcome the flow rate of the flue gas. However, the solution may not be so simple. The flue gas supply will be pulsed (because it is used to regulate pH), whereas the airlift is continuous. Thus, we might create a strongly modulated fluid flow rate that is not favorable to the microalgae cultures. Other solutions could involve (a) decreasing bubble size of the flue gas to provide for higher dissolution rates, or (b) automatic modulation of the airlift flow rate to offset the counter-flow of flue gas.

If we introduce a flue gas containing 5 to 10% CO_2 in the down-flowing section where pure CO_2 is currently introduced, the 10 to 20-fold increase in flow rate could create a substantial back-pressure on the airlift-driven circulation. We may be able to solve this problem by simply increasing the flow rate of the airlift supply to overcome the flow rate of the flue gas. However, the solution may not be so simple. The flue gas supply will be pulsed (because it is used to regulate pH), whereas the airlift is continuous. Thus, we might create a strongly modulated fluid flow rate that is not favorable to the microalgae cultures. Other solutions could involve (a) decreasing bubble size of the flue gas to provide for higher dissolution rates, or (b) automatic modulation of the airlift flow rate to offset the counter-flow of flue gas.

5.2   Selection of Microalgae

Our objective was to select microalgae best suited for carbon recovery from flue gases. Our selection criteria consisted, first, of temperature, pH and simulated flue gas tolerance (untreated) and, second, ability to maintain high photosynthetic rates under those conditions, produce high value products and ability to induce carbon precipitation into carbonate minerals.

5.2.1   Characterization of Physiology, Metabolism and Requirements of Microalgae

Temperature tolerance

We grew 54 microalgal strains in batch culture at 15, 20, 25, 30 and 35ºC and found that five did not grow at 15ºC, one each did not grow at 20ºC and 30ºC and eleven did not grow at 35ºC. Microalgal cultures exposed to flue gases may experience relatively high temperatures unless the temperature of the flue gas is controlled. Thus, temperature range may be a limiting factor in the selection of microalgal strains for specific applications in carbon sequestration from flue gases. We found that, on average, locally isolated strains (Hawaii), had higher temperature tolerances than strains maintained in culture collections.

pH tolerance

We grew 20 microalgal strains in chemostat cultures at 6.5, 7.5 and 8.5 pH. We found that biomass levels in the chemostats were dependent on the pH conditions of the cultures. Lower culture biomass at 8.5 pH was interpreted as indicative of carbon limitation of growth while lower culture biomass at 6.5 ph was interpreted as a detrimental effect due to the acidity of the medium. Interestingly, the photochemical efficiency of the cultures was not affected by the different pH conditions except for two Cyanobacterial strains.

Flue gas tolerance

We grew 24 microalgal strains in chemostat cultures at 7.5 pH and exposed either to pure CO2 or one of five simulated gas mixtures. We found that, for all strains, exposure to simulated flue gases (0-3504 ppm SO_2, 0-328 ppm NO, and 0-126 ppm NO_2) did not result in reductions in the photochemical efficiency of the cultures as long as the culture pH was controlled.

5.2.2   Achievable Photosynthetic Rates, High Value Product Potential and Carbon Sequestration into Carbonates

Achievable Photosynthetic Rates

We found that photosynthetic carbon capture rates were quite variable for each strain and dependent on the pH and simulated flue gas that the cultures were exposed to. The rates ranges from 0 (no carbon uptake)to as high as 0.13 mg CO_2 l^{-1} min^{-1}. Independent of the specific photosynthetic carbon capture rates we found that the efficiency of carbon capture by the cultures (the ratio of the net photosynthetic rate to the rate at which inorganic carbon disappeared from the culture medium either *via* photosynthesis or degassing) was dependent on the pH of the

cultures but not on the type of simulated flue gas. We also found that the effects of the ph of the culture were consistent over a large range of photosynthetic rates. This provides us a tool to choose the appropriate microalgal strains for real world applications in which maximum algal productivity (m^{-2}) is more desirable than high carbon capture efficiency.

High Value Component

Microalgal cultivation is expensive (tens of US$ kg-1 of carbon sequestered in biomass). Thus, microalgal-mediated carbon sequestration becomes attractive from a cost point of view when high value byproducts can be obtained from the biomass produced. In this work we analyzed the pigment (carotenoids and phycobiliproteins) content of 34 microalgal strains. These pigments have applications as colorants, nutritional supplements, feed ingredients and in medical diagnostics. We identified several strains, and their growth conditions, that would produce viable strategies for high value chemical production, the revenues from which would offset the cost of the carbon capture and sequestration.

Carbon Sequestration into Carbonates

Here we have described microalgal growth conditions that result in changes in the chemical make up of the growth medium that are conducive to carbon precipitation in the form of carbonates. Specifically, we have described culture conditions that will induce the precipitation of carbon into $CaCO_3$ *via* photosynthetically mediated changes in medium pH. In principle, this strategy can be used with any microalgal species and, thus, is not limited to species that produce cellular structures made up of $CaCO_3$.

5.3   Optimization and Demonstration of Industrial Scale Photobioreactor

The objective of this Task was to investigate microalgal mediated carbon sequestration at a commercially significant scale while using actual combustion flue gases. This was done in three phases. First, we conducted pilot evaluations using small enclosed outdoor photobioreactors where the cultures were grown either on pure CO_2 or actual combustion gases from a coal combustor. Second, we conducted full scale production runs in enclosed outdoor photobioreactors where the cultures were grown either on pure CO_2 or actual combustion gases from a propane combustor. Third, we conducted experiments to determine the costs associated with harvesting the produced biomass since this has been identified as one of the significant costs associated with microalgal cultivation and is dependent on strain morphology.

5.3.1   Pilot Evaluation

Seven microalgal strains were grown in pilot scale (up to 2,000 liter capacity) outdoor photobioreactors and exposed to either pure CO_2 or actual coal combustion gases.

Our data on microalgal productivity and photosynthesis indicated that outdoor microalgal cultures can be quite variable as they depend, for example, on the availability of sunlight. This is reflected in the daily values for carbon capture obtained. Even with all that variability, the data from these experiments reflect what was learned in Task 2, that a large fraction of the CO_2 that is

available in the culture medium will simply escape (degassing) and will not be captured by the microalgae.

From these experiments, we have also confirmed the relationship between culture pH (and medium CO_2 concentration) and carbon capture efficiency that was described in the laboratory scale experiments (Task 2).

We also found a detrimental characteristic of coal combustion gases that we had not detected in the previous chemostat experiments. Use of raw coal combustion gases result in a decrease in the alkalinity of the culture medium, presumably because of the presence of acid gases, mainly SO_X. At any one pH, lower medium alkalinity translates into lower dissolved inorganic carbon species available in the medium for photosynthesis-mediated carbon capture and sequestration. However, no other negative effect of coal combustion gases was found in these microalgal cultures. Thus, if the coal combustion flue gases were to be scrubbed to eliminate SO_X, it would appear that microalgal photosynthesis represents a viable alternative to reduce CO_2 emissions from such combustion sources.

5.3.2   Full Scale Production Runs

Six microalgal strains were grown in commercial scale (up to 25,000 liter capacity) outdoor photobioreactors and exposed to either pure CO_2 or actual propane combustion gases.

As was the case for the pilot scale experiments, our data indicated large variability in daily photosynthetic rates by the cultures. Similarly, a large fraction of the CO_2 introduced into the cultures was simply lost to degassing.

From these experiments at commercial scale, we have also confirmed the relationship between culture pH (and medium CO_2 concentration) and carbon capture efficiency that was described in the laboratory scale experiments (Task 2) and in the pilot scale experiments (Subtask 3.1). Further, we found that the large photobioreactors were more efficient than the small ones since the rate of CO_2 degassing was lower in the former.

As opposed to the pilot scale cultures grown on coal combustion gases, no detrimental effects were found in the full scale cultures grown on propane combustion gases (no measurable SO_X). This indicates that propane (and, presumably, natural gas) combustors can be used, without scrubbing, in mitigation strategies that take advantage of microalgal photosynthesis.

5.3.3   Algae Separation and Final Product

We conducted experiments to determine the costs associated with harvesting the produced biomass since this has been identified as one of the significant costs associated with microalgal cultivation and is dependent on strain morphology.

Twenty two strains were tested in a benchtop centrifugation protocol designed to measure harvest efficiencies for the different strains under a standard set of conditions. We found that the

relative centrifugation efficiencies ranged over five orders of magnitude and was related to strain morphology

Furthermore, five microalgal strains of very different morphology (from 3 μm diameter coccoid cells to filaments several mm long) were tested in large scale centrifugation experiments using a commercial centrifuge. In these experiments, we confirmed the effects of strain morphology on harvest efficiencies which will translate in differences in harvesting costs.

Finally, we tested the applicability of lamellar settling to microalgal harvesting as this promises to be a less costly alternative to centrifugation. In these experiments we found that lamellar settling would probably be useful in the harvesting of microalgal biomass if the cells are substantially denser that the growth medium, as is the case for stressed *Haematococcus* cells.

5.4   Carbon Sequestration System Design

5.4.1   Photobioreactor Design Concept

A new type of photobioreactor was developed. The photobioreactor maximizes availability of the PAR spectra for microalgae; and utilize the solar radiation outside of PAR spectra for generating electric power that potentially offset the sequestration cost. In this photobioreactor concept, the solar radiation from the concentrator is directed to a selective spectral reflector which reflects only the PAR spectra while the longer wavelength components are transmitted to the PV cells.

This photosynthetic reaction requires solar spectra typically between 400 nm and 700 nm, called photosynthetically active radiation (PAR). Solar spectra outside of the PAR wavelength regime are not utilized by microalgae.   The solar spectral energy between 400 nm and 700 nm (PAR) is 424 W/m^2, which is 44% of the total solar spectral energy of 962 W/m^2 on the ground.

In the past, PSI conducted a series of experiments for electrical power generation utilizing the GaSb cell, one of the low-bandgap PV cells. The test results showed that it is possible to convert the solar IR spectra into electric power at efficiencies theoretically predicted, e.g., 15.5% for the GaSb cell, while the PAR spectra are transmitted to the plant growth facility

As the area required for photosynthetic process by microalgae is a key cost driving factor, a photobioreactor design which makes efficient use of solar light was developed.   Solar radiation was separated into PAR and non-PAR components. The PAR components was fed to microalgae while the non-PAR solar spectra was converted to electric power by using low bandgap photovoltaic cells.

Based on the current commercial PV cell cost, potential economic merit of this photobioreactor was calculated. It was shown that that the cost benefit associated with simultaneous CO_2 sequestration and electricity generation is not likely due to the state of the art the PV cost. However, if the cost of the PV cells fall below 10% of the current cost, then electric power generation using non-PAR solar spectra will work towards lowering the CO_2 sequestration cost.

5.4.2   System Integration and Modeling

A process model of a commercial scale hybrid photobioreactor/open pond microalgae production system was developed to optimize harvesting strategy to maximize carbon capture (i.e., cumulative yield). As part of this development, the carbon balance over the photobioreactor was investigated and relationships were derived for the partitioning of carbon between the different carbon pools including DIC in the liquid media, organic carbon in the cell biomass, and losses to the headspace and by venting. The relationship between carbon assimilation and cell division was also determined.

The data suggest that the carbon capture efficiency of the present photobioreactor system is modest. Between 7% and 39%, with a cumulative average of 25%, of the carbon sparged into the media is eventually assimilated into the cell biomass. Most of the remaining carbon is lost via degassing and venting. To maximize carbon capture efficiency, a closed system in which vented gas is recirculated back into the photobioreactor should be explored.

Process model verification tests indicate that cell population growth is predicted reasonably well; however, additional comparisons with operational data should be performed.

Simulations were conducted to identify harvesting scenarios that would maximize cell biomass yield (and, hence, carbon capture). It was determined that reducing harvesting quantities while increasing target cell concentrations in the photobioreactor could provide significant increases in cumulative yield (about 10%) compared to the harvesting strategy currently applied by Mera Pharmaceuticals, Inc. Unfortunately, this would require daily harvests and additional ponds. A target cell concentration of 5.5×10^5 cells/mL and a harvesting cell quantity of 3.2×10^{12} cells produced a realistic (i.e., achievable with the current labor force and ponds) cumulative yield of 3.12×10^{13} cells; however, this is only 2.57×10^{11} cells greater than the cumulative yield of the current harvesting strategy. The current harvesting strategy appears to represent the best possible scenario when real constraints imposed by the limited labor force and number of available open ponds are taken into consideration. Nevertheless, the present results suggest that a process model can be a valuable tool to optimize carbon capture and revenue streams when planning new facilities.

Since optimizing a harvesting strategy for large-scale production of microalgae is a new concept in microalgal modeling, further research in this area is warranted. One area of potential interest is to incorporate microalgal models that predict culture growth rate as a function of light intensity, light/dark cycle effects induced by cell position in the depth of the culture, average solar irradiance, or non-limiting nutrients into the model for optimizing a harvesting strategy (Csögör et al., 1999; Molina Grima et al., 1996; Pruvost et al., 2002; Zonneveld, 1996).

5.5   Economic Analysis

A detailed economic model was developed for the production of high value substances from microalgae in a carbon sequestration scheme. Using over 500 input variables, the model calculates capital and operating costs as well as land, labor and utility requirements. It also generates cash flow and balance sheets for the first 15 years of operation given market price and

sales expectations. The model was developed to be as flexible as possible and accommodating of any microalgae and type of processing that microalgae would require to produce the valuable end product, the sale of which would produce the revenues necessary to cover the costs of the carbon sequestration.

The viability of three different types of products were examined in this report: *Spirulina* biomass for the nutraceutical market, astaxanthin gelcaps for the nutraceutical market and *Haematococcus pluvialis* biomass for the feed market. The model showed that only certain products were able to generate sufficient cash to cover all costs associated with the microalgal-based carbon sequestration scheme and, in the case of the nutraceutical astaxanthin, it had potential to generate significant profits.

Sensitivity analysis was also carried out to look at the effects of varying variables such as % biomass that consists of the high value product, kg biomass produced/kg carbon captured by a growth unit, and price of kg of product on net returns and breakeven prices for the product. We have also examined the effect of diversification using markers for solvency, liquidity and profitability to determine the viability of the algae project. This analysis will be useful when investigating specific microalgal-based carbon sequestration schemes as they will point to the areas of the process in which investment in optimization will bear the largest potential for cost reduction of carbon sequestration.

We conclude that microalgal-based carbon sequestration schemes can, in principle, not only cover the cost of carbon capture and sequestration but also produce a profit. The scheme's viability will be dependent on the high value product produced and its markets.

REFERENCES

American Society for Horticultural Science, Kent Kobayashi, Using computer simulation software to enhance student learning (2004). http://www.ashs.org/resources/horteducator/Kobayashi.html. 12 September 2004.

Becker, E.W., Microalgae: Biotechnology and Microbiology (Cambridge University Press, Cambridge, New York, 1994), pp. 1-2 and 11-13.

Bischoff, H.W. and Bold H.C., Phycological studies. IV. Some algae from Enchanted Rock and related algal species (The Univ. of Texas. Publ. 6318, 1963) 95 pp.

Borowitzka, M.A., "Microalgae as sources of pharmaceuticals and other biologically active compounds," *J. Appl. Phycol.* 7, 3-15 (1995).

Brown, L.W., "Uptake of carbon dioxide from flue gas by microalgae," *Energy Conv. Manag.* 37, 1363-1367 (1996).

Chang, E.H. and Yang, S.S., "Microalgae for biofixation of carbon dioxide," *Bot Bull Acad Sin.* 44, 43-52 (2003).

Clesceri, L.S., Greenberg, A.E. and Eaton, A.D., Standard methods for the examination of water and wastewater,. (Baltimore: United Book Press, 1998).

Csögör, Z., Herrenbauer, M., Perner, I., Schmidt, K., and Posten, C., "Design of a photo-bioreactor for modeling purposes," *Chemical Engineering Processing* 38(4-6), 517-523 (1999).

Geider, R.J. and Osborne, B.A., Algal Photosynthesis: the Measurement of Algal Gas Exchange. Current Phycology 2, (Chapman and Hall, New York, 1992), pp. 24-25.

Guerin, M., Huntley, M., and Olaizola, M., "*Haematococcus* astaxanthin: health and nutritional applications," 1st Congress of the International Society for Applied Phycology/9th International Conference on Applied Phycology. Almeria, Spain, pp.1-19 (2002).

Hanagata, N., Takeuchi, T., Fukuju, Y., Barnes, D.J. and Karube, I., "Tolerance of microalgae to high CO2 and high temperature," *Phytochem.* 31, 3345-3348 (1992).

IEA (International Energy Agency), *Carbon Dioxide Capture from Power Stations,* 1998.).

Jeffrey, S.W., Mantoura, R.R.C. and Wright, S.W., "Phytoplankton pigments in oceanography," (UNESCO Publishing, France 1997).

Kim, J.M., Araki, S., Kim, D.J., Park, C.B., Takasuka, N., Baba-Toriyama, H., Ota, T., Nir, Z., Khachik, F., Shimidzu, N., Tanaka, Y., Osawa, T., Uraji, T., Murakoshi, M., Nishino, H., Tsuda, H., "Chemopreventive effects of carotenoids and curcumin on mouse colon carcinogenesis after 1,2-dimethylhydrazine initiation," *Carcinogenesis* 19(1), 81-5, 1998

Kirk, J.T.O., Light and Photosynthesis in Aquatic Ecosystem (University Press, Cambridge, 1983).

Law, A.M. and McComas, M.G., How to build valid and credible simulation models. *In* Proceedings of the 2001 Winter Simulation Conference, B.A. Peters, J.S. Smith, D.J. Medeiros, and M.W. Rohrer (Eds.). Arlington, Virginia, pp. 22-29 (2001).

Lee, J.S., Kim, D.K., Lee, J.P., Park, S.C., Koh, J.H., Cho, H.S. and Kim, S.W., "Effects of SO_2 and NO on growth of Chlorella sp," *KR-1. Biores. Biotechnol.* 82,,1-4 (2002).

Lee. J.N., Lee, J.S., Shin, C.S., Park, S.C. and Kim, S.W., "Methods to enhance tolerances of Chlorella KR-1 to toxic compounds in flue gas," *Appl. Biochem. Biotechnol.* 84-86, 329-342 (2000).

Leung, P.S., Hochman, E., Wanitprapha, K., Shang, Y.C., and Wang, J.K., "Optimal harvest schedule for maricultured shrimp: a stochastic sequential decision model," Research Series 060. College of Tropical Agriculture and Human Resources, Honolulu, Hawai'i, pp. 2-3 (1989).

Libes, SM., An introduction to marine biogeochemistry (Wiley & Sons Inc., New York, 1992), p, 242-261.

Maeda, K., Owada, M., Kimura, N., Omata, K. and Karube, I., CO_2 fixation from the flue gas on coal-fired thermal power plant by microalgae," *Energy Conv Manag.* 36, 717-720 (1995).

Mazzuca-Sobczuk, T., García-Camacho, F., Camacho-Rubio, F., Acién-Fernández, F.C. and Molina-Grima, E., "Carbon dioxide uptake efficiency by outdoor microalgal cultures in tubular airlift photobioreactors," *Biotechnol Bioeng.* 67, 465-475 (2000).

McCabe, W.L. and Smith, J.C., Unit Operations of Chemical Engineering (McGraw-Hill, New York, pp. 697-700, 1976).

Millero, F.J., The thermodynamics of the carbonate system in seawater," *Geochimica et Cosmochimica Acta* 43, 1651-1661 (1979).

Molina Grima, E., Fernández Sevilla, J.M., Sánchez Pérez, J.A., and García Camacho, F., "A study on simultaneous photolimitation and photoinhibition in dense microalgal cultures taking into account incident and averaged irradiances," *Journal of Biotechnology* 45(1), 59-69 (1996).

Molina-Grima, E., Belarbi, E.-H., Acién-Fernández, F.G., Robles-Medina, A. and Chisti, Y., "Recovery of microalgal biomass and metabolites: process options and economics," *Biotechnol Adv.* 20, 491-515 (2003).

Murakami, M. and Ikenouchi, M., "The biological CO2 fixation and utilization by RITE (2) Screening and breeding of microalgae with high capability in fixing CO_2," *Energy Conv Manag.* 38, S493-497 (1997).

Nagase, H., Yoshihara, K.I., Eguchi, K., Okamoto, Y., Murasaki, S., Yamashita, R., Hirata, K. and Miyamoto, K., "Uptake pathway and continuous removal of nitric oxide from flue gas using microalgae," *Biochem. Eng. J.* 7, 241-246 (2001).

Nagase, H., Yoshihara, K.I., Eguchi, K., Yokota, Y., Matsui, R., Hirata, K. and Miyamoto, K., "Characteristics of biological NOx removal from flue gas in a *Dunaliella tertiolecta* culture system," *J. Ferm. Bioeng.* 83, 461-465 (1997).

Nakamura, T., "Optical Components for Space Based Plant Lighting," NASA SBIR Contract NAS10-01056, NASA/KSC, November 2001.

Nakamura, T., Fraas, L. M., and Avery, J. E., "Solar Plant Lighting with Electric Power Generation," Paper Number 188., 32nd International Conference on Environmental Systems, San Antonio, TX, July 2002

NEDO Report, "Sequestration and Utilization of CO_2 by Bacteria and Microalgae," March 2000.

Negoro, M., Shioji, N., Miyamoto, K. and Miura, Y., Growth of microalgae in high CO_2 gas and effects of SOx and NOx," *Appl. Biochem. Biotechnol.* 28-29, 877-886 (1991).

Nyholm, N. and Peterson, H.G., "Laboratory bioassays with microalgae," In Plants for environmental studies (CRC Press. Florida, 1997), Wang W, Gersuch JW, and Hughes JS, editors.

Olaizola, M., "Commercial production of astaxanthin from Haematococcus pluvialis using 25,000-liter outdoor photobioreactors," *J. Appl. Phycol.* 12, 499-506 (2000).

Perry, R.H. and Chilton, C.H., *Chemical Engineer's Handbook* (McGraw-Hill, New York, 1973).

Pruvost, J., Legrand, J., Legentilhomme, P., and Muller-Feuga, A., "Simulation of microalgae growth in limiting light conditions: flow effect," *AIChE Journal* 48(5), 1109-1120 (2002).

Rice, S.K., Brown, G.E. and Willing, R.P., "Computer simulation modeling using STELLA to enhance investigative learning in a biology curriculum: what is STELLA," http://www1.union.edu/~rices/STELLA/stella_intro.html. 12 September 2004 (2002).

Robbins, L.L. and Yates, K.K., "Microbial lime-mud production and its relation to climatic change," In Geological Perspectives of Global Climate Change (American Association of Petroleum Geologists, Tulsa, 2001); Gerhard, L.C.; Harrison, W.E., Hanson, B.M., Eds.; p. 267-283.

Schreiber, U., Schliwa ,U. and Bilger, W., "Continuous recording of photochemical and non-photochemical chlorophyll fluorescence quenching with a new type of modulation fluorometer," *Photosyn. Res.* 10, 51-62 (1986).

Sung, K.D., Lee, J.S., Shin, C.S., Park, S.C. and Choi, M.J., "CO_2 fixation by Chlorella sp. KR-1 and its cultural characteristics," *Biores. Biotechnol.* 68, 269-273 (1999).

Tredici, M., "Mass production of algae: photobioreactors," In Microalgal Culture (Blackwell Publishing, Oxford, 2003), Richmond, A, editor, 178-214.

U.S. Department of Energy, Energy Information Agency, *Emissions of Greenhouse Gases in the United States 1996*, DOE/EIA-0573(96), October 1997.

UNESCO, "Thermodynamics of the carbon dioxide system in seawater" (Technical Papers in Marine Science. Paris, France, 1987), pp. 51.

United Technologies Research Center, *Final Engineering Development of Coal-Fired High Performance Power Systems, Phase II*, Quarterly Progress Report for July 1-September 30, 1999, Contract DE-AC22-95PC95144 (1999)

Yamamoto, H.Y. and Kamite, L., "The effects of dithiothreitol on violaxanthin de-epoxidation and absorbance changes in the 500-nm region," *Biochim Biophys. Acta.* 267, 538-543 (1972).

Zapata, M., Rodriguez, F., Garrido, J.L., "Separation of chlorophylls and carotenoids from marine phytoplankton: a new HPLC method using a reversed phase C_8 column and pyridine-containing mobile phase," *Mar Eco Prog Ser*. 195, 29-45, (2000)

Zonneveld, C., Modelling the kinetics of non-limiting nutrients in microalgae," *Journal of Marine Systems* 9(1-2), 121-136 (1996).